Université catholique de Louvain
Faculty of Science
Department of Geography
Earth and Life Institute
Georges Lemaître Centre for Earth
and Climate Research

Aix-Marseille Université
Ecole Doctorale des Sciences de
l'Environnement (ED251)
Centre Européen de Recherche et
d'Enseignement des Géosciences
de l'Environnement

DATA-MODEL FUSION APPROACH USING TREE-RING WIDTH SERIES, A MECHANISTIC GROWTH MODEL AND AN EARTH SYSTEM MODEL TO RECONSTRUCT THE LARGE-SCALE CLIMATE VARIABILITY

DOCTORAL DISSERTATION PRESENTED BY

JEANNE REZSÖHAZY

IN PARTIAL FULFILLMENT OF THE REQUIREMENTS FOR THE DEGREE OF
DOCTOR IN SCIENCES OF THE UNIVERSITÉ CATHOLIQUE DE LOUVAIN
AND DOCTOR OF THE AIX-MARSEILLE UNIVERSITÉ

THESIS COMMITTEE:

Prof. Hugues Goosse (Supervisor)	Université catholique de Louvain, Belgium
Dr. Joël Guiot (Supervisor)	Aix-Marseille Université, France
Prof. Marie-Laurence De Keersmaecker (Chair)	Université catholique de Louvain, Belgium
Prof. Thierry Fichefet (Examiner)	Université catholique de Louvain, Belgium
Dr. Mathieu Jonard (Examiner)	Université catholique de Louvain, Belgium
Dr. Franck Torre (Examiner)	Aix-Marseille Université, France
Prof. Jan Esper (Reviewer)	Gutenberg University, Germany
Dr. Philippe Peylin (Reviewer)	Laboratoire des Sciences du Climat et de l'Environnement, France

LOUVAIN-LA-NEUVE
NOVEMBER 2021

Je soussignée, Jeanne Rezsöhazy, déclare par la présente que le travail présenté dans ce manuscrit est mon propre travail, réalisé sous la direction scientifique de Joël Guiot et Hugues Goosse, dans le respect des principes d'honnêteté, d'intégrité et de responsabilité inhérents à la mission de recherche. Les travaux de recherche et la rédaction de ce manuscrit ont été réalisés dans le respect à la fois de la charte nationale de déontologie des métiers de la recherche et de la charte d'Aix-Marseille Université relative à la lutte contre le plagiat.

Ce travail n'a pas été précédemment soumis en France, en Belgique ou à l'étranger dans une version identique ou similaire à un organisme examinateur.

Fait à Louvain-la-Neuve le 20 octobre 2021



Cette œuvre est mise à disposition selon les termes de la Licence Creative Commons Attribution - Pas d'Utilisation Commerciale - Pas de Modification 4.0 International.

Bon, voilà la fin d'un chapitre dans ma petite vie, pas grand chose me direz-vous à l'échelle de l'humanité, mais bon enfin quand même quelque chose à mon échelle. Alors, je me retourne pour me remémorer les circonstances et les personnes qui ont façonné ces quatre dernières années.

L'avantage lorsqu'on entreprend une thèse en cotutelle – mises à part les démarches administratives –, c'est que cela nous offre l'opportunité d'être encadrée par deux promoteurs (ou directeurs de thèse, au choix). Une situation finalement idéale pour ma part, puisque de cette façon je pouvais répartir mes questionnements et incertitudes entre deux personnes, sans (trop) risquer de les épuiser (enfin, je crois?); je pouvais aussi me plaindre deux fois plus de ma thèse (ça m'arrive); je pouvais recevoir deux fois plus de conseils, discuter deux fois plus, donc parler deux fois plus, ce qui m'arrangeait bien. Que demander de plus? Je souhaiterais donc tout d'abord remercier mon promoteur Hugues Goosse et mon directeur de thèse Joël Guiot. Hugues et Joël, chacun dans un style complémentaire, votre optimisme à toute épreuve (contrastant probablement avec cette tendance que j'ai à être un peu pessimiste), votre très grande disponibilité et nos discussions éclairantes m'ont indubitablement permis de mener cette thèse à son terme. Merci de m'avoir donné l'opportunité de pérégriner un peu, quand cela était encore possible, entre conférences, école d'été et terrain, ces expériences stimulantes scientifiquement et humainement feront assurément partie des plus beaux souvenirs de ma thèse. Merci pour votre confiance, merci pour tout!

La cotutelle m'a également permis de descendre dans cette contrée du sud de la France que l'on appelle Marseille pour découvrir un climat méditerranéen (un peu trop chaud à mon goût, je dois bien l'avouer) et une région accueillante. Je garderai un très bon souvenir de mes séjours à Marseille et au CEREGE (et sa belle pinède), bien que quelque peu compromis ces deux dernières années. J'y ai rencontré de très chouettes personnes (un petit bonjour à Macha et Fanny! vous rencontrer fut un réel plaisir!), y ai découvert des spécialités locales et moins locales au bout de la rue Sylvabelle et plus loin, jusqu'à Endoume, et y ai aussi travaillé, finalement. Merci Joël pour ton accueil! Je souhaiterais aussi adresser un très grand merci à Isabelle Hammad au CEREGE, sans qui cette cotutelle

n'aurait probablement jamais pu aboutir, car les démarches administratives, sans vouloir jeter la pierre à un des deux pays, furent ardues.

I would also like to thank the members of my jury, Mathieu Jonard, Thierry Fichefet, Franck Torre, Philippe Peylin and Jan Esper. Thank you very much for the careful reading of my manuscript, but also for your comments and feedbacks that have definitely improved the quality of the thesis. Un très grand merci également à la présidente de mon jury, Marie-Laurence De Keersmaecker, pour l'organisation et l'encadrement convivial et professionnel de la soutenance.

Je souhaiterais adresser un merci particulier à Fabio Gennaretti qui, depuis mon mémoire de fin d'études déjà lors de ma première expérience au CEREGE, et puis tout au long de ces quatre années de thèse, m'a aidée à m'y retrouver dans les méandres de MAIDEN, m'a conseillée et m'a guidée dans la bonne direction. Fabio, merci beaucoup pour ton écoute, ta disponibilité et ta patience, malgré mes innombrables questions et interrogations, probablement pas toujours toutes pertinentes.

J'aimerais également remercier Etienne Boucher et Dominique Arseneault qui m'ont permis de connaître l'expérience du terrain dans la taïga canadienne. Ma thèse n'aurait pas été la même sans cette expérience enrichissante. Je n'aurais jamais pensé pouvoir me retrouver là un jour, aussi bien entourée, merci infiniment!

Je souhaiterais aussi remercier tous mes collègues du Mercator, qui le rendent si spécial! Avant que tout ne parte un peu en ... cacahuète ... ces nombreux verres et soirées en votre compagnie durant lesquels nous pouvions échanger sur nos joies et désespoirs de thèse, mais aussi les oublier, étaient une vraie bouffée d'oxygène! Le télétravail sans vous, c'était franchement moins sympa. Un merci spécial à Charles, qui m'a permis de m'évader dans les montagnes pour écrire les dernières lignes de ma thèse. C'était définitivement une bonne idée. Un merci spécial aussi à François et Quentin qui m'ont permis de clôturer la dernière étape de ma thèse en moins de temps qu'il ne faut pour le dire, ou certainement en moins de temps qu'il ne m'aurait fallu!

Merci finalement à ma famille qui est là et me soutient quelle que soit la situation. Merci à mes parents, à Elise et Romain, pour ce noyau familial et l'oreille attentive! Un merci tout particulier à Q., tes compétences en code ont été particulièrement appréciables tout au long de ce parcours, mais pas que. Voilà on y est!

Résumé

Avant le 19ème siècle, peu de données instrumentales existent pour caractériser la variabilité climatique. Les enregistrements indirects du climat, appelés aussi proxys, issus des archives naturelles comme les cernes des arbres permettent de reconstruire le climat passé au-delà de la période instrumentale. La largeur des cernes d'arbres et la densité du bois représentent les proxys les plus couramment utilisés en paléoclimatologie, en raison de leur disponibilité à large échelle. Traditionnellement, la relation entre le climat et les proxys issus des cernes des arbres est modélisée statistiquement, souvent sur base d'une régression linéaire. Or, cela repose sur différentes hypothèses, entre autres la linéarité et la stationnarité de la relation entre le climat et la croissance des arbres, qui peuvent ne pas être adaptées pour de nombreux enregistrements. A l'inverse, on dispose de modèles mécanistes capables de simuler une relation potentiellement non-linéaire entre le climat et la croissance des arbres en considérant l'influence combinée de facteurs climatiques et non-climatiques au sein des processus biologiques sous-jacents à la croissance des arbres.

Au cours des dernières décennies, des méthodes d'assimilation de données ont été de plus en plus utilisées en paléoclimatologie. Elles combinent de manière optimale les sorties des modèles climatiques et les observations indirectes du climat, en particulier issues des cernes des arbres, afin de fournir des reconstructions de champs climatiques aussi cohérentes que possible en tenant compte de la physique du climat, des données disponibles et des incertitudes associées aux modèles et aux données. Dans ce cadre, l'utilisation de modèles de type *proxy system models* permet de faire le lien entre les observations indirectes du climat ou proxys et les sorties des modèles climatiques. Or, jusqu'à présent, l'assimilation de données incluant des données de largeur de cernes s'est basée exclusivement sur l'utilisation de *proxy system models* statistiques.

Dans cette thèse, nous posons donc la question de recherche suivante: Est-il possible d'améliorer les reconstructions climatiques à large échelle sur base des séries de largeurs de cernes en prenant en compte explicitement les liens entre le

climat et la croissance des arbres avec un modèle dendroclimatique mécaniste? Pour ce faire, nous avons inclus, pour la première fois, un modèle mécaniste de la croissance des arbres, le modèle écophysiologique MAIDEN, au sein d'une procédure d'assimilation de données de manière à améliorer les reconstructions de champs climatiques.

Afin d'y parvenir, un protocole de calibration du modèle MAIDEN à large échelle a été mis en place, depuis l'initialisation à la validation du modèle, en passant par sa calibration. En particulier, une méthode de calibration bayésienne des paramètres les plus sensibles du modèle a été développée afin d'appliquer le modèle MAIDEN à large échelle de la manière la plus automatisée possible. La méthode de calibration bayésienne a ensuite été testée sur le 20ème siècle avec des arbres aussi différents que ceux de l'Europe et du Canada. Cela a permis de mettre en évidence la possibilité d'utiliser le modèle à large échelle. Pour ce faire, il est nécessaire de calibrer le modèle sur une période de temps suffisamment longue (50 ans) avec des données climatiques d'entrée à haute résolution, mais également de valider le modèle sur une période indépendante, afin d'éviter autant que possible de potentiels problèmes de surcalibration (*overfitting*).

Dans un second temps, le protocole de calibration a été appliqué et amélioré en utilisant le réseau global de séries de largeurs de cernes de la base de données PAGES2k sur le 20ème siècle. La performance de MAIDEN a également été comparée à celle de VS-Lite, un modèle semi-mécaniste de croissance des arbres qui a déjà été appliqué à large échelle en raison de sa simplicité de calibration. Nous avons pu confirmer que le modèle MAIDEN peut être appliqué à large échelle avec une performance comparable au modèle VS-Lite et avec d'importants avantages associés à sa complexité. Par exemple, la performance de MAIDEN ne dépend pas de la présence d'un signal climatique fort au sein de la série de croissance, contrairement à VS-Lite, ce qui limite l'application de ce dernier pour de nombreux endroits où la relation entre le climat et la croissance des arbres est complexe. Par ailleurs, en moyenne, le modèle MAIDEN tend à mieux simuler la dépendance de la croissance au climat que le modèle VS-Lite, qui a tendance à la surestimer dans les séries simulées. Cependant, l'application de MAIDEN est restreinte par le manque d'informations fournies au modèle pour son initialisation et sa calibration (larges *priors* des paramètres, absence de données journalières de la productivité primaire brute pour calibrer les paramètres liés au module de la photosynthèse dans le modèle, par exemple).

Finalement, sur base de ces développements, le modèle MAIDEN a pu être inclus avec succès au sein d'une procédure d'assimilation de données. La procédure a ensuite été testée aux moyennes et hautes latitudes de l'hémisphère Sud afin de reconstruire différents champs atmosphériques (température de surface, précipitation, vents) sur les quatre derniers siècles. Les reconstructions résultantes ont été évaluées par rapport aux observations sur la période instrumentale

et leur performance comparée à des reconstructions obtenues sur base d'une procédure d'assimilation de données incluant une régression linéaire pour faire le lien entre le climat et la croissance des arbres. Les reconstructions obtenues avec MAIDEN sont au moins aussi bonnes qu'avec un modèle de régression, ce qui est encourageant et offre de belles perspectives. En particulier, étant donné les améliorations qui peuvent toujours être faites dans le modèle MAIDEN lui-même et son protocole de calibration, contrairement au modèle de régression pour lequel les perspectives sont limitées, le modèle MAIDEN pourrait, dans le futur, devenir un outil important permettant de dépasser les limitations des modèles statistiques et ainsi améliorer les reconstructions climatiques avec l'assimilation de données.

Contents

Contents ix

List of abbreviations xi

1 Introduction 1
- 1.1 Studying climates of the past . . . 1
- 1.2 Proxies of climate . . . 3
- 1.3 Tree-ring proxy development in paleoclimatology . . . 8
- 1.4 Reconstructing climate from tree rings: the statistical approach . . . 15
- 1.5 Tree-growth process models for reconstructing climate . . . 24
- 1.6 Objectives and outlines of the thesis . . . 27

2 Application and evaluation of the process-based model MAIDEN 31
- 2.1 Introduction . . . 32
- 2.2 Material and methods . . . 34
- 2.3 Results and discussion . . . 43
- 2.4 Conclusions . . . 52

3 Testing the performance of dendroclimatic models at global scale 57
- 3.1 Introduction . . . 58
- 3.2 Material and methods . . . 61
- 3.3 Results . . . 65
- 3.4 Discussion and conclusions . . . 77

4 Using a mechanistic dendroclimatic PSM in a data assimilation framework 81
- 4.1 Introduction . . . 81
- 4.2 Data assimilation . . . 84
- 4.3 Experiment design and diagnostics . . . 92

4.4 Results and discussion 94
4.5 Conclusion 110

5 Conclusions and perspectives 113
5.1 How to calibrate MAIDEN in an automatised way with limited information? 114
5.2 To which extent is MAIDEN adapted for application at global scale? 115
5.3 What is the added value of MAIDEN for reconstructing climate? . . 116
5.4 General conclusions 117
5.5 Perspectives 118

A Supplement to Chapter 1 123
A.1 Dendroclimatic models 123

B Supplement to Chapter 2 133
B.1 Supplementary tables 133
B.2 Supplementary figures 136

C Supplement to Chapter 3 141
C.1 Supplementary tables 141
C.2 Supplementary figures 149

D Supplement to Chapter 4 159
D.1 Data assimilation and particle filtering in paleoclimatology 159
D.2 Supplementary tables 162
D.3 Supplementary figures 164

E List of publications related to the thesis 173

References 175

List of abbreviations

BHM	Bayesian Hierarchical Model
CESM	Community Earth System Model
CFR	Climate field reconstruction
CE	Common Era
DA	Data assimilation
ENSO	El Niño-Southern Oscillation
ESM	Earth System Model
GCM	General Circulation Model
GPP	Gross Primary Production
IPCC	Intergovernmental Panel on Climate Change
LAI	Leaf Area Index
MAIDEN	Modelling and Analysis In DENdroecology
MDF	Model-data fusion
MXD	Maximum latewood density
NDVI	Normalized Difference Vegetation Index
NH	Northern Hemisphere
NPP	Net Primary Production
PAGES2k	Past Global Changes of the last two millennia
PSM	Proxy system model
RCS	Regional curve standardization
SAM	Southern Annular Mode
SH	Southern Hemisphere
TRW	Tree-ring width
VS	Vaganov-Shashkin

1 Introduction

1.1 Studying climates of the past

The rapid and global change occurring since the beginning of the industrial era, and in particular the rapid increase of global temperature [IPCC, 2019], has motivated the study of past climate variability in order to place the recent changes into a longer-term context. The Earth's climate has always changed on all timescales, both globally and regionally [Huybers and Curry, 2006; Goosse, 2015]. The climate variability is governed by external forcing and by the internal dynamics of the climate system. The main natural forcings that represent the orbital variations, solar and volcanic activities have shaped the Earth's climate for millions of years [Goosse, 2015]. For instance, long ice archives show glacial-interglacial alternations with strong variations in the ice volume covering the continents and in the subsequent sea level over the last 800ka. These alternations are driven by the orbital forcing which leads the distribution of the insolation on Earth at the scale of the Quaternary geological period, which started around 2.5 million years ago [Berger, 1978; Imbrie et al., 1984; Jones and Mann, 2004].

On shorter timescales, before the increase of anthropogenic influence, the climate variations of the past millennium have partly resulted from the interplay of the solar irradiance forcing along with the volcanic eruptions [Jones et al., 2001; Jones and Mann, 2004; Hegerl et al., 2003; Crowley et al., 2008]. The internal dynamics of the global climate system also contributes to the variations of the climate over the last thousand years [Jones et al., 2001; Goosse et al., 2006, 2012; Camenisch et al., 2016]. Among the most important modes of internal climate variability, the Southern Annular Mode (SAM), the El Niño-Southern Oscillation (ENSO) and the North Atlantic Oscillation play a large role on interannual to decadal timescales.

Most recently, the anthropogenic forcing has started to have a dominant influence on the variability of the climate system, through the increasing emission of greenhouse gases, land use changes or, over the past century, the sulphate aerosol loading [Keeling et al., 1976; Mann et al., 1998; Jones and Mann, 2004; Myhre et al., 2013].

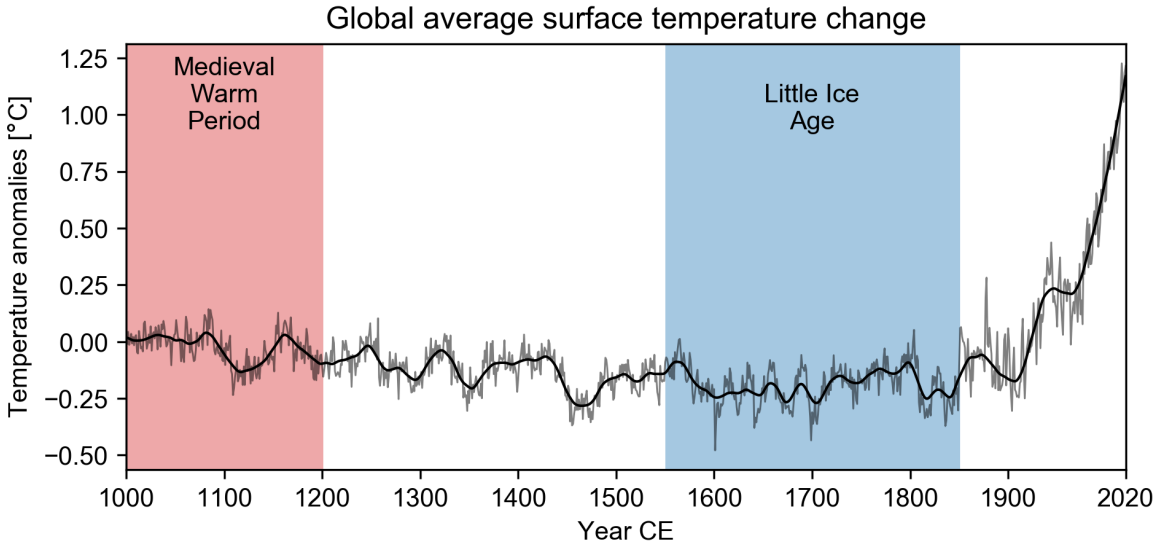


Figure 1.1: *Global near-surface air temperature anomalies (relative to 1901-2000 CE) over the past millennium. The reconstruction of near-surface air temperature from Neukom et al. [2019] has been used over the 1000-1849 CE time period. It is based on paleoclimate proxy records, mostly tree-ring width. The HadCRUT version 5 dataset [Osborn et al., 2021] incorporates all the available near-surface air temperature observations over 1850-2020 CE. The annual mean of near-surface air temperature is represented by the thin gray line. A lowess filter has been applied to the annual time series to produce a 30-year smoothed near-surface air temperature time series, represented with a thick black line. The approximate time coverage of the Medieval Warm Period and of the Little Ice Age during the last millennium is represented in red and blue, respectively.*

The climate variations of the last millennium have been increasingly studied over the past decades, in particular the past variations of surface temperature [Mann et al., 1998, 1999; Goosse et al., 2006; Mann et al., 2008, 2009; Neukom et al., 2011, 2014; Wilson et al., 2016; Anchukaitis et al., 2017; Tardif et al., 2019]. All the large-scale climate reconstructions characterize the past 1000 years with two significant climate periods, in addition to the recent industrial period (Fig. D.1). First, the so-called Medieval Warm Period, spanning around 900–1200 CE, displays relatively warmer conditions in comparison with the following five centuries, particularly on the Northern Hemisphere continents [Hughes and Diaz, 1994]. Following this warm period, the cooler Little Ice Age spans approximately the 1550–1850 CE time period and is characterized by frequent volcanic eruptions [Bradley

and Jonest, 1993]. However, except for the recent rapid and global warming of the 20th century, large uncertainties still remain on the timing and the amplitude of the temperature changes, as well as their spatial extent and the underlying causes of the changes [e.g. Goosse et al., 2005; Guiot and Corona, 2010; Neukom et al., 2019].

Reconstructing the Earth's past climate is fundamental to understand and characterize the internal and forced variability of the climate system and disentangle the anthropogenic impact on climate from the natural climate variability, and finally to anticipate the future of Earth's climate. However, prior to the instrumental period, very few instrumental observations of climate variations are available, and the spatial and temporal distribution of such records decrease drastically as we go back in time [Harris et al., 2020; Jones and Mann, 2004]. Indirect records of climate from natural archives, also known as proxies (Section 1.2), can be used to characterize the past variability of the climate system over longer timescales, at regional, hemispheric and global scales [e.g. Mann et al., 1999; Cook et al., 2010; PAGES 2k Consortium, 2013; Neukom et al., 2014; PAGES 2k Consortium, 2017; Neukom et al., 2019]. In this regard, the last millennium offers an ideal framework as this period has the richest network of proxy records [Jones et al., 2009; PAGES 2k Consortium, 2017].

Different high-resolution (annual) proxies exist to characterize the past climate variability (Sect. 1.2), among which tree-ring proxies are the most commonly used thanks to their large-scale availability (Sect. 1.3). In order to decipher the climate signal from tree-ring series, statistical models linking climate and tree growth are traditionally used (Sect. 1.4). However, this approach may have serious shortcomings related to their assumptions of linearity and stationarity of the tree-growth-to-climate relationship. Tree-growth process-based models incorporate most of the important biological processes of tree growth, and are a solution to overcome these limitations (Sect. 1.5).

1.2 Proxies of climate

A *proxy* of climate is generally defined as the observations that have been recorded into a *natural archive* through physical, chemical or biological properties, as a response of a *sensor* to climate [Evans et al., 2013]. For example, a tree (the sensor) can respond to its surrounding environment in its annual rings (the archive) with varying ring width (the proxy). The tree-ring width of a year is therefore considered as an indirect observation of the climate conditions that the tree experienced during this specific year. Various natural archives exist that indirectly record different aspects of climate variability over different timescales and with different temporal resolution. Some archives cannot register a high-resolution climate signal. This is for instance the case for nonvarved sediment cores, low accumulation

ice cores, glacial moraine evidence, terrestrial and ice boreholes and preserved pollen, used to characterize at best the centennial climate variability. On the other hand, high-resolution climate proxies can describe the past climate variations at an annual to seasonal resolution over centuries, and up to millennia for some of them [Jones and Mann, 2004]. We briefly present here below the main archives providing high-resolution proxies for paleoclimatology: coral, ice cores, varved sediments, speleothems and tree rings (Table 1.1).

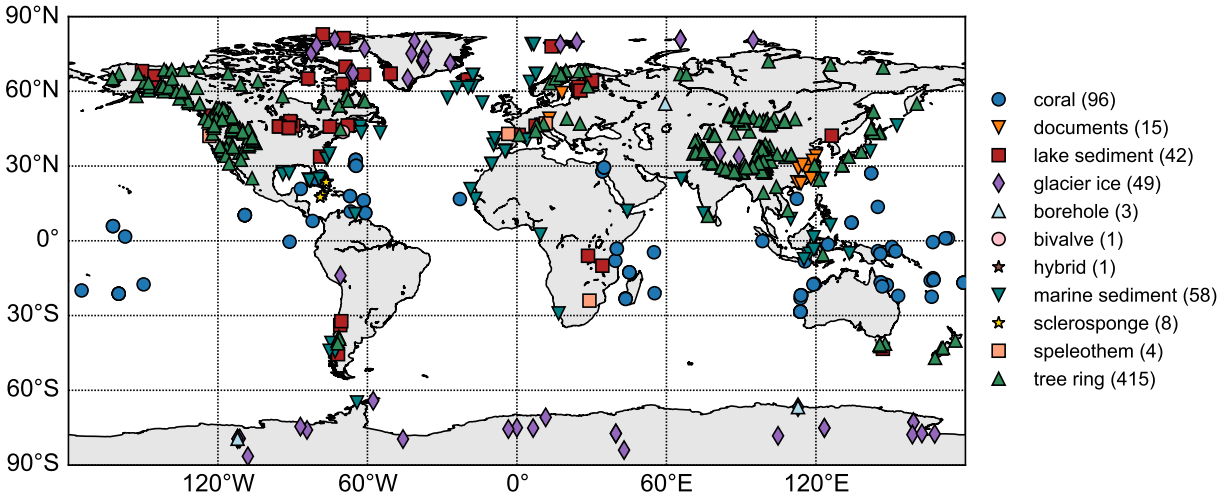


Figure 1.2: *Location of the 692 proxy records of the PAGES2k database [PAGES 2k Consortium, 2017] by archive type. The hybrid type is a tree ring/borehole record. Background map from Hunter [2007].*

The aragonite structure of which coral is made has several geochemical (e.g., the ratio of stable isotopes oxygen δ^{18}O or the ratio of strontium to calcium chemical elements Sr/Ca) or coral growth characteristics (e.g., the coral calcification rate) that provide proxy climate information in tropical and subtropical oceans (see Fig. 1.2 for the spatial distribution of coral proxy records in the PAGES2k database; PAGES 2k Consortium, 2017; more details on the PAGES2k database below) with an annual to seasonal resolution [Dunbar and Cole, 1999; Lough, 2010; Jones and Mann, 2004; Jones et al., 2009]. The records have been primarily used to describe the ENSO variability, sea-surface temperature and sea water salinity variations in the tropics over several decades [e.g. Evans et al., 2002; Wilson et al., 2006; Ault et al., 2009; Hereid et al., 2013; Tierney et al., 2015; Zinke et al., 2016; Jimenez et al., 2018]. However, coral proxy records rarely span several centuries (see Fig. 1.3 for the temporal availability of coral proxy records in the PAGES2k database). Ideally, the records should be replicated to increase the confidence in the resulting chronology, for example by reducing the uncertainties related to the dating of each individual core, or by enabling the emergence of a common climate signal among the cores. Yet, this is almost never the case for coral and most high-resolution

proxies, except tree-ring proxies, often due to the cost of sample recovery or the analytical cost of replication [Hughes et al., 2011].

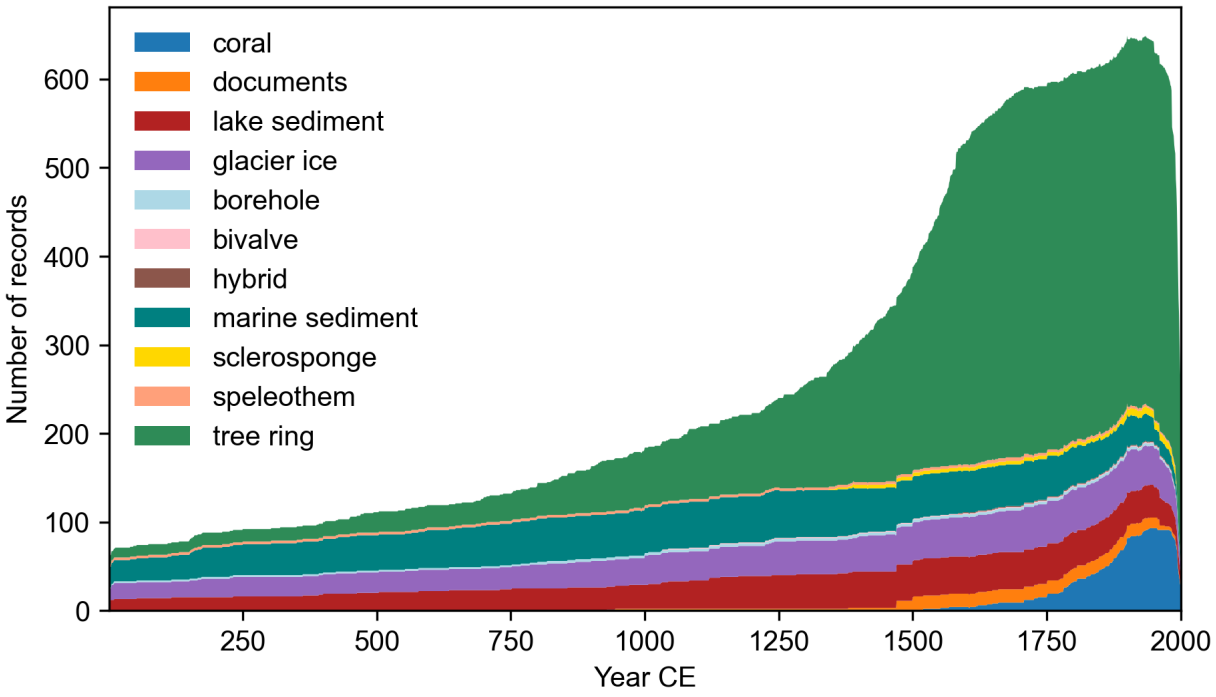


Figure 1.3: *Temporal availability of the 692 proxy records of the PAGES2k database [PAGES 2k Consortium, 2017] by archive type over the past two millennia. The hybrid type is a tree ring/borehole record.*

On the other hand, the continental ice core records provide climate information on ice sheets and glaciers (Fig. 1.2) up to several millennia, at a theoretical annual to subannual resolution (in practice rarely achievable due to the difficulty of dating) [Jones and Mann, 2004; Jones et al., 2009]. On the contrary to coral, they are less broadly available. Among the different proxies retrieved from ice cores, the ratio of stable isotopes oxygen δ^{18}O has been the most commonly used for decades, owing to its relationship with local air temperature and more generally the hydrological cycle [Craig, 1961; Dansgaard, 1964; Dansgaard et al., 1982; Jouzel et al., 1987; Petit et al., 1999; Fisher et al., 1996; Vinther et al., 2003]. However, the costs for collecting and extracting relevant climate information from ice cores are extremely high in terms of money and time.

Varved or annually laminated sediment cores can also provide climate information at an annual to subannual resolution. They are commonly found in lakes in the form of clastic, biogenic or endogenic (i.e., consisting of minerals formed by chemical precipitation) sediments, or a combination of these classes. Information on past climatic changes can potentially be retrieved from the variations in the structure, composition and thickness of the varves [Zolitschka et al., 2015]. The varve thickness, for example, can be related to seasonal precipitation or sum-

mer temperature as they control the volume of meltwater discharge as well as the sediment load in glacial lakes [e.g. Bird et al., 2009; Cook et al., 2009]. In marine environments, some rare varved sediments can also provide information on past climates for example from the oxygen isotopes or microfossil assemblages [e.g. Black et al., 1999; Barron et al., 2015]. However, the use of varved sediments for high-resolution paleoclimate reconstruction requires a good knowledge of the regional climatology and sedimentation processes in order to establish a reliable chronology of the varve and a reliable relationship between climate and varve characteristics [Weinheimer and Biondi, 2003; Jones et al., 2009].

Speleothems are high-resolution proxy indicators that result from the precipitation of calcium carbonate from ground water in calcareous caves, for example in the form of stalagmites. Many proxies can be retrieved from speleothems, such as growth rates, isotopic composition from oxygen or carbon isotopes, trace elements or luminescent laminae [Lauritzen and Lundberg, 1999; Wong and Breecker, 2015; White, 2019; Jones et al., 2009]. They can be related to the environmental changes on the land surface above the cave, in particular the local and regional hydroclimate over centuries to millennia [e.g. Fleitmann et al., 2007; Mangini et al., 2005; Partin et al., 2007; Baker et al., 2015]. However, despite clear advantages of speleothems (e.g., fast growth rates and widespread existing records), dating uncertainties can still be large, especially in the absence of replication, which is often the case. The relationship between simple climate parameters, such as temperature, can also be difficult to elaborate due to the influence of multiple external factors. This complicates their use for paleoclimate reconstruction so that they have been underexploited in the field until recently [Wong and Breecker, 2015; Jones et al., 2009]. The use of speleothems in paleoclimatology has started to extend with the development of proxy databases incorporating numerous speleothem records, for instance through the SISAL (Speleothem Isotopes Synthesis and AnaLysis) working group [Atsawawaranunt et al., 2018; Comas-Bru et al., 2020], or the Iso2k initiative focusing on the study of Common Era hydroclimate with water isotopes [Konecky et al., 2020].

Finally, tree rings are the most commonly used archive for regional and large-scale climate reconstructions at high temporal resolution (annual to subannual) over centuries to millennia [Fritts, 1976; Mann et al., 1998; Cook et al., 1999, 2002; Mann et al., 2008; Büntgen et al., 2011, 2013; Luterbacher et al., 2016; Wilson et al., 2016; Anchukaitis et al., 2017; Esper et al., 2018; Büntgen et al., 2020]. Their associated proxies are indeed the most widely and extensively available, particularly in the extratropical latitudes of the Northern Hemisphere (Fig. 1.2), and over the last millennium (Fig. 1.3. They are precisely dated and easily replicated (both in space and in time). The spatial distribution of tree-ring proxies are, in this regard, complementary to ice core (alpine and polar regions) and coral (tropical and subtropical maritime regions) proxy records. The International

Tree-Ring Data Bank (ITRDB; https://www.ncdc.noaa.gov/data-access/paleoclimatology-data/datasets/tree-ring) assembles more than 4000 sites with publicly available tree-ring data from all around the world. The ITRDB was established at the First International Workshop on Dendroclimatology (April 1974), organized by Harold C. Fritts. It is clear from the distribution of the tree-ring network of the ITRDB (Fig. 1.4) that still few tree-ring records are located in the Southern Hemisphere, partly because dendrochronological research began later in the Southern Hemisphere compared to the Northern Hemisphere. The continental area of the Southern Hemisphere and the associated forests are also less widespread. In the tropical regions, dendrochronology still raises numerous challenges so that few records are available there [Stahle, 1999].

The tree-ring width (TRW) and, to a lesser extent, the maximum latewood density (MXD) are the most frequently used proxies from tree rings, in particular for reconstructing past seasonal temperature [e.g. Esper et al., 2002; Büntgen et al., 2013; Luterbacher et al., 2016; Anchukaitis et al., 2017] and hydroclimate (in particular, drought events) [e.g. Cook et al., 2007; Touchan et al., 2011b; Cook et al., 2015; Hessl et al., 2018]. Compared with other high-resolution proxies, tree-ring proxies relationship with climate is far better understood and characterized, thanks to the long history of ecophysiological studies of tree growth [Fritts, 1976; Schweingruber, 1996; Vaganov et al., 2006]. The characteristics of the tree-ring archive will be addressed in more detail in Sect. 1.3.

Over the past decade, efforts have been made to improve reconstructions of the past millennium climate variability with the development of multi-proxy databases through different projects and consortia [PAGES 2k Consortium, 2013; Wilson et al., 2016; Anchukaitis et al., 2017; PAGES 2k Consortium, 2017; Tardif et al., 2019; Konecky et al., 2020]. For example, the international consortium of PAGES2k (Past Global Changes of the last two millennia) has collected 692 temperature-sensitive records from various archives (tree rings, coral, marine and lake sediments, glacier ice, speleothems, boreholes, ice cores, documentary evidence, sclerosponges and bivalves), but tree rings are by far the most represented (ring-width and density, 415 records) [PAGES 2k Consortium, 2017]. The temporal resolution of the records is mostly annual but can range from biweekly to centennial. The spatial coverage of the proxies is global, but most records are located in the Northern Hemisphere (Fig. 1.2). All proxy records have been screened to meet different criteria. In particular, the record must be temperature sensitive. Only records for which the original study describes a relationship between temperature and the proxy or for which the correlation between local instrumental temperature and the proxy is significant at the 95% confidence level were included in the database. Other criteria include the chronological accuracy, a minimum record duration (which can vary depending on the proxy), a minimum record resolution (which can also vary depending on the proxy), and, finally, the public availability of the record

Table 1.1: *Characteristics of the main high-resolution archives for paleoclimatology. The information in this table are indicative and cannot be considered as an exhaustive listing of all the studies in the associated scientific field. SST stands for sea surface temperature; SSS for sea surface salinity; T for temperature; D for drip rate; Hy for hydroclimate.*

Archive	Main proxies	Environment	Temporal coverage	Abundance	Main reconstructed variables
Coral	δ^{18}O, Sr/Ca, coral calcification rate	tropical and subtropical oceans	decades to centuries	middle	SST, SSS
Ice core	isotopes (δ^{2}H, δ^{18}O)	ice sheets and glaciers	millennia	middle	T, atmospheric composition
Varve	varve thickness, chemical composition, micropaleontological assemblage	mostly glacial lakes	millennia	low	T, Hy
Speleothem	growth rates, isotopic composition, trace elements	calcareous caves	millennia	low	Hy, D
Tree ring	tree-ring width, density, isotopes (δ^{18}O, δ^{13}C)	mostly extratropical continents	millennia	high	T, Hy

[PAGES 2k Consortium, 2017]. All these objective criteria, along with its accessibility and ease of use, make the PAGES2k database an appealing candidate for paleoclimate exercises.

1.3 Tree-ring proxy development in paleoclimatology

In the previous section, we briefly summarized the different high-resolution archives in paleoclimatology. Here, we focus on tree rings, which are of specific interest in this thesis. Tree-ring proxies are the most appropriate indirect climate observations for large-scale paleoclimate exercises focusing on the continental climate interannual variability over the past millennium, as is the case in this thesis. More generally, dendroclimatology can be defined as the science that allows for the inference of past climates from tree rings [Fritts, 1976; Sheppard, 2010; Hughes et al., 2011]. In this section, we first briefly review the process of formation of tree rings (Sect. 1.3.1). We then describe how, in dendroclimatology, we move from

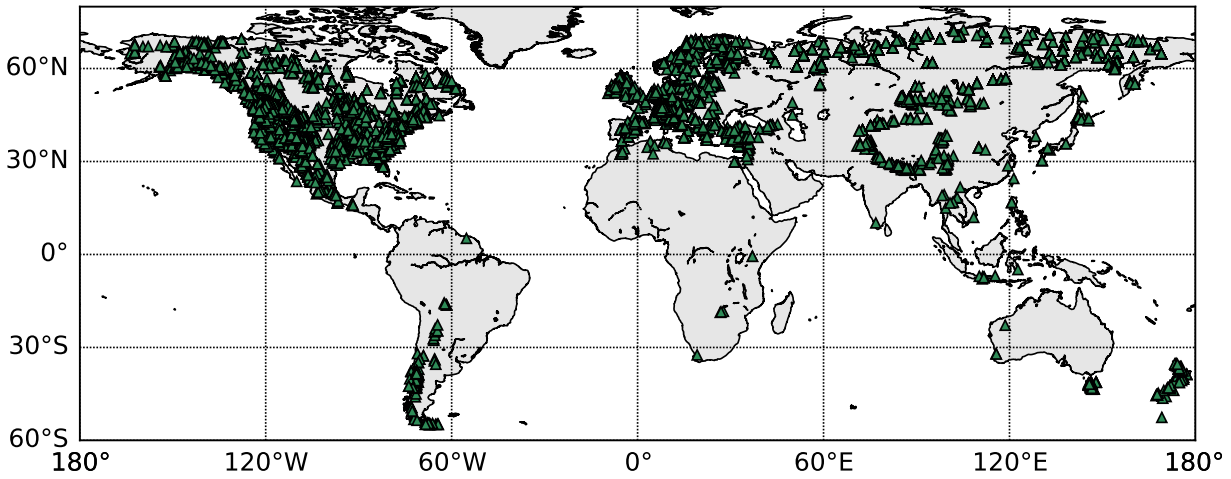


Figure 1.4: *Location of the tree-ring records publicly available in the International Tree-Ring Data Bank. Coordinates extracted from Zhao et al. [2019]. Background map from Hunter [2007].*

a simple core in a tree to a tree-ring growth time series, with a special focus on tree-ring width (Sect. 1.3.2).

1.3.1 How tree rings form

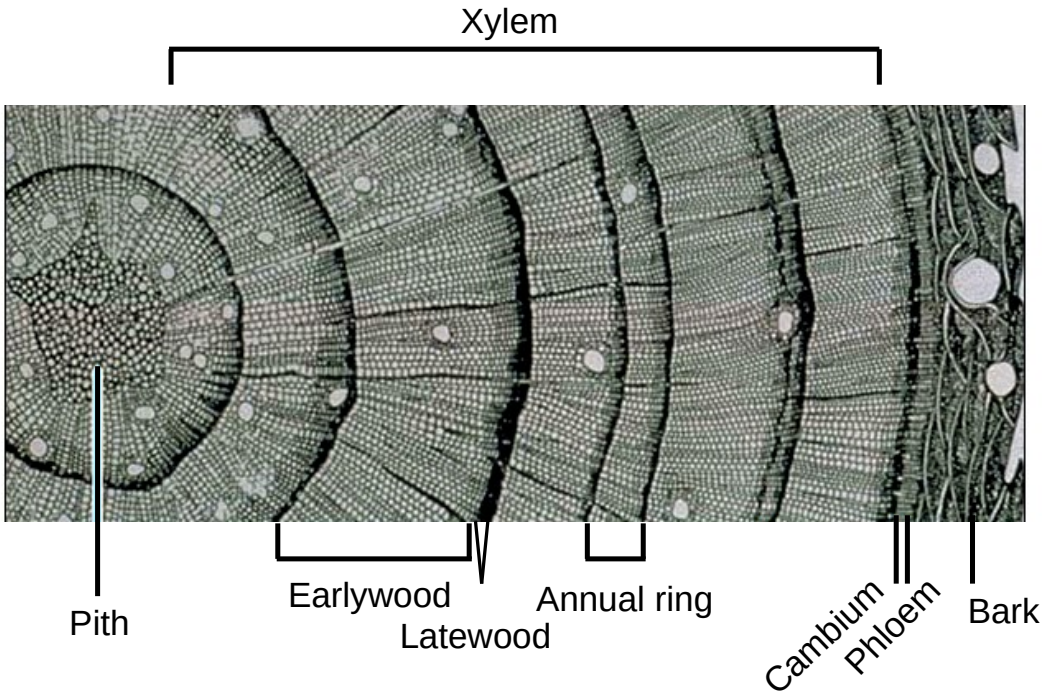


Figure 1.5: *Diagram of rings in a young conifer from Fritts [1976]. Adapted from National Oceanic and Atmospheric Administration (NOAA) Paleoclimatology Program (Photo Credits).*

Trees undergo two types of growth: the primary growth responsible for the lengthening of the tree, and the secondary growth, responsible for the widening of the tree. In the stem, the vascular cambium is made up of a thin layer of meristamic cells (Fig. 1.5; meristamic cells are non-differentiated, totipotent, embryonic cells that divide rapidly and eventually differentiate) that envelops the stem. They are called the cambial initial cells. A cambial initial generates two types of mother cells: the xylem mother cells, generated inward toward the pith, and the phloem mother cells, generated outward toward the bark. The mother cells can in turn divide into new undifferentiated cells. These mother cells then give rise to secondary tissues: the secondary xylem (i.e, the wood, Fig. 1.5) and the secondary phloem (i.e, the living bark, Fig. 1.5). The xylem mother cells produce four to ten times more undifferentiated cells than the phloem mother cells so that the cambium and the secondary phloem are progressively pushed outward [Rathgeber et al., 2016; Delpierre et al., 2016; Hughes et al., 2011; Vaganov et al., 2006]. The activity of the cambium is subject to a seasonal periodicity, determined by regular environmental fluctuations [Denne and Dodd, 1981]. In the extratropical region, the cambial activity is set by the alternation of winter (dormant cambium) and spring and summer (active cambium) climatic conditions [Delpierre et al., 2016]. In the tropical region, the cambium may be dormant during the dry season and active during the wet season, as it is often the case for teak in south Asia [Breitsprecher and Bethel, 1990; Pumijumnong et al., 1995; D'Arrigo et al., 2006b; Schöngart et al., 2006; D'Arrigo et al., 2011; Zaw et al., 2020]. This seasonal activity of the cambium gives rise to annual rings (Fig. 1.5). However, for vast areas of equatorial and tropical forests, trees do not undergo any climatic stress, preventing the production of reliable annually resolved tree rings.

In particular, each spring in the extratropical region, the cambium reactivates with the fast division of mother cells, when the temperature and day length increase [Rossi et al., 2007, 2008; Prislan et al., 2013; Huang et al., 2020; Rathgeber et al., 2016]. The new produced cells appear as radial files. In the early growing season in spring, trees produce wood (earlywood; Fig. 1.5) with larger cells and thinner cell walls than later in the growing season, in summer (latewood; Fig. 1.5). The contrast between those earlywood cells that efficiently transport water and nutrients from the roots to the canopy, and latewood cells, that provide an efficient mechanical support, creates this typical tree-ring structure (Fig. 1.5) [Rathgeber et al., 2016; Vaganov et al., 2006; Hughes et al., 2011]. The transition between early and latewood generally happens around the summer solstice, i.e., when the photoperiod is at its highest [Rossi et al., 2006]. The cambial activity stops when the water or temperature conditions become unfavorable, i.e, in autumn or even earlier [Delpierre et al., 2016; Rossi et al., 2008; Gruber et al., 2010].

1.3.2 From the sample to the series

To optimize the climatic signal, the most suitable regions for sampling trees are at the limit of their climatic distribution because they are more likely to strongly respond to the climate variability of the limiting climatic factors. However, reliable climate signal may be extracted from trees that have grown under more favorable conditions [Cook and Kairiukstis, 1990]. In the case of a study on hydroclimate variability, for example, the most appropriate site would be in a dry region where tree growth is likely limited by precipitation. If interested in reconstructing temperature variability, the selected site should not present any water shortage, and rather be located in cold regions (high latitude or altitude sites) where temperature would likely be the limiting factor of tree growth. Once a site has been selected, the replication of samples within the site ensures a better common climatic signal and the smoothing of the other non-climatic sources of tree-growth variability in the mean chronology. The number of sampled trees depends on the aim of the study. At least 20 to 30 trees are generally needed to build the mean chronology, but this can be less if there is a strong common climatic signal among trees, and vice versa [Cook and Kairiukstis, 1990; Hughes et al., 2011].

More generally, the choice for sampling a tree is based on the absence of disturbance evidence related to non-climatic factors and on a sufficient age of the trees (depending on the type of study). Different strategies of stand and trees selection are applied to minimize the non-climatic noise (competition, fires, wind impacts, human impacts). For instance, to minimize the influence of forest management and to get sufficiently long chronologies, old-growth forests are preferred. However, fires and human influence may be difficult to avoid, especially in Western and Mediterranean Europe. At the scale of the tree, to reduce the individual variability of growth, two cores are usually sampled at breast height, away from a wound or reaction wood [Fritts, 1976; Cook and Kairiukstis, 1990; Sheppard, 2010].

Some trees, and more generally some tree species, may not be adapted for dendrochronology because they do not display annual rings or a sufficient ring-to-ring variability for crossdating (i.e., matching patterns of wide and narrow rings across trees in order to date the tree-ring series; Douglass, 1941), for example. As stated before (Sect. 1.3.1), many trees in the tropics do not produce annual rings or rings that can be crossdated [Stahle, 1999]. In Asia, Americas and Europe, tree-ring studies have been primarily performed with species of pine (*Pinus* sp.), spruce (*Picea*), oak (*Quercus* sp.) and Douglas Fir (*Pseudotsuga* sp.) [Zhao et al., 2019; Pearl et al., 2020], for which reliable relationships between annual growth and environmental factors have been demonstrated. In the Southern Hemisphere, species from *Nothofagus* have shown to be valuable [Cook and Kairiukstis, 1990; Zhao et al., 2019].

Once the samples have been collected, generally using an increment borer, they will be prepared for the rings to be readable, then dated and crossdated [Douglass, 1941]. Subfossil trees (most found in rivers, lakes, marine deposits or in peat bogs and permafrost soils), historical or archaeological timbers (most found in human settlements and burial places) can be used to extend the tree-ring chronology from living trees with crossdating [Cook and Kairiukstis, 1990; Gennaretti et al., 2014b; Rydval et al., 2017].

Different parameters can then be measured from individual tree-ring cores, depending on the climate signal of interest. The most commonly used and easily measured property of tree rings is structural, i.e, the total ring width (TRW). TRW is known to reflect the climate variability of the most limiting factor of tree growth, for example precipitation in moisture-limited sites of the Mediterranean region [e.g. Touchan et al., 2017]. Alternatively, early or latewood width may help to capture seasonal climate variability [Griffin et al., 2013]. Maximum latewood density (MXD; the density of wood cell during the late growing season; Schweingruber et al., 1978) exhibits a strong signal of summer temperatures and has shown to be more skillful than TRW to reconstruct temperatures [Briffa and Jones, 1992; Büntgen et al., 2010; Yuan et al., 2013; Esper et al., 2015; Wilson et al., 2016; Anchukaitis et al., 2017]. On the contrary, TRW may better reflect low-frequency variability, while MXD may display more interannual variability [Büntgen et al., 2010; D'Arrigo et al., 2014]. Nevertheless, MXD chronology development is still associated with high costs in terms of time and money compared to TRW. Most recently, blue intensity (or blue reflectance; McCarroll et al., 2002) has emerged as a new proxy of tree rings to reconstruct past summer temperature variability [McCarroll et al., 2002; Dolgova, 2016; Heeter et al., 2019] with a similar skill but lesser cost than MXD [McCarroll et al., 2002; Rydval et al., 2014; Björklund et al., 2014; Kaczka et al., 2018]. In particular, blue intensity measures the amount of blue light reflected by tree rings associated with the lignin (one of the key components of wood, in particular in cell walls) content of cell walls, which is particularly dependent on summer and late summer temperatures [Björklund et al., 2014; Tsvetanov et al., 2020]. Tree-ring parameters can also be retrieved from wood composition. Stable isotopes of carbon and oxygen have been increasingly used to reconstruct past climate variability in temperate regions [Saurer et al., 1995; Hemming et al., 1998; McCarroll and Loader, 2004; Cernusak and English, 2015; Lavergne et al., 2017], for example air temperature [Liu et al., 2014; Naulier et al., 2015], precipitation [Masson-Delmotte et al., 2005; Rinne et al., 2013] and drought [Kress et al., 2010; Masson-Delmotte et al., 2005; Labuhn et al., 2016], among others.

Once the crossdating and measurement of the tree-ring variable of interest have been achieved and verified [Holmes, 1983; Grissino-Mayer, 2001], each individual tree-ring series are standardized [Fritts, 1976], in order to remove as much as possible any low frequency (red) noise that may be related to non-climatic fac-

tors and to isolate the target common climatic signal. In this regard, tree-ring series may be seen as the combination of several signals, among which the climatic signal is of interest for dendroclimatic studies, and the others are considered as noise. The other objective of standardization is to transform the individual series into indexes to account for the differences related to the age of the trees or to the overall rate of growth, in order to produce a stationary mean chronology [Fritts, 1976; Cook and Kairiukstis, 1990]. In particular, there is a typical negative exponential decline of ring width (from the pith to the bark), related to the geometrical constraint of adding a certain amount of biomass to an increasing stem radius. In practice, this exponential decay can be deeply altered by competition and disturbances, particularly in closed-canopy forests. First, tree-growth variability may be influenced by local (endogenous) disturbances that are related to gap-phase stand development, i.e. when individual trees are removed from the canopy, creating an opening in the canopy of the forest and affecting the trees close to the removed trees. Other disturbances may affect the stand as a whole (exogenous disturbances), for example fire, insects, logging, disease or extreme weather events (such as high winds or severe frosts). On the contrary to local disturbances, the pattern of ring width associated with these kinds of disturbances is common to all trees in the stand [Cook and Kairiukstis, 1990; Sheppard, 2010].

A variety of standardization methods exists to estimate the growth trend resulting from non-climatic factors [Cook and Kairiukstis, 1990; Fritts, 1976]. We will here focus on the case of TRW standardization techniques. The empirical curve fitting method has been primarily used to describe the growth trend by fitting a smooth curve to each individual ring-width series (Fig. 1.6). The growth trend can be estimated with deterministic unimodal models such as a simple linear trend model or a modified negative exponential curve [Fritts et al., 1969], among others [Cook and Kairiukstis, 1990], or with polynomial models [Jonsson and Matern, 1974; Fritts, 1976]. In order to estimate the growth trend with more flexible curves, stochastic methods of standardization have been investigated, such as the cubic smoothing spline [Cook and Peters, 1981]. The standardization is most commonly achieved by dividing each tree-ring width by its expected value as given by the estimated growth trend, so that the tree-ring indices have a mean of one and a stabilized variance [Cook and Kairiukstis, 1990; Helama et al., 2004].

However, such standardization techniques may remove some low-frequency signal related to climate variability. Cook et al. [1995] highlighted that building a millennia-long chronology from several short series hampers the study of the long-term climate variability over timescales longer than the typical segment length of the single series. The regional curve standardization (RCS) was primarily applied in dendroclimatology by Becker [1989] in order to mitigate those effects. On the contrary to fitted curves, the method aligns the series relative to their cambial age (and not the calendar date) and empirically derives a single mathematical smooth-

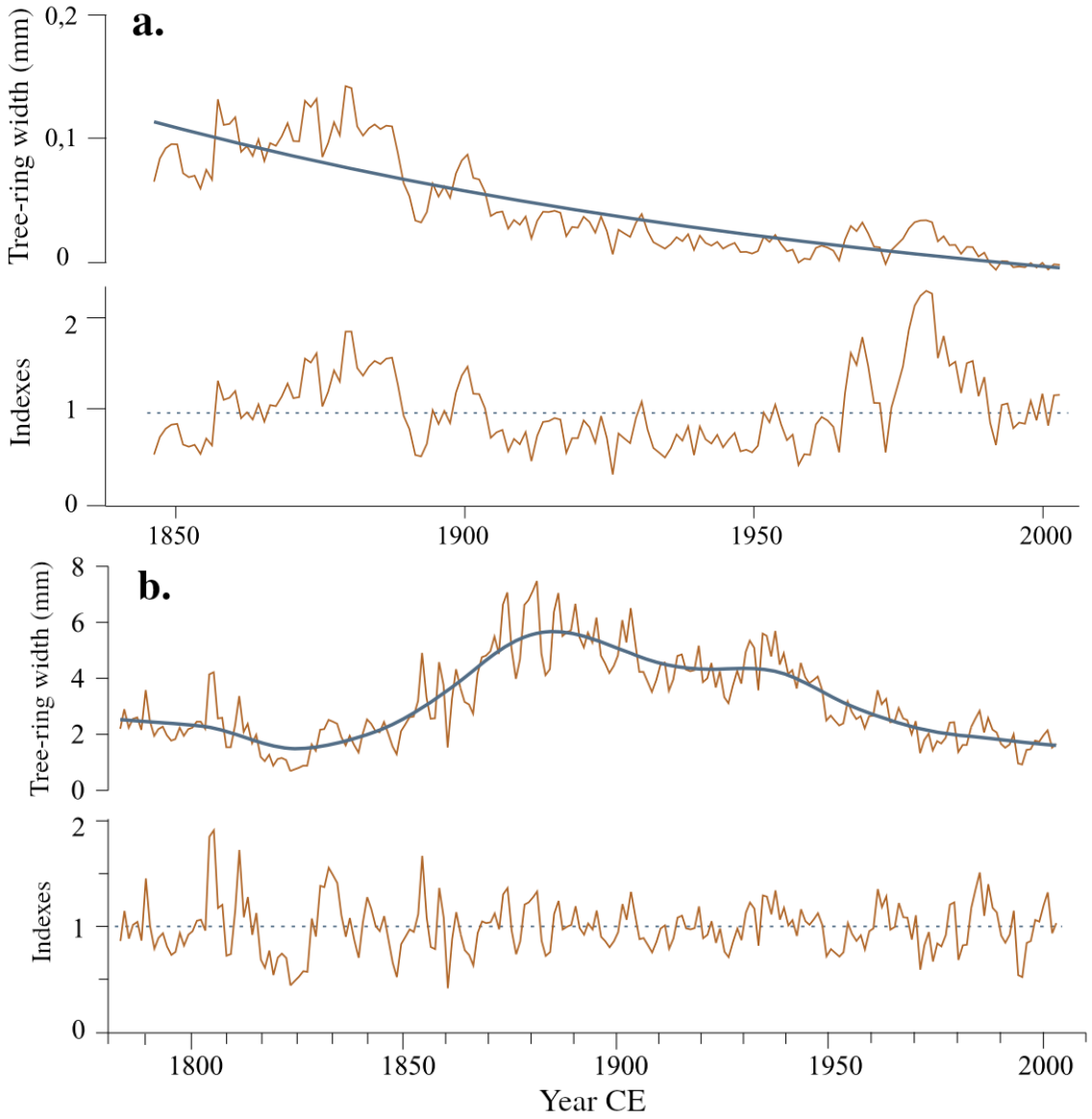


Figure 1.6: *Examples of empirical curve fitting methods. (a) Modified negative exponential curve. (b) Cubic smoothing spline. The tree-ring index series obtained by dividing each tree-ring width by its expected value as given by the estimated growth trend is also shown. Figures from Nicault et al. [2010a].*

ing function from the averaged tree-ring measurement values, for one species in a particular region [Briffa et al., 1992; Esper et al., 2003; Melvin et al., 2007]. Subsequently, each tree-ring width is generally divided by its expected value as estimated by the RCS curve with respect to the cambial age. This standardization technique requires a large number of tree-ring series covering all age classes, and tree-ring samples that hit or are close to the pith [Cook et al., 1995; Helama et al., 2017]. The idea behind the ordering of tree-ring series by cambial age is to obtain a RCS curve that does not include any signal related to climate variability when deriving the estimated growth trend from the means of ring width, because the climate variance is assumed to be distributed randomly between the series. In this context, any deviations from the estimated growth trend are the result of the climate forcing alone. In practice, the growth of each individual tree can also be influenced by differences in microclimate, competition or soil characteristics, for instance, that can result in a biased form of the RCS curve [Fritts, 1976; Hughes et al., 2011]. In either case (fitting curves or RCS standardization), the individual standardized series are generally merged into one mean chronology using the arithmetic mean of the detrended tree-ring indexes relative to the calendar year. Many standardization techniques have emerged from the initial RCS, for example the age band decomposition [Briffa et al., 2001] that allows for large spatial scale tree-ring datasets with various species to be standardized, or the adaptive regional growth curve method [Nicault et al., 2010b] that considers the differences of productivity within a site [Helama et al., 2017]. The chosen method of standardization can have important effects on the resulting mean chronology [Cook and Kairiukstis, 1990; Helama et al., 2004].

1.4 Reconstructing past climate variations from tree rings: the statistical approach

1.4.1 Transfer function approach

The relationship between the mean chronologies (Sect. 1.3.2) and different climate factors have primarily been investigated and estimated using various statistical methods, in the light of the available knowledge on how climate conditions affect tree-ring growth and wood structure [Fritts et al., 1971; Fritts, 1976; Cook and Kairiukstis, 1990; Vaganov et al., 2006]. In particular, significant correlations may be established over the period covered by meteorological observations between tree-ring variations and one or several climate factors known to influence tree growth. Monthly mean air temperature and total precipitation are the most used (from the current or previous year). In Fritts et al. [1971], a general scheme is elaborated to establish a statistical relationship (most of the time linear) between tree-ring series and climate variables. The climate variables are the predictors that

allow the tree-ring series – the predictand – to be estimated. These kinds of models are called response functions. They describe the response of tree-ring growth to climate and, consequently, determine the climatic information contained in each tree-ring width chronology, in terms of climate variables but also in terms of timing, i.e., which part of the year or season tree-ring growth responds to. The set of coefficients of the response function provides the magnitude and direction of the response of tree growth to climate over the calibration interval. They are used as a support for the inverse model, called transfer function, where the climate variables (predictands) are estimated from the tree-ring series (predictors). Transfer functions are used to directly reconstruct past climate variations from past variations of tree growth beyond the period covered by instrumental data by focusing on the climate variables best correlated with most of the tree-ring series used (Fig. 1.7). As required by statistical models, calibrated equations are verified on independent observations, i.e. those not used for the calibration. This implies to divide the available meteorological datasets into two (not necessarily equal) parts, the so-called calibration and verification periods [Fritts et al., 1971; Cook and Kairiukstis, 1990; Briffa, 1999].

While such transfer functions can be estimated at the scale of the sampling site using local climate data (as is typically the case for response functions), dendroclimatology offers the opportunity to work at larger spatial scale, thanks to the availability of tree-ring records over vast areas of the extratropical latitudes. Networks of chronologies can be built from multiple sites in a region to capture regional climate signal by minimizing the non-climatic noise of growth variations linked to site specificities, but can also cover the continental to hemispheric and even global scales [Hughes et al., 2011]. Those networks have provided numerous reconstructions of past variations of different climate variables aggregated over space, mostly surface temperature [e.g Mann et al., 1999; Briffa et al., 2001; Esper et al., 2002; D'Arrigo et al., 2006a; Mann et al., 2008; Büntgen et al., 2013; Stoffel et al., 2015; Wilson et al., 2016; Büntgen et al., 2020] and hydroclimate [e.g. Touchan et al., 2005a; D'Arrigo et al., 2006b; Esper et al., 2007; Davi et al., 2009; Büntgen et al., 2011; Cooper et al., 2013; Malevich et al., 2013; Yang et al., 2014]. While those reconstructions provide single time series of the target climate variable, tree-ring chronology networks can also be used to infer past variations of large-scale spatially gridded climate fields, a procedure also known as climate field reconstruction (CFR). There is a long history of CFRs in dendroclimatology [Fritts et al., 1971; Fritts, 1976, 1991], in particular for past temperatures over the last millennium and Common Era, at the global scale [e.g Mann et al., 1998, 2009; Rutherford et al., 2005], hemispheric scale [e.g. Anchukaitis et al., 2017] or regional to continental scale [e.g. Neukom et al., 2011; Cook et al., 2013; Linderholm et al., 2015]. A particular attention has also been given to past drought events at the regional scale [e.g. Nicault et al., 2008; Touchan et al., 2011a] and at the sub-

continental to continental scale with the development of drought atlases in North America [Cook et al., 2004], Asia [Cook et al., 2010], Europe and the Mediterranean basin [Cook et al., 2015], European Russia [Cook et al., 2020], Mexico [Stahle et al., 2016] and Eastern Australia and New Zealand [Palmer et al., 2015]. Other CFRs have focused on precipitation [Touchan et al., 2005b; Pauling et al., 2006; Neukom et al., 2010], sea level pressure [Fritts et al., 1971; Briffa et al., 1986] or sea surface temperature [Evans et al., 2001; Wilson et al., 2010], among others. CFRs from tree-ring proxy networks give the opportunity not only to characterize regional to global climate changes, but also to describe spatial patterns of atmospheric circulation, large-scale modes of internal climate variability, or external climate forcings [Evans et al., 2001; Kaufman, 2014]. Note that, although many reconstructions can also incorporate other proxies than tree-ring proxies, they are always the dominant proxy used in the reconstruction [e.g. Mann et al., 1998].

Most classically, CFRs are obtained on the basis of linear multivariate regressions of the climate fields of interest on proxy records calibrated over the instrumental period [Fritts et al., 1971; Mann et al., 1998; Cook et al., 2004; Rutherford et al., 2005; Mann et al., 2007; Cook et al., 2010; Wang et al., 2015]. This often implies the transformation of the instrumental data, the proxy data or both into a certain number of leading principal components on which the multivariate regressions are made [Jones et al., 2009; Mann et al., 1998; Cook et al., 1999, 2004; Neukom et al., 2010, 2011; Anchukaitis et al., 2017]. For example, in some approaches, the linear relationships may be considered between the dominant patterns of climate variability as represented by the leading principal components and all the proxy records [e.g. Mann et al., 1998]. The reconstructed principal component time series are then converted to a climate field. Other approaches may define the principal components of the tree-ring chronologies that are located within a certain distance of the grid point, and use them in separate multivariate regressions for each grid point to reconstruct the climate field of interest (point-by-point regression), for example drought [e.g. Cook et al., 1999, 2004, 2015]. Some studies have also been based on the use of pseudoproxies, i.e., synthetic proxy climate indicators, for evaluating CFR methods in a controlled environment [Mann and Rutherford, 2002; Von Storch et al., 2004; Mann et al., 2007; Riedwyl et al., 2009; Smerdon et al., 2010; Wang et al., 2014].

More recently, new techniques have emerged for reconstructing climate fields, i.e., Bayesian Hierarchical Models (BHMs) [e.g. Tingley and Huybers, 2013; Luterbacher et al., 2016; Werner et al., 2018; Zhang et al., 2018] and data assimilation (DA) [e.g. Goosse et al., 2010; Tardif et al., 2019]. On the contrary to the traditional transfer function approach, where the climate fields are expressed according to the proxies ("inverse mode"), such techniques give the opportunity to consider the relationship between climate and tree growth in the natural direction (i.e., the response of tree growth to climate), through the use of a forward proxy system

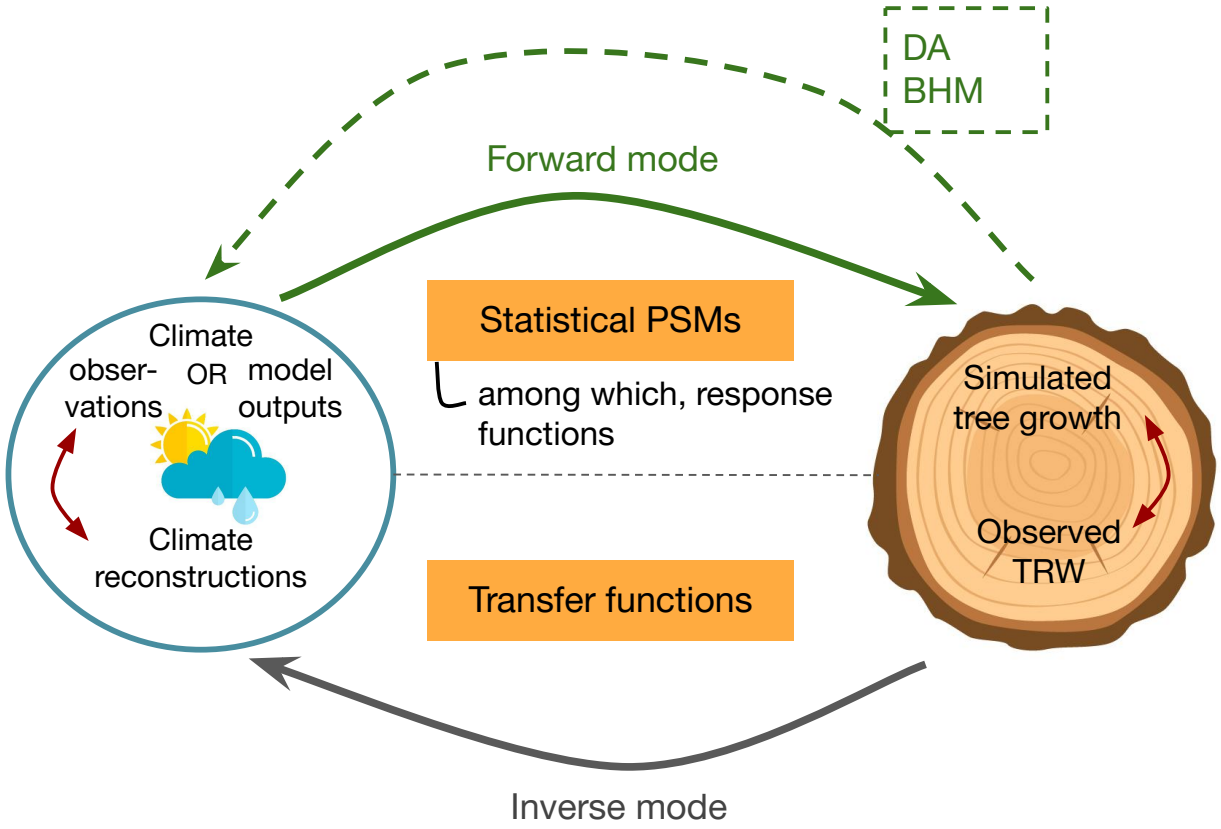


Figure 1.7: *Schematic representation of the different statistical approaches used to reconstruct climate variations from tree-ring proxies (e.g., tree-ring width). In the forward mode (green arrow), statistical proxy system models (PSMs) are driven by climate observations (response functions) or climate model results (data assimilation or DA, and Bayesian Hierarchical Models or BHMs) to simulate tree-ring growth series that can be compared with the observations of tree-ring width (TRW; red arrow). Based on the comparison of simulated and observed tree-ring growth, BHMs and DA provide reconstructions of past climate variations (green dashed arrow) that can be compared with climate observations over the instrumental era (red arrow). In the inverse mode (gray arrow), transfer functions, developed on the basis of response functions, provide reconstructions of climate variations from the past variations of observed TRW that can also be compared with climate observations (red arrow). Images: freepik.com*

model (PSM) (Fig. 1.7). In light of the definition given above for the proxy (Sect. 1.2), a proxy system model may be defined as a model that simulates the development of measured variables (the proxy data; e.g., tree-ring width) in an archive as a response of the sensor to climate variations, using a simplified representation of the processes (biological, chemical or physical) governing the relationship between climate and the proxy observations. In the forward mode, PSMs can be used to transfer climate observations (e.g., with response functions) or climate models results (e.g., with BHMs and DA) into a variable that can be directly compared with the actual proxy observations [Evans et al., 2013; Dee et al., 2016]. In this regard, response functions for tree-ring proxies may be seen as part of this larger group of models that have been formalized more recently. To date, both BHMs and DA have focused on the use of statistical forward PSMs, developed on the basis of a linear regression.

1.4.2 Bayesian Hierarchical Models

The BHM consists of three components, each of them occupying one level of the hierarchy. In paleoclimatology, the data (or observation) level of the hierarchical model contains the forward PSM, which informs on the response of the proxy to the climate variable of interest. The climate variable is also represented by a model, for instance a first-order autoregressive model [Tingley and Huybers, 2010a,b], at the process level. The third level of the BHM includes the prior information on the unknown statistical parameters related to the models. Following the Bayes theorem, the prior distributions are updated on the basis of the available proxy observations in order to provide the posterior distribution of the parameters and of the climate field of interest, by incorporating all the known sources of error and providing complete uncertainty estimates of the reconstruction in each grid cell. In this framework, the forward PSM makes the link between the climate variable and the indirect observations of climate from proxies. With the definition of a spatial covariance matrix (in a simple parametric form), BHMs provide spatially gridded reconstructions at places where there are no proxy observations. For instance, spatially resolved reconstructions of past surface temperature at the regional to hemispheric scale has already been provided from tree rings with BHMs [Tingley and Huybers, 2013; Luterbacher et al., 2016; Werner et al., 2018; Zhang et al., 2018]. However, the computational cost of such method is still high, even with simple models. Moreover, the inference of multiple climate variables with a BHM remains difficult [Tolwinski-Ward et al., 2015]. In the framework of Tingley and Huybers [2010b] ("Bayesian Algorithm for Reconstructing Climate Anomalies in Space and Time"; BARCAST), thereafter used in other studies [Tingley and Huybers, 2013; Werner and Tingley, 2015; Werner et al., 2018; Luterbacher et al., 2016], the spatial covariance of the climate field is assumed to exponentially de-

cay with distance, which does not account for any features that may not be related to distance, for example the presence of moutains or dominant wind direction.

1.4.3 Data assimilation

Over the past decades, data assimilation has been increasingly used in paleoclimatology to produce a climate field reconstruction by combining the information brought by proxy records with the physics of the climate system as represented by climate models (Fig. 1.8) [Kalnay, 2003; Goosse et al., 2010; Widmann et al., 2010; Steiger et al., 2014; Hakim et al., 2016; Franke et al., 2017; Steiger et al., 2018; Tardif et al., 2019]. Climate models explicitly incorporate the main physical processes governing the climate system [Schneider and Dickinson, 1974]. When focusing on the global scale, General Circulation Models (GCMs) offer a representation of the climate system at the highest possible spatial resolution. Currently, GCMs encompass at least the atmosphere, ocean and sea ice components, that are coupled together. When the dynamic vegetation, the carbon cycles (terrestrial and marine) and the ice sheet components are also included, GCMs are more commonly referred to as Earth System Models (ESMs) [Goosse, 2015]. Global climate simulations provide a complete spatial picture of the climate changes. However, climate models display biases and they could not be able to properly reproduce the timing of the past variations. On the other hand, proxy observations give an insight into the past climate changes but at a limited number of locations.

In the paleoclimate DA framework, following the Bayes theorem, the prior state of the climate system as given by the climate model is updated with the available proxy records to produce a posterior estimation of the state of the climate system (i.e., the reanalysis). Using the spatial covariance of the model, the DA procedure spreads the information given by the proxy observations in space, i.e., where no proxy records are available. Using the covariance between the climate variables of the model, this information is also propagated to variables for which we do not have any assimilated observations. The dynamical consistency of the reconstructed climate fields is thus ensured in space and between the variables by relying on the physics of the climate system as included in the climate model. In this regard, the relationships between the reconstructed climate fields are represented much more naturally than would be the case with statistical approaches, for example in the BHM framework. Similarly to BHMs, the paleoclimate DA framework also gives the opportunity to incorporate a forward PSM (called an observation operator in the DA framework), to make the link between the outputs of the climate model and the proxy observations, without the need to reconstruct the climate variables of interest from the proxy observations [e.g. Tardif et al., 2019].

Two approaches of DA have been commonly applied in paleoclimatology: the offline approach of DA (or no-cycling method) and the online approach [e.g. Mat-

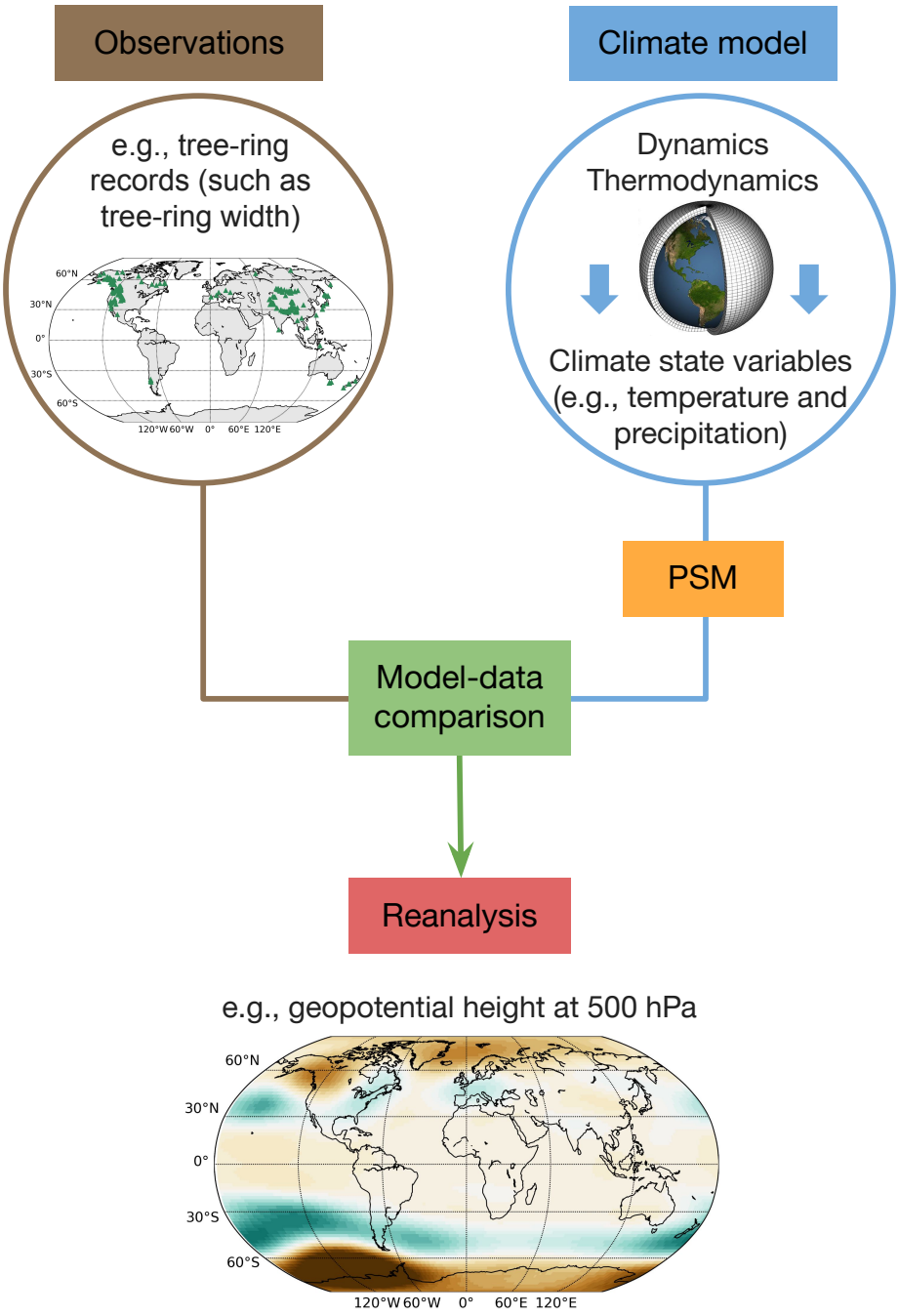


Figure 1.8: *Schematic representation of a procedure of data assimilation in paleoclimatology. The information brought by proxy records (e.g., tree-ring width) are combined with the physics of the climate system as represented by climate models in order to produce a reanalysis of different climate fields (e.g., the geopotential height at 500 hPa). Here, the distribution of the tree-ring width proxies is from the PAGES2k database [PAGES 2k Consortium, 2017]. The figure used to illustrate the climate models is from the National Oceanic and Atmospheric Administration (NOAA). The reanalysis is from the Last Millennium Reanalysis [Tardif et al., 2019] and represents the anomalies of geopotential height at 500 hPa in 1940 CE relative to 0-2000 CE. The brown (green) color stands for a positive (negative) anomaly. A darker (lighter) color represents a higher (lower) anomaly. Figure based on Goosse [2016] and Hakim et al. [2016].*

sikaris et al., 2015]. With the online approach, an ensemble of model simulations is updated at regular intervals (for example one year if annual tree-ring data are assimilated), so that the updates made on a time step depend on the previous ones, which considerably increases the computational time [e.g. Goosse, 2017; Perkins and Hakim, 2017]. In the offline approach, the prior state of the climate system is estimated by sampling different years (assumed to be independent of each other) in an existing ensemble of climate model simulations, which has the advantage of saving a large amount of computational time. On the contrary to the online approach, the updates made on the previous time steps are not transferred to the next ones. This holds as long as the predictability of the climate variables of interest is shorter than the temporal resolution of the DA procedure. Due to the chaotic nature of the atmosphere, Matsikaris et al. [2015] have shown that the online approach does not bring additional information compared to the offline approach when reconstructing atmospheric variables.

The first DA-based reconstructions incorporated information from proxy records with temperature reconstructions derived from proxies on the basis of a statistical relationship [e.g. Crespin et al., 2009; Goosse et al., 2012]. Lately, paleoclimate DA studies have started to make use of statistical forward PSMs as a way to directly assimilate tree-ring proxy records with uni- or multivariate linear regressions, providing large-scale reconstruction of hydroclimate [Steiger et al., 2018; Erb et al., 2020] or surface temperature [Hakim et al., 2016; Tardif et al., 2019; King et al., 2021], for instance, and giving insight into large-scale patterns of climate variability [e.g Zhu et al., 2020].

1.4.4 Limitations of the statistical approach

There are clear advantages related to the statistical approach. In particular, statistical methods are easy to implement and to interpret for any site without any a priori knowledge of the response of the studied species to climate. Statistical models may be used to easily unravel some of the relationships between climate variables and tree-ring growth. However, it relies on different assumptions that may not be appropriate for many records. First, climate is assumed to be the ultimate cause of past variations of tree growth, while other non-climatic factors are negligible. Moreover, it assumes that the statistical relationship calibrated over the instrumental period is also valid for the past, i.e, that the relationship is stationary. Most tree-ring based reconstructions also rely on the presumed linearity of the response of tree growth to climate, even if non-linear statistical techniques also exist and are sometimes used (e.g., artificial neural networks; Guiot et al., 1995; Nicault et al., 2008). Finally, the environmental conditions in which the trees are growing today are also supposed to be analogous to past conditions [Cook and Kairiukstis, 1990; Hughes et al., 2011]. However, tree-growth variations are known to

result from complex and multivariate biological processes related to climatic and non-climatic factors [Fritts, 1976; Anchukaitis et al., 2006; Vaganov et al., 2006; Evans et al., 2006] that can give rise to non-linear and non-stationary responses of tree-ring proxies to climate, questioning the statistical approach [Hughes et al., 2010; Babst et al., 2018; Wilmking et al., 2020].

For instance, Briffa et al. [1998a] have first highlighted a reduced response of tree growth to temperature changes in formerly temperature-limited sites of the high-latitude forests of the Northern Hemisphere, starting around the mid-20th century. This appears in the form of a loss of tree-growth sensitivity to temperature changes and/or a divergence of tree-ring width and density records from mean annual temperature time series [D'Arrigo et al., 2008]. It has, since then, been reported in many sites and for many species [Briffa et al., 1998a,b; Vaganov et al., 1999; Büntgen et al., 2006; Wilson et al., 2007; D'Arrigo et al., 2008; Visser et al., 2010; Babst et al., 2019; Hofgaard et al., 2019]. The causes of this tree-growth-to-climate relationship have still not been fully elucidated [Hughes et al., 2011; Wilmking et al., 2020]. For instance, this may be the result of complex non-linear or thresholded growth responses to climate [Vaganov et al., 1999; D'Arrigo et al., 2004]. This could also be related to the recent change in atmospheric composition that may have altered the growth response to climate [D'Arrigo et al., 2008; Hughes et al., 2011]. Whatever the reason, this example of non-stationarity in the relationship between climate and tree growth may have important implications when using statistical models calibrated over the recent decades to reconstruct past variations of temperature from tree rings [D'Arrigo et al., 2008; Wilmking et al., 2020].

On the contrary to statistical models, process-based tree-growth PSMs explicitly incorporate the biological processes driving tree growth, considering the combined influence of both climatic and non-climatic factors (for example atmospheric CO_2 concentration) to simulate a potentially non-linear response of tree growth to climate. In this regard, they may be able to overcome some of the assumptions related to the commonly used linear statistical models [Hughes et al., 2010; Guiot et al., 2014]. However, there are also limitations associated with such complex models. Despite their sophisticated representation of biological processes, they may not include an adequate representation of some of them to be widely applied in contrasted conditions. They also include numerous parameters, which often require high spatial and temporal observations, in particular meteorological and ecophysiological data for an accurate calibration and application. This is especially limiting when willing to use such models at large spatial scale, because the data may not be available or easily retrievable for the model to be applied skillfully.

1.5 Tree-growth process models for reconstructing past climate variations

Since the onset of dendroclimatology, careful attention has been given to understand the climate controls on tree growth, in order to shed light on the statistical models [Fritts, 1976]. This knowledge has been formalized with process-based models that explicitly incorporate the mechanisms by which tree-ring growth and wood structure react to tree environment, and more specifically to climate. Many process-based models of tree growth exist with different characteristics and different processes included [e.g Misson, 2004; Dufrêne et al., 2005; Vaganov et al., 2006; Drew et al., 2010].

For example, the mechanistic Vaganov-Shashkin (VS) model [Vaganov et al., 2006, 2011; Evans et al., 2006; Anchukaitis et al., 2006] is based on the fact that the environmental conditions, among which climate variations, directly affect the cellular processes occurring in the cambium, which in turn influence the structure and size of annual rings [Denne and Dodd, 1981; Vaganov et al., 2006; Rossi et al., 2006, 2007; Deslauriers et al., 2008; Vaganov et al., 2011; Rathgeber et al., 2016]. The VS model incorporates the primary controls of daily temperature, precipitation (used as inputs of the model) and sunlight on cambial activity and secondary xylem development of conifers to simulate the characteristics of annual tree rings at the stand level. The principle of limiting factor [Fritts, 1976] determines the daily growth rate relative to temperature, soil moisture and light using threshold growth response functions in the "growth block", which in turn determines the xylem development in the "cambial block". Tolwinski-Ward et al. [2011] have recently developed a light version of the VS model, Vaganov-Shashkin-Lite (VS-Lite), which uses monthly climate inputs (mean temperature and cumulative precipitation) to simulate annual tree-growth indexes on the same basis as the VS model, i.e. the principle of limiting climatic factor and threshold growth response functions, but without the cambial block. It has the advantage of being far more easily calibrated and applied at large spatial scale than the full VS model [e.g. Breitenmoser et al., 2014; Seftigen et al., 2018], whilst allowing for a non-linear response of tree growth to climate. However, it cannot be considered as fully mechanistic as it does not include any biological processes related to the xylem development, as in the VS model. While the VS [Anchukaitis et al., 2006; Evans et al., 2006; Shi et al., 2008; Zhang et al., 2011] and VS-Lite [Breitenmoser et al., 2014; Lavergne et al., 2015; Seftigen et al., 2018] models have already been successfully used in investigating tree-growth response to climate, they do not include any other internal or external drivers of tree growth than climate variables, and do not simulate explicitly other biological processes such as photosynthesis, respiration or carbon allocation [Evans et al., 2006; Babst et al., 2018].

On the contrary, the ecophysiological model MAIDEN (Modelling and Analysis In DENdroecology; Misson, 2004; Gea-Izquierdo et al., 2015; Gennaretti et al., 2017) is based on a source-sink approach of the climate control on tree-ring growth at the stand-level [Fatichi et al., 2014; Körner, 2015], but does not include any representation of the wood structure. The photosynthesis is directly affected by the more or less favorable climate variations, which determines the available quantity of carbon (i.e., the source) on a daily basis. The available carbon from photosynthesis and stored non-structural carbon is then allocated to the different sink tissues (stem, canopy, roots, storage), on the basis of allocation and climate-dependent rules that are defined according to phenology. Through the storage pool, MAIDEN can account for the temporal autocorrelation in the stem increment. When working with tree-ring width observations, the annual quantity of carbon allocated to the stem is assumed to be proportional to observed TRW (i.e., the mean standardized chronology; Sect. 1.3.2) [e.g. Gennaretti et al., 2017]. This implies to normalize both the observed TRW and simulated growth increment for comparison (i.e., by removing the mean and dividing by the standard deviation of the time series over the period of interest), which hampers the evaluation of the error in the simulated variance. Gennaretti et al. [2018] combine density and width measurements to produce a wood biomass index that is directly comparable with forest carbon accumulation simulated by MAIDEN. On the opposite, VS and VS-Lite simulate an index that is more directly comparable to the standardized tree-ring width series (Sect. 1.3.2; i.e., standardized tree-ring indices expected in the absence of any other controls on tree growth than local climate).

The MAIDEN model works at a daily time step, using maximum and minimum temperature and cumulative precipitation as inputs, and, most importantly, atmospheric CO_2 concentration, on the contrary to the VS model. Atmospheric CO_2 concentration has dramatically increased over the past fifty years (by around 30%; Myhre et al., 2013), reaching unprecedented levels (416.34 ppm in March 2021; `https://gml.noaa.gov/ccgg/trends/global.html`), and is expected to pursue an exponential increase during the upcoming century under the RCP8.5 scenario [Myhre et al., 2013]. While it is still difficult to estimate and take into account the actual effects of CO_2 concentration in dendroecological studies, it is known to be a key driver of the forest carbon fluxes [Körner et al., 2005; Silva et al., 2010; Peñuelas et al., 2011; Lévesque et al., 2014; Girardin et al., 2016b; Giguère-Croteau et al., 2019; Marchand et al., 2020]. As a consequence, considering the influence of atmospheric CO_2 concentration is crucial for dendroclimatic process-based models so as to account for its effects on forest carbon fluxes and potentially on the resulting tree growth. In particular, since these models are calibrated over the recent period, stationarity problems may arise if CO_2 concentration is not taken into account, which could induce an improper calibration of model pa-

rameters and important bias in the resulting climate reconstruction [D'Arrigo et al., 2008; Babst et al., 2018].

Process-based models can be used to reconstruct past climate variations using model-data fusion (MDF) approaches. More generally, MDF aims at enhancing the performance of a complex model (e.g., a process-based dendroclimatic model or a climate model) on the basis of available observations (e.g., tree-ring width series). To do so, MDF technique can optimize or refine the unknown parameters and initial conditions of the model or improve its predictive capacity using observations to constrain the model. Each MDF approach shares the same characteristics: (1) a model simulating the evolution of state variables (e.g., near-surface temperature or tree-growth-related variables); (2) observations that can be compared to the model output state variables; (3) an objective function combining observations and output state variables with the available prior information; and (4) an optimization technique that modifies the model parameters, the model input or output state variables in order to produce an estimate of the state variables which is as accurate as possible regarding the observations [Peng et al., 2011; Guiot et al., 2014].

MDF incorporates model calibration, model inversion and data assimilation in models (Sect. 1.4.3). Calibration consists in estimating some model parameters using observations. In paleoclimatology, inverse modelling consists in estimating one or several input climate variables that are directly or indirectly related to output observations by means of a process-based model [Guiot et al., 2000]. Inverse modelling to reconstruct past climates is thus based on the assumption that the process-based model perfectly reproduces the relationship between the output observations and climate. In reality, the model is not analytically inverted. Instead, for each given year of the period covered by tree-ring observations, for instance, the method iteratively runs the process-based model with climate inputs randomly sampled in the climate space (defined as the probability distribution of a chosen reference or average year), in order to converge towards the most likely climate conditions that gave rise to the observed tree-ring growth index [Guiot et al., 2014]. An inversion method has already been successfully applied to MAIDEN by Boucher et al. [2014], in order to reconstruct past variations of summer temperature and precipitation in the Fontainebleau forest (France).

At the moment, this approach only provides single time series of the climate variables used as inputs of the dendroclimatic model, and for a limited area. To produce large-scale and spatially gridded reconstructions of several climate variables with a process-based tree-growth PSM, data assimilation offers a more attractive framework (Sect. 1.4.3). However, while the use of process-based tree-growth models is theoretically possible with DA, so far it has never been done with actual tree-ring proxy data, but only with pseudoproxies, using the simple VS-Lite model [Dee et al., 2016; Acevedo et al., 2017; Steiger and Smerdon, 2017].

1.6 Objectives and outlines of the thesis

The mechanistic understanding of the climate impact on tree growth potentially increases our ability to retrieve meaningful climate information from tree-ring proxy networks. In turn, this may improve the reconstructions of past climate variations and, thereby, contribute to a better comprehension of internal and forced climate variability. In this framework, the general research question of the thesis is the following:

Can we improve large-scale climate reconstructions based on tree-ring width proxies by taking into account explicitly the links between climate and tree growth with a process-based dendroclimatic model?

To this end, we propose to incorporate a process-based dendroclimatic model into a data assimilation procedure. Specifically, the ecophysiological MAIDEN model is used as a forward PSM to make the link between the outputs of an Earth system model and tree-ring width proxy data. We elaborate the main equations and parameters of the MAIDEN model in Appendix A. To date, the MAIDEN model has been successfully calibrated and applied in the temperate regions [Misson, 2004; Boucher et al., 2014], the Mediterranean basin [Gea-Izquierdo et al., 2015], the Eastern Canadian taiga [Gennaretti et al., 2017] and Argentina [Lavergne et al., 2017]. As is the case for all process-based models, the large-scale application of MAIDEN is still hindered by the calibration of the numerous parameters and the setting of the model constants related to the site conditions. In particular, some parameters linked to the photosynthesis and carbon allocation modules require a site-by-site fitting. This site-by-site calibration generally requests local meteorological (at high temporal resolution; daily, in the case of MAIDEN), environmental (e.g., soil conditions) and physiological data, for example related to photosynthesis, which may be difficult to retrieve at large spatial scale. As the ultimate goal of the thesis is to incorporate MAIDEN into a data assimilation procedure, MAIDEN will be run using climate model outputs at low spatial and temporal resolution as inputs of the model. This requires major changes in the way MAIDEN is usually applied and is thus an important challenge.

As a consequence, to answer our research question, the thesis is divided into three chapters, each of them addressing a specific question:

1. What is the adequate method to robustly calibrate MAIDEN in an automatised way when only limited information on the local conditions are available? (Chapter 2, published in *Climate of the Past*)

2. To which extent is a complex dendroclimatic model such as MAIDEN adapted for application to a large number of sites? (Chapter 3, published in *Climate Dynamics*)

3. What is the added value of using a dendroclimatic process-based model as a proxy system model in reconstruction of past climates with data assimilation? (Chapter 4)

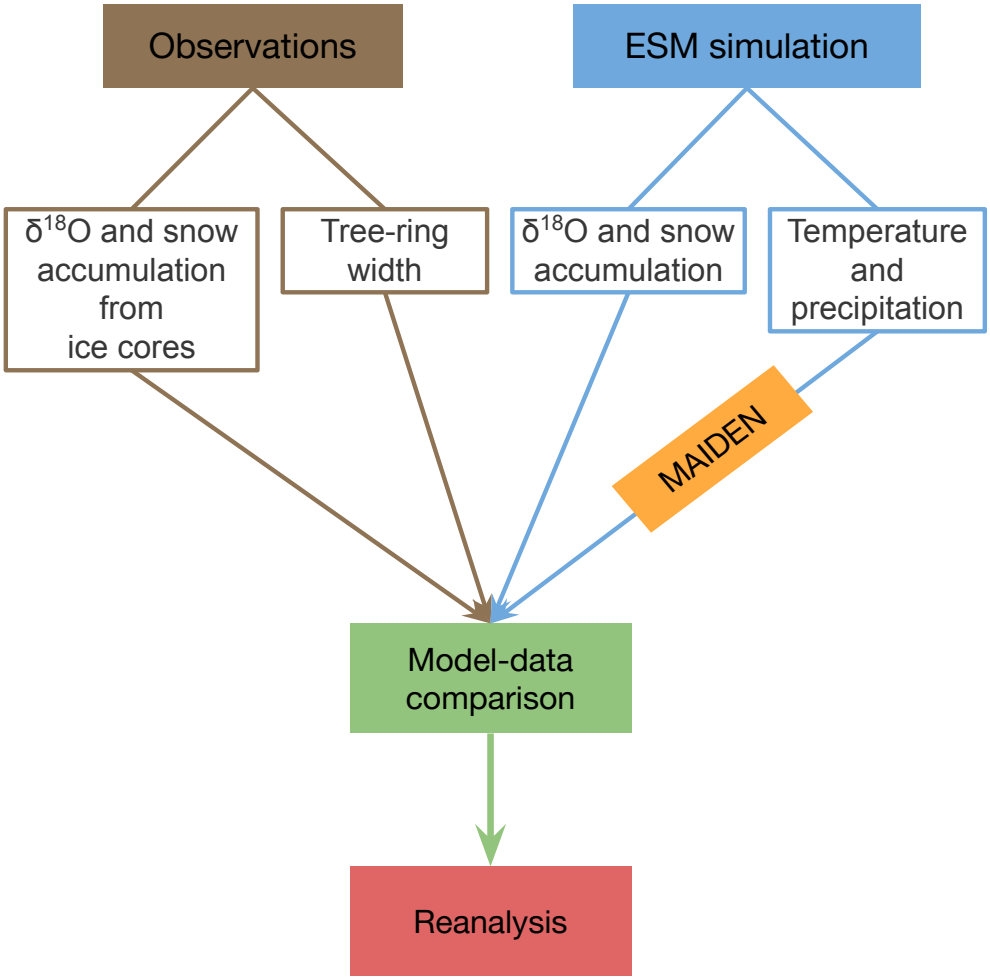


Figure 1.9: *Schematic representation of the procedure of offline data assimilation incorporating the dendroclimatic process-based model MAIDEN in a forward mode to assimilate tree-ring width records. Ice core records ($\delta^{18}O$ and snow accumulation) are also incorporated and directly compared with the outputs of the Earth system model (ESM) to produce a reanalysis. Figure based on Goosse [2016].*

In Chapter 2, we aim at developing a Bayesian calibration procedure of the MAIDEN model which allows for a good performance of the model at large spatial scale while being the most automatised as possible. In particular, our protocol focuses on the most sensitive parameters of the model as defined by Gennaretti et al. [2017]. The calibration procedure is then tested by applying MAIDEN to an Eastern Canadian taiga network of *Picea mariana* chronologies, as well as to three European chronologies of various tree species, over the last century. This gives the opportunity to test the model applicability to two different site configurations, i.e., a network of sites and three independent sites. The performance of the

MAIDEN model at those two sets of site chronologies is compared to the performance of the simple VS-Lite model. The VS-Lite model (Sect. 1.5) is a simple dendroclimatic model that has been frequently used at large spatial scale [e.g. Breitenmoser et al., 2014] and in pseudoproxy experiments with data assimilation [e.g. Dee et al., 2016; Acevedo et al., 2017; Steiger and Smerdon, 2017]. It is a potential good candidate for paleoclimate data assimilation exercises willing to go beyond the commonly used linear regression. In this chapter, VS-Lite is used as a benchmark to evaluate the advantage of a more complex dendroclimatic model as MAIDEN for large-scale paleoclimate applications. More details on the VS-Lite model are given in Appendix A. Finally, we assess the sensitivity of the model calibration to the quality of the climate inputs.

The objective of the Chapter 3 is to underline the benefits and potential limitations linked to the use of a process-based dendroclimatic model such as MAIDEN at large spatial scale for paleoclimate reconstructions. To this end, the calibration protocol developed in Chapter 2 is evaluated and updated by applying the MAIDEN model at the global scale over the last century. We use the TRW network of the PAGES2k database, including 354 TRW chronologies of various tree species (PAGES 2k Consortium, 2017; Sect. 1.2). As in Chapter 2, the performance of the MAIDEN model is compared to the performance of VS-Lite.

In Chapter 4, we aim at evaluating the potential of the process-based model MAIDEN to improve large-scale DA-based reconstructions of past climate variability. To this end, MAIDEN is incorporated into an offline DA procedure (using a particle filter; see Sect. D.1 for details on the procedure) as a forward PSM to combine TRW records with ESM simulations (Fig. 1.9). On the basis of the developments made in Chapter 3 with the TRW PAGES2k database, we test our DA approach in the mid- to high-latitudes of the Southern Hemisphere and compare it with a DA experiment incorporating the commonly used regression-based PSM. The mid-to-high latitudes of the Southern Hemisphere represent an interesting test case as few reconstructions have been performed to now in this region [Neukom et al., 2011, 2014]. We focus on the reconstruction (or reanalysis) of continental near-surface air temperature, precipitation and winds over the past 400 years. Specifically, we also include ice core records (δ^{18}O and snow accumulation) in the DA procedure, to make more consistent the reconstruction of the large-scale circulation pattern. In this regard, data assimilation is particularly convenient as it allows for the combination of multiple types of proxy records. Ice core proxies and TRW constitute the best continental proxies available at high temporal resolution in the Southern Hemisphere [PAGES 2k Consortium, 2017]. On the contrary to TRW observations, ice core records can be directly compared to the outputs of the climate model without a PSM (Fig. 1.9).

Finally, in Chapter 5, we provide the main conclusions and contributions of this thesis, and discuss the perspectives.

2

Application and evaluation of the dendroclimatic process-based model MAIDEN during the last century in Canada and Europe

Abstract

Tree-ring archives are one of the main sources of information to reconstruct climate variations over the last millennium with annual resolution. The links between tree-ring proxies and climate have usually been estimated using statistical approaches, assuming linear and stationary relationships. Both assumptions may be inadequate but this issue can be overcome by ecophysiological modelling based on mechanistic understanding. In this respect, the model MAIDEN (Modeling and Analysis In DENdroecology) simulating tree-ring growth from daily temperature and precipitation, considering carbon assimilation and allocation in forest stands, may constitute a valuable tool. However, the lack of local meteorological data and the limited characterization of tree species traits can complicate the calibration and validation of such a complex model, which may hamper paleoclimate applications. The goal of this study is to test the applicability of the MAIDEN model in a paleoclimate context using as a test case tree-ring observations covering the 20th century from 21 Eastern Canadian taiga sites and 3 European sites. More specifically, we investigate the model sensitivity to parameter calibration and to the quality of climatic inputs, and we evaluate the model performance using a validation procedure. We also examine the added value of using MAIDEN in paleoclimate applications compared to a simpler tree growth model, i.e. VS-Lite. A Bayesian

This chapter is based on: Rezsöhazy, J., Goosse , H., Guiot, J., Gennaretti, F., Boucher, E., André, F., and Jonard, M. (2020). Application and evaluation of the dendroclimatic process-based model MAIDEN during the last century in Canada and Europe, *Climate of the Past*, **16**, 1043–1059, https://doi.org/10.5194/cp-16-1043-2020. Supplementary materials are in Appendix B or available online as a supplement of the paper for Tables S4–S11 and Figures S1–S58.

calibration of the most sensitive model parameters provides good results at most of the selected sites with high correlations between simulated and observed tree-growth. Although MAIDEN is found to be sensitive to the quality of the climatic inputs, simple bias correction and downscaling techniques of these data improve significantly the performance of the model. The split-sample validation of MAIDEN gives encouraging results but requires long tree ring and meteorological series to give robust results. We also highlight a risk of overfitting in the calibration of model parameters that increases with short series. Finally, MAIDEN has shown higher calibration and validation correlations in most cases compared to VS-Lite. Nevertheless, this latter model turns out to be more stable over calibration and validation periods. Our results provide a protocol for the application of MAIDEN to potentially any site with tree-ring width data in the extratropical region.

2.1 Introduction

Instrumental data inform on past climate only back to the 19th century because few continuous records exist before this period [Harris et al., 2014; University of East Anglia Climatic Research Unit (CRU), 2017]. Complementary, indirect climate records from natural archives such as tree rings offer a longer-term perspective. In this context, dendroclimatology, defined as the science that allows for the inference of past climates from tree rings, enables climate reconstructions at high temporal resolution (annual) over several centuries or millennia [Fritts, 1976; Hughes et al., 2011]. Thanks to the availability of tree-ring observations in many regions, they represent the main data source in most large-scale hemispheric reconstructions covering the last millennium [e.g. Cook et al., 1999; Jones et al., 2009; Mann et al., 2009; Wilson et al., 2016; Anchukaitis et al., 2017; PAGES 2k Consortium, 2017; Esper et al., 2018; St. George and Esper, 2019].

Reconstructing past climate on the basis of tree rings first requires us to establish a relationship between measured variables, such as tree ring width or density, and climate. This has been classically done using statistical approaches [Fritts, 1976; Cook and Kairiukstis, 1990] and often reducing the problem to empirical linear relationships. Consequently, numerous temperature reconstructions are based on multiple linear regressions, calibrated using temperature during the instrumental period [e.g. Fritts, 1991; Jones et al., 1998; Mann et al., 1999, 2008]. When using those statistical models for the entire period covered by dendroclimatic data, we assume both linear and stationary relationships [Guiot et al., 2014], while those assumptions may be inadequate for many records [Briffa et al., 1998b; Wilson and Elling, 2004; Wilson et al., 2007; D'Arrigo et al., 2008].

Process-based tree-growth models are able to overcome those limitations of statistical models by explicitly representing the processes at the origin of the recorded signal [Guiot et al., 2014]. They are also one kind of a larger group of mod-

els called proxy system models (PSM). PSMs simulate the development of measured variables (here in tree rings) based on climatic variables as inputs. They integrate a simplified representation of the mechanisms governing the relationship between climate and observations used to capture paleoclimatic information [Evans et al., 2013]. These models can be applied in an inverse mode to estimate the climatic conditions that gave rise to the measured characteristics [Guiot et al., 2014; Boucher et al., 2014]. Alternatively, they can be forced by climate model results (direct mode), thereby allowing us to compare model results with indirect climate records and without the need to reconstruct the climate from these observations [Evans et al., 2013; Dee et al., 2016]. In addition to major advantages for model–data comparisons, proxy system models can facilitate the assimilation of proxy data in long climate model runs [Dee et al., 2016; Goosse, 2016]. In paleoclimatology, the objective of data assimilation is to optimally combine the results of one climate model and the observations to obtain an estimate of the state of the climate system as accurate as possible [Kalnay, 2003]. This technique is now used regularly to obtain reanalyses, providing estimates of different climatic variables, such as temperature, precipitation and atmospheric and ocean circulation for the last decades. Similar procedures are being developed in palaeoclimatology [e.g. Goosse et al., 2012; Franke et al., 2017; Tardif et al., 2019]. However, so far, physically based tree-ring PSMs have not been used in published reconstructions based on data assimilation using actual data. This implies additional uncertainties when reconstructing temperatures.

Several models developed to simulate tree growth have been applied in dendroclimatology [Guiot et al., 2014]. Among them, the VS-Lite model is a deterministic numerical model that simulates the primary response of ring width to climate based on the principle of limiting climatic factors (i.e. temperature and soil moisture; Tolwinski-Ward et al., 2011). Because of its simplicity and the small number of inputs required, it has been used in a wide range of conditions in a large number of paleoclimate studies [e.g. Breitenmoser et al., 2014; Lavergne et al., 2015; Dee et al., 2016; Steiger and Smerdon, 2017; Seftigen et al., 2018; Fang and Li, 2019]. However, VS-Lite is not able to reproduce tree-growth observations for numerous sites, particularly when the dependence on climatic conditions is complex [Breitenmoser et al., 2014]. More comprehensive models such as the full Vaganov–Shashkin model [Vaganov et al., 2006] or MAIDEN (Modeling and Analysis In DENdroecology; Misson, 2004) could be more adapted to those conditions. One of the strengths of the MAIDEN model is to include the influence of atmospheric CO_2 concentration on growth. This is essential when we know that the atmospheric concentration of CO_2 increased by 30% during the last 50 years [Myhre et al., 2013; Boucher et al., 2014]. As models are calibrated over this recent period, not taking into account CO_2 concentration could potentially induce stationarity problems which can, ultimately, have an impact on the calibration of

parameters, such as the ones related to temperature or water use efficiency that can covary with CO_2. Unfortunately, those more comprehensive models including explicitly complex biological processes such as photosynthesis and carbon allocation may need careful initialization and calibration for each set. They may thus require specific information on the sites that may not be available. This may then hamper a systematic application of the model to a large number of sites as done for instance with VS-Lite [Breitenmoser et al., 2014].

Before applying a mechanistic model to a wide range of tree-ring records covering the past centuries, testing its applicability over the 20th century when data allow for an estimation of the model skill appears necessary, which is the goal of our study. For a specific study site, local meteorological data and measurements of several ecophysiological variables allow for a precise calibration of many individual processes included in the model. However, this is a rare case and likely one of the main limitations in the application of the model to a wide range of sites and soil conditions or when driven by climate model results that have known biases [Flato et al., 2013]. We first present in Sect. 2.2.1 the two dendroclimatic models that are compared in this study, namely the complex model MAIDEN and the more simple model VS-Lite. MAIDEN and VS-Lite are applied to selected sites of the Northern Hemisphere (described in Sect. 2.2.2), covering a range of environmental conditions and tree species. A first set of data consists of a large number of sites from the same region with similar environmental conditions but with low in situ replication, while a second set only contains a few sites but with good replication. In this way, we test the applicability of MAIDEN to two datasets contrasted in terms of site documentation. This allows us to evaluate the extent to which MAIDEN can be applied. We compare the calibration methods adopted for VS-Lite [Tolwinski-Ward et al., 2013] and MAIDEN [Hartig et al., 2019] in Sect. 2.2.3. Different strategies to select the value for the most sensitive parameters of the MAIDEN model as well as the sensitivity of parameter calibration to the quality of climatic inputs are tested in Sect. 2.3.1, 2.3.2 and 2.3.3. Finally, we compare calibration and validation statistics of both models and discuss their applicability to a wide range of sites and species in Sect. 2.3.4 and 2.3.5.

2.2 Material and methods

2.2.1 Tree-growth models

2.2.1.1 The MAIDEN model

The dendroclimatic model MAIDEN has initially been developed by Misson [2004]. It explicitly includes biological processes, namely photosynthesis and carbon allocation to different tree compartments, to simulate an annual tree-growth incre-

ment. The model uses daily climatic inputs (i.e. CO_2 atmospheric concentration, precipitation and minimum and maximum air temperature). Up to now, MAIDEN has been applied in the Mediterranean [Gea-Izquierdo et al., 2015] and temperate regions [Misson, 2004; Boucher et al., 2014], in the Eastern Canadian taiga [Gennaretti et al., 2017], and in Argentina [Lavergne et al., 2017]. Currently, there are two versions of the model from Gea-Izquierdo et al. [2015], developed for the Mediterranean forests, and Gennaretti et al. [2017], for boreal tree species. A unified version from those two versions has also been developed by Fabio Gennaretti (unpublished). In this study, all tests have been conducted using the unified version of MAIDEN. This unified version gives the opportunity to choose between the version from Gennaretti et al. [2017] or from Gea-Izquierdo et al. [2015] and, if needed, to test equations from both versions to evaluate their impact. However, here, only the version from Gennaretti et al. [2017] is used as it is the most adapted to the selected sites.

MAIDEN simulates photosynthesis on a daily basis and allocates the daily available carbon from photosynthesis and stored non-structural carbohydrates to different pools (leaves, roots, stem and storage). The allocation is based on functional rules defined following the ongoing phenological phase (five phases per year: winter 1 with no accumulation of growing degree-days (GDD), winter 2 with active GDD accumulation, budburst, summer and fall). At the end of the year, the model sums all the daily carbon inputs allocated to the stem to get an annual tree-growth increment (yearly Dstem, hereafter Dstem, in grams of carbon per square metre of stand per year). Dstem is assumed to be proportional to tree-ring growth so that we can build simulated tree-ring index time series and compare it with tree-ring width (hereafter TRW) observations (Sect. 2.2.3.1) [Gea-Izquierdo et al., 2015; Gennaretti et al., 2017]. The structure of the MAIDEN model is provided online (`https://figshare.com/articles/MAIDEN_ecophysiological_forest_model/5446435/1`, last access: 17 November 2019; Gennaretti, 2017), and its modules are available upon request.

Tree-ring observation site and climate station (corresponding to a single location or grid cell as a function of the climatic dataset) constants of the MAIDEN model (Table B.1) are derived from observations, as far as possible. For practical reasons, we were not able to retrieve slope and aspect information from a digital elevation model, for example, because it requires field knowledge of the site and for each sample, which we cannot systematically obtain given our global-scale goals. Thus, slope and aspect constants are set to zero. The soil is divided into four layers (1-15 cm; 15-30 cm; 30-65 cm; 65-100 cm). Clay and sand fractions are extracted from the Harmonized World Soil Database (hereafter HWSD) v1.2 at 30 arcsec resolution [FAO/IIASA/ISRIC/ISSCAS/JRC, 2012] at the nearest cell with observed value which is always at a distance smaller than 100 km to the site and assigned as follows: 1-30cm parameters from the HWSD for the two first soil

layers in MAIDEN; 30-100 cm parameters from the HWSD for the two deepest soil layers in MAIDEN. Soil layer thickness is fixed at the same value for all sites, as for fine root fractions.

2.2.1.2 The VS-Lite model

VS-Lite was developed by Tolwinski-Ward et al. [2011] as a simplified version of the full Vaganov–Shashkin model [Vaganov et al., 2006]. The model reproduces the primary response of ring width to climate using an approach based on the limiting factors principle (i.e. temperature and soil moisture) and on threshold growth response functions. It does not model any biological processes explicitly so it cannot be considered fully mechanistic. The model needs monthly climate data (cumulated precipitations and average temperature) as input as well as latitude of the study site. The main output of VS-Lite used here is a unitless annual tree-growth increment [Tolwinski-Ward et al., 2011].

2.2.2 Study sites and climate data

2.2.2.1 Study sites

A network of tree-ring width chronologies of *Picea mariana* collected in similar conditions is available for the Eastern Canadian taiga (Nicault et al., 2014; Boucher et al., 2017; `http://dendro-qc-lab.ca/trw.html`, last access: 30 March 2019). We use here the tree-ring series directly derived from this compilation, without any modification. The chronologies have been previously standardized using the age-band regional curve standardization (or RCS) method proposed by Briffa et al. [2001] and further applied to a similar boreal dataset by Nicault et al. [2014]. We also use the Eastern Canadian taiga chronology for *Picea mariana* from Gennaretti et al. [2017] (hereafter *QC_taiga*), standardized using a site-specific RCS [Gennaretti et al., 2014b]. The latter is highly replicated [Gennaretti et al., 2014b] compared to the other Eastern Canadian sites from Nicault et al. [2014] and Boucher et al. [2017], which cover a broader spatial range, and provides additional observations to calibrate the model. From this network, we have only selected sites from Nicault et al. [2014] and Boucher et al. [2017] ending at least in 2000, with an expressed population signal (defined as the amount of variance of a population chronology infinitely replicated explained by a finite subsample; Buras, 2017) equal to or above 0.8, and replication equal to or above 15. We have also kept the site from Gennaretti et al. [2017] as a control site. At the end of the selection process, we get 21 sites (Fig. 2.1a). In order to increase replication, the Canadian sites from Nicault et al. [2014] and Boucher et al. [2017] are aggregated based on a 1° grid by averaging tree-ring width chronologies (Fig. 2.1b). From this, we get five aggregated sites (Table 2.1). Note that *QC_taiga* is not included

into the aggregation process to keep it as a reference. The aggregation allows us to get relatively good intersite correlations inside the same 1° grid, ranging from 0.442 to 0.732 with an average of 0.558. This observational network represents an archetypal example of a singular species that covers an important hydroclimatic gradient. Sites located along the western (near James Bay, WNFLV1, Fig. 2.1a) and eastern (near Labrador sea, WL32, Fig. 2.1a) margins of the study area present the warmest growing seasons in the network (864 growing degree-days above 5℃ for the 1976-2005 period; Hutchinson et al., 2009). Sites located in the centre of the Quebec–Labrador peninsula (WHM2, Fig. 2.1a) present a much shorter growing season (692 growing degree-days above 5℃), much like the sites located further north (WLECA, Fig. 2.1a, 573 growing degree-days above 5℃). Annual precipitation increases from west to east, passing from 668 mm (WNFLV1, Fig. 2.1a) to 907 mm (WL32, Fig. 2.1a), and significantly decreases with latitude, reaching only 567 mm at WLECA (Fig. 2.1a) for the 1976-2005 period [Hutchinson et al., 2009]. This makes this network a relevant candidate for our calibration and validation exercises.

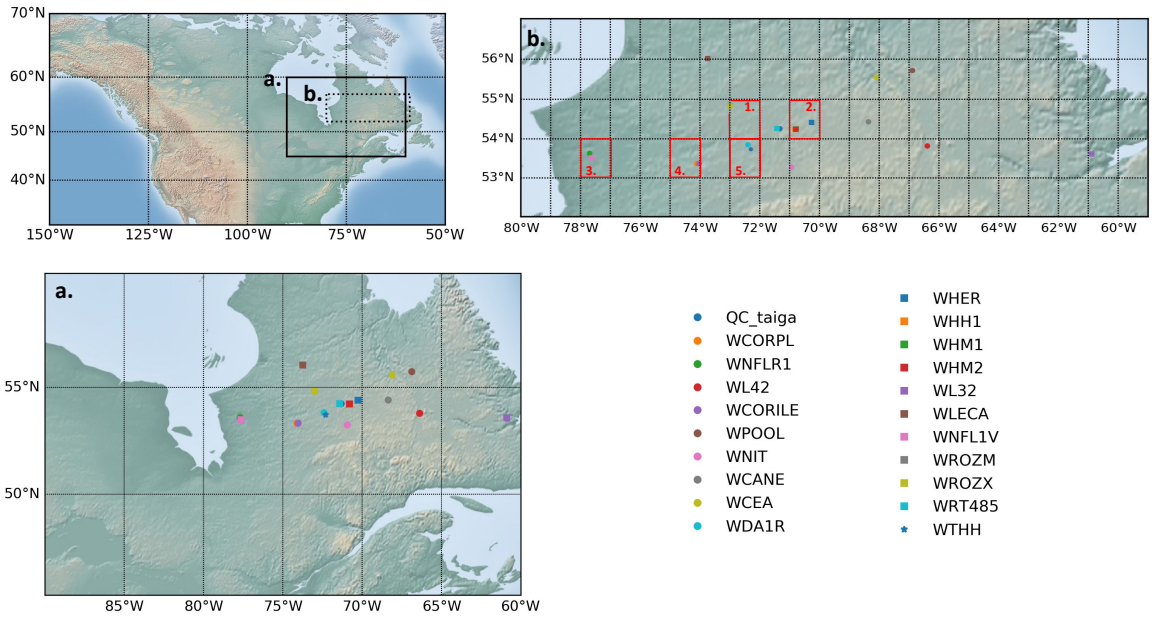


Figure 2.1: *Location of (a) 21 Eastern Canadian taiga sites (20 sites from Nicault et al., 2014 and Boucher et al., 2017 and 1 site called here QC_taiga from Gennaretti et al., 2017), and (b) aggregated Eastern Canadian taiga sites from Nicault et al. [2014] and Boucher et al. [2017] based on a 1° grid (red numbered grid cells). Background map from Hunter [2007].*

Three additional tree-ring width chronologies (hereafter European sites) are used to perform tests on sites with good replication, especially at the European

Table 2.1: *Aggregated Eastern Canadian taiga sites based on the individual sites from Nicault et al. [2014] and Boucher et al. [2017] (Fig. 2.1a and b).*

Aggregated site name	Individual sites	Grid cell number
WROZ	WROZM, WROZX	1
WH	WHER, WHH1, WHM1, WHM2	2
WNFL	WNFL1V, WNFLR1	3
WCOR	WCORILE, WCORPL	4
WDA1R_WTHH	WDA1R, WTHH	5

Alps site, and long nearby series from meteorological stations (Fig. 2.2): EALP (47° N, 10.7° E; 2050m; European Alps; *Pinus cembra* and *Larix decidua*; Büntgen et al., 2011; processed data available in the PAGES2k database; PAGES 2k Consortium, 2017); SWIT179 (46.77° N, 9.82° E; 1800m; *Picea abies*; standardized with a cubic-smoothing spline with a 50% frequency cut-off at 35 years; Seftigen et al., 2018; unprocessed data archived at the International Tree Ring Data Bank, `https://www.ncdc.noaa.gov/data-access/paleoclimatology-data`) and FINL045 (68.07° N, 27.2° E; *Pinus sylvestris*; standardized using a spline with a 50% frequency cut-off response at 32 years; Babst et al., 2013; processed data available in the Supplement of Babst et al., 2013). Similarly to the Eastern Canadian taiga chronologies, the tree-ring series were not modified here. Those three European sites exemplify a situation where we only have access to individual sites with different species and from different environmental conditions that are not part of a larger network of tree-ring width observations.

2.2.2.2 Climate data

Daily climatic inputs are needed to run MAIDEN (Sect. 2.2.1.1). Monthly climatic inputs for VS-Lite are computed from those daily data. Note that monthly-average temperature has been computed by averaging daily maximum and minimum temperatures, which could lead to a small bias. Three daily climatic datasets with different spatial resolutions (Table 2.2) were selected for our analysis on the Eastern Canadian taiga network (Fig. 2.1a and b). First, a dataset at a high spatial resolution of 5 minutes from the gridded interpolated Canadian database of daily minimum–maximum temperature and precipitation (Hutchinson et al., 2009, hereafter NRCAN). The *Global Meteorological Forcing Dataset for land surface modeling* (v1) (`http://hydrology.princeton.edu/data.php`, last access: 4 January 2019; Sheffield et al., 2006) at 1° resolution is used as a mid-resolution climatic dataset (hereafter GMF). The NOAA-CIRES 20th Century Reanalysis V2c

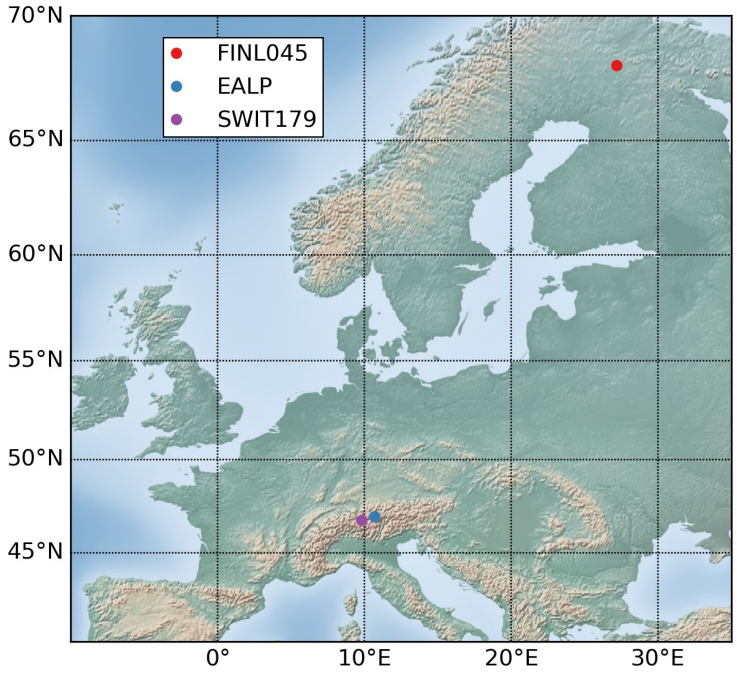


Figure 2.2: *Location of three European sites with tree-ring width observations used in this study. Background map from Hunter [2007].*

(https://www.esrl.noaa.gov/psd/data/gridded/data.20thC_ReanV2c.monolevel.html, last access: 4 January 2019) at 2° resolution is used as a low-resolution dataset (hereafter 20CRv2c). Finally, the 20CRv2c dataset was modified to match the monthly-mean seasonal cycle of the high-resolution dataset NRCAN (hereafter 20CRv2c corr.). This simple bias correction and downscaling to the location of the site is done by removing the difference between the monthly-mean seasonal cycle of 20CRv2c (2°) and NRCAN (5 arcmin) from the maximum and minimum temperature data. In order to avoid negative values, daily precipitations are multiplied by the ratio between the monthly-mean seasonal cycle of NRCAN (5 arcmin) and 20CRv2c (2°). The time series are extracted from the grid cells nearest to the studied individual sites. The climatic data are averaged over the individual site data for the aggregated Eastern Canadian sites (Table 2.1).

The Global Historical Climate Network Daily (Table 2.2; see Table B.2 for details on selected stations; Menne et al., 2012a,b; hereafter GHCN) is used to perform analysis on the European sites (FINL045, EALP, SWIT179, Fig. 2.2).

Daily atmospheric CO_2 concentration data are linearly interpolated from the annual data from Sato and Schmidt (https://data.giss.nasa.gov/modelforce/ghgases/, last access: 3 December 2018).

Table 2.2: *Description of all daily climatic datasets used in this study (abbreviation, climatic dataset, spatial resolution and source), time periods on which MAIDEN and VS-Lite simulations are performed with each specific climatic dataset (time period), and sites where climate data are used (sites). European and Canadian sites refer to Fig. 2.1 and 2.2, respectively.*

Abbreviation	Climatic dataset	Spatial resolution	Source	Time period	Sites
GHCN	Global Historical Climate Network Daily	station	Menne et al., 2012a,b	1909-1944 or 1910-1949;1950-2000	European sites
NRCAN	Canadian database of daily minimum-maximum temperature and precipitation	5 minutes	Hutchinson et al., 2009	1950-2000	Canadian sites
GMF	Global Meteorological Forcing Dataset for land surface modeling	1 degree	Sheffield et al., 2006	1950-2000	Canadian sites
20CRv2c	NOAA-CIRES 20th Century Reanalysis V2c	2 degrees	NOAA-CIRES	1950-2000;1900-2000	Canadian sites
20CRv2c corr.	NOAA-CIRES 20th Century Reanalysis V2c corrected for bias in the mean seasonal cycle based on NRCAN	2 degrees	-	1950-2000;1900-2000	Canadian sites

2.2.3 Calibration

2.2.3.1 The MAIDEN model

We have developed a protocol to systematically and automatically calibrate the model through a Bayesian procedure with Markov Chain Monte Carlo sampling carried out using the DREAMzs algorithm [Hartig et al., 2019]. The calibration procedure focusses on the most sensitive parameters of the model identified in Gennaretti et al. [2017]: 6 parameters influencing the simulated stand growth primary production and 12 parameters involved in the modelling of the daily quantity of carbon allocated to different tree compartments (Table B.3). Those 6+12 parameters are calibrated by comparison between simulated Dstem and tree-ring width observations. The comparison relies on the computation of the model likelihood defined as the sum of the logarithms of the normal probability densities of the residuals between the model simulation and the observations. The prior distributions of the 6+12 parameters are assumed to be uniform over an acceptable range,

as in Gennaretti et al. [2017]. The calibration procedure is made up of three steps. During the first step, we calibrate the 12 carbon allocation parameters, while fixing the 6 photosynthesis parameters to arbitrary values in their acceptable ranges. We run three Markov chains of 10 000 iterations with a five-iteration thinning (i.e. we only consider one random sample out of five) to calibrate the parameters. During the second step, we fix the 12 carbon allocation parameters at the values obtained from the first step. We calibrate the 6 photosynthesis parameters by also running three Markov chains of 10 000 iterations with a five-iteration thinning. Finally, during the third step, the 6 photosynthesis parameters are fixed at the values obtained from the second step, and the 12 carbon allocation parameters are calibrated, by running three Markov chains of 30 000 iterations, with a five-iteration thinning as well. Each of those nine chains starts from random initial values of the parameters in their acceptable ranges. At the end of each calibration step, we select the set of parameters with the highest posterior (maximum a posteriori value or MAP, Hartig et al., 2019) from all iterations considering a burn-in period (i.e. the number of initial iterations of a chain that are not considered in the calibration) of 1000 iterations (first and second steps) and 3000 iterations (third step). At the end of the calibration process, we thus have 6 calibrated parameters from the second calibration step and 12 carbon allocation parameters from the third one. The calibration method has been tested for convergence of Markov chains with Gelman–Rubin statistical indicators [Hartig et al., 2019].

The MAIDEN model was calibrated at the 21 Eastern Canadian taiga sites and at the 5 aggregated sites over the 1950-2000 time period using the high- (NRCAN), mid- (GMF) and low-resolution (20CRv2c) datasets as inputs, as well as the bias-corrected low-resolution dataset (20CRv2c corr.), and over the 1900-2000 time period using the 20CRv2c and 20CRv2c corr. datasets as climatic inputs. MAIDEN was also calibrated at the three European sites using GHCN station data over 1950-2000 (FINL045; EALP; SWIT179), 1909-1944 (FINL045) and 1910-1949 (EALP and SWIT179). Calibrated parameters values for the 1950-2000 time period are available in Tables S4–S7. Parameter posterior frequency distributions for the NRCAN (5 arcmin) high-resolution climatic dataset are available in Fig. S1–S58. Pearson correlation coefficients between observed TRW and simulated Dstem were computed, as well as the corresponding confidence level. To compare observed and simulated tree-ring growth data after the optimization of the model parameters, both observed tree-ring width series and simulated time series have been normalized to unitless indexes. Ideally, an exhaustive quantitative evaluation of MAIDEN would require a comparison of the variable simulated by MAIDEN to represent tree-growth directly with observations. However, this would imply the use of other tree-growth observations such as tree-ring density measurements, while tree-ring width represents the most widely available tree-growth observations which makes it a relevant candidate given our global-scale goals.

The disadvantage is that this normalization forbids us to assess error in the variance. This is why we only analyse the correlations for simplicity as using other metrics like the RMSE would not help us in this aspect.

2.2.3.2 The VS-Lite model

The VS-Lite parameters are calibrated at each location following a Bayesian approach described in Tolwinski-Ward et al. [2013]. In this study, four VS-Lite parameters, corresponding to the lower and upper temperature (respectively T_1 and T_2 in Tolwinski-Ward et al., 2011) and soil moisture (respectively M_1 and M_2 in Tolwinski-Ward et al., 2011) thresholds of the model, have been optimized. The other parameters were fixed to default values. The method is based on a standard Markov chain Monte Carlo approach, a Metropolis–Hastings algorithm embedded within a Gibbs sampler. The VS-Lite model was calibrated at the same sites and over the same time periods as MAIDEN, using the same climatic data (Sect. 2.2.3.1). Calibrated parameters values for the 1950-2000 period are available in Tables S8–S11. Pearson correlation coefficients between TRW observations and simulated tree-growth indexes were also computed. Observed time series have been normalized to unitless indexes as well.

Running MAIDEN takes around 2.5 seconds on one CPU for a 50-year time span while running VS-Lite takes around 0.30 seconds. Currently, calibrating MAIDEN with our method takes around 18 hours on one CPU for a site due to the high number of iterations and calibrated parameters, while the calibration method used for VS-Lite and developed by Tolwinski-Ward et al. (2013) takes only a few seconds.

2.2.4 Validation

Split-sample validation are performed by dividing the available data into two subperiods: one for calibration and one for validation, and viceversa. In order to test the influence of time series length, we validate the two models for both short (1950-1974 and 1975-2000) and long (1909-1944 and 1950-2000 or 1910-1949 and 1950-2000) time periods. For each validation experiment, Pearson correlation coefficients between observed TRW and simulated tree-growth indexes were computed, as well as the corresponding confidence level.

Split-sample validation was preferred over other validation methods such as h-block jackknife which are computationally intensive. Additionally, removing years may be inappropriate for the validation because of the autocorrelation characterizing yearly TRW observations. Similar problems arise from a bootstrap technique [Gea-Izquierdo et al., 2017].

2.3 Results and discussion

Our results and discussion are structured into five sections that allow us together to fulfil our objective of testing the applicability of MAIDEN over the 20th century (Table 2.3). At first, we want to determine the best set of parameters for MAIDEN at our study sites and test the sensitivity of calibration to the quality of climatic inputs (Sect. 2.3.1, 2.3.2 and 2.3.3). In a context of paleoclimate model–data comparison where MAIDEN will be driven by climate model outputs at low resolution, this is a crucial point of our analysis. For example, bias correction and downscaling techniques could be good options to improve the robustness of the model calibration if the model is sensitive to the quality of climatic inputs.

We first test the possibility of using calibrated parameters from a well-documented site at other similar sites in terms of environment (here the Eastern Canadian taiga) and tree species (here *Picea mariana*) in Sect. 2.3.1. Another option is to calibrate each site individually, as in Sect. 2.3.2 following the calibration protocol detailed in Sect. 2.2.3.1. We thirdly test in Sect. 2.3.3 an alternative calibration method which consists of calibrating the MAIDEN model over the mean of a tree-ring width observations network with similar environmental conditions and then applying the resulting calibrated parameters to the individual sites. From another perspective, this experiment could also be seen as an alternative method for the validation of the MAIDEN model when the climate and/or tree-ring width observation time series are too short for a split-sample validation. In this case, the individual sites are considered nearly independent validation data. To test the sensitivity of the model to the quality of climatic inputs, we have selected four climatic datasets at different spatial resolutions (Sect. 2.2.2.2, Table 2.2) that will be used in Sect. 2.3.2 to drive MAIDEN at the Eastern Canadian taiga sites. As a second sensitivity experiment, we have applied the parameters calibrated with MAIDEN using the high-resolution climatic data (NRCAN) to the Eastern Canadian taiga sites driven by the low-resolution data without or with bias correction (20CRv2c and 20CRv2c corr.).

The validation of MAIDEN in Sect. 2.3.4 is essential to evaluate the robustness of the calibration. The last section of our study consists of comparing the performance of the complex model MAIDEN with the performance of the simple model VS-Lite so as to assess the benefits of using a complex tree-growth model as MAIDEN for past climate reconstruction compared to a simple one (Sect. 2.3.5).

2.3.1 Application of prior MAIDEN parameters to all Canadian sites

At first, the *QC_taiga* parameters as calibrated by Gennaretti et al. [2017] (12 carbon allocation and 6 photosynthesis parameters) were applied to the other 20 Eastern Canadian sites and 5 aggregated sites from Nicault et al. [2014] and

Table 2.3: *Description of each experiment performed in our study: experiment name, sites and climate dataset used for the experiment, time period of the experiment, and short description of the experiment. Information on climate datasets can be found in Table 2.2. Individual and aggregated Eastern Canadian taiga sites refer to Fig. 2.1 and European sites refer to Fig. 2.2.*

Experiment name	Sites	Climate dataset	Time period	Description
Calibration strategies for MAIDEN				
Application of prior MAIDEN parameters to all Canadian sites (Sect. 2.3.1)	Individual and aggregated Eastern Canadian taiga sites	NRCAN	1950-2000	We apply *QC_taiga* parameters as calibrated by Gennaretti et al. [2017] to all Eastern Canadian taiga sites
Site-specific calibration of the MAIDEN parameters and sensitivity to the quality of climatic inputs (Sect. 2.3.2)	Individual and aggregated Eastern Canadian taiga sites	NRCAN, GMF, 20CRv2c, 20CRv2c corr.	1950-2000 ;1900-2000 (20CRv2c and 20CRv2c corr. only)	We calibrate each Eastern Canadian taiga sites with a bayesian procedure and evaluate the sensitivity of the calibration to the climate inputs quality
Regional calibration of MAIDEN (Sect. 2.3.3)	Individual and aggregated Eastern Canadian taiga sites	NRCAN	1950-2000	We evaluate the performance of MAIDEN at the Eastern Canadian taiga sites using a regional calibration
Validation of MAIDEN				
Split-sample validation of MAIDEN calibration (Sect. 2.3.4)	Aggregated Eastern Canadian taiga sites (AC) and European sites (E)	NRCAN (AC); GHCN (E)	1950-1974/1975-2000 (AC, E); 1909-1944 or 1910-1949/1950-2000 (E)	We validate our calibration procedure for MAIDEN using a split-sample method
Comparison between models				
Comparison between VS-Lite and MAIDEN (Sect. 2.3.5)	Individual Eastern Canadian taiga sites (IC) and European sites (E)	NRCAN (IC); GHCN (E)	1950-1974/1975-2000 (E); 1909-1944 or 1910-1949/1950-2000 (E); 1950-2000 (IC)	We compare VS-Lite and MAIDEN calibration and validation statistics

Boucher et al. [2017] using the NRCAN (5 arcmin) climate data (Table 2.2) over the 1950-2000 time period. Correlations between observations and simulations with MAIDEN using *QC_taiga* calibrated parameters (Fig. 2.3) are low and non-significant at most sites. Several reasons can explain the low skill of MAIDEN using those parameters. These results could be linked to the lower replication level at the sites from Nicault et al. [2014] and Boucher et al. [2017] - even when aggregated - compared to the site from Gennaretti et al. [2017] that weakens the climatic signal in the series. This may also be due to a high sensitivity of parameter calibration to an unstable climate–species relationship among sites that are different from each other in many aspects (such as soil type, vegetation, nutrient availability). Additionally, the long-term trends of forest growth in the Eastern Canadian taiga mostly depend on the past fire history [e.g. Payette et al., 2008; Gennaretti et al., 2014a; Erni et al., 2017]. This represents the main natural disturbance factor that has shaped the North American boreal ecosystem by determining forest structure and composition as well as carbon stocks and interacting with climate on a long timescale. Yet, MAIDEN does not account for disturbances. To evaluate the effect of those disturbances on our experiment, the long-term decadal trends have been removed in both observations and simulations following Gennaretti et al. [2017] (Fig. B.1). With only the high-frequency signal, the agreement between TRW observations and simulations with MAIDEN using *QC_taiga* calibrated parameters is far better for most individual and aggregated sites.

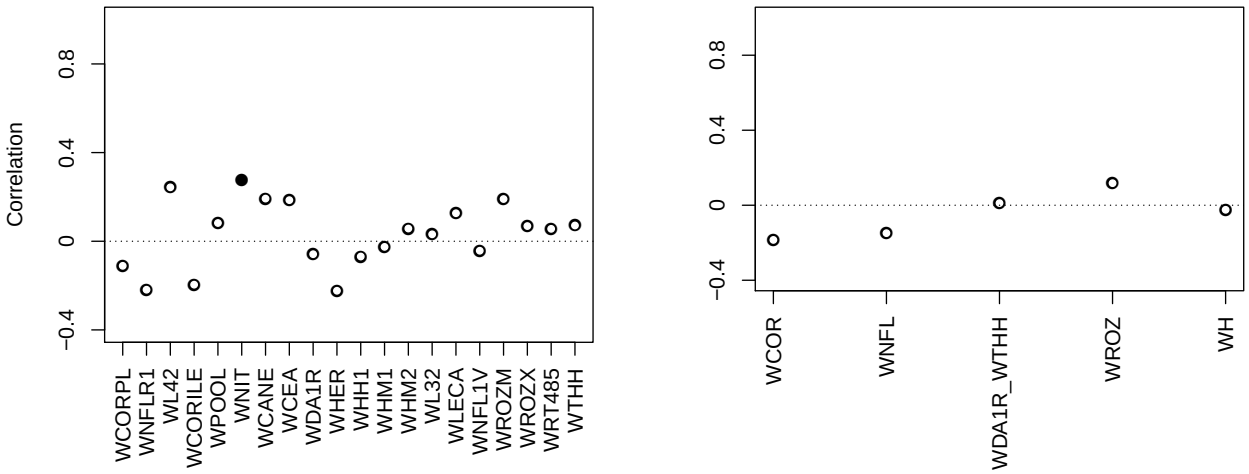


Figure 2.3: *Pearson correlation coefficients between tree-growth observations and simulations at the Eastern Canadian taiga sites (Fig. 2.1) with MAIDEN using NRCAN (5 arcmin) as climatic inputs (Table 2.2) for the 1950-2000 period with QC_taiga calibrated parameters from Gennaretti et al. [2017]. Individual (left) and aggregated sites (right). White inner circles stand for non-significant correlations (p-value > 0.05). Plain circles stand for significant correlations (p-value < 0.05).*

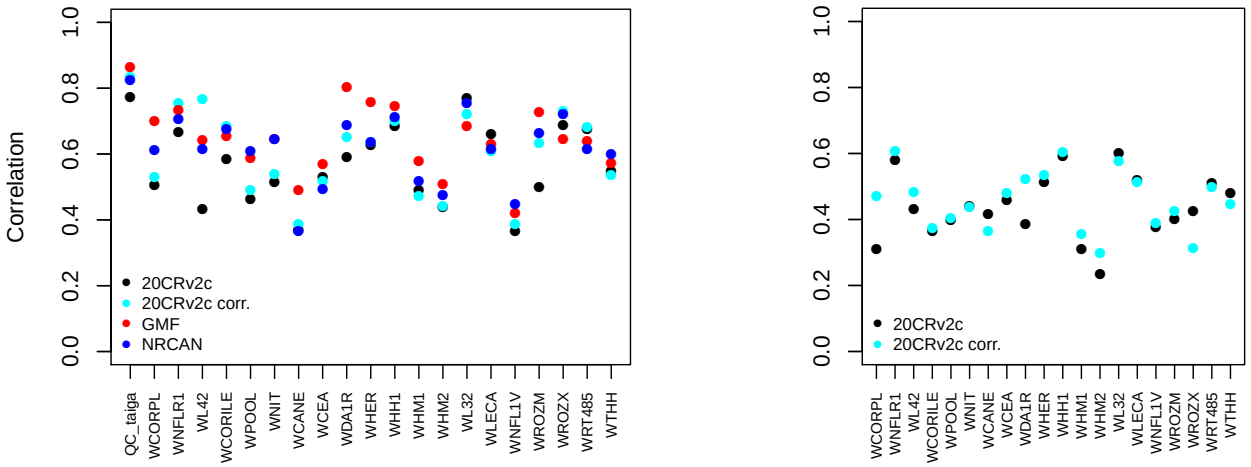
2.3.2 Site-specific calibration of the MAIDEN parameters and sensitivity to the quality of climatic inputs

A second option is to calibrate each of the 21 Eastern Canadian taiga sites as well as the 5 aggregated Eastern Canadian taiga sites (Fig. 2.1) using the calibration procedure detailed in Sect. 2.2.3.1. Correlations between tree-growth observations and simulations with MAIDEN for the 1950-2000 calibration period at the Eastern Canadian taiga sites are good and significant for all the climatic datasets (Fig. 2.4a). Correlations are in general slightly higher for the higher-resolution datasets (NRCAN (5 arcmin) and GMF (1°) datasets, with an average correlation of 0.62 and 0.65, respectively compared with 0.57 for 20CRv2c (2°) and 0.61 for 20CRv2c corr. (2°)). At the aggregated sites (Fig. 2.5a), correlations for each dataset increase a little bit compared to the average of individual correlations but the general picture is the same. The bias correction (20CRv2c corr. (2°)) can slightly improve correlations for the 20CRv2c (2°) climatic dataset in some cases (e.g. WL42 and WROZM). Consequently, those results do not indicate that using higher-resolution datasets effectively increase correlations. This is likely due to the calibration procedure that might be able to compensate for specific biases in each climatic dataset. This implies large variations of calibrated parameters between experiments (Fig. B.2 and B.3), questioning the robustness of the selected values. The calibration method can also compensate potential biases of tree-ring observations and of sampling procedures, which have important impacts on long-term decadal trends (e.g. biases due to disturbance origin and tree selection criteria) [Johnson and Abrams, 2009; Gennaretti et al., 2014a; Duchesne et al., 2019].

Many potential biases of tree-ring observations due to the specific physiology of selected trees – that may not be representative of forest processes – and the chronology building process exist that may dampen the comparison with what MAIDEN simulates, i.e forest carbon accumulation and not forest demographic processes [Johnson and Abrams, 2009; Duchesne et al., 2019]. Ideally, considering those biases, we should find a better way to transform tree-ring data in time series with meaningful units to improve model–data comparisons. For example, Gennaretti et al. [2018] compute a wood biomass production index, which is closer to what MAIDEN simulates. This implies that we have access to both tree-ring width and density measurements.

Pearson correlation coefficients between TRW observations and tree-growth index simulations by MAIDEN for the 1900-2000 calibration period (Fig. 2.4b) are in most cases lower than those of the 1950-2000 calibration period. The bias correction can slightly improve correlations in some cases but the latter stay smaller. At the aggregated sites (Fig. 2.5b), correlations for each dataset decrease slightly compared to the mean of individual correlations. The low correlation for the whole 20th century can be explained by the large uncertainty of the 20CRv2c (2°) cli-

matic dataset before 1950 there, as measured by the large spread of the 20CRv2c ensemble spread at that time (Fig. B.4).

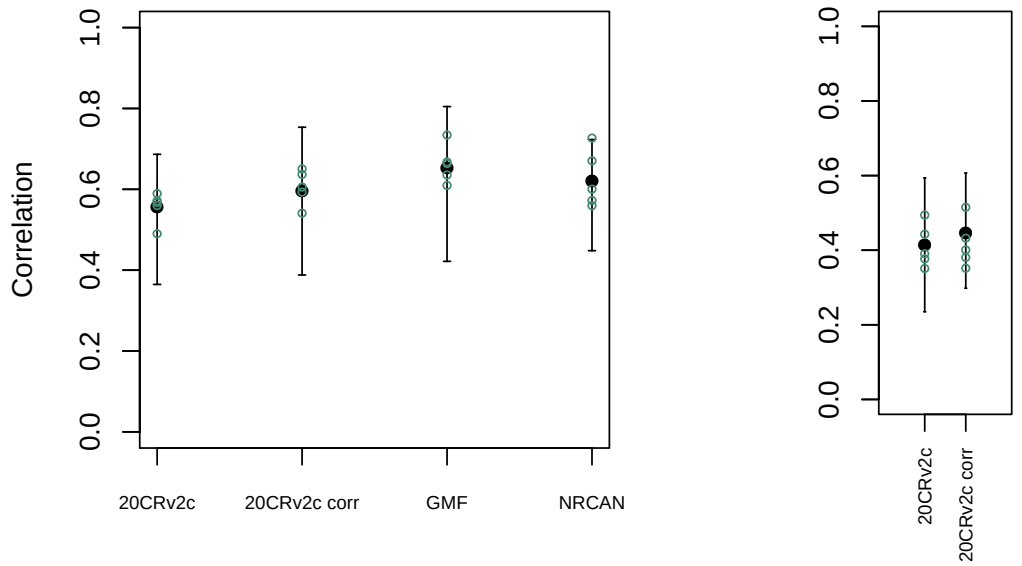


(a) 1950-2000 **(b)** 1900-2000

Figure 2.4: *Pearson correlation coefficients between tree-growth observations and simulations at the Eastern Canadian taiga sites (Fig. 2.1a) with MAIDEN using the different climatic datasets described in Table 2.2 as inputs for the 1950-2000 (a) and 1900-2000 (b) calibration periods. White inner circles stand for non-significant correlations (p-value > 0.05). Here, all circles are plain because correlations are all significant.*

When applying the parameters calibrated using the highest resolution dataset, NRCAN (5 arcmin), as climatic inputs to the Eastern Canadian taiga sites driven by the 20CRv2c (2°) dataset (Fig. 2.6, right, in red), correlations are on average much lower. Mean correlation is 0.17 in that case compared to 0.57 when the parameters are calibrated using 20CRv2c (2°) as climatic inputs. With the 20CRv2c corr. (2°) dataset as climatic inputs – i.e. the low-resolution dataset corrected for bias in the mean seasonal cycle – (Fig. 2.6, left, in red) we see that the performance of the MAIDEN model when applying NRCAN (5 arcmin) parameters is less good compared to the case when the parameters are calibrated using 20CRv2c corr. (2°) as climatic inputs (in black). Nevertheless, correlations are far better than with 20CRv2c (2°) (Fig. 2.6, right, in red). Indeed, the mean correlation is 0.36 when applying NRCAN (5 arcmin) parameters and 0.61 when applying 20CRv2c corr. (2°) parameters. Consequently, the bias correction of the 20CRv2c (2°) increases the robustness of the calibration of the MAIDEN parameters. Additionally, this shows that the MAIDEN model parameter calibration is highly sensitive to the quality of the climatic dataset used as inputs.

At the aggregated sites (Fig. 2.7), the general picture is the same but with far lower correlations. The mean correlations are 0.07 when applying the parameters calibrated using NRCAN (5 arcmin) to the aggregated sites driven by 20CRv2c (2°) dataset and 0.56 when the parameters are calibrated using 20CRv2c (2°). With the



(a) 1950-2000 **(b)** 1900-2000

Figure 2.5: *Pearson correlation coefficients (aggregated Eastern Canadian taiga sites (Fig. 2.1b), green circles), and mean and range of correlations (individual Eastern Canadian taiga sites used in aggregation (Fig. 2.1a and b), in black) between tree-growth observations and simulations with MAIDEN using the different climatic datasets described in Table 2.2 as inputs for the 1950-2000 (a) and 1900-2000 (b) calibration periods.*

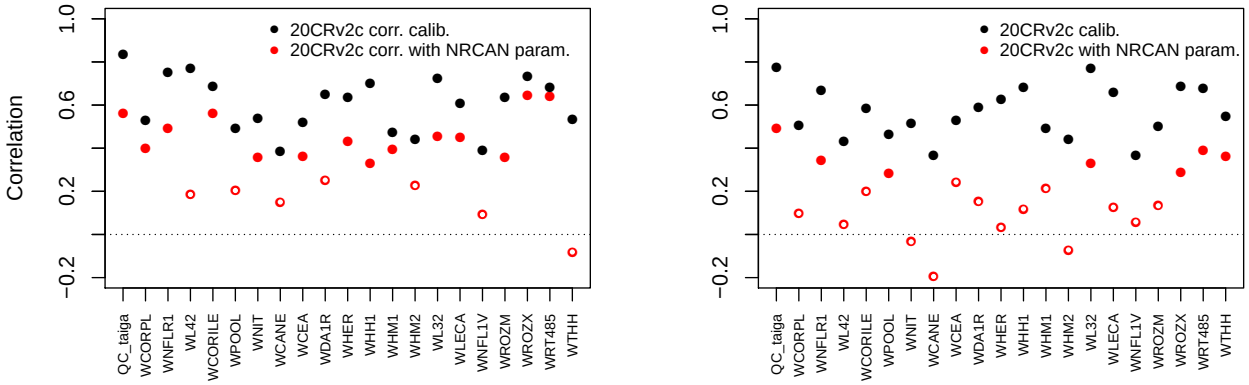


Figure 2.6: *Pearson correlation coefficients between tree-growth observations and simulations at the Eastern Canadian taiga sites (Fig. 2.1a) with MAIDEN using the 20CRv2c corr. (2°) (left) or 20CRv2c (2°) (right) climatic dataset for the 1950-2000 period with parameters calibrated using NRCAN (5 arcmin) (with NRCAN param.) climatic inputs and with parameters calibrated using 20CRv2c corr. (2°) (left) or 20CRv2c (2°) (right) (calib.) climatic inputs (Table 2.2). White inner circles stand for non-significant correlations (p-value > 0.05).*

20CRv2c corr. (2°) dataset as climatic inputs, mean correlations are respectively 0.18 and 0.61 with NRCAN (5 arcmin) and 20CRv2c corr. (2°) parameters. Those results would require a case-by-case analysis as it seems that higher replication does not provide better performance in this specific experiment.

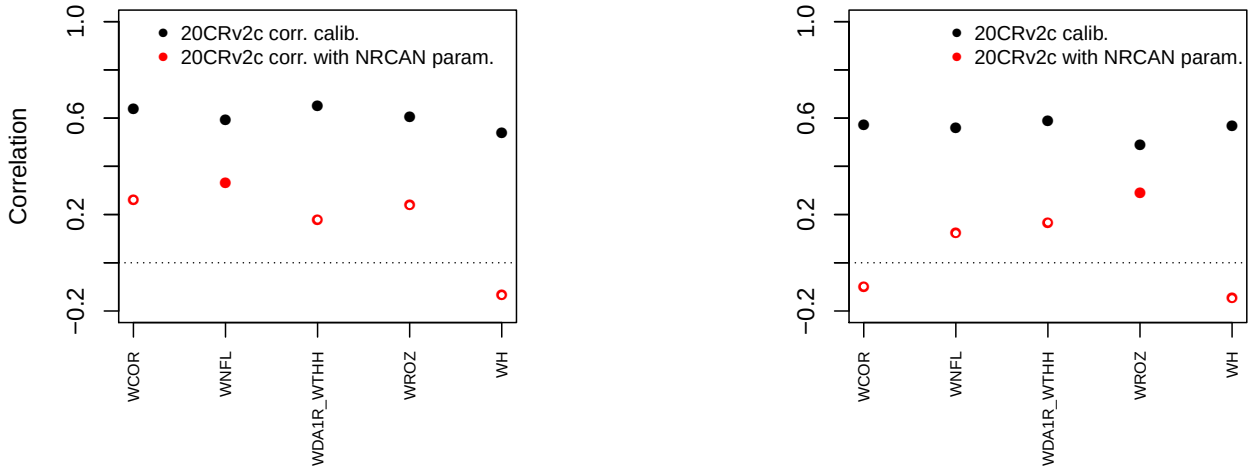


Figure 2.7: *Pearson correlation coefficients between tree-growth observations and simulations at the aggregated Eastern Canadian taiga sites (Fig. 2.1b) with MAIDEN using the 20CRv2c corr. (2°) (left) or 20CRv2c (2°) (right) climatic dataset for the 1950-2000 period with parameters calibrated using NRCAN (5 arcmin) (with NRCAN param.) climatic inputs and with parameters calibrated using 20CRv2c corr. (2°) (left) or 20CRv2c (2°) (right) (calib.) climatic inputs (Table 2.2). White inner circles stand for non-significant correlations (p-value > 0.05).*

2.3.3 Regional calibration of MAIDEN

At last, we apply the parameters calibrated against the mean of TRW observations from the 20 Eastern Canadian taiga sites (Fig. 2.8) to the 5 aggregated sites (Fig. 2.8, right) and to the individual sites used in the aggregation procedure (Fig. 2.8, left). For this experiment, we use the NRCAN (5 arcmin) climate data (Sect. 2.2.2.2, Table 2.2) averaged over individual sites for each aggregated site (Table 2.1). The main parameters linked to site conditions and control parameters (Table B.1) are fixed to their mode (soil parameters), mean (site latitude, elevation and isohyet, station elevation and isohyet) or common value (*exp_site*, slope and aspect parameters). Overall, correlations between TRW observations and simulations by MAIDEN with parameters calibrated based on the mean of the observed TRW time series are low and non-significant for the individual sites (Fig. 2.8, left). At the more replicated aggregated sites (Fig. 2.8, right), correlations between TRW observations and simulations get better with three significant correlations out of 5 sites. However, this result should be viewed in parallel with the individual correlations (Fig. 2.8, left) and sites implied in the aggregation (Table

2.1). Indeed, aggregated sites with higher correlations are made up of individual sites with higher correlations as well. This means that probably not only higher replication is at the origin of higher correlations for most aggregated sites but also the specific conditions at each individual site as well as site ecological history, as previously mentioned (Sect. 2.3.1).

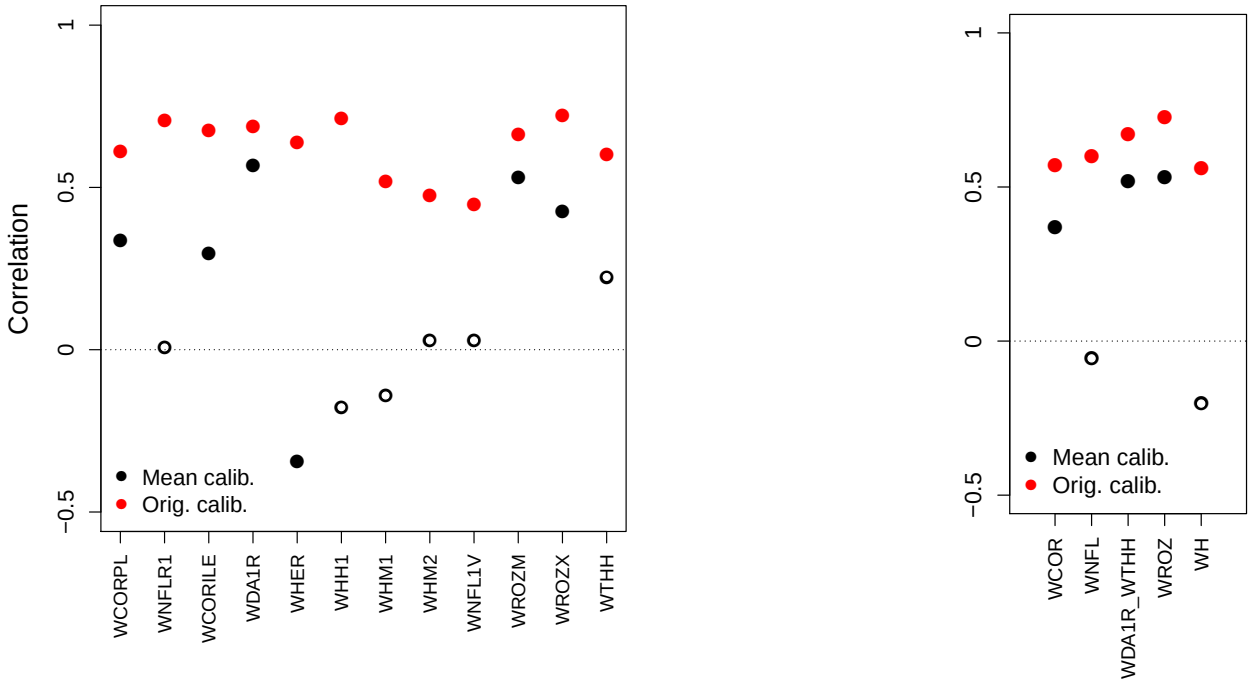


Figure 2.8: *Pearson correlation coefficients between tree-growth observations and simulations at the individual (left) and aggregated Eastern Canadian taiga sites (right) (Fig. 2.1a and b) with MAIDEN using the NRCAN (5 arcmin) climatic dataset (Table 2.2) with site-specific calibration of the parameters (Orig. calib., in red) and with parameters calibrated based on the mean of the observed TRW time series (Mean calib.) for the 1950-2000 period. White inner circles stand for non-significant correlations (p-value > 0.05).*

2.3.4 Split-sample validation of MAIDEN calibration

Depending on the available years, we have selected different time periods at the European sites (Table 2.4) and at the aggregated Eastern Canadian taiga sites (Table 2.5), using each period once for the calibration and once for the validation. At the European sites, 25 years is clearly a period of time that is too short to get robust results, while the validation is generally successful for the longer period as indicated by the significant correlations – except in one case – (Table 2.4). Similarly, at the aggregated Eastern Canadian sites – where we only have 50 years of reliable climate data (see Sect. 2.3.2) – , a 25-year subperiod is not enough for a robust calibration and validation (Table 2.5). However, even on the long time period (Table 2.4), we can see a clue of some overfitting, especially at the

SWIT179 site, where the correlation for the validation period is far lower compared to the correlation for the calibration period. Those results show that because of the large number of parameters, the validation of MAIDEN is difficult. It requires long observation series, but the skill of the model still decreases significantly for the validation period.

Table 2.4: *Pearson correlation coefficients between tree-growth observations and simulations at the European sites (Fig. 2.2) with MAIDEN and VS-Lite using GHCN as climatic inputs (Table 2.2) for the 1950-1974 and 1975-2000 and for the 1910-1949 (EALP, SWIT179) or 1909-1944 (FINL045) and 1950-2000 calibration and validation periods and vice versa. Asterisks stand for significant correlations (p-value < 0.05).*

European sites	Model	1950-1974		1975-2000	
		Calibration	Validation	Calibration	Validation
EALP	MAIDEN	0.831*	0.443*	0.886*	0.546*
	VS-Lite	0.629*	0.618*	0.603*	0.599*
SWIT179	MAIDEN	0.744*	0.284	0.783*	0.325
	VS-Lite	0.260	0.181	0.435*	0.396*
FINL045	MAIDEN	0.827*	0.0358	0.610*	0.135
	VS-Lite	0.415*	0.209	0.271	0.143
		1910-1949 or 1909-1944		**1950-2000**	
		Calibration	**Validation**	**Calibration**	**Validation**
EALP	MAIDEN	0.880*	0.626*	0.856*	0.569*
	VS-Lite	0.491*	0.487*	0.656*	0.656*
SWIT179	MAIDEN	0.721*	0.163	0.659*	0.306*
	VS-Lite	0.490*	0.489*	0.350*	0.353*
FINL045	MAIDEN	0.751*	0.428*	0.670*	0.394*
	VS-Lite	0.320	0.304	0.315*	0.263

2.3.5 Comparison with VS-Lite

On average, over the 1950-2000 calibration period at the individual Eastern Canadian taiga sites, VS-Lite has lower correlations for the highest-resolution dataset (NRCAN) compared with MAIDEN, i.e. 0.106 and 0.62 mean correlations for VS-Lite and MAIDEN, respectively (Fig. 2.9). Results for the other climatic datasets over the 1950-2000 period (GMF (1°), 20CRv2c (2°) and 20CRv2c corr. (2°)) and over the 1900-2000 calibration period (20CRv2c (2°) and 20CRv2c corr. (2°) cli-

Table 2.5: *Pearson correlation coefficients between tree-growth observations and simulations at the aggregated Eastern Canadian sites (Fig. 2.1b) with MAIDEN using NRCAN (5 arcmin) as climatic inputs (Table 2.2) for the respectively 1950-1974 and 1975-2000 calibration and validation periods and vice versa. Asterisks stand for significant correlations (p-value < 0.05).*

Canadian sites	1950-1974		1975-2000	
	Calibration	Validation	Calibration	Validation
WCOR	0.693*	0.146	0.783*	0.589*
WNFL	0.619*	0.103	0.804*	0.429*
WDA1R_WTHH	0.480*	0.737*	0.610*	0.332
WROZ	0.674*	0.577*	0.841*	0.270
WH	0.549*	0.008	0.718*	-0.011

matic datasets) also show lower correlations compared to MAIDEN (Fig. B.5). As for split-sample validation over the long time period, the performance of VS-Lite is more stable (less fall of validation from calibration correlation) compared with MAIDEN (Table 2.4) even if correlations are, except for SWIT179, lower than MAIDEN. Similarly, over the short time period, the performance of VS-Lite is less good than over the long time period but still more stable than MAIDEN (Table 2.4). Compared to VS-Lite, MAIDEN has shown lower skill over short-time-period validation, which indicates that we should only use MAIDEN when a long enough period is available for validation. As for a long validation period, MAIDEN has shown a stronger decrease in correlations compared to VS-Lite but still with higher correlations than VS-lite on average. This would indicate that the MAIDEN calibration is not always prone to overfitting.

As our objective is to provide a first test of our calibration methodology using only a few sets of tree-ring sites, the obtained results only give an incomplete view of the MAIDEN model performance and its comparison with VS-Lite, focussing over a limited range of climate regimes. More experiments in different conditions are required in the future to exhaustively evaluate and compare the performance of both models.

2.4 Conclusions

In this paper we have tested the applicability of the ecophysiological tree-growth model MAIDEN for potential dendroclimatological applications during the 20th century at 21 Eastern Canadian taiga sites and 3 European sites using tree-ring width

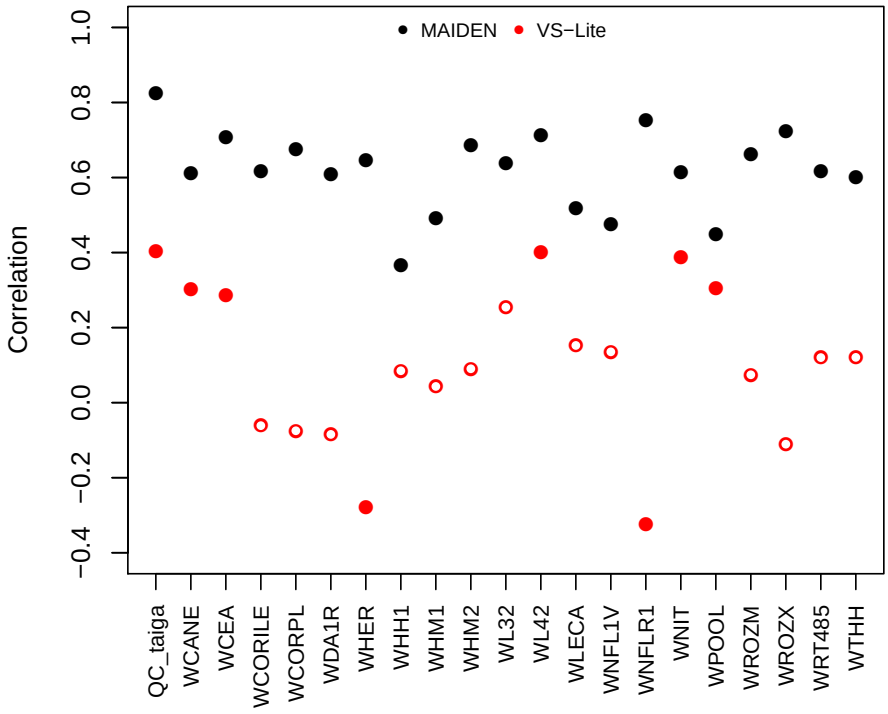


Figure 2.9: *Pearson correlation coefficients between tree-growth observations and simulations at the Eastern Canadian taiga sites (Fig. 2.1a) with VS-Lite (in red) and MAIDEN (in black) using NRCAN (5 arcmin) as climatic inputs (Table 2.2) for the 1950-2000 calibration period. White inner circles stand for non-significant correlations (p-value > 0.05).*

observations. Our results provide a protocol for the application of MAIDEN to potentially any site with tree-ring width data in the extratropical region, i.e. from climatic data selection to validation, through automatized Bayesian calibration of the most sensitive parameters. As the ultimate goal is to use MAIDEN in a context of paleoclimatic reconstruction, forced by low-resolution climate models outputs, we also analysed the sensitivity of the model to parameter calibration and to the quality of climatic inputs. The performance of MAIDEN was compared to the one of a simple tree-growth model, VS-Lite, to evaluate the advantages of using a complex tree-growth model for past climate reconstruction.

Different strategies have been tested to select the value for the most sensitive parameters of the MAIDEN model. When applying calibrated parameters from a well-documented site at other sites with the same species and similar environmental conditions, very low correlations between tree-ring width observations and simulations by the MAIDEN model are found. However, when removing the long-term trend to account for the past disturbance history of these sites that is not represented in MAIDEN, correlations get higher. In the future, this strategy can be used by selecting sites carefully to avoid disturbances. At our study sites, the Bayesian

calibration of the most sensitive parameters of the model can provide good and significant correlations between tree-growth observations and simulations.

Secondly, sensitivity of the MAIDEN model parameter calibration to the quality of the climatic data used as inputs has been highlighted. In a context of paleoclimatic applications, where MAIDEN will be driven by climate model outputs at low resolution, bias correction and downscaling techniques could be good options to improve climate inputs and calibration quality, thereby leading to reasonable correlations with observed tree-ring width.

Our split-sample validation experiments are encouraging. However, when a calibration interval of only a few decades is available, the calibration displays large overfitting for individual sites as indicated by the very low correlation with observations over the validation period. Similar split-sample experiments on longer series show much better results, with potentially some overfitting but still with relatively high and generally significant correlations over the validation period. When working with a network of similar sites, the alternative validation technique, i.e. applying calibrated parameters from the mean of a network of tree-ring width observation series with the same species and environmental conditions to the individual sites, should be preferred if not enough data (climate and TRW observations) are available for split-sample validation.

Lastly, at our study sites, MAIDEN has shown higher calibration and validation correlations in most cases compared to VS-Lite. VS-Lite correlations over the calibration period are especially far lower for sites with low replication (i.e. the Eastern Canadian taiga sites from Nicault et al., 2014, and Boucher et al., 2017). However, VS-Lite stays more stable over both calibration and validation periods. Consequently, VS-Lite has a lower ability to reproduce tree growth at our sites but is less prone to overfitting than MAIDEN. Most importantly, we have shown that to limit overfitting, MAIDEN should not be used with short and low-replicated tree-ring width observation time series. VS-Lite is less risky to use in such situations as there is potentially less overfitting in the calibration and probably easier to apply over a large network of tree-ring width time series. However, VS-Lite does not include CO_2 nor biological processes and may thus not be able to take into account changes in conditions between the recent calibration period and the more distant past.

In the future, MAIDEN will be applied at a larger spatial scale in a systematic way, using the protocol that has been developed here, by selecting hundreds of sites from the commonly used databases in paleoclimate reconstruction based on tree-ring proxies, covering a wide range of environmental conditions and tree species, such as PAGES2k [PAGES 2k Consortium, 2017] and NTREND [Wilson et al., 2016; Anchukaitis et al., 2017]. This broader analysis will allow us to refine the protocol developed here in order to identify the sites where MAIDEN can

be successfully applied and estimate the uncertainty associated with the use of MAIDEN for many more different sites.

Although some limitations could remain in our calibration protocol, we have shown the ability of MAIDEN to simulate tree-growth index time series that can fit robustly tree-ring width observations under certain conditions (well-replicated tree-ring width observation time series, high-resolution or downscaled climate data, long time period), as well as its potential to be used as a complex mechanistic proxy system model in paleoclimatic applications and more specifically in data assimilation.

3

Testing the performance of dendroclimatic process-based models at global scale with the PAGES2k tree-ring width database

Abstract

Tree-rings are one of the most commonly used proxies for reconstructing past climates at annual resolution. The climate information is generally deduced from tree-rings using statistical relationships, but the assumed linearity and stationarity may be inadequate. Process-based models allow for non-stationarity and non-linearity; however, many challenges are associated with their application for global scale reconstructions. In this study, we aim to test the feasibility of using the mechanistic model MAIDEN at the global scale for paleoclimate reconstructions based on data assimilation by applying it to the PAGES2k tree-ring width database. We also compare its performance with the simpler model VS-Lite, often used in global applications. Both models are skillful in terms of calibration and verification correlations for a similar number of sites (63 and 64 for VS-Lite and MAIDEN, respectively). VS-Lite tends to perform better for sites where the climate signal in tree-rings is strong and clear. By contrast, MAIDEN's performance is likely mostly limited by the lack of data (for example, daily Gross Primary Production data or phenological timings) needed to accurately calibrate the model. However, when the calibration is robust, both models reproduce well the observed link between climate and tree-growth. In general, VS-Lite tends to overestimate the climate signal in tree-rings compared to MAIDEN, which better reproduces the magnitude of the climate signal on average. Our results show that both models are complemen-

This chapter is based on: Rezsöhazy, J., Gennaretti, F., Goosse, H., Guiot, J. (2021). Testing the performance of dendroclimatic process-based models at global scale with the PAGES2k tree-ring width database, *Climate Dynamics*, **57**, 2005-2020, https://doi.org/10.1007/s00382-021-05789-7. Supplementary materials are in Appendix C.

tary and can be applied at the global scale to reconstruct past climates using an adequate protocol designed to exploit existing tree-ring data.

3.1 Introduction

Studying past climates prior to the instrumental period requires the use of indirect records of climate variations from natural archives, commonly referred to as proxies [Jones et al., 2009]. Different projects and consortia have emerged in recent years to improve global climate reconstructions using the development of global multi-proxy databases spanning last millennium [PAGES 2k Consortium, 2013; Wilson et al., 2016; Anchukaitis et al., 2017; PAGES 2k Consortium, 2017; Tardif et al., 2019; Konecky et al., 2020]. Among available records, tree-rings are one of the most commonly used proxies for reconstructing past climates at high temporal (annual) resolution, due to their large spatial coverage and availability [Fritts, 1976; Jones et al., 2009; Mann et al., 2009; Wilson et al., 2016; Anchukaitis et al., 2017; Esper et al., 2018; Anderson et al., 2019; St. George and Esper, 2019].

To make the link between climate and indirect observations of paleoclimate variations from proxies, proxy system models (PSMs; i.e. models that simulate the development of measured variables, for example tree-ring width, in response to a climate forcing; Evans et al., 2013; Dee et al., 2016) must be used. Such models can be applied in the forward mode, for example to compare proxy data directly with climate model simulations when these simulations are used as inputs of the PSM. In the inverse mode, PSMs can reconstruct the climate variations that produce the measured variables [Guiot et al., 2000; Evans et al., 2013].

In the case of tree-growth proxy data (such as tree-ring width, hereafter TRW, or density), the climate information is generally deduced on the basis of a statistical relationship calibrated over the instrumental period [Fritts, 1976; Cook and Kairiukstis, 1990; Fritts, 1991; Jones et al., 1998; Mann et al., 1999, 2008]. Therefore, many climate reconstructions of the period covered by dendroclimatic data have been developed with linear regressions between climate variables and proxy records [Fritts, 1991; Jones et al., 1998; Mann et al., 1999, 2008]. This raises concern about the assumed linearity and stationarity of the relationship deduced from the calibration [Briffa et al., 1998b; Wilson and Elling, 2004; Wilson et al., 2007; D'Arrigo et al., 2008; Guiot et al., 2014]. A complementary approach that has been expanded over the past decade is data assimilation, which combines information from the physics of the system included in climate models and indirect climate observations provided by proxy data, such as TRW [e.g. Goosse et al., 2012; Franke et al., 2017; Steiger et al., 2018; Tardif et al., 2019]. So far, the studies using tree-ring proxy data with data assimilation have focused on the use of statistical PSMs (i.e., univariate or multiple linear regressions) to provide a large-scale reconstruction over the past millennia [e.g. Tardif et al., 2019].

As a complement to statistical methods, the link between climate and tree-ring proxy data can be established from process-based PSMs. Mechanistic modelling of tree-growth dependency on climate explicitly states the processes that govern the relationship between climate and tree-growth and allows for non-stationarity and non-linearity [Guiot et al., 2014]. While in regression-based PSMs, tree-growth is assumed to be only dependent on the chosen climate target variables, mechanistic modelling introduces the influence of other climate variables, for example atmospheric CO_2 concentration. Additionally, tree-ring-based reconstructions are often limited to sites where tree-growth is driven by one limiting climatic factor. Yet, process-based tree-growth models are able to extract a climate signal from tree-rings at sites where tree-growth is driven by multiple climatic factors. Accordingly, they may expand the area of dendroclimatic reconstructions to a wide range of regions away from extreme growth environments [Breitenmoser et al., 2014; Babst et al., 2018]. To date, such models have only been used for local reconstructions [e.g. Boucher et al., 2014]. While global scale reconstructions are theoretically possible with a data assimilation procedure including a process-based PSM, such models have only been applied in a pseudo-proxy context [Dee et al., 2016; Acevedo et al., 2017; Steiger and Smerdon, 2017]. A further step would be to introduce such mechanistic models in the data assimilation procedure using actual proxy data to possibly improve the quality of the reconstruction.

However, many challenges are associated with the use of process-based tree-ring PSMs for global scale reconstructions. In particular, the inclusion of complex biological processes, for example photosynthesis and carbon allocation, usually implies a cautious initialization and calibration of the model at each particular site of interest, depending on the site environment or the tree species. This information is not readily available at global coverage with the necessary detail. Running and calibration time of such models can also be an obstacle to their utilization.

Among the many available process-based dendroclimatic models, the Vaganov-Shashkin-Lite model (VS-Lite; Tolwinski-Ward et al., 2011) has been used in several paleoclimate studies [Breitenmoser et al., 2014; Lavergne et al., 2015; Dee et al., 2016; Steiger and Smerdon, 2017; Seftigen et al., 2018; Fang and Li, 2019]. The model is not considered as fully mechanistic. Indeed, VS-Lite does not include any explicit representation of tree-growth processes, but relies instead on the principle of limiting factors (soil moisture and temperature; Tolwinski-Ward et al., 2011) to mimic the response of tree-ring growth to climate conditions. The model has faced difficulties in simulating tree-growth where the dependence on climate is not dominated by one limiting factor, such as precipitation or temperature [Breitenmoser et al., 2014].

Process-based dendroclimatic models that describe more mechanistically the response of proxy data to climate could overcome those limitations. Among the complex mechanistic models [e.g. Misson, 2004; Dufrêne et al., 2005; Vaganov

et al., 2006; Drew et al., 2010], we will focus here on the model MAIDEN (Modelling and Analysis In DENdroecology; Misson, 2004) that explicitly includes biological processes and has the potential to be applied at the global scale. Unlike VS-Lite, MAIDEN also takes into account atmospheric CO_2 concentration as an input, allowing the user to consider the non-stationary dependency of tree-growth on the recent exponential increase of CO_2 concentration [Myhre et al., 2013; Boucher et al., 2014]. Another important difference between MAIDEN and VS-Lite is the theoretical basis of the models. VS-Lite is a "sink" model in the sense that it only considers the climate constraints on tree-rings (the carbon sink tissues at the tree-level; see Körner, 2015; Fatichi et al., 2014, 2019). MAIDEN is a "source-sink" mechanistic model in the sense that it first determines the carbon availability by modelling photosynthesis, and second, it allocates the available carbon to the sink tissues based on allocation and climate-dependent rules. Feedbacks between allocation and photosynthesis are also considered in MAIDEN. So far, MAIDEN has been applied to the European temperate forests [Misson, 2004; Boucher et al., 2014], to the Mediterranean forests [Gea-Izquierdo et al., 2015, 2017], to the eastern Canadian taiga [Gennaretti et al., 2017] and to Argentine forests [Lavergne et al., 2017]. However, unlike VS-Lite, MAIDEN has not been applied at the global scale yet, due to its level of complexity. In particular, the need for daily climate data at high spatial resolution and for measurements of ecophysiological variables to calibrate the model parameters represents the main limitation for its systematic application in different regions. In Rezsöhazy et al. [2020], a protocol has been developed to calibrate and apply MAIDEN automatically at any site globally that contains TRW observations in the extratropical regions.

To date, the new protocol applying MAIDEN globally has not been demonstrated. To this end, this study highlights the advantages and potential limitations of using a process-based model like MAIDEN at the global scale. In the future, such mechanistic PSM could be utilized for paleoclimate reconstructions based on data assimilation. Specifically, we perform a comparative analysis of the performance of the simpler VS-Lite and the more complex MAIDEN process-based models. Both models have been applied over the last century to the global TRW data network of PAGES2k [PAGES 2k Consortium, 2017], including 354 TRW records. Studies such as this which lend insight into the mechanisms controlling tree-ring width and tree-growth elevate our ability to extract meaningful climate information from tree-ring networks. This information is required to improve our understanding of natural and forced decadal climate variability, and to potentially improve reconstructions of past climate variability.

First, we describe MAIDEN and VS-Lite in Sect. 3.2.1, as well as the TRW data network (Sect. 3.2.2) and climate data (Sect. 3.2.3) used in this study. The calibration (Sect. 3.2.4) and verification (3.2.5) procedure of both models is then presented. The models are calibrated and applied to the PAGES2k TRW data-

base in Sect. 3.3.1. We provide explanations on the performance of the models in Sect. 3.3.2. The ability of MAIDEN and VS-Lite to reproduce the climate signal in tree-rings is then evaluated in Sect. 3.3.3 and, finally, the implications of including atmospheric CO_2 concentration as an input of MAIDEN are assessed in Sect. 3.3.4.

3.2 Material and methods

3.2.1 Tree-growth models

3.2.1.1 MAIDEN

MAIDEN [Misson, 2004; Gea-Izquierdo et al., 2015; Gennaretti et al., 2017] is a complex tree-growth model that explicitly includes biological processes (photosynthesis and carbon allocation to different tree compartments) to simulate, among other outputs, the annual quantity of carbon allocated to the stem. This key variable is hereafter referred to as Dstem, in grams of carbon per square meter of stand per year. In this study, Dstem is assumed to be proportional to tree-ring growth so as to compare it with TRW observations. The model runs on a daily basis with maximum and minimum air temperature, cumulative precipitation and atmospheric CO_2 concentration as inputs.

In this study, we use a combined version of the model from Gea-Izquierdo et al. [2015] (initially developed for Mediterranean forests; hereafter GI2015) and Gennaretti et al. [2017] (initially developed for boreal tree species; hereafter Ge2017) developed by Fabio Gennaretti (unpublished) that gives the possibility to switch between those two versions. The versions from GI2015 and Ge2017 only differ in some mechanistic rules used in the photosynthetic and allocation modules, but they are identical otherwise. The structure of the MAIDEN model is provided online (`https://figshare.com/articles/MAIDEN_ecophysiological_forest_model/5446435/1`, last access: 16 May 2020) and its modules are available upon request.

The model includes constants to describe the conditions at the tree-ring observations site and the climate station (Table C.1). As in Rezsöhazy et al. [2020], the constants are derived from observations. However, slope and aspect constants are set to zero, as we do not have the field knowledge needed to extract the information from a Digital Elevation Model. MAIDEN includes a four-layer soil module (1-15cm; 15-30cm; 30-65cm; 65-100cm) for which we have to provide the main characteristics (clay and sand fractions; Table C.1). The soil characteristics are obtained from the Harmonized World Soil Database (hereafter HWSD) v1.2 at a 30 arc-second spatial resolution [FAO/IIASA/ISRIC/ISSCAS/JRC, 2012], as in Rezsöhazy et al. [2020].

3.2.1.2 VS-Lite

The Vaganov-Shashkin Lite model [Tolwinski-Ward et al., 2011] is a simple tree-growth model that simulates a unitless annual tree-growth increment based on latitude, monthly cumulative precipitation and average temperature of the study site as inputs. It is based on the limiting factors principle (temperature and soil moisture) and on the use of threshold growth response functions. VS-Lite is derived from the full process-based Vaganov-Shashkin model [Vaganov et al., 2006] that has been developed to explicitly quantify the influence of climate and environmental variables on tree-ring formation. While the full model is a two-block model, i.e. a block with cell growth, division and multiplication in the cambium and a growth block based on the limiting factor principle, the Lite version just uses the second block.

3.2.2 PAGES2k tree-ring width data

The PAGES2k working group aims to reconstruct the climate of the last two millennia based on proxy records [PAGES 2k Consortium, 2017]. Their community database contains 692 temperature-sensitive proxy records from different archives (trees, ice, sediment, coral, speleothems, documentary evidence, and other archives), among which 354 TRW time series are of interest for our work [PAGES 2k Consortium, 2017]. We were able to retrieve the species information needed to run MAIDEN at 307 sites. Time series ending before 1979 were excluded to allow for a long enough calibration period (at least 30 years starting from 1950, Sect. 3.2.4), leaving 302 TRW time series for our analysis (Fig. 3.1). The resulting TRW network covers a large range of environmental conditions and tree species (evergreen and deciduous), but is mostly located in the Northern Hemisphere, specifically in North America and Asia. As a consequence, the TRW network is dominated by cold and dry sites (Fig. C.1). The tree-ring proxy records in the PAGES2k database have been specifically selected for their local sensitivity to temperature [PAGES 2k Consortium, 2017]. However, correlations with other environmental variables can be significant as well, for example with precipitation, and a gradient of environmental sensitivity is thus obtained (water limited sites, temperature limited sites or unclear limiting factor). This can be illustrated by the comparison of the correlations of TRW observations with annual cumulative precipitation against the correlations with mean annual temperature over 1901-2000 (Fig. C.2). A wide range of values in the correlations is observed with both variables, with the mean being slightly higher for temperature (0.07 mean correlation, compared to 0.05 for precipitation). TRW data are available online [PAGES 2k Consortium, 2017].

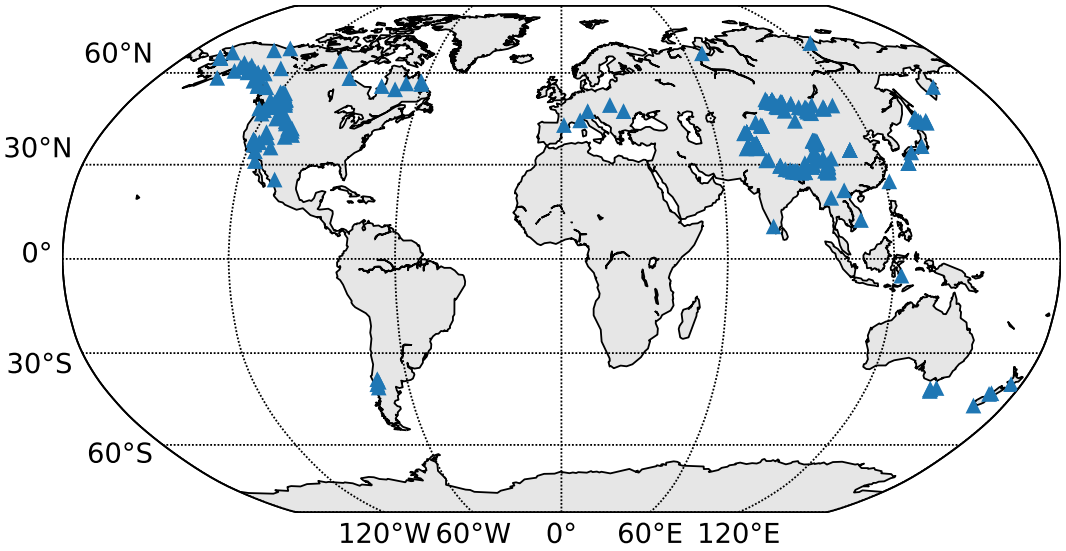


Figure 3.1: *PAGES2k [PAGES 2k Consortium, 2017] tree-ring width sites used in this study (302 sites). Background map from Hunter [2007].*

3.2.3 Climate data

Daily climatic inputs are needed to run MAIDEN (Sect. 3.2.1.1) while VS-Lite needs monthly climate inputs (Sect. 3.2.1.2). In this study, we use the *Global Meteorological Forcing Dataset for land surface modelling* (v2) (`http://hydrology.princeton.edu/data.php`, last access: 13 March 2020; Sheffield et al., 2006) at 0.5° resolution over the 1901-1949 and 1950-2000 time periods. Daily maximum and minimum temperature and daily cumulative precipitation were extracted for MAIDEN from the grid cell closest to each individual site. Daily mean temperature and cumulative precipitation were averaged and summed, respectively, for VS-Lite at a monthly time step. Annual atmospheric CO_2 concentration data are from Sato and Schmidt (`https://data.giss.nasa.gov/modelforce/ghgases/`, last access: 6 January 2020) and were linearly interpolated at a daily time step. Note that for the Southern Hemisphere climate data start in July instead of January to match the seasonality of tree-growth.

3.2.4 Calibration

3.2.4.1 MAIDEN

A protocol has been developed in Rezsöhazy et al. [2020] to calibrate MAIDEN in a systematic and automatic way following a Bayesian procedure with Markov Chain Monte Carlo sampling using the DREAMzs algorithm [Hartig et al., 2019]. Because we are working with the two versions of MAIDEN here [Gea-Izquierdo et al., 2015; Gennaretti et al., 2017], the procedure has been adapted to the ver-

sion from Gea-Izquierdo et al. [2015], that was not used in Rezsöhazy et al. [2020]. The Bayesian procedure allows for calibration of the most sensitive parameters of the model. This includes parameters influencing the simulated stand growth primary production or GPP (6 parameters in the Ge2017 version and 5 parameters in the GI2015 version) and parameters influencing the simulated daily quantity of carbon allocated to different tree compartments (12 parameters in the Ge2017 version and 13 parameters in the GI2015 version). Those parameters are referenced hereafter as photosynthesis and carbon allocation parameters, respectively. The calibration starts from prior distributions, assumed to be uniform over an acceptable range, to produce posteriors for each of the 18 calibrated parameters. It is based on the comparison between the normalized (i.e. with a null mean and a standard deviation of 1) simulated annual quantity of carbon allocated to the stem or Dstem and normalized observed TRW time series. Tables C.2 and C.3 give the definition of each calibrated parameter for both versions. The ranges of the parameters are available for both versions in Tables C.4 and C.5.

Ideally, photosynthesis parameters should be calibrated by comparing simulated against observed GPP instead of simulated Dstem against observed TRW and prior ranges would be more informative for each species or biome [Misson, 2004; Danis et al., 2012; Gea-Izquierdo et al., 2015, 2017; Gennaretti et al., 2017; Lavergne et al., 2017]. However, this is not possible here as the information is lacking for the majority of sites. Furthermore, the tree-growth index simulated by MAIDEN, which is derived from the annual quantity of carbon allocated to the stem, is not directly comparable to TRW without standardization. We are thus unable to both calibrate the variance and evaluate the error variance of tree-growth [Rezsöhazy et al., 2020]. Information is thus missing to guide the Bayesian calibration towards a biologically plausible set of parameters. For example, we miss information to properly constrain phenology. Consequently, the selection of parameters for our simulations has been slightly updated compared to Rezsöhazy et al. [2020]. The set of photosynthesis parameters with the highest posterior (Maximum *a posteriori* value or MAP; Hartig et al., 2019) is selected as in Rezsöhazy et al. [2020]. The carbon allocation parameters are then calibrated as in Rezsöhazy et al. [2020]. In addition, after the calibration procedure, the model is iteratively run over the top 10% carbon allocation parameters. The photosynthesis parameters are fixed at their calibrated values. To avoid unrealistic growth period lengths, a parameter set which simulates a growth period of less than 20 days for each year of the calibration period (hereafter, phenological criterion) is excluded. At the end of the iterations, we keep the set of parameters with the highest likelihood. Note that if none of the parameter sets meet the phenological criterion, the MAIDEN calibration is considered as non-valid for this site with the forcing used.

MAIDEN was calibrated at the TRW sites with at least 30 TRW observations available over the 1950-2000 period, using the climate data described in Sect. 3.2.3. For simplicity, the calibration period will be referred to as 1950-2000.

3.2.4.2 VS-Lite

The Bayesian approach proposed in Tolwinski-Ward et al. [2013] was used to calibrate the four VS-Lite parameters linked to the growth response (lower and upper temperature and soil moisture thresholds of the model; T_1 and T_2, and M_1 and M_2, respectively, in Tolwinski-Ward et al., 2011). This Bayesian approach is based on a standard Markov Chain Monte Carlo method to sample the posterior distribution, i.e., a Metropolis-Hastings algorithm embedded within a Gibbs sampler. Default values were given to the other parameters (six soil moisture parameters and two integration window parameters) as provided in the standard version of the model code (`https://www.ncei.noaa.gov/pub/data/paleo/softlib/vs-lite/`, last access: 16 March 2021).

VS-Lite was optimized at the 302 TRW sites over the same time period as MAIDEN and using the climate dataset described in Sect. 3.2.3.

3.2.5 Verification

Both models were tested over the 1901-1949 time period, with the same climate data as described in Sect. 3.2.3. Models were run over the verification period using the parameters calibrated over the 1950-2000 time period as in Sect. 3.2.4. Pearson correlation coefficients and their corresponding confidence levels were calculated at each site between simulated tree-ring indexes from MAIDEN or VS-Lite and observed TRW on both the calibration and the verification time periods.

3.3 Results

Section 3.3.1 assesses and compares the general performance of both VS-Lite and MAIDEN models with respect to calibration (Sect. 3.2.4) and independent verification (Sect. 3.2.5), in order to determine the sites with the best performance. Section 3.3.2 explains the performance of both models, by focusing on its relationship with different environmental characteristics, such as climate and tree leaf traits. Section 3.3.3 evaluates the ability of both PSMs to reproduce the climate signal recorded in tree-rings, and then their potential for paleoclimate reconstructions based on data assimilation. Finally, Section 3.3.4 assesses the effect of CO_2 concentration in the MAIDEN model with a sensitivity analysis.

3.3.1 Applying MAIDEN and VS-Lite to the PAGES2k TRW sites

Substantial challenges arose in the calibration of MAIDEN. In particular, at some sites, we were unable to properly set phenology due to the lack of information available for calibration (Sect. 3.2.4.1). From all 302 calibration experiments (Sect. 3.2.4.1), 113 sites for Ge2017 and 142 sites for GI2015 were excluded based on the phenological criterion (Sect. 3.2.4.1). The remaining sites (189 sites for Ge2017 and 160 sites for GI2015) will be referred to as MAIDEN selected sites. All the analyses for MAIDEN are performed on these selected sites. From all calibration (Sect. 3.2.4.1) and verification (Sect. 3.2.5) experiments for both versions [Gea-Izquierdo et al., 2015; Gennaretti et al., 2017] of MAIDEN (Figs. C.3 – C.6), we consider a site as well-fitted only if the following conditions are fulfilled, whatever the model version used: (i) a significant (at the 95% confidence level) calibration (1950-2000) and verification (1901-1949) correlation $\geq$ 0.3; (ii) a growth period length of at least 20 days for each year of the calibration (Sect. 3.2.4.1) and verification period. If conditions are fulfilled for both versions, the version leading to the highest verification correlation at the site is kept. Based on these criteria, we retained 64 well-fitted sites (Fig. 3.2a).

For VS-Lite (Sect. 3.2.4.2 and 3.2.5; Figs. C.7 and C.8), the condition for retaining a site is also to have a significant (at the 95% confidence level) calibration (1950-2000) and verification (1901-1949) correlation $\geq$ 0.3. As for MAIDEN, VS-Lite simulated time series were checked for consistency as correlation is not able to account for all artefacts in simulated chronologies. Two sites were considered as invalid since estimated tree-growth indexes were found constant (no growth) for more than 10 successive years. Based on these criteria, we retained 63 well-fitted sites (Fig. 3.2b).

Considering the loss of correlation from calibration to verification, VS-Lite appears more stable than MAIDEN (Fig. 3.3, see Fig. C.9 for by-site correlations). Calibrating MAIDEN at the global scale without overfitting is indeed a challenge. The mean calibration and mean verification correlations for MAIDEN are 0.68 (with a standard deviation of 0.10) and 0.43 (0.10) respectively, and 0.49 (0.14) and 0.43 (0.11) for VS-Lite. 18 well-fitted sites are in common between VS-Lite and MAIDEN (Fig. 3.4). On average, verification correlations are 0.47 for MAIDEN and 0.48 for VS-Lite with a standard deviation of 0.10 and 0.14 respectively. MAIDEN and VS-Lite are skillful at a similar number of mostly different sites, spread all over the globe. The reasons behind their performance are consequently also different and will be addressed in the next section. However, at the common sites, their respective performances are equivalent.

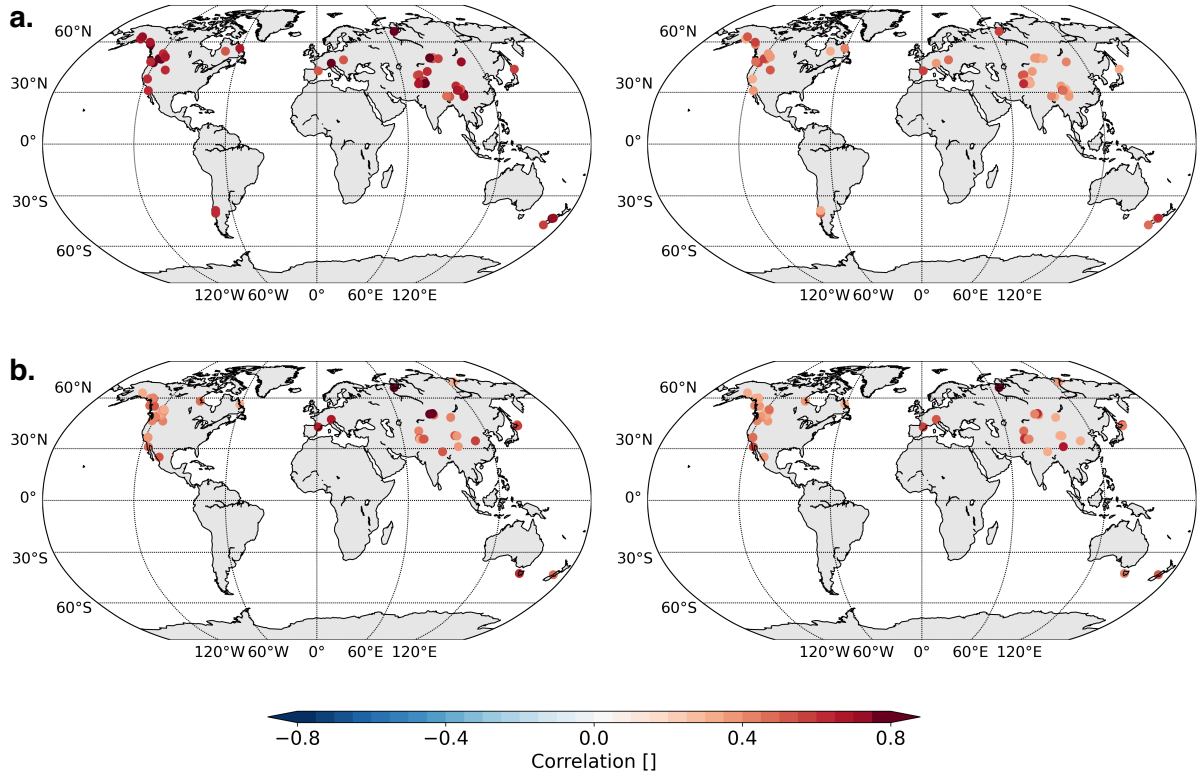


Figure 3.2: *(a) MAIDEN (64 sites) and (b) VS-Lite (63 sites) calibration (left) and verification (right) correlations for well-fitted sites (Sect. 3.3.1). All correlations are significant at the 95% confidence level. Background maps from Hunter [2007].*

3.3.2 Explaining the performance of VS-Lite and MAIDEN

In this section, we want to understand the underlying factors driving the performance of both models. We focus on two site characteristics: tree leaf traits and climate. The relationship between models performance and altitude, latitude or calibration period length (ranging from 30 to 51 years) was also checked but none of these variables were found to be a significant driver of model skill. We are here considering all calibrated sites (Sect. 3.2.4), irrespective of whether they were identified as well-fitted in the previous section or not.

Verification correlations as a function of tree leaf traits (deciduous or evergreen) are shown on Fig. 3.5 for both versions of MAIDEN and for VS-Lite. VS-Lite performance (Fig. 3.5c) does not seem to be influenced by leaf trait, with an average correlation of 0.184 and 0.221 for deciduous and evergreen trees respectively. 13 sites out of 63 well-fitted sites are deciduous which is comparable to the proportion of deciduous sites in the PAGES2k TRW database (64 deciduous out of 302 sites, i.e. around 20%). For MAIDEN (Fig. 3.5a and b), verification correlations are also very close on average for deciduous (0.073 for GI2015 and 0.101 for Ge2017) and evergreen trees (0.087 for GI2015 and 0.113 for Ge2017). However, there is a low proportion of deciduous trees for Ge2017 (Fig. 3.5b) that passes

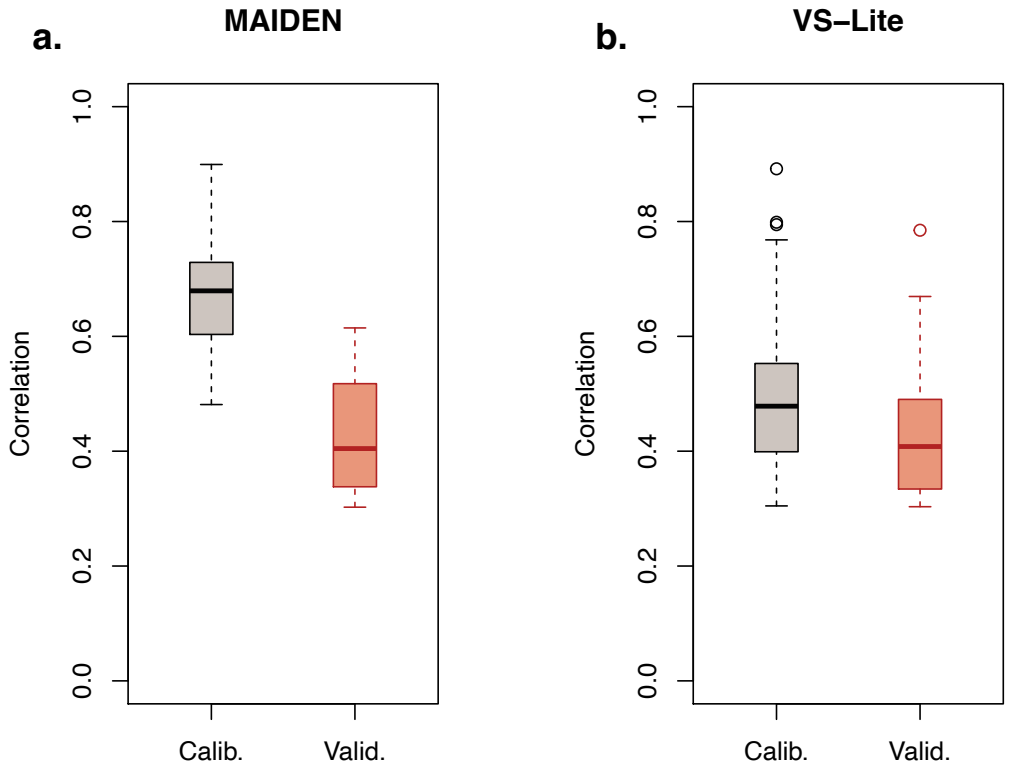


Figure 3.3: *(a) MAIDEN (64 sites) and (b) VS-Lite (63 sites) calibration (1950-2000) and verification (1901-1949) correlations (all significant at the 95% confidence level) boxplots for well-fitted sites (Sect. 3.3.1).*

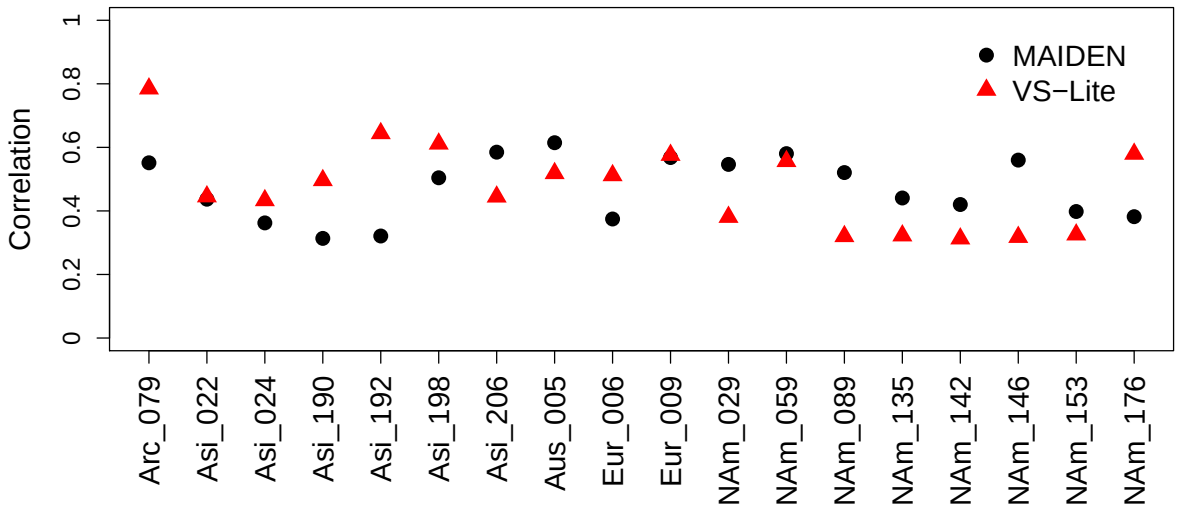


Figure 3.4: *MAIDEN and VS-Lite verification (1901-1949) correlations (all significant at the 95% confidence level) for common well-fitted sites (Sect. 3.3.1) (18 sites, with names from the PAGES2k database: NAm for North American sites; Asi for Asian sites; Eur for European sites; Arc for Arctic sites; Aus for Australian, Tasmanian or New Zealand sites; SAm for South American sites).*

the phenological criterion for the calibration described in Sect. 3.2.4.1 (9 out of 64 sites) compared to evergreen trees (180 out of 238 sites). Conversely, this proportion is far higher for GI2015 (36 sites out of 64; Fig. 3.5a) and comparable to evergreen trees (124 sites out of 238). Besides, seven sites out of 64 well-fitted sites are deciduous which is less than the proportion of deciduous sites in the PAGES2k TRW database (64 out of 302 sites). Only one deciduous well-fitted site is simulated by Ge2017, and six by GI2015. A possible reason is that only the version from Gea-Izquierdo et al. [2015] has already been applied to deciduous trees sites (*Quercus Pyrenaica*; Gea-Izquierdo et al., 2017). Consequently, we were able to use the initialization parameters already applied to deciduous trees in this version solely. The version from Gennaretti et al. [2017] has never been specifically calibrated for deciduous trees and some initialization parameters are likely not adapted in that case. This exemplifies the fact that the calibration and initialization of MAIDEN are probably the main obstacles for a better performance of the model at the global scale.

To study the influence of climate on the performance of both models, we focus on different climate indicators: cumulative October to September precipitation, annual mean temperature and mean July-August-September temperature. In general, correlations of climate indicators with verification scores at all sites are low and not significant for both VS-Lite and MAIDEN (Table C.6). This means that the performance of both models does not depend primarily on the mean climate at a site. Another hypothesis to test is whether the models perform better for sites where tree-ring growth is strongly controlled by climate. To this end, we compare the correlations between climate variables and observed TRW to the verification correlations (Table 3.1). Since none of the correlations in Table 3.1 are significant (p-value < 0.05) for MAIDEN, its performance does not rely significantly on tree-growth correlation with climate. On the contrary, VS-Lite performance shows a higher dependency on tree-growth correlation with climate, especially temperature (Table 3.1). Indeed, all correlations between the tree-growth relationship with climate and verification scores for VS-Lite are significant and particularly high for annual (0.467) and July-August-September (0.506) temperature. We obtain the same result for VS-Lite when the analysis is restricted to the MAIDEN selected sites (Sect. 3.2.4.1) (Table C.7). This dependence of VS-Lite performance to the presence of a strong climate driver of tree-growth is consistent with what has been highlighted in Breitenmoser et al. [2014]. It is likely due to the structure of VS-Lite on itself (Sect. 3.2.1.2), as tree-growth directly depends on the identified limiting climatic factor (temperature or soil moisture) at the site in the model. VS-Lite tends to be better where tree-growth is predominantly driven by climate, which can be limiting for its application in many regions of the world away from the treeline environments (for example high-altitude or high-latitude environments), often not considered for paleoclimate reconstruction [Breitenmoser et al., 2014; Babst et al.,

2018]. Conversely, in MAIDEN, multiple biological processes shape the links that exist between climate and tree-growth. This potentially brings a better suitability of MAIDEN to work in a larger range of environments than VS-Lite, where the relationship between climate and tree-growth is more complex.

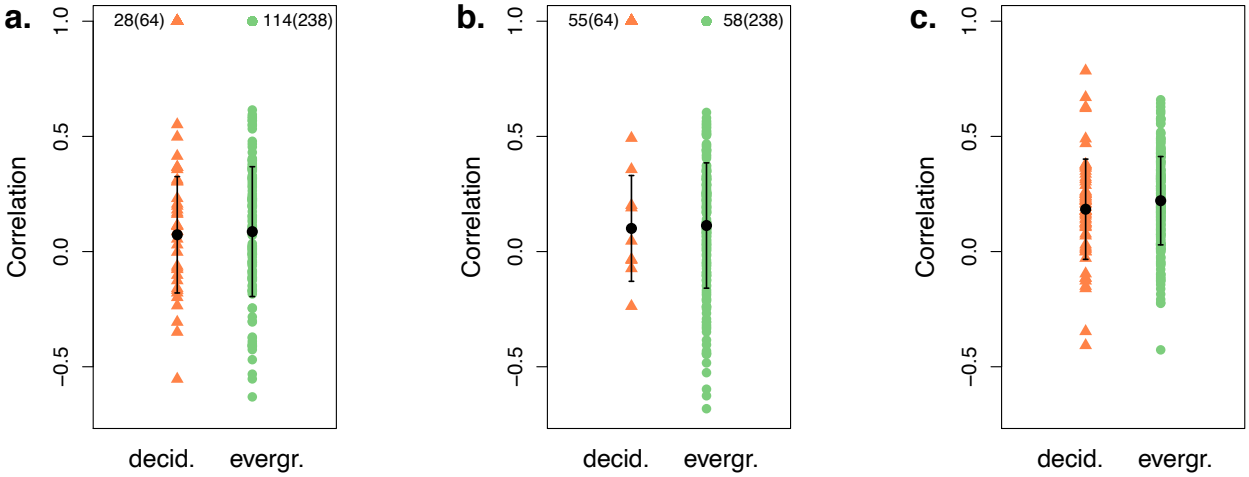


Figure 3.5: *Verification correlations, mean and standard deviation by tree types (deciduous or evergreen) for the MAIDEN version of GI2015 (a) and Ge2017 (b), for selected sites (160 sites for GI2015 and 189 for Ge2017, Sect. 3.2.4.1; others have been put to 1; the number of sites that have been put to 1 is indicated by category with the total number of sites in each category in brackets) and VS-Lite, for all 302 sites (c).*

3.3.3 Assessing the ability of MAIDEN and VS-Lite to reproduce climate relationship with tree-growth

One of the ultimate purposes of PSMs like VS-Lite and MAIDEN is to be used to reconstruct past climates, for example by including them in a data assimilation procedure [Evans et al., 2013; Dee et al., 2016]. Therefore, we have to assess if these models are able to reproduce well the climate signal recorded in TRW. In the previous section, we established if the models ability to reproduce tree-growth depends on the presence of a strong climate signal recorded in the tree rings. In this section, we want to evaluate if the simulated climate signal, whatever its predominance, is consistent with its recording by tree-ring indexes. This is based on the comparison of the correlations of different climate indicators with tree-growth in simulations and in observations: firstly, by means of scatterplots (Figs. 3.6, 3.7 and 3.8) and secondly, by means of correlations (Table 3.2).

For MAIDEN (Figs. 3.6 and 3.7), over- and underestimations of the climate dependencies of tree-growth are more balanced than for VS-Lite (Fig. 3.8) as the dots in the scatterplots tend to spread more equally around and are closer to the 1:1 line, particularly for temperature. Conversely, the scatterplots of VS-Lite (Fig.

Table 3.1: *Pearson correlations between correlations of observed TRW with different climate indicators and MAIDEN or VS-Lite verification correlations (1901-1949). O-S stands for the year starting from October (previous year) to September (current year); P for precipitation; JAS for July-August-September; T for temperature. Asterisks stand for significant correlations (p-value < 0.05). The difference in the number of sites on which correlations are computed is due to the phenological criterion that has been applied to MAIDEN calibrated sites (see Sect. 3.2.4.1 for more details).*

Model (version)	**Correlation**
Correlations between observed TRW and O-S P correlation and verification correlation	
MAIDEN (Ge2017; 189 sites)	0.114
MAIDEN (GI2015; 160 sites)	0.155
VS-Lite (302 sites)	0.149*
Correlations between observed TRW and annual T correlation and verification correlation	
MAIDEN (Ge2017; 189 sites)	0.074
MAIDEN (GI2015; 160 sites)	0.059
VS-Lite (302 sites)	0.467*
Correlations between observed TRW and JAS T correlation and verification correlation	
MAIDEN (Ge2017; 189 sites)	-0.039
MAIDEN (GI2015; 160 sites)	-0.097
VS-Lite (302 sites)	0.506*

3.8) show a stronger overestimation of the climate dependency of tree-growth at most sites, as most of the dots are far above the diagonal. This bias is particularly large for temperature. Indeed, for VS-Lite, the correlation for mean annual temperature is overestimated by more than 0.4 at 43% of the sites (12% for GI2015 and 18% for Ge2017), at 47% of the sites for mean July-August-September temperature (7% for GI2015 and 13% for Ge2017), and at 28% of the sites for October-September cumulative precipitation (17% for GI2015 and 12% for Ge2017). The same conclusion is still valid for VS-Lite when we restrict the analysis to the MAIDEN selected sites (Sect. 3.2.4.1) (Figs. C.10–C.15). This overestimation of the climate signal enhanced by the model is a crucial feature to consider when using such PSMs in paleoclimatology, as it can lead to biased climate reconstruction. Again, the structure of VS-Lite is likely responsible for the overestimation of the climate influence on tree-growth as tree-growth is not driven by any other internal or external drivers than limiting climatic factors. The very high correlations (r>0.7) between the VS-lite simulations and basic climate indicators in Fig.

3.8 at many sites indicate the simplicity of the climate dependence of tree-growth in this PSM. In MAIDEN, many biological processes are in play to frame the climate dependence of tree-growth. MAIDEN uses different functional rules specific to the ongoing phenological phase to allocate at a daily time step the available carbon from photosynthesis and stored non-structural carbohydrates to different tree compartments. The functional rules directly depend on climate factors, such as growing degree days, soil water content or temperature, and are specific to the phenological phase. Simultaneaously, the daily photosynthesis is simulated following the biochemical model of Farquhar et al. [1980] and dynamically interacts with the allocation module. The combination and interaction of these processes may smooth out the direct climate signal on tree-ring growth.

Correlations between observed and simulated (MAIDEN or VS-Lite) tree-growth dependency on climate at all sites (referred to as correlations of correlations in Table 3.2) are generally low (ranging from 0.053 to 0.515), particularly for temperature, even if mostly significant. The correlations for VS-Lite when we restrict the analysis to the MAIDEN selected sites (Sect. 3.2.4.1) are in Table C.8 and are similar to the results for all 302 sites. In other words, when considering all sites, both models have low skill in reproducing correctly the actual climate signal observed in tree-rings. However the well-fitted sites (Sect. 3.3.1) have better correlations, ranging from 0.648 (annual temperature) to 0.759 (July-August-September temperature) for MAIDEN and 0.678 (annual temperature) to 0.837 (October-September precipitation) for VS-Lite. Both models are thus able to accurately mimic the climate signal in tree-ring observations if the sites are carefully selected (Sect. 3.3.1). When focusing on the common well-fitted sites between VS-Lite and MAIDEN, VS-Lite is slightly better at reproducing climate, specifically for annual temperature (0.608 correlation for MAIDEN and 0.772 for VS-Lite) and precipitation (0.747 for MAIDEN and 0.886 for VS-Lite).

3.3.4 Sensitivity analysis of MAIDEN to atmospheric CO_2 concentration

In this section, we perform a sensitivity analysis of the MAIDEN model to atmospheric CO_2 concentration. The CO_2 concentration is a key driver of the forest carbon fluxes but its actual effects are still difficult to consider and evaluate in dendroecological studies [Körner et al., 2005; Silva et al., 2010; Peñuelas et al., 2011; Lévesque et al., 2014; Van Der Sleen et al., 2015; Girardin et al., 2016a; Hararuk et al., 2019; Giguère-Croteau et al., 2019; Marchand et al., 2020]. Yet, the CO_2 concentration has increased by 30% over the last 50 years and might increase up to 1000 ppm at the 2100 horizon (RCP 8.5; Myhre et al., 2013) relative to the current 414.49 ppm (December 2020, `https://www.esrl.noaa.gov/gmd/ccgg/trends/global.html`, last access: 19 March 2021), which will have an impact

Table 3.2: *Pearson correlations of correlations between different climate indicators and tree-ring width observations with correlations between the same climate indicators and MAIDEN or VS-Lite tree-growth simulations (1901-1949 verification period). O-S stands for the year starting from October (previous year) to September (current year); P for precipitation; JAS for July-August-September; T for temperature; TRindex for tree-ring index. Asterisks stand for significant correlations (p-value < 0.05). The difference in the number of sites on which correlations are computed is due to the phenological criterion that has been applied to MAIDEN calibrated sites (see Sect. 3.2.4.1 for more details).*

Model (version)	**Correlation**
Correlations between observed TRW and O-S P correlation and simulated TRindex and O-S P correlation	
MAIDEN (Ge2017; 189 sites)	0.388*
MAIDEN (GI2015; 160 sites)	0.322*
VS-Lite (302 sites)	0.515*
MAIDEN (well-fitted sites only)	0.694*
VS-Lite (well-fitted sites only)	0.837*
MAIDEN (common well-fitted sites only)	0.747*
VS-Lite (common well-fitted sites only)	0.886*
Correlations between observed TRW and annual T correlation and simulated TRindex and annual T correlation	
MAIDEN (Ge2017; 189 sites)	0.053
MAIDEN (GI2015; 160 sites)	0.171*
VS-Lite (302 sites)	0.241*
MAIDEN (well-fitted sites only)	0.648*
VS-Lite (well-fitted sites only)	0.678*
MAIDEN (common well-fitted sites only)	0.608*
VS-Lite (common well-fitted sites only)	0.772*
Correlations between observed TRW and JAS T correlation and simulated TRindex and JAS T correlation	
MAIDEN (Ge2017; 189 sites)	0.130
MAIDEN (GI2015; 160 sites)	0.216*
VS-Lite (302 sites)	0.338*
MAIDEN (well-fitted sites only)	0.759*
VS-Lite (well-fitted sites only)	0.704*
MAIDEN (common well-fitted sites only)	0.739*
VS-Lite (common well-fitted sites only)	0.787*

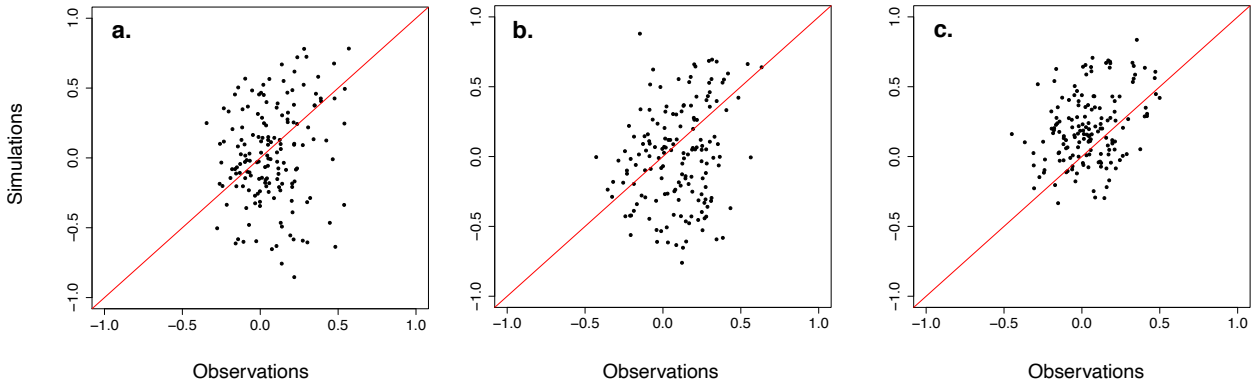


Figure 3.6: *Correlations between mean annual temperature (a), mean July-August-September temperature (b), October-September cumulative precipitation (c) and MAIDEN (GI2015) Dstem simulations as a function of correlations between the same climate indicators and TRW observations for selected sites (160 out of 302 sites; Sect. 3.2.4.1) over the 1901-1949 verification period.*

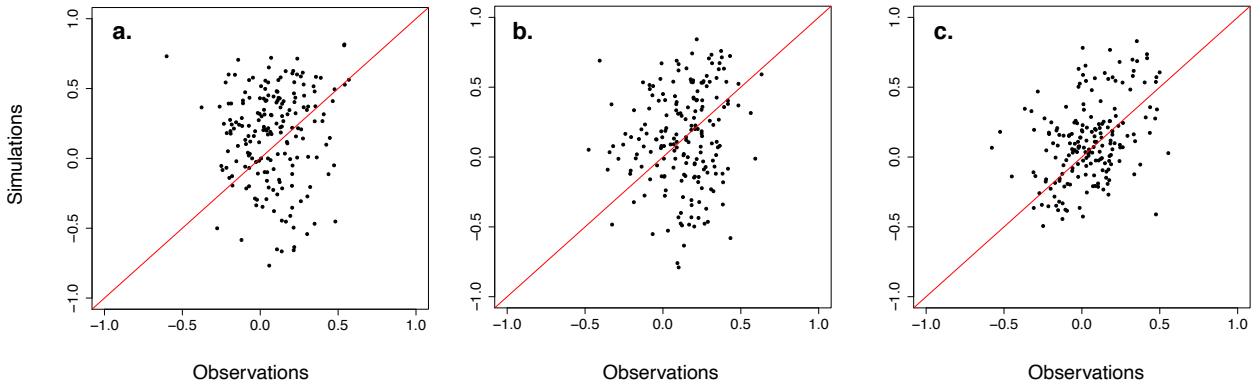


Figure 3.7: *Correlations between mean annual temperature (a), mean July-August-September temperature (b), October-September cumulative precipitation (c) and MAIDEN (Ge2017) Dstem simulations as a function of correlations between the same climate indicators and TRW observations for selected sites (189 out of 302 sites; Sect. 3.2.4.1) over the 1901-1949 verification period.*

on the forest carbon fluxes. This effect should be taken into account in dendroecological analysis [Babst et al., 2018]. In MAIDEN, the CO_2 influences the forest carbon fluxes through the coupled modelling of photosynthesis and stomatal conductance [Farquhar et al., 1980; Leuning, 1995] with environmental dependencies related to temperature and soil water content [Gea-Izquierdo et al., 2015; Gennaretti et al., 2017], and the feedbacks between the coupled photosynthesis-stomatal conductance system and the carbon allocation.

Here, we evaluate the influence of the inclusion of the CO_2 concentration increase in MAIDEN by comparing its performance in the standard configuration with a sensitivity experiment in which the CO_2 concentration is kept constant, for the

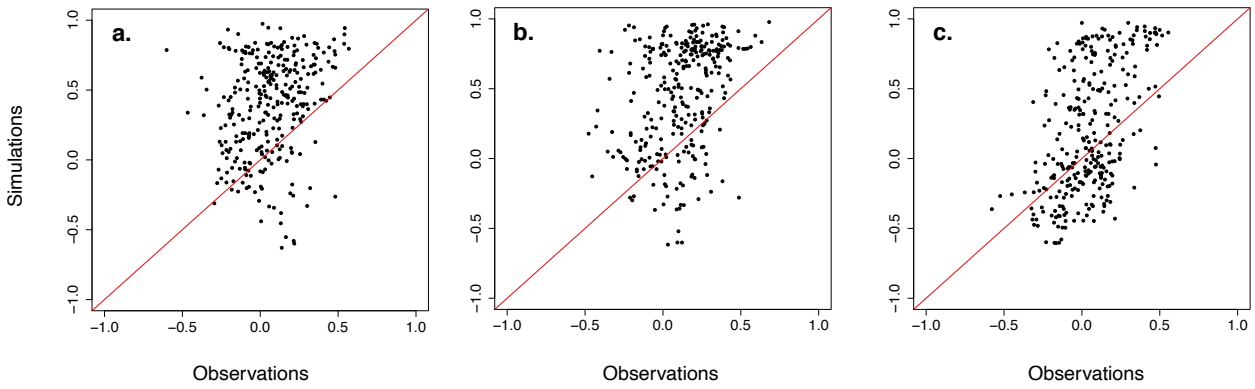


Figure 3.8: *Correlations between mean annual temperature (a), mean July-August-September temperature (middle), October-September cumulative precipitation (b) and VS-Lite tree-ring index simulations as a function of correlations between the same climate indicators and TRW observations for all sites (302) over the 1901-1949 verification period.*

64 well-fitted sites (Sect. 3.3.1), with parameters calibrated based on the CO_2 increasing scenario. The CO_2 is fixed at its 1st January 1980 value for the Northern Hemisphere (339 ppm), and at its 1st July 1980 value for the Southern Hemisphere (340 ppm).

At each site, we computed the difference between normalized MAIDEN tree-ring growth simulations and normalized TRW observations from 1990 with increasing CO_2 and constant CO_2. We performed our analysis on the 60 sites out of 64 well-fitted sites that end at least in 1990. Note that both simulations were normalized over 1950-2000 based on the mean and standard deviation of the original simulation, i.e. with increasing CO_2, over the same time period. The density distributions of the difference for both experiments are shown on Fig. 3.9a. The Pearson's Chi-squared test indicates a significant difference between the two experiments distributions (p-value < 0.05). The mean for both experiments are -0.209 and 0.182 for the constant CO_2 and increasing CO_2 experiment, respectively. In other words, while not taking into account CO_2 tends to underestimate the actual tree-growth on average, taking into account the increase of CO_2 in MAIDEN leads to overestimate it. Ecophysiological models are indeed known to overestimate the actual effect of CO_2 [Peñuelas et al., 2011; Gea-Izquierdo et al., 2017]. However, the CO_2 concentration has certainly an impact on the tree carbon assimilation [Marchand et al., 2020] that should be properly considered to avoid potential biases in climate and growth trend reconstructions derived from tree-ring data. This impact can be taken into account by ecophysiological models such as MAIDEN, but potential overestimations must be carefully envisaged due to the generic default of such models.

The trend of simulated and observed tree-growth was also computed and compared at each of the 60 sites. It corresponds to the coefficient of regression of the

normalized tree-growth simulations or observations from 1970 up to 1990 at least, versus the years. The simulated trend by MAIDEN may reproduce the generally positive trend that is observed from 1970 in TRW time series (Fig. 3.9b) in correlation with the increasing CO_2 concentrations.

Consequently, our results show that the growth trends simulated by MAIDEN are significantly influenced by the CO_2 increase and that MAIDEN simulated tree-growth is closer to the observed TRW when including the CO_2 concentration increase. This limited analysis is not sufficient to draw conclusions regarding CO_2 fertilization in trees but it highlights a potential CO_2 effect based on a model that takes into account a commonly used biochemical formulation of photosynthesis [Farquhar et al., 1980]. Including the effect of CO_2 in a mechanistic model like MAIDEN is a potential advantage over statistical and simple process-based models such as VS-Lite that are not able to account for these processes strongly influencing the forest carbon fluxes. However, because of the remaining uncertainties on the associated processes, an improved representation of the effect of CO_2 in process-based dendroecological models is needed to analyse past and future growth trends and variability.

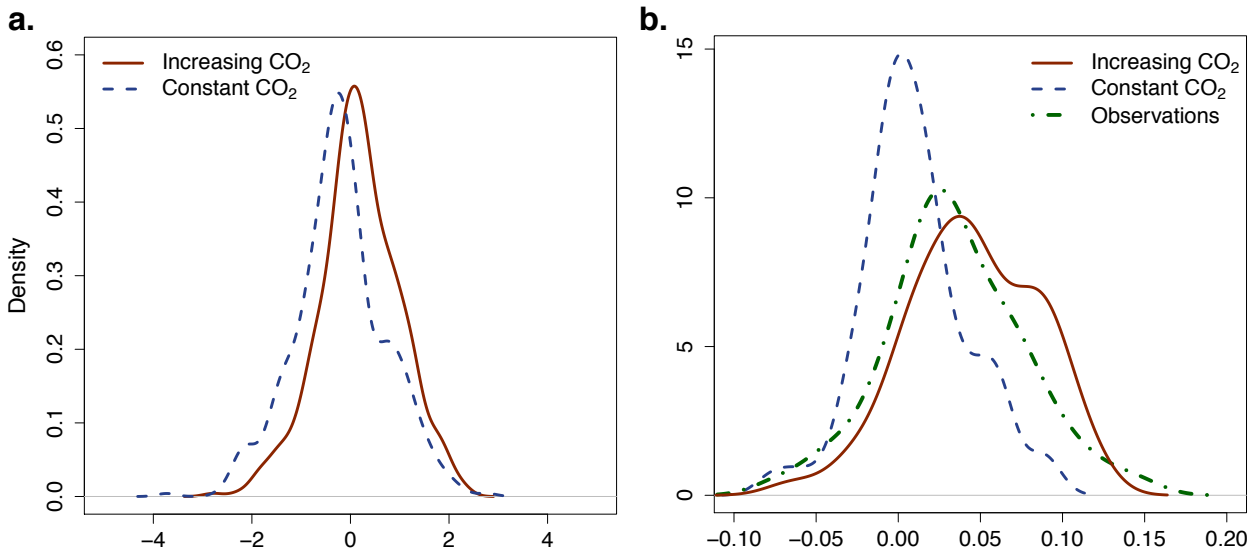


Figure 3.9: *Density distributions of (a) the difference between normalized tree-ring index simulations by MAIDEN and observed tree-ring width from 1990 with increasing CO_2 concentration (red solid line, i.e. the original configuration), and constant CO_2 concentration (blue dashed line); (b) the trend from 1970 of normalized tree-ring index simulations by MAIDEN with increasing CO_2 concentration (red solid line, i.e. the original configuration) or with constant CO_2 concentration (blue dashed line), and of normalized tree-ring width observations (green dot-dashed line); at 60 out of 64 well-fitted sites (Sect. 3.3.1).*

3.4 Discussion and conclusions

In this paper, we have applied and compared two dendroclimatic process-based models of different complexity levels, VS-Lite and MAIDEN, using the global PAGES2k TRW database over the last century. We have evaluated their respective abilities and advantages to be used at the global scale as PSMs for paleoclimate reconstructions based on data assimilation.

The models appear to be skillful for a similar number of mostly different sites (63 sites for VS-Lite and 64 sites for MAIDEN, 18 sites in common), spread over all continents. The performance of the models is comparable in terms of calibration and verification correlations. VS-Lite generally results in more stable correlations between the calibration and verification periods. When focusing on the factors that can drive the performance of both models, VS-Lite displays a strong correlation between its verification scores and tree-growth correlations with temperature, while MAIDEN does not. This means that VS-Lite tends to perform better at sites where observed tree-growth strongly correlates with temperature. In other words, the model's performance is improved in environments characterized by extreme temperatures. This feature hampers its application in many regions of the world away from the treeline, already rarely considered for paleoclimate reconstruction. In contrast, MAIDEN performance is less sensitive to the climate signal in TRW time series. We presume that MAIDEN performance is mainly limited by the lack of information needed to accurately calibrate and initialize the model at each specific site. As mentioned above, the information needed to calibrate MAIDEN is a key limitation of complex tree-growth models in general for use at a broader scale. This lack of data (for example, the observed Gross Primary Productivity data) also hinders a complete evaluation and identification of the factors driving the performance of MAIDEN.

At the sites where each model works well in terms of calibration and verification correlations, both VS-Lite and MAIDEN are on average able to successfully retrieve the climate signal in tree-rings. A careful selection of the tree-ring sites provides the opportunity to focus on the most robust simulated relationship between climate and tree-growth. However, VS-Lite appears to predominantly overestimate the observed dependence of tree-growth on climate, while there is no systematic biases for MAIDEN. The overestimation of the climate signal recorded in tree-rings has to be carefully taken into account when using such tree-growth models for data assimilation based reconstructions as it can result in biases. This is a clear disadvantage when using less complex dendroclimatic models, such as VS-Lite, in which the climate and tree-growth relationship is simplified.

Consequently, we may recommend using MAIDEN especially when the relationship between climate and tree-growth is complex with interacting limiting factors. VS-Lite would be a good candidate if tree-growth is mostly limited by only

one climatic factor (e.g. summer temperature), although it may overestimate these climate dependences, particularly for temperature, leading to overconfident reconstructions. In this case, MAIDEN should produce more plausible results. However, if not enough data are available to properly set and calibrate MAIDEN (for example long daily climate data or soil characteristics), VS-Lite should be preferred. As shown in Rezsöhazy et al. [2020], MAIDEN cannot be properly calibrated if used with short and low-replicated TRW time series (periods shorter than 50 years).

It has also been shown in this study that the inclusion of atmospheric CO_2 concentration has a significant impact on the MAIDEN simulations. More generally, MAIDEN appears as a potential good candidate to account for the non-stationarity of the tree-growth-to-climate relationship linked to changing CO_2 conditions in paleoclimate reconstructions. In particular, ecophysiological models, such as MAIDEN, could be useful tools to solve the so-called divergence problem in dendroclimatology [D'Arrigo et al., 2008]. Conversely, from a paleoclimate perspective, not taking into account changing CO_2 concentration when using PSMs for data assimilation based reconstructions could lead to inaccurate climate reconstructions. More specifically, models such as VS-Lite could wrongly assign a trend in TRW series due to CO_2 concentration changes to the effect of rising temperatures. In turn, this will lead to an overestimation of the climate sensitivity of tree-growth and thus to an overestimation of the amplitude of past reconstructions. However, the impact of CO_2 concentration on tree carbon assimilation in more complex ecophysiological models should be evaluated carefully to properly take this process into account.

Consequently, future reconstructions and data assimilation could benefit from the use of complex ecophysiological models such as MAIDEN. Despite the obvious challenges that are associated with the calibration of such models, their potential for improving the quality of the reconstructions makes their complexity worthy. In particular, they widen the range of environments where tree-ring observations can be used for dendroclimatic reconstructions, including regions where the relationship between TRW and climate is more complex. They also account for the potential non-stationarity of tree-growth, for example due to increasing CO_2 concentration. Finally, they can prevent from systematic bias in the reconstruction of the climate signal recorded in TRW observations. Additionally, ecophysiological models like MAIDEN are continuously benefiting from improvements made in ecophysiology, in particular in the modelling of the links between climate and tree-growth through complex biological processes. However, in order to optimally use these complex models, we need to (1) have additional site knowledge to properly initialize the model such as data on the root profile, (2) use additional observations to verify specific processes such as phenology and photosynthetic rates, and (3) verify that the tree-ring chronologies are not affected by sampling biases that can distort the growth trends or are linked to non-climatic processes such as tree on-

togeny and demographic changes in the sampled stands [Duchesne et al., 2019]. Finally, to properly calibrate a complex model such as MAIDEN at the global scale, multiple data information sources should be mixed in the future. For example, tree phenology is hard to set with tree-ring data only. The phenology of MAIDEN could be informed more efficiently using satellite data (e.g. NDVI). On the other hand, simple dendroclimatic models like VS-Lite, through their ease of use and calibration, coupled with a satisfying performance in reproducing tree-growth, are also appealing candidates for paleoclimate reconstructions based on data assimilation. VS-Lite and MAIDEN thus bring complementary assets for reconstructing past climates. The user must select the model according to the goal of the study (temperature or hydroclimate reconstruction), the data availability at the proxy site and the climate dependence of the TRW observations (one or multiple climate drivers).

More generally, the simultaneous evaluation of tree-growth PSMs of different complexity is essential for any future paleoclimate data assimilation exercises willing to use TRW proxy data and tree-ring PSMs at the global scale. Such study helps to select the adequate PSM and identify the limitations and the advantages of mechanistic modelling in a paleoclimate perspective compared to statistical methods. It is a necessary step to increase our ability to robustly reconstruct past climates from tree-rings. In particular, our study has shown that the mechanistic approach has great potential to enhance the skill of reconstructions of past climate variability from tree-rings. Consequently, the next step will be to include such models in a data assimilation procedure to reconstruct the climate of the last millennium in regions where the models perform well. On this basis, we will be able to fully evaluate how process-based dendroclimatic models can contribute to the improvement of large-scale reconstructions of past climate variability and justify the added complexity of the procedure compared to the linear regressions classically used up to now.

4

Using a process-based dendroclimatic proxy system model in a data assimilation framework: a test case in the Southern Hemisphere over the past centuries

Abstract

To date, data assimilation-based reconstructions of past climate variations from tree-ring proxies have only used statistical proxy system models to make the link between the climate model outputs and the indirect observations from tree rings. However, the linearity and stationarity assumptions of the statistical approach may have limitations. In this study, we incorporate the process-based dendroclimatic model MAIDEN into a data assimilation procedure, using as a test case the reconstruction of near-surface air temperature, precipitation and winds in the mid-latitudes of the Southern Hemisphere over the past 400 years. We compare our results with a data assimilation approach including a linear regression as a proxy system model for tree-ring width proxies. Overall, when compared to instrumental data, the reconstructions using MAIDEN as a proxy system model offer a skill equivalent to the experiment using the regression model. However, our test does not incorporate enough tree-ring width records so that the reconstructions underestimate the variance, especially at large spatial scale. Knowing the advantages that a process-based model can bring and the improvements that can still be made with MAIDEN, those results are promising.

4.1 Introduction

Indirect observations of climate from proxies such as tree-ring width (hereafter TRW) or isotopic content in ice cores and coral inform on past climate variability

This chapter is based on a paper in preparation. Supplementary materials are in Appendix D.

beyond the instrumental era [Jones et al., 2009]. Those proxy records have been used in numerous studies for providing historical climate variability over the last millennium. This has been usually achieved by using empirical (i.e., statistical) relationship between climate variables of interest and proxy observations, mostly from tree rings [e.g. Mann et al., 1999; Luterbacher et al., 2004; Mann et al., 2008; Büntgen et al., 2011; Neukom et al., 2011; Tingley and Huybers, 2013]. They represent the most available proxy to reconstruct past climates at high temporal resolution and large spatial scale [Fritts, 1976; Jones et al., 2009; Cook et al., 1999; Esper et al., 2002; Wilson et al., 2016; Anchukaitis et al., 2017; Esper et al., 2018].

Although the network of TRW records is well developed, mostly in the extratropical latitudes of the Northern Hemisphere [PAGES 2k Consortium, 2017], these records only provide insight about past climates on a limited area. Statistical methods have been developed in order to provide spatially gridded climate reconstructions of the past centuries, generally on the basis of linear regressions between the network of proxy records and the climate field of interest, calibrated over the instrumental period [Fritts et al., 1971; Mann et al., 1998, 2007; Cook et al., 2010; Wang et al., 2015]. The use of linear regression is based on the assumption that the relationship between climate and tree growth is linear and stationary over time. However, many studies have highlighted the shortcomings associated with these assumptions for TRW records [Wilmking et al., 2020; Briffa et al., 1998b; Wilson and Elling, 2004; Wilson et al., 2007; D'Arrigo et al., 2008; Guiot et al., 2014; Babst et al., 2018].

On the other hand, global climate model simulations offer a complete spatial picture of the past climate variability. Nevertheless, these simulations, if used alone, do not include any information on the performance of the models. Over the last decades, data assimilation (DA) has been increasingly used in paleoclimatology to bring together the information from both indirect climate records from proxies and climate models to provide a complete picture of the climate changes [Goosse et al., 2010; Widmann et al., 2010; Goosse et al., 2012; Steiger et al., 2014; Franke et al., 2017; Steiger et al., 2018; Tardif et al., 2019].

Initially, the DA-based reconstructions were developed using temperature reconstructions derived from the statistical relationship between temperature and proxy observations, and not the proxy time series themselves [e.g. Crespin et al., 2009; Goosse et al., 2010]. More recently, the use of forward proxy system models (hereafter, PSMs) has emerged in order to directly assimilate the proxy time series. Specifically, the PSMs make the link between the outputs of the climate model included in the DA procedure and the assimilated proxy observations, for example TRW [Evans et al., 2013; Dee et al., 2016]. To date, the DA studies using tree-ring proxy data have only included statistical PSMs (uni- or multivariate regressions; e.g. Franke et al., 2017; Steiger et al., 2018; Tardif et al., 2019).

Contrary to statistical models, process-based dendroclimatic PSMs are able to account for the complexity of the relationship between climate and tree-ring proxy data by explicitly simulating the biological processes governing the climate dependency of tree-ring growth. However, so far, they have never been used in a DA procedure with actual tree-ring proxy data, but only with pseudoproxies [Dee et al., 2016; Acevedo et al., 2017; Steiger and Smerdon, 2017]. In these studies, the simple VS-Lite model [Tolwinski-Ward et al., 2011] has shown to significantly improve the quality of the reconstruction. However, VS-Lite can not be considered as entirely process-based as it does not include any biological processes to drive tree growth, but is rather based on the implementation of the principle of limiting factor with threshold growth response functions [Tolwinski-Ward et al., 2011].

In this study, we introduce a process-based dendroclimatic model in an offline data assimilation procedure with actual tree-ring width records. Among all the available mechanistic tree-growth models [e.g Misson, 2004; Dufrêne et al., 2005; Vaganov et al., 2006; Drew et al., 2010; Tolwinski-Ward et al., 2011], we chose to work with the complex ecophysiological model MAIDEN (Modelling and Analysis In DENdroecology; Misson, 2004). MAIDEN includes the atmospheric CO_2 concentration among other inputs, which represents a major advantage for taking into account the potential effect of the recent exponential increase of CO_2 on tree growth [Myhre et al., 2013; Boucher et al., 2014]. In Rezsöhazy et al. [2021], the MAIDEN model has been applied to the PAGES2k TRW database using the calibration protocol developed in Rezsöhazy et al. [2020]. Rezsöhazy et al. [2021] have highlighted the potential of MAIDEN to be used as a PSM for DA-based reconstruction of past climate variability at the global scale, and to improve the quality of the DA-based paleoclimate reconstructions.

Here, we perform a comparative analysis on the impact of a simple regression model or a process-based dendroclimatic model as PSMs for TRW records in the DA framework. The goal is to evaluate if and how a complex process-based model of tree growth like MAIDEN can contribute to the improvement of large-scale DA-based reconstructions of past climate variability compared to the regression model classically used so far. To this end, different DA experiments are first performed over the last century and evaluated against state-of-the-art gridded climate datasets (Sect. 4.4.1 and 4.4.2). Because MAIDEN has shown to be skillful in different regions of the Southern Hemisphere (SH) [Rezsöhazy et al., 2021], we focus on that region and provide climate reconstruction of near-surface air temperature, precipitation and winds in the mid- to high-latitudes of the SH over the past 400 years (Sect. 4.4.3). The Southern Hemisphere also constitutes an interesting study case, as few reconstructions have been performed in this region so far [Neukom et al., 2011, 2014]. The DA experiments are based on both TRW and ice core (δ^{18}O and snow accumulation) proxy data to ensure the consistency of the reconstructed large-scale circulation pattern. They both represent the best

available continental annually resolved proxies in the SH [PAGES 2k Consortium, 2017]. To match the seasonality of tree growth in the Southern Hemisphere, all the analysis in this study are performed on a July-June year.

4.2 Data assimilation

In paleoclimatology, the objective of data assimilation is to optimally combine the information from the physics of the climate system as included in climate models and indirect observations of climate from proxies [Kalnay, 2003; Goosse et al., 2010; Widmann et al., 2010; Steiger et al., 2014; Franke et al., 2017; Tardif et al., 2019]. More specifically, the DA procedure is based on the Bayes theorem: starting from the prior estimate of the state of the climate system provided by the model, the DA produces a reconstruction of the climate system as accurate as possible (i.e, the posterior) given the information provided by the climate observations. The updated estimate of the climate system is called a reanalysis. One of the advantages of DA is its ability to propagate the information brought by the observations both in space and between the climate variables, by relying on the spatial covariance and the covariance between different variables in the model. In other words, the DA gives the opportunity to reconstruct the climate at places where there is no proxy sites, and for variables for which we do not have any observations to assimilate.

In this study, we use an offline DA approach, by opposition with the online DA approach. The offline approach samples a pre-existing ensemble of climate model simulations to build the prior state of the climate system. This has the great advantage of being considerably computational time saving. In this configuration, the different years of the sampled ensemble are assumed to be independent of each other. This assumption is reasonable if the predictability of the variables of interest is smaller than the temporal resolution of DA (i.e, one year in our study), as is the case for atmospheric variables. With the online approach, the prior state of the climate system is sequentially updated. In this case, the years are not assumed to be independent of each other. Instead, the update made at the previous time step is transferred to the next one. When focusing on the atmosphere, as in our study, the online approach is not expected to outperform the offline approach [Matsikaris et al., 2015].

Here, the offline approach is based on a particle filter method described in Sect. 4.2.1. For more details on paleoclimate data assimilation and on the particle filter, see Sect. D.1. In addition, the framework of DA includes three main components: (1) prior climate model simulations (Sect. 4.2.2); (2) indirect observations of climate provided by proxy data (Sect. 4.2.3); and (3) proxy system models, to make the link between climate models outputs and indirect observations of climate (Sect. 4.2.4). The error associated with the data used in the DA procedure is also

considered and defined in Sect. 4.2.5. Finally, in Sect. 4.3, we elaborate the DA experimental design and diagnostics of this study.

4.2.1 Particle filter

In this study, the offline DA procedure uses a particle filter as in Dubinkina et al. [2011]. The particle filter [van Leeuwen, 2009] describes the prior of each climate variable by a probability density function, which is represented discretely on the basis of independent states of the model (Sect. 4.2.2), i.e., the particles. The model states are sampled at a chosen frequency in the model simulations. This frequency of sampling determines the number of sampled particles and will be characterized later in Sect. 4.3. The prior stays the same throughout the DA procedure. As the observations are annually resolved (see Sect. 4.2.3), the time step of the DA is also annual. As a consequence, the particles are defined as the annual mean of the model state variables (for example near-surface air temperature and precipitation, depending on the observations).

For each year of the reconstruction period (i.e, the period covered by observations), all the particles are compared to the available observations, directly or through the use of a PSM (Sect. 4.2.4). This allows estimating the likelihood of each particle knowing the observations at that time. This computation also takes into account all known sources of errors (see Sect. 4.2.5). The likelihood then determines the weight given to each particle. The weight given to a particle will be higher if the particle is closer to the observations, and lower if further to the observations. In this way, starting from a prior distribution where all the particles have the same weight, the particle filter produces a posterior distribution where the weights of the particles are redistributed according to the observations, for each year of the reconstruction. In this framework, the dynamical consistency of the model is preserved, since only the weights of the particles are updated. At the end of the DA procedure, the weighted mean of the particles for each year over the assimilation period provides an estimate of the climate variables (i.e., the ensemble mean). The weighted standard deviation of the particles is used to estimate the range of the reconstruction (i.e., the ensemble spread).

4.2.2 Climate model simulations

We use the ensemble of three simulations performed with the isotope-enabled Community Earth System Model version 1 (iCESM1; Brady et al., 2019; Stevenson et al., 2019; publicly available at `https://www.earthsystemgrid.org/dataset/ucar.cgd.ccsm4.CESM_CAM5_LME.html`; last access: 12 May 2021) as a basis for building the prior of our data assimilation experiments. The iCESM1 is a coupled atmosphere–ocean–sea-ice model at 1.9° latitude and 2.5° longitude

resolution for the atmosphere component and around 1° for the ocean–sea-ice component. The model simulations include the anthropogenic (aerosol emissions and land use changes) and volcanic aerosol forcings, the greenhouse gas emissions, solar irradiance variations and Earth's orbital changes [Brady et al., 2019; Stevenson et al., 2019]. The annually resolved iCESM1 simulations used in this study span the July 850 – June 2005 CE time period. For our DA experiments (Sect. 4.3), all the particles are sampled in the three iCESM1 members for a total of 3465 particles.

4.2.3 Proxy data

In this study, we make use of three types of proxy data from two types of archives: first, tree-ring width (Sect. 4.2.3.1) and, second, δ^{18}O (i.e, the ratio of stable isotopes oxygen in the ice core) and snow accumulation from ice cores (Sect. 4.2.3.2). They represent the best available continental proxies in the SH continents (South America, Australia, Tasmania, New Zealand and Antarctica) for reconstructing the past climate at high-resolution [PAGES 2k Consortium, 2017].

4.2.3.1 Tree-ring width data

The PAGES2k working group have collected 692 proxy records [PAGES 2k Consortium, 2017] selected for reconstructing the global temperature of the last two millennia. The records are from a variety of archives (tree rings, ice cores, lake sediments, coral, speleothems, documentary evidence, etc). The PAGES2k database (hereafter PAGES2k2017) includes 354 TRW records, among which 12 are located below 30°S, in New Zealand (four records), Tasmania (four records) and South America (four records). The previous version of the PAGES2k TRW database (PAGES 2k Consortium, 2013; hereafter PAGES2k2013) contains 28 TRW records below 30°S. Nine records have been excluded from the recent version of the PAGES2k database because they were too short (less than 300 years). Those records are also included in this study and are all located in South America. The location of the 21 TRW records from the two databases can be seen on Fig. D.2 (blue stars). The location of the 15 TRW records that are actually used in this study can be seen on Fig. 4.1 (see Sect. 4.2.4.1 and 4.2.4.2 for more details on the included sites). The TRW records are normalized (i.e, with a null mean and a standard deviation of 1) relative to the 1900–2000 CE time period for a use with the MAIDEN model (Sect. 4.2.4.1). For the regression-based model (Sect. 4.2.4.2), TRW anomalies are also computed relative to the 1900–2000 CE time period.

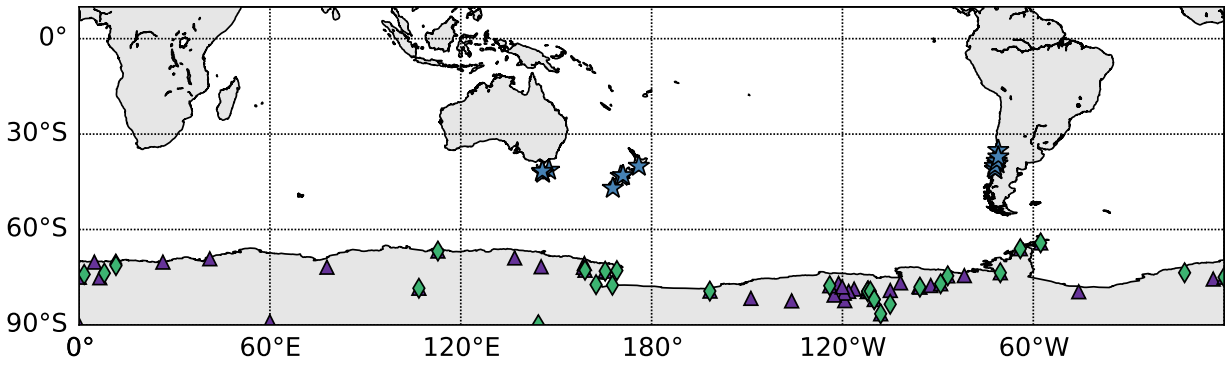


Figure 4.1: *Location of the 15 tree-ring width (TRW) records (blue stars) from the PAGES2k databases [PAGES 2k Consortium, 2013, 2017] used in this study; the 49 ice core snow accumulation records (purple triangles) from Thomas et al. [2017] and Medley et al. [2018]; and the 29 $\delta^{18}O$ records (green diamonds) from Stenni et al. [2017] (Sect. 4.2.3). Background map from Hunter [2007].*

.

4.2.3.2 Ice core data

The ice core data included in this study are the same as in Dalaiden et al. [2021], a study focusing on the mechanisms behind the West Antarctic climate changes. The 48 annually resolved ice core snow accumulation records in Antarctica from the database of Thomas et al. [2017] are included in this study. They span the last millennium [Medley and Thomas, 2019]. The B40 ice core snow accumulation record of Medley et al. [2018] has also been added. Finally, as in Dalaiden et al. [2021], we use the 29 annually resolved $\delta^{18}O$ records in Antarctica from Stenni et al. [2017]. The location of the snow accumulation and $\delta^{18}O$ records used in this study can be seen on Fig. 4.1 (purple triangles and green diamonds, respectively). They are mostly situated in West Antarctica. The ice core records are averaged over a 500 km grid in order to reduce the non-climatic noise in the observations. The anomalies of the ice core data are computed relative to 1900–2000 CE.

4.2.4 Proxy System Models

Proxy System Models, also referred to as observation operators, are a crucial component of the DA framework that makes the link between the climate state variables of the prior such as near-surface air temperature and precipitation and the assimilated indirect observations from proxies, here tree-ring width. In this study, we make use of two types of tree-ring PSMs, at opposite ends of the PSM spectrum: first, a complex process-based ecophysiological model, MAIDEN (Sect. 4.2.4.1); second, a simple linear regression model (Sect. 4.2.4.2). In the case of ice core records, the observations (snow accumulation and δ^{18}O) are directly com-

parable with the climate model as iCESM1 simulates these two variables. In particular, the difference between precipitation and sublimation/evaporation ($P - E$) from iCESM1 is compared to the snow accumulation observations. It has already been shown in different studies that the main contributor to the snow accumulation variability is indeed $P - E$, especially when working at large spatial scale [Agosta et al., 2019; Souverijns et al., 2018; van Wessem et al., 2018]. Finally, the ratio of stable isotope oxygen δ^{18}O is simulated in iCESM1 and can be directly compared to δ^{18}O records.

4.2.4.1 MAIDEN

MAIDEN (Modelling and Analysis In DENdroecology; Misson, 2004; Gea-Izquierdo et al., 2015; Gennaretti et al., 2017) is a process-based dendroclimatic model which simulates the course of photosynthesis and the allocation of carbon to different pools (stem, roots, leaves, storage) on a daily time step as a response to climatic drivers (daily maximum and minimum temperature, precipitation and atmospheric CO_2 concentration). The annual quantity of carbon which is allocated to the stem (hereafter Dstem) is assumed to be proportional to tree-ring growth and comparable to TRW data, after normalization. We use a combined version of the model from Gea-Izquierdo et al. [2015] and Gennaretti et al. [2017], developed by Fabio Gennaretti (unpublished).

We must first determine where the MAIDEN model can be skillfully applied among the 21 PAGES2k sites (Sect. 4.2.3.1). MAIDEN was calibrated at the 12 SH sites from PAGES2k2017 in Rezsöhazy et al. [2021] using the daily maximum and minimum temperature and precipitation from the *Global Meteorological Forcing Dataset for land surface modelling* (v2) (`http://hydrology.princeton.edu/data.php`, last access: 5 May 2021; Sheffield et al., 2006) at 0.5° resolution (hereafter GMF), over 1950–2000 CE. The model was validated using the same dataset over the 1901–1949 CE time period. The calibration method is based on a Bayesian procedure with Markov Chain Monte Carlo sampling using the DREAMzs algorithm [Hartig et al., 2019]. This Bayesian approach is used to calibrate the most sensitive parameters of the model from the photosynthesis and carbon allocation modules (18 parameters). MAIDEN was found to be well calibrated with significant (95% confidence level) calibration and verification correlation greater than 0.3 at five sites south of 30°S. The same methodology was used for calibrating and validating MAIDEN at the nine records of PAGES2k2013. One site was found to be well calibrated and validated with a consistent phenology. The six sites on which MAIDEN will be run during the DA procedure can be seen on Fig. D.3 (orange circles). There is no site in Tasmania.

The iCESM1 data used in the DA framework are available at a monthly resolution. Yet, MAIDEN runs on a daily basis. To convert monthly data into daily

data, we apply the same methodology to any particle throughout the DA procedure. We use a reference year of the daily GMF dataset (1950) which we modified to match the mean seasonal cycle over 1950–2000 CE, i.e., a climatological seasonal cycle. Then, for a given particle, the monthly anomalies of the iCESM1 data relative to 1950–2000 CE are added (near-surface air temperature) or multiplied (precipitation) to the reference year of the daily GMF data. Note that the iCESM1 does not include maximum and minimum temperature data. We use the anomalies of iCESM1 near-surface air temperature on both maximum and minimum daily GMF temperature. As for atmospheric CO_2 data, the annual data from Rubino et al. [2019] (154–1996 CE; publicly available at `https://doi.org/10.25919/5bfe29ff807fb`, last access: 10 January 2021) followed from 1996 by the annual data from Sato and Schmidt (1880–2011 CE; `https://data.giss.nasa.gov/modelforce/ghgases/`, last access: 10 January 2021) were linearly interpolated at a daily time step.

The temporal autocorrelation in the simulated Dstem can be important, through the storage pool [Gea-Izquierdo et al., 2015; Gennaretti et al., 2017; Guiot et al., 2014], so that the performance of the model in reproducing the observed tree growth of one year highly depends on the performance of the previous years. As a consequence, we cannot run the MAIDEN model independently for each year driven by the iCESM1 data as is the case with the linear regression (Sect. 4.2.4.2). The linear regression can be run using as inputs any single year of the ensemble of three iCESM1 simulations (Sect. 4.2.2). For each year of the reconstruction, the particles are then directly sampled from the simulated tree-ring indexes and compared to the observations as in Sect. 4.2.1. Instead, MAIDEN is sequentially run year by year using the reconstructed climate for the previous years and thus accounting for the effect of past climate history on tree-ring growth. For any particle, we use the CO_2 data corresponding to the assimilated year.

The tree-growth index simulated by MAIDEN is not directly comparable with TRW data. The observations are thus normalized a priori (Sect. 4.2.3.1) to produce unitless indexes. However, this is not possible for the tree-growth simulations as we sequentially run MAIDEN and, by construction, we can not know a priori the final values required for the normalization. The mean and standard deviation of a reference run of MAIDEN with iCESM1 inputs over 1900–2000 CE are thus used to normalize the annual Dstem output throughout the DA procedure.

4.2.4.2 Linear regression

A regression-based model was developed for each of the 21 TRW records (Sect. 4.2.3.1), similarly to Dalaiden et al. [2021] and to the Last Millennium Reanalysis [Tardif et al., 2019]. Different annually resolved climate variables were considered to model the relationship between climate and tree-ring growth. They are either re-

lated to temperature or precipitation. For temperature, we considered the current year July to next June temperature, the December-January-February (i.e., austral summer) temperature and the September to March or growth period temperature. For precipitation, we considered the July to June precipitation, the July-August precipitation and the July-August-September precipitation. We built the different climate variables by averaging the monthly near-surface air temperature and precipitation from the GMF interpolated on the iCESM1 grid (Sect. 4.2.2) over the period of months of interest. The climate data were extracted from the continental grid cell closest to each individual TRW record. The statistical model can be univariate (temperature or precipitation) or bivariate (temperature and precipitation).

Similarly to the MAIDEN calibration, the regression parameters of each statistical PSM were first calibrated over the 1950–2000 CE time period using the ordinary least squares method. For each record, we tested all the possible combinations of climatic variables. As in Dalaiden et al. [2021], the best model was selected for each TRW record using the *Bayesian Information Criterion* or BIC [Schwarz, 1978], which has the advantage to penalize the complexity (i.e, the number of explanatory variables) of a model.

The regression models were then run independently over the 1901–1949 CE verification time period. Among the 21 sites, only two sites were validated following the same criterion as MAIDEN (Sect. 4.2.4.1), i.e, a significant calibration and verification correlations greater than 0.3 (Table D.1). As a consequence, the validity of the regression models out of the calibration interval is not ensured for most of them. Alternatively, we decided to calibrate the regression parameters using the same method over the entire period covered by climate data, i.e., 1901–2000 CE, in order to better account for the possible non-stationarity of the relationship between climate and tree growth. We then excluded the sites for which the explanatory climate variables were not significantly and positively correlated with observed TRW series. This selection criterion is similar to what is generally done in paleoclimate DA-based reconstruction using TRW proxies with a statistical model (e.g., the Last Millennium Reanalysis; Tardif et al., 2019). Nine sites are excluded (one in New Zealand and eight in South America). The 12 sites included in the DA procedure with the regression model (hereafter, selected sites) can be seen on Fig. D.4 (blue circles). A criterion based on the calibration only could not be used to select the TRW records for MAIDEN. The complexity of the model and the number of calibrated parameters make it more prone to overfitting problems and biological inconsistency during the calibration [Rezsöhazy et al., 2020, 2021]. As a consequence, the selection of the TRW records has to be more restrictive but may also lead to a better stability of the model.

For comparison with the observed TRW series, anomalies of the simulated tree-ring indexes are computed relative to 1900–2000 CE.

4.2.5 Observation error

In the DA framework, the observation error determines the confidence that we can have in the climate information retrieved from the available proxy records. It directly influences the magnitude of the weight given to a particle when compared to an assimilated proxy observation, which has in turn direct consequences on the resulting reanalysis. We generally identify three types of observation error [e.g. Badgeley et al., 2020].

The first type of error is related to the inaccuracy of the PSM in reproducing the proxy dependency on climate. The PSMs can not fully account for the complexity of the processes by which tree growth responds to climate and non-climatic drivers. The error of MAIDEN is computed using the standard deviation of the residuals over the verification period (1901–1949 CE; Sect. 4.2.4.1). The error of the TRW regression-based PSM (Sect. 4.2.4.2) is computed as in Tardif et al. [2019], using the standard deviation of the residuals over the calibration period (1901-2000 CE). However, computing the error over the calibration period can have serious shortcomings. It does not account for the actual skill of the model to accurately estimate tree growth outside the calibration interval and is biased by possible overfitting problems associated with any statistical model. This could result in an underestimation of the error associated with the statistical PSM and, as a consequence, to overconfidence in the PSM performance and finally in the climate reconstruction. The snow accumulation and δ^{18}O records can be directly compared to the model outputs (Sect. 4.2.4) so that a PSM is not necessary.

Second, the representativeness error [e.g. Oke and Sakov, 2008] corresponds to the uncertainty related to the unresolved processes at the resolution of the climate model relative to the smaller scale potentially represented by proxy observations (tree-ring width, snow accumulation and δ^{18}O in our study). For the regression-based TRW PSM, we consider that the representativeness error is implicitly taken into account by computing the error related to the PSM using observed data at the same resolution as the iCESM1 data (Sect. 4.2.4.2). However, for MAIDEN, Rezsöhazy et al. [2020] have shown that calibrating the model with input climate data at low-resolution can have important consequences on the performance of the model. We thus used high-resolution data to calibrate MAIDEN at the TRW sites. In the DA procedure, the bias correction applied to the iCESM1 data with the high-resolution GMF data (Sect. 4.2.4.1) is associated with an error but we assume that it is weaker compared to the error related to the PSM.

Regarding the ice core records (snow accumulation and δ^{18}O), the representativeness error was computed as in Dalaiden et al. [2021], on the basis of an Antarctic simulation performed with the latest version of the Regional Atmospheric Climate MOdel (RACMO2.3p2, hereafter RACMO) at 27 km horizontal resolution [van Wessem et al., 2018]. They computed the standard deviation of the differ-

ences between the annual RACMO time series (1979–2016 CE) of snow accumulation averaged on all the ice core sites and the time series averaged over the 500 km grid, following the same approach as in Valler et al. [2020]. As for the δ^{18}O, the same methodology was applied but with the iCESM1 linearly interpolated on the RACMO grid over 1950–2005 CE, as RACMO does not simulate the water isotopes. The error was then corrected to account for the underestimation of spatial variability of snow accumulation and δ^{18}O in models (i.e., RACMO and iCESM1), by multiplying the resulting standard deviation by a factor 3 (see Dalaiden et al., 2021 for more details).

The last type of error is the instrumental error related to the measurement of the proxy data, often negligible, particularly in paleoclimatology [Steiger et al., 2018; Tardif et al., 2019].

4.3 Experiment design and diagnostics

Different DA experiments are run in this study (Table 4.1), varying between them by (1) the tree-ring PSMs included, (2) the records assimilated (3) the PSM error and (4) the period of the reconstruction.

A first set of experiments is conducted over the 1900–2000 CE time period and compared with state-of-the-art gridded climate datasets in order to evaluate the performance of our DA-based reconstructions regarding the use of statistical (TIC-reg) and process-based (TIC-MDN) dendroclimatic models separately, assimilating both ice core and tree-ring proxies.

A second set of experiments is performed over the 1900-2000 CE time period and compared with state-of-the-art gridded climate datasets in order to evaluate the contribution of tree-ring proxies in the data assimilation framework over the last century. Specifically, we perform an experiment assimilating tree-ring proxies only with the regression (TREES-reg) and MAIDEN (TREES-MDN) models and an experiment assimilating ice core proxies only (IC). The impact of the observation error associated with the tree-growth PSMs (Sect. 4.2.5) on the performance of the reconstruction is also evaluated by reducing the error by two in the experiments constrained by tree-ring proxies only (TREES-reg-05 and TREES-MDN-05).

Lastly, we perform a DA-based reconstruction over the period covered by a sufficient number of TRW proxy records, i.e., 1600–2000 CE, with the regression model (TIC-reg) and the MAIDEN model (TIC-MDN), with both tree-ring and ice core proxies.

Our analysis concentrate on four regions or sub-regions of the mid-latitudes of the SH: South America, defined between 25° and 56°S and between 55° and 85°W (SA); the South-Western Andes, where the TRW proxy sites are located, defined between 35° and 42.5°S and between 70° and 85°W (SAmSW); New Zealand, defined between 29° and 51°S and between 160° and 179°E (NZ); and

Tasmania, defined between 39.5° and 47°S and between 140° and 154°E (Tas). We did not include Antarctica in our study as tree-ring records have not shown to significantly affect the reconstruction in this region (see Dalaiden et al. [2021] for more details on the reconstructions in Antarctica).

Table 4.1: *Data assimilation (DA) experiments in this study and experimental design: experiment name; types of proxies assimilated; Proxy System Model (PSM) used to assimilate the proxy data; the error associated with the PSM; the calibration period of the PSM; the proxy records assimilated. N.A stands for Not Applicable. See Sect. 4.2.4.1 and 4.2.4.2 for details on the Validated and Selected sites, respectively. The number of tree-ring width records assimilated is in brackets.*

Experiment name	Proxies	PSM	PSM error	Calibration period of PSM	Proxy records
TIC-reg	Ice cores Tree-ring width	N.A Regression-based	N.A Calibration	N.A 1901–2000 CE	All Selected (12)
TIC-MDN	Ice cores Tree-ring width	N.A MAIDEN	N.A Validation	N.A 1950–2000 CE	All Validated (6)
TREES-reg	Tree-ring width	Regression-based	Calibration	1901–2000 CE	Selected (12)
TREES-MDN	Tree-ring width	MAIDEN	Validation	1950–2000 CE	Validated (6)
IC	Ice cores	N.A	N.A	N.A	All
TREES-reg-05	Tree-ring width	Regression-based	Calibration error divided by two	1901–2000 CE	Selected (12)
TREES-MDN-05	Tree-ring width	MAIDEN	Validation error divided by two	1950–2000 CE	Validated (6)

We evaluate our reconstructions against the most recent atmospheric reanalysis from the ECMWF, ERA5 [Hersbach et al., 2020] over the 1979–2000 CE time period, and against the GMF dataset (see Sect. 4.2.4.1 for more details on the dataset) over 1901–2000 CE, after interpolating them on the iCESM1 grid (Sect. 4.2.2). We focus on the near-surface air temperature, the cumulative precipitation and the geopotential height at 500 hPa (ERA5 only). The Southern Annular Mode index (hereafter SAM index) is from Marshall [2003] (1957–2000 CE). They will be hereafter referred to as observations. The SAM is the principal mode of atmospheric variability in the extratropics of the SH [Marshall, 2003]. It is associated with the north-south movement of the Westerlies and often defined as the difference between the normalized monthly zonal mean sea-level pressure at 40° and

65°S [Gong and Wang, 1999; Marshall, 2003], as chosen here. For each of the experiments, the same diagnostics are performed and based on the computation of two statistical indicators: the Pearson correlation coefficient (r; considered as significant at the 95% confidence level) and its associated p-value; and the coefficient of efficiency (hereafter CE). The coefficient of efficiency is computed as in Nash and Sutcliffe [1970]:

$$CE = 1 - \sum_{i=1}^{n} \frac{(x_i - y_i)^2}{(x_i - \bar{x})^2} \tag{4.1}$$

with n, the number of samples; x, the observation vector; y, the reconstruction vector. The overbar characterizes a time-averaged vector of values. The average is made over 1901-2000 CE in all experiments, except the SAM index when compared to the observations from Marshall [2003], as they only cover the 1957-2000 CE period. While the Pearson correlation coefficient gives an estimation of the linear fit between the reconstructed and observed values, the CE also informs on the amplitude of the observed and reconstructed signal. For regional near-surface air temperature and precipitation, the metrics are computed between the mean of the reconstruction and the mean of the ERA5 or GMF data over the continental mass that lies in the region delimited by the latitudes and longitudes above.

4.4 Results and discussion

4.4.1 Comparison of data assimilation with regression- and process-based tree-growth models over the last century

The spatial distribution of the correlation coefficients between different ERA5 and reconstructed climate fields over the recent period (1979–2000 CE) indicates a general good agreement of the reconstruction using MAIDEN as a PSM south of 30°S (TIC-MDN; Fig. 4.2a). When compared with the DA experiment including the regression model to assimilate 12 TRW records (TIC-reg; Fig. 4.2b), the hemispheric 500 hPa geopotential height, near-surface air temperature and precipitation fields are reconstructed with a quite similar performance in both cases. The spatial distribution of the correlation coefficients between the ERA5 and the reconstructed climate fields zoomed on the different regions (Sect. 4.3) can be seen on Figs. D.5–D.10.

At the regional scale and over the recent period (1979–2000 CE), the correlation coefficients of the ERA5 and GMF near-surface air temperature with the reconstructed near-surface air temperature in the four regions (Table 4.2) are generally similar for both TIC-reg and TIC-MDN. Except in Tasmania (Tas), where the TIC-MDN near-surface air temperature is highly and significantly correlated with

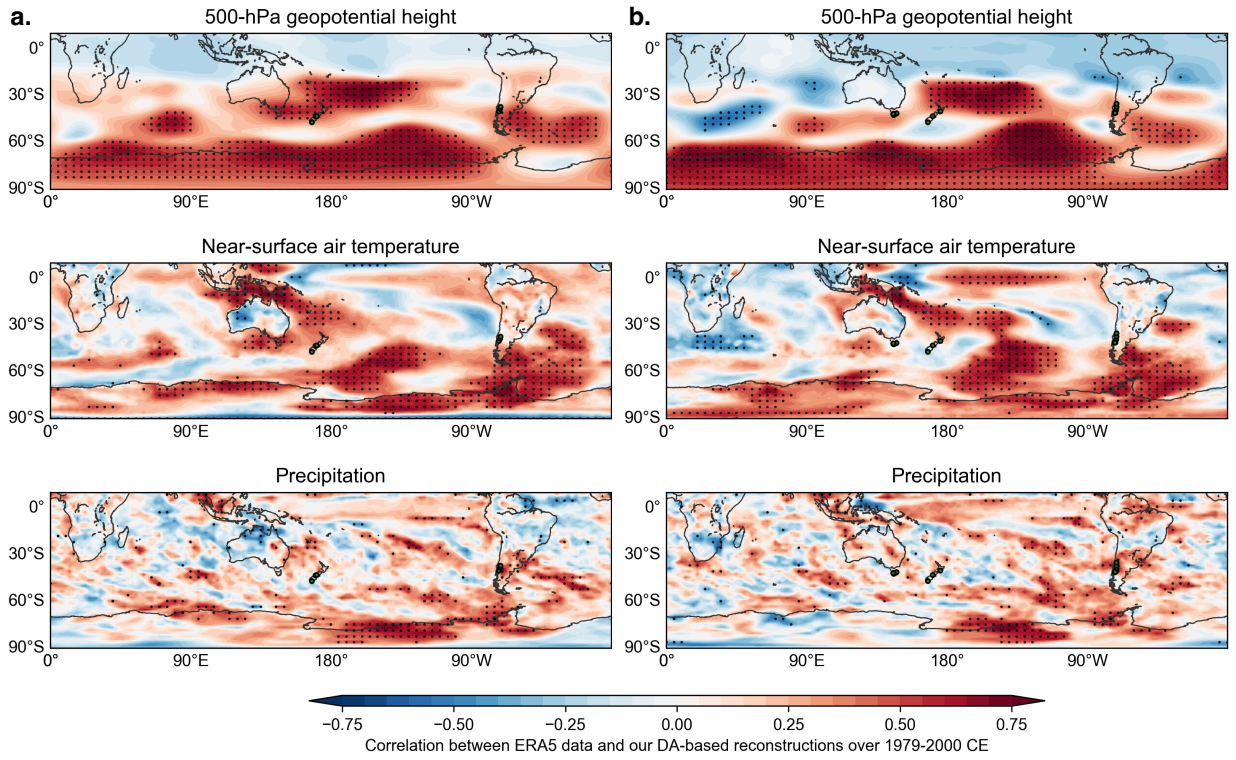


Figure 4.2: *Pearson correlation coefficient between the reconstructed and ERA5 geopotential height at 500 hPa, near-surface air temperature or cumulative precipitation over 1979–2000 CE for the TIC-MDN (a) and TIC-reg (b) experiments (see Sect. 4.3 and Table 4.1 for details on the experiments). The green dots indicate the localization of the assimilated tree-ring width records. The black dots indicate a significant correlation coefficient at the 95% confidence level.*

both ERA5 and GMF, the correlation coefficients are low and not significant for both experiments. This differs from the good general pattern previously noted (Fig. 4.2). Locally, the correlations can indeed be lower (see Figs. D.5–D.10 for the regional pattern of the correlations). It is also important to highlight that these correlations have been computed between the integrated fields and are not the average of the correlations represented on the map, which may result in slight differences (Sect. 4.3). Regarding precipitation (Table 4.2), the correlation coefficients are particularly high and significant in South America (SA) and in the South-Western Andes (SAmSW) for TIC-reg and TIC-MDN.

Over the whole century (1901–2000 CE), both DA experiments have similar skills (ranging from -0.12 to 0.60 for the correlation coefficients, and from -0.12 to 0.36 for the CE, for the four regions; Fig. 4.3; Table 4.3) in reconstructing the near-surface air temperature when compared to the GMF climate dataset. Except in the South-Western Andes region (SAmSW in Table 4.3), the correlation coefficients and CE between reconstructed and GMF temperature are close for both experiments and particularly high in New Zealand (NZ). In Tasmania, no TRW records

Table 4.2: *Pearson correlation coefficient between the reconstructed and GMF and ERA5 near-surface air temperature or precipitation over 1979–2000 CE for different DA experiments with both ice core and tree-ring proxies (Table 4.1) and for different regions (Sect. 4.3). SA stands for South America; SAmSW for the South-Western border of South America in the Andes where the TRW proxy sites are located; NZ for New Zealand; Tas for Tasmania. Asterisks stand for significant correlation coefficients at the 95% confidence level.*

	ERA5		**GMF**	
	TIC-reg	TIC-MDN	TIC-reg	TIC-MDN
Near-surface air temperature				
SA	-0.07	0.04	0.12	0.20
SAmSW	-0.15	0.13	-0.21	0.14
NZ	0.11	0.33	0.14	0.32
Tas	0.05	0.56*	0.17	0.52*
Precipitation				
SA	0.72*	0.71*	0.65*	0.64*
SAmSW	0.54*	0.44*	0.53*	0.44*
NZ	0.25	0.26	0.28	0.44*
Tas	0.10	0.00	0.16	0.14

have been assimilated with MAIDEN, which explains the lower CE (Table 4.3) for the TIC-MDN experiment, while the correlation coefficients are similar between both experiments. As for precipitation (Table 4.3 and Fig. 4.4), both TIC-MDN and TIC-reg are more skillful in the vicinity of the South American TRW proxies (SAmSW), with significant correlation coefficients of 0.35 and 0.37, respectively, and positive CE.

Overall, the reconstructed variance of the climate changes is far smaller than the observed variance, for both near-surface temperature and precipitation (Figs. 4.3 and 4.4). Since this pattern is apparent in both experiments, i.e., when using a regression and when using a process-based model as a PSM, this is likely not predominantly related to the intrinsic characteristics of each model. Our DA experiments only include 6 and 12 TRW proxy sites in the mid-latitudes of the SH for TIC-MDN and TIC-reg, respectively. Comparatively, in the high-latitudes, the ice core records are far more numerous (78 records aggregated over a 500 km grid; Sect. 4.2.3.2). However, the ice core records can only have an influence on the reconstructed variance over a limited area. As a consequence, the number of assimilated TRW proxies in the mid-latitudes is probably not sufficient to effectively constrain the climate model simulations during the DA procedure. In the DA framework, when no proxy is assimilated, the posterior as defined in Sect.

Table 4.3: *Pearson correlation coefficient and coefficient of efficiency (CE) between the reconstructed and GMF near-surface air temperature or precipitation over 1901–2000 CE for different DA experiments with both ice core and tree-ring proxies (Table 4.1) and for different regions (Sect. 4.3). SA stands for South America; SAmSW for the South-Western border of South America in the Andes where the TRW proxy sites are located; NZ for New Zealand; Tas for Tasmania. Asterisks stand for significant correlation coefficients at the 95% confidence level.*

	Correlation		**CE**	
	TIC-reg	TIC-MDN	TIC-reg	TIC-MDN
Near-surface air temperature				
SA	0.07	-0.12	-0.06	-0.12
SAmSW	0.34*	0.00	0.12	-0.07
NZ	0.55*	0.54*	0.30	0.27
Tas	0.60*	0.52*	0.36	0.18
Precipitation				
SA	0.12	-0.05	0.00	-0.06
SAmSW	0.37*	0.35*	0.12	0.12
NZ	-0.01	0.10	-0.12	-0.02
Tas	0.08	0.04	-0.02	-0.02

4.2.1 is equivalent to the prior, in which all the particles have the same weight. The posterior and the resulting ensemble mean are thus the same for each year of the reconstruction. As a consequence, the reconstruction has, by construction, a variance equal to zero. For a small number of proxies providing a weak constrain, many particles receive a similar weight, resulting in a small variance too. By contrast, the uncertainty of the reconstruction (as measured by the standard deviation of the posterior or the ensemble spread; Sect. 4.2.1) remains large. Additionally, both the MAIDEN and regression models work on the basis of normalized observed and simulated tree-ring growth indexes. Consequently, in the DA procedure, the error in the simulated variance of the climate signal is likely not properly assessed with the TRW PSMs. It is in practice possible to transform tree-ring data in order to directly compare them with the output of the MAIDEN model, without normalization [Gennaretti et al., 2018]. This implies to combine both tree-ring width and density measurements, that are less widely available [PAGES 2k Consortium, 2017]. This could improve the model-data comparison in the DA procedure, and, consequently, the resulting reconstruction. This is not the case for the regression model.

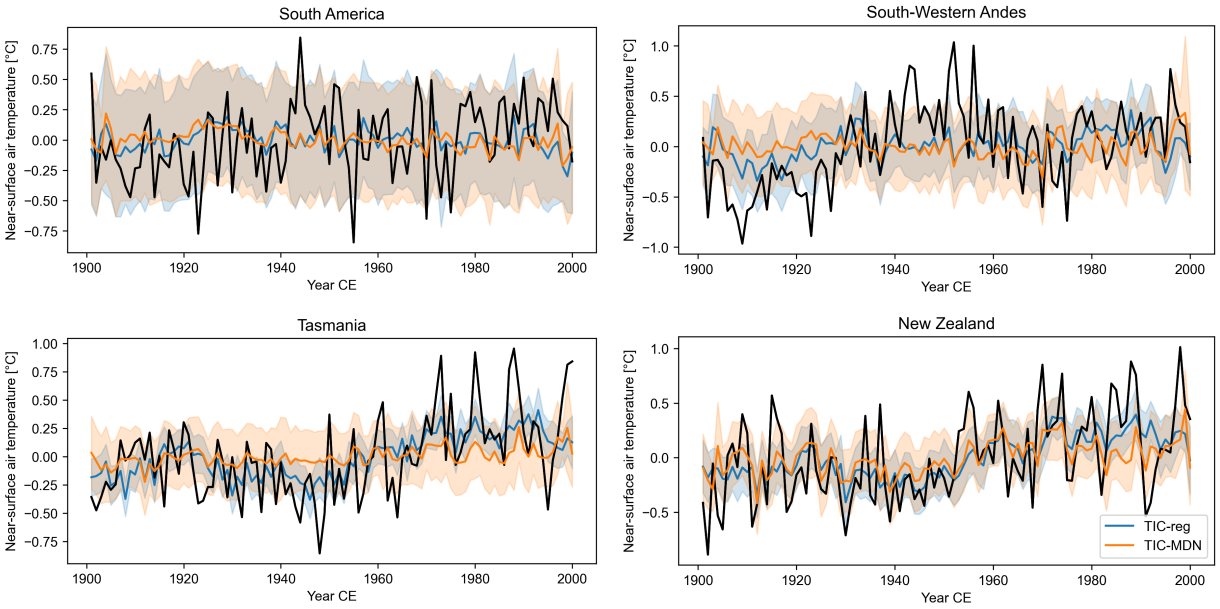


Figure 4.3: *Reconstructed (in color) and GMF (in black) near-surface air temperature anomalies (in ℃; relative to 1901–2000 CE) over 1901–2000 CE for different DA experiments with both ice core and tree-ring proxies (Table 4.1) in different regions (Sect. 4.3). The uncertainty associated with each reconstruction is represented by the shaded areas.*

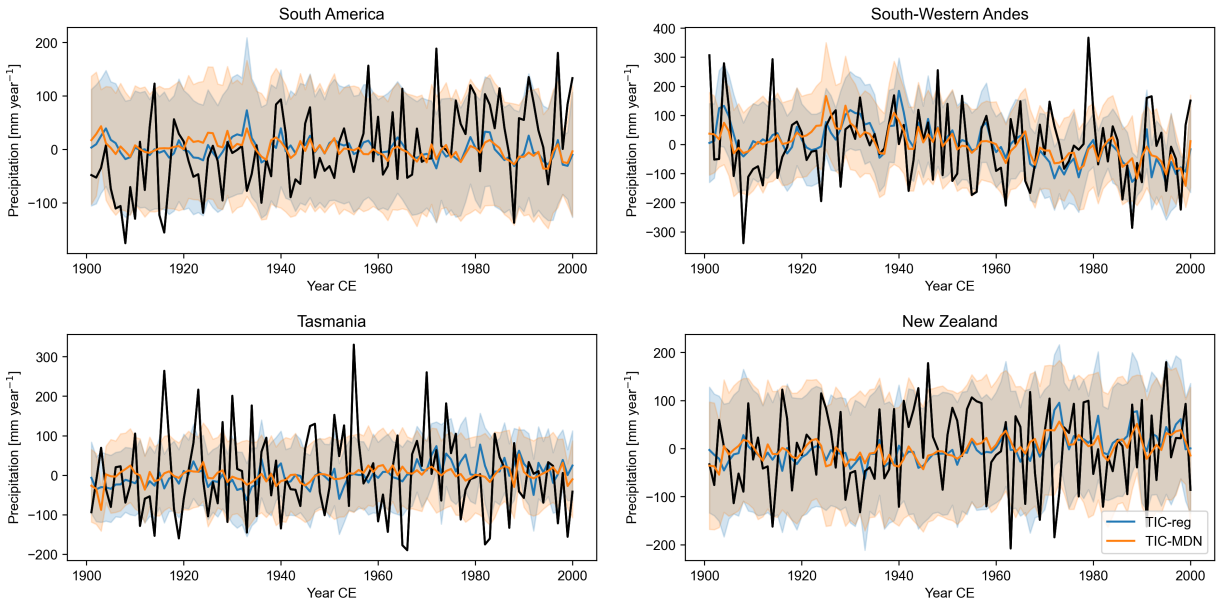


Figure 4.4: *Reconstructed (in color) and GMF (in black) precipitation anomalies (in mm year^{-1}; relative to 1901–2000 CE) over 1901–2000 CE for different DA experiments with both ice core and tree-ring proxies (Table 4.1) in different regions (Sect. 4.3). The uncertainty associated with each reconstruction is represented by the shaded areas.*

The DA procedure seeks to identify the climate conditions (i.e., the inputs of the TRW PSM) that gave rise to the observed TRW. As a consequence, to fully verify our DA procedure, we must also establish if the reconstruction of near-surface air temperature and precipitation translates into a local ability of the MAIDEN model to reproduce tree growth at the six assimilated TRW sites over the 20th century. Note that depending on the sites, the last year of TRW observations may slightly vary (from 1993 up to 2000). First, we have retrieved the monthly climate fields from the annual TIC-MDN reanalysis using the temporal covariance of the iCESM1 model. Then, the monthly climate inputs have been converted to daily inputs as in Sect. 4.2.4.1. For consistency, the tree-growth time series of the MAIDEN model have been normalized with the mean and the standard deviation of the reference run used in the DA procedure (Sect. 4.2.4.1). If we only look at the correlation coefficients between the observed and simulated tree-growth indexes (Fig. D.11), MAIDEN has been successfully run over 1900–2000 CE with the TIC-MDN reanalysis of near-surface air temperature and precipitation as inputs at most assimilated sites (with a mean correlation of 0.59). The TRW sites displaying lower correlation coefficients between the observed and simulated tree-ring indexes are the ones associated with higher PSM errors (Sect. 4.2.5), i.e., Aus_002 and SAm_024. This result is logical as the proxy records with lower PSM errors are expected to be better reconstructed than the records with a higher PSM error. A lower confidence is given to the latter in the particle filter (Sect. 4.2.1), so that the climate variability reconstructed at the local scale is less influenced by those records. However, the simulated variance is strongly underestimated compared to the observations, as seen on Fig. D.11. This underestimation of the variance of tree growth directly comes from the underestimation of the variance in the reconstructed near-surface air temperature and precipitation, as highlighted above. In turn, this underestimation of the variance in the reconstruction likely comes from the low number of TRW proxies included in the DA procedure. The same pattern of small simulated variance is observed with the tree-ring indexes simulated with the linear regression.

Finally, the reconstructed SAM index is well and significantly correlated with the SAM index from Marshall [2003] for TIC-MDN (0.46) and TIC-reg (0.50) over the 1957–2000 CE period (Fig. 4.5). However, the TIC-reg experiment slightly better captures the positive trend of the SAM index, with a significant reconstructed trend of 0.34 and non-significant reconstructed trend of 0.20 standard deviation per decade for TIC-reg and TIC-MDN, respectively, and a significant observed trend of 0.28 standard deviation per decade over 1957–2000 CE. However, both reconstructions display negative values for the CE, which indicates that they are unable to accurately reproduce the observed amplitude of the SAM index.

Overall, the DA experiment using MAIDEN as a PSM for assimilating the TRW records does not outperform the experiment using the regression model. However, its skill is always as good as the TIC-reg experiment, with less TRW proxy

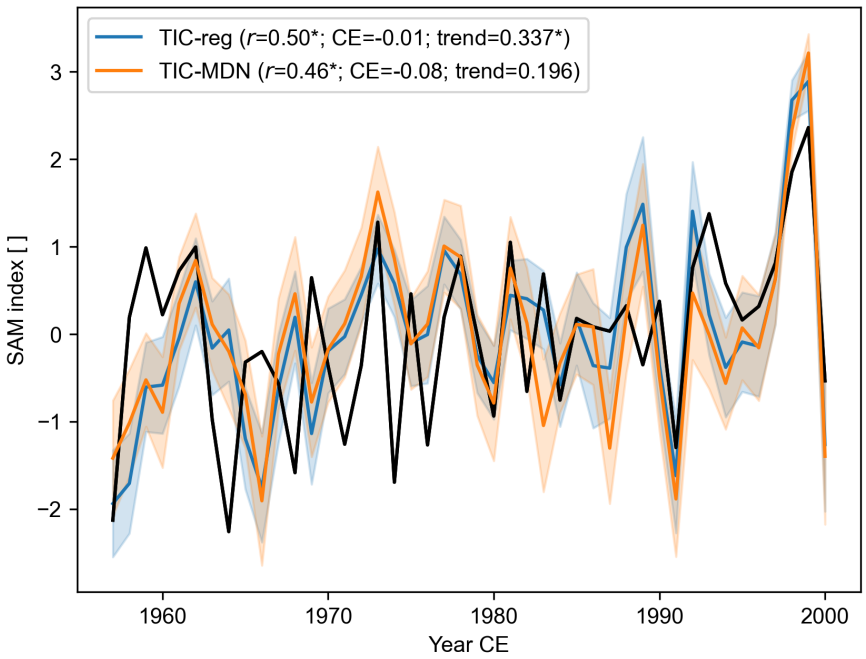


Figure 4.5: *Z-scored (relative to 1957-2000 CE) Southern Annular mode (SAM) index of Marshall [2003] (in black) and reconstructed SAM index (in color) over 1957–2000 CE for different DA experiments with both ice core and tree-ring proxies (Table 4.1); Pearson correlation coefficient (r), coefficient of efficiency (CE), and decadal trend of the reconstructed SAM index (trend). Asterisks stand for a significant correlation coefficient or trend at the 95% confidence level. The observed trend of the SAM index is 0.28* standard deviation per decade over 1957–2000 CE. The uncertainty associated with each reconstruction is represented by the shaded areas.*

sites assimilated, and a potential better stability of MAIDEN through time, since it has been independently validated at the assimilated sites (Sect. 4.2.4.1; contrary to the sites assimilated with the regression model; Sect. 4.2.4.2). It is also worth noting that the DA experiments with MAIDEN or the regression model have some characteristics that can influence their respective skills. Firstly, the DA experiment with the regression model includes twice the number of TRW records compared to the experiment with MAIDEN (12 and six, respectively, see Sect. 4.2.4.1 and 4.2.4.2 for more details on the selection of TRW records). The TRW records can also be located at different places which may result in different local skills of the DA experiments (e.g., in Tasmania). Secondly, the regression model was calibrated over the whole century (1901–2000 CE), while MAIDEN was calibrated over the second half of the century. This may confer a comparative advantage to the regression-based DA experiment, particularly when evaluated against the GMF climate dataset over 1901–2000 CE (Sect. 4.3).

4.4.2 Contribution of tree-ring proxies in the data assimilation framework over the last century

For evaluating the contribution of the different types of proxy included into the data assimilation framework, we focus on the regions and climate variables for which the reconstructions over the last century are the most consistent regarding the observations, i.e., precipitation in South America and near-surface air temperature in New Zealand (Sect. 4.4.1). In South America (SA; Table 4.4 and Fig. 4.6), the correlations with observations are low for the experiments with tree-ring proxies alone (TREES-reg and TREES-MDN). Ice core proxies alone (IC) perform better than the tree-ring proxies alone (TREES-reg and TREES-MDN) or when combined with the tree-ring proxies (TIC-reg and TIC-MDN) in terms of correlation coefficients, but not in terms of reconstructed variance (standard deviation for TIC-reg, TIC-MDN, TREES-reg or TREES-MDN higher than IC). However, as previously noted, it is clear from the reconstruction of precipitation that, even though the reconstructions with tree-ring proxies display a higher variance, none of the DA experiments accurately reconstruct the observed variance of the climate changes (Fig. 4.6).

At the more local scale, in the South-Western Andes (SAmSW), the tree-ring proxies alone provide a better reconstruction skill than for the South America when it comes to the correlation coefficients and to the reconstructed variance (TREES-reg and TREES-MDN; Table 4.4). The correlation coefficients are, however, slightly lower than when combined with ice core proxies or with the ice core proxies alone. Nevertheless, it is associated with a higher reconstructed variance compared to ice core proxies only, in particular for TREES-reg, even though it is still underestimated compared to the observations (Fig. 4.6). The combination of both tree-ring and ice core proxies (TIC-reg and TIC-MDN) provides the best reconstruction in the South-Western Andes, in terms of correlation coefficients and of reconstructed variance.

At the scale of the proxy site (i.e., the grid cell closest to the proxy site; e.g., SAm_11, the tree-ring proxy site assimilated both with MAIDEN and the regression model), the correlation coefficients are similar for all the experiments, so that the different proxy records all bring some information, but when tree-ring records are included, an improvement of the reconstructed variance is obtained. However, SAm_11 is the only tree-ring proxy site (out of three) assimilated with MAIDEN in South America where the reconstructed variance is higher for TREES-MDN than for IC (Table 4.4). The reconstructed variance is higher for TREES-reg than for IC at three out of five assimilated tree-ring proxy sites. Additionally, the reconstructed variance at the scale of the proxy site increases compared to the South-Western Andes (SAmSW) at two out of three assimilated sites for TREES-MDN and three

out of five assimilated sites for TREES-reg (among which SAm_11). It always increases compared to South America (SA).

Table 4.4: *Pearson correlation coefficient between the reconstructed and GMF near-surface air temperature or precipitation over 1901–2000 CE for different DA experiments (Table 4.1, with ice core proxies only, with tree-ring proxies only or with both) in different regions (Sect. 4.3) and proxy sites (Fig. 4.1). Standard deviation of the reconstruction in °C (near-surface air temperature) or in mm year^{-1} (precipitation). SA stands for South America; SAmSW for the South-Western border of South America in the Andes where the TRW proxy sites are located; NZ for New Zealand. Aus refers to a site in New Zealand and SAm, in South America. Asterisks stand for significant correlation coefficients at the 95% confidence level.*

	Correlation				
	TIC-reg	TIC-MDN	IC	TREES-reg	TREES-MDN
Precipitation					
SA	0.12	-0.05	0.28*	0.02	-0.20*
SAmSW	0.37*	0.35*	0.34*	0.33*	0.26*
SAm_11	0.26*	0.22*	0.22*	0.22*	0.14
Near-surface air temperature					
NZ	0.55*	0.54*	0.50*	0.53*	0.52*
Aus_005	0.20*	0.26*	0.29*	0.19	0.24*
Aus_030	0.49*	0.41*	0.30*	0.57*	0.48*

	Standard deviation				
	TIC-reg	TIC-MDN	IC	TREES-reg	TREES-MDN
Precipitation					
SA	17.82	15.29	8.31	17.22	18.53
SAmSW	63.59	51.79	33.79	52.00	38.50
SAm_11	59.51	41.84	17.63	57.74	41.38
Near-surface air temperature					
NZ	0.19	0.15	0.11	0.18	0.13
Aus_005	0.21	0.17	0.11	0.21	0.16
Aus_030	0.17	0.13	0.07	0.18	0.13

In New Zealand, the correlations with observations are similar in all the experiments (NZ; Table 4.4). In other words, tree-ring proxies only are able to provide a skill at the scale of the New Zealand, even without assimilating ice core proxies, and with a slightly higher reconstructed variance (especially for TREES-reg). The contrast between the reconstructed variance in IC and TREES-reg or TREES-MDN experiments is stronger at the scale of the proxy site (Aus_005 and Aus_030, the tree-ring proxy sites assimilated both with MAIDEN and the regression model). At the Aus_030 proxy site the correlation coefficients are even higher for the ex-

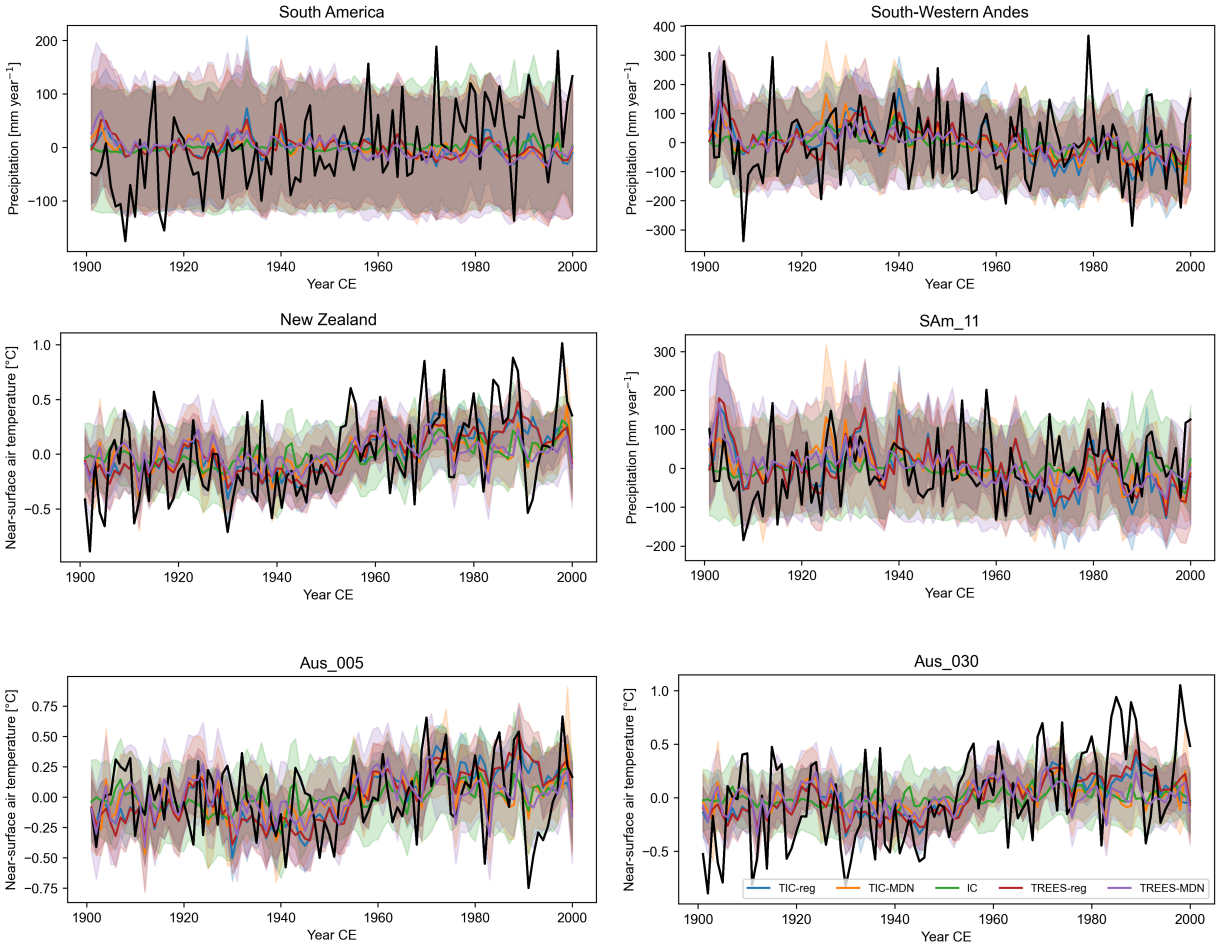


Figure 4.6: *Reconstructed (in color) and GMF (in black) temperature (in ℃; relative to 1901–2000 CE) or precipitation anomalies (in mm year^{-1}; relative to 1901–2000 CE) over 1901–2000 CE for different DA experiments (Table 4.1, with ice core proxies only, with tree-ring proxies only or with both) in different regions (Sect. 4.3) and proxy sites (Fig. 4.1). Aus refers to a site in New Zealand and SAm, in South America. The uncertainty associated with each reconstruction is represented by the shaded areas.*

periments assimilating tree-ring proxies only compared to ice core proxies only. Similar results are obtained at the other assimilated tree-ring proxy sites. The reconstructed variance can slightly increase at the scale of the proxy site compared to the whole New Zealand. However, the reconstructed variance is still underestimated compared to observations (Fig. 4.6).

Reducing the error associated with the PSMs (Sect. 4.2.5) by two increases the reconstructed variance at all spatial scales in both South America (precipitation) and New Zealand (near-surface air temperature; Table 4.5 and Fig. 4.7). This does not translate, however, into higher correlation coefficients, since they virtually remain unchanged (Table 4.5).

Table 4.5: *Pearson correlation coefficient between the reconstructed and GMF near-surface air temperature or precipitation over 1901–2000 CE for different DA experiments (Table 4.1, with tree-ring proxies only, with the full observation error or the half of the observation error; see Sect. 4.3 for more details) in different regions (Sect. 4.3) and proxy sites (Fig. 4.1). Standard deviation of the reconstruction in ℃ (near-surface air temperature) or in mm year^{-1} (precipitation). SA stands for South America; SAmSW for the South-Western border of South America in the Andes where the TRW proxy sites are located; NZ for New Zealand. Aus refers to a site in New Zealand and SAm, in South America. Asterisks stand for significant correlation coefficients at the 95% confidence level.*

	Correlation			
	TREES-reg	TREES-MDN	TREES-reg-05	TREES-MDN-05
Precipitation				
SA	0.02	-0.20	-0.05	-0.19
SAmSW	0.33*	0.26*	0.37*	0.24*
SAm_11	0.22*	0.14	0.21*	0.16
Near-surface air temperature				
NZ	0.53*	0.52*	0.51*	0.50*
Aus_005	0.19	0.24*	0.23*	0.25*
Aus_030	0.57*	0.48*	0.57*	0.48*

	Standard deviation			
	TREES-reg	TREES-MDN	TREES-reg-05	TREES-MDN-05
Precipitation				
SA	17.22	18.53	25.12	26.73
SAmSW	52.00	38.50	75.51	60.58
SAm_11	57.74	41.38	79.44	60.13
Near-surface air temperature				
NZ	0.18	0.13	0.23	0.21
Aus_005	0.21	0.16	0.27	0.26
Aus_030	0.18	0.13	0.22	0.22

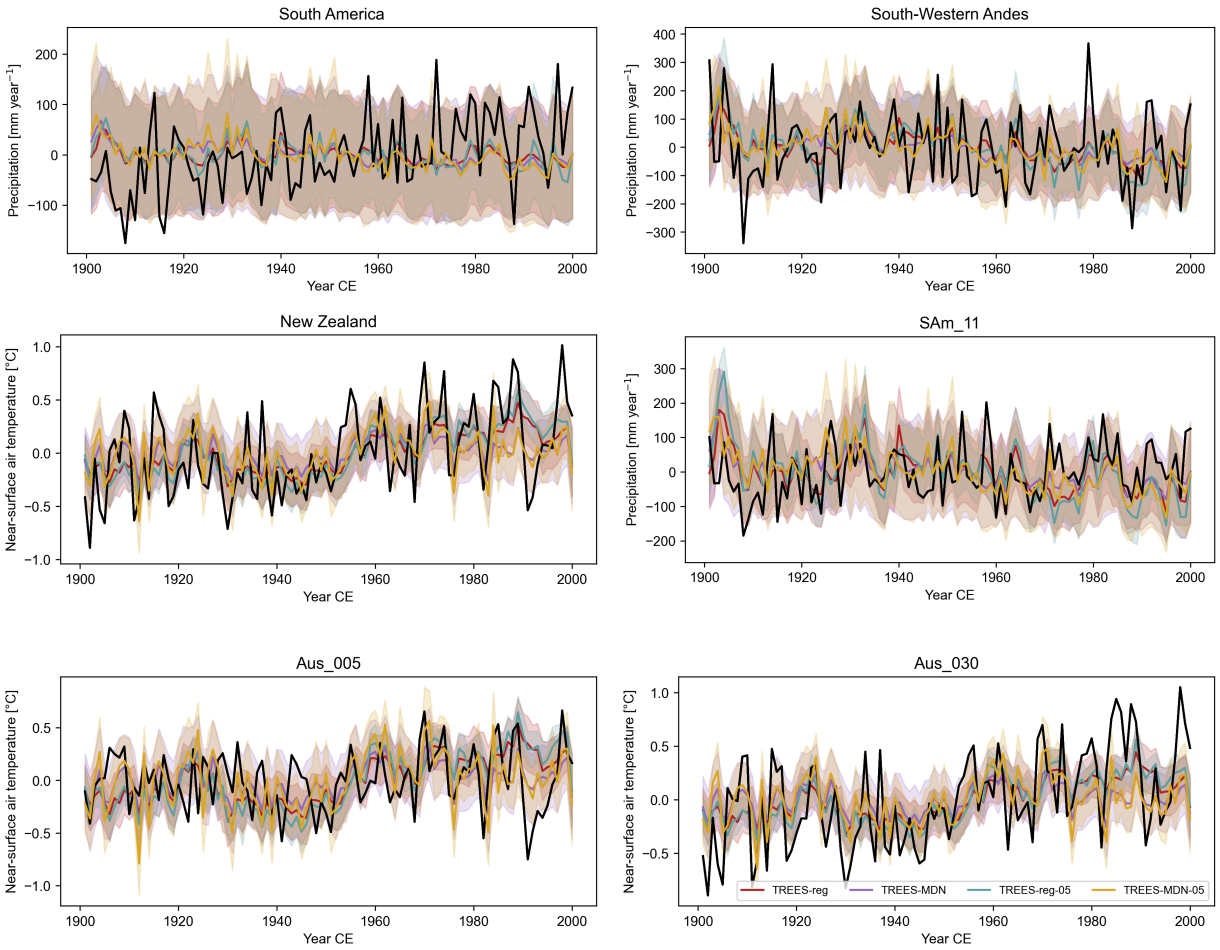


Figure 4.7: *Reconstructed (in color) and GMF (in black) temperature (in °C; relative to 1901–2000 CE) or precipitation anomalies (in mm year^{-1}; relative to 1901–2000 CE) over 1901–2000 CE for different DA experiments (Table 4.1, with tree-ring proxies only, with the full observation error or the half of the observation error; see Sect. 4.3 for more details) in different regions (Sect. 4.3) and proxy sites (Fig. 4.1). Aus refers to a site in New Zealand and SAm, in South America. The uncertainty associated with each reconstruction is represented by the shaded areas.*

More generally, this sensitivity analysis shows that tree-ring proxies have a positive effect on the reconstructed mid-latitude climate changes in our framework, especially at the regional to local scale, both on the correlation with observations and on the reconstructed variance. The fact that the reconstructed variance can increase at the more local scale when assimilating tree-ring proxies alone indicates that the number of tree-ring proxies assimilated in our experiments likely has an impact on the reconstructed variance. If more proxies were available, we could expect that this local increase in the variance would lead to an increase at larger spatial scale. The definition of the error related to the PSMs likely plays a role as well. In particular, the computation of the error for MAIDEN is stricter than for the regression model (i.e., computed on the verification period and on the calibration period, respectively; Sect. 4.2.5) and the number of proxy records assimilated with MAIDEN is lower as well, which may advantage the regression-based PSM.

4.4.3 Data assimilation based reconstruction of the Southern Hemisphere climate over the last 400 years

If we first look at the regional reconstructions of near-surface air temperature (Fig. 4.8) and precipitation (Fig. 4.9) for the four regions (Sect. 4.3), we observe that the ensemble spread is in general large, contrasting with an interannual variability of the reconstructions that is generally small. As highlighted before, this is at least partly due to the small number of assimilated TRW proxies in the mid-latitudes that prevents the climate model to be effectively constrained by the available observations. This pattern is stronger when the spatial scale is large (e.g., South America), and weaker when the spatial scale is small (e.g., Tasmania), i.e., closer to the proxy sites. This is particularly true for MAIDEN, for which we assimilated half the number of TRW proxy records compared with the regression model.

In New Zealand, both TIC-reg and TIC-MDN display a smaller spread and larger variability of the reconstructed near-surface air temperature compared to the other regions (Fig. 4.8), which suggests that the DA has been more effective in updating the climate model simulations with the available proxy records. The reconstructed near-surface air temperature in New Zealand was also well evaluated against GMF observations over 1901–2000 CE in Sect. 4.4.1 (Table 4.3). The trend followed by the two reconstructions over the last 400 years is relatively similar overall, with a very small trend before the industrial era (until around 1850-1900 CE) followed by an increase in temperature. TIC-reg and TIC-MDN display a significant trend of 0.047 and 0.023 °C per decade after 1900 CE (against 0.062 °C per decade in the GMF observations) and a significant trend of 0.001 and non-significant trend of 0 °C per decade before 1900 CE, respectively. The significant correlation coefficient between both reconstructions is 0.63, which indicates that the trend and timing of the reconstructions are close to each other. However, TIC-

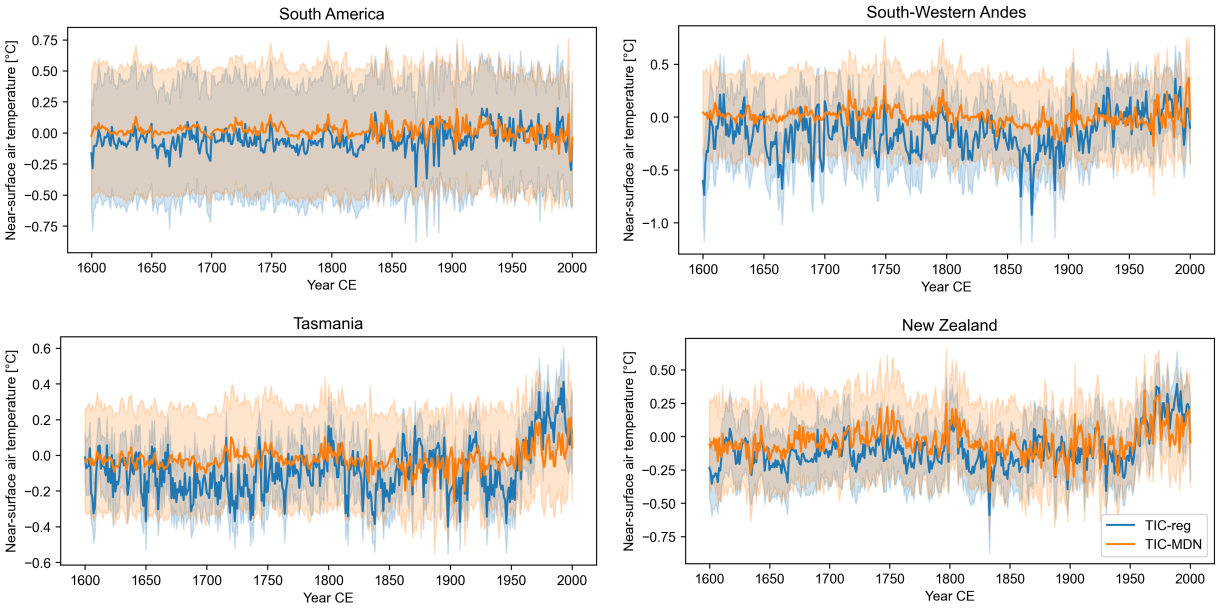


Figure 4.8: *Reconstructed TIC-reg (in blue) and TIC-MDN (in orange) near-surface air temperature anomalies (in ℃; relative to 1901–2000 CE) over 1600–2000 CE (Table 4.1) in different regions (Sect. 4.3). The uncertainty associated with each reconstruction is represented by the shaded areas.*

MDN displays higher near-surface air temperature anomalies before 1850 CE than TIC-reg (-0.05℃ in average for TIC-MDN, against -0.14℃ for TIC-reg, relative to 1901-2000 CE). In Tasmania, there are no assimilated sites for MAIDEN (Figs. D.3 and D.7) and four assimilated sites for the regression over a very small area (Figs. D.4 and D.10), which may explain the difference between the reconstructed near-surface air temperature of TIC-reg and TIC-MDN (Fig. 4.8).

For precipitation (Fig. 4.9), the South-Western Andes is the region for which the ensemble spread is the smallest and the interannual variability is the largest for both TIC-reg and TIC-MDN. Both experiments are also skillful for reconstructing precipitation in this region when compared with the state-of-the-art climate datasets over the last century (Table 4.3; Sect. 4.4.1). The correlation coefficient between both reconstructions is 0.58 and is significant, so that the trend and timing of the reconstructions are close to each other. Both reconstructions display a very small trend before 1900 CE (a significant trend of -0.586 and a non-significant trend of -0.042 mm year^{-1} per decade for TIC-reg and TIC-MDN, respectively) and a negative trend after 1900 CE (a significant trend of -12.79 and -8.89 mm year^{-1} per decade for TIC-reg and TIC-MDN, respectively; against a non-significant trend of -1.26 mm year^{-1} per decade in the GMF observations). However, TIC-MDN displays higher anomalies before 1900 CE than TIC-reg (28.23 mm year^{-1} in av-

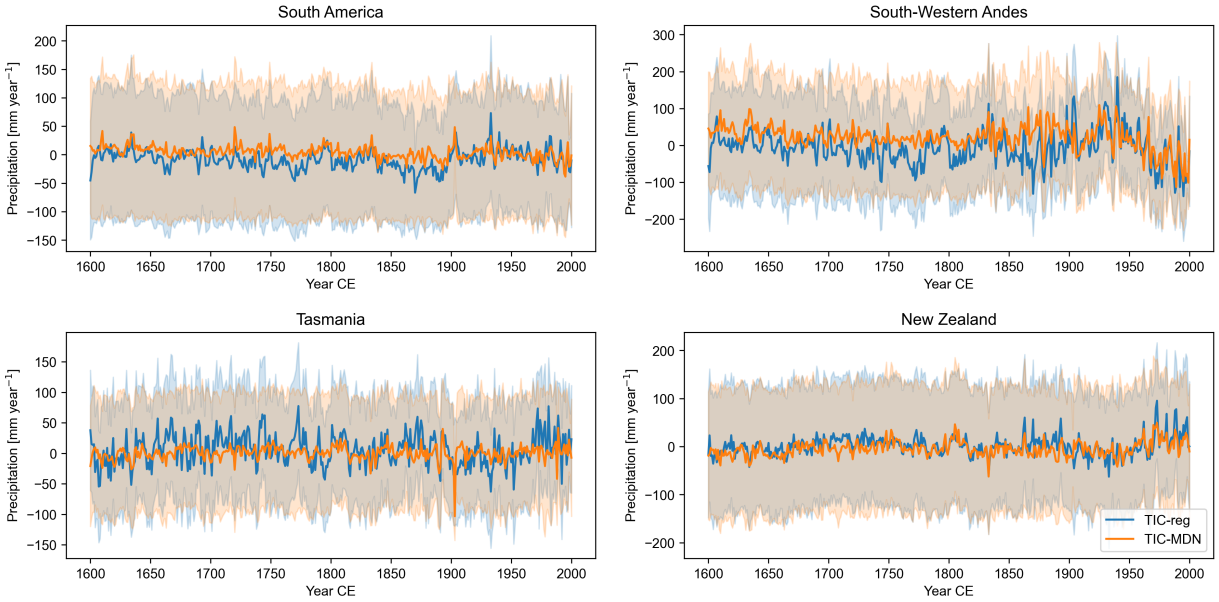


Figure 4.9: *Reconstructed TIC-reg (in blue) and TIC-MDN (in orange) precipitation anomalies (in mm year^{-1}; relative to 1901–2000 CE) over 1600–2000 CE (Table 4.1) in different regions (Sect. 4.3). The uncertainty associated with each reconstruction is represented by the shaded areas.*

erage for TIC-MDN against -5.70 mm year^{-1} for TIC-reg, relative to 1901-2000 CE).

At the regional scale (in New Zealand and in the South-Western Andes in particular), we have highlighted from the reconstructed near-surface air temperature and precipitation that the experiments with the statistical or process-based PSM show different amplitudes of climate change over the past 400 years, even if close in terms of correlation (i.e, the trend and timing of change). It is not possible, of course, to determine which one is better. This point would need further investigation with more TRW proxy records assimilated. Indeed, this difference in the reconstructions could also be related to the number of proxies, but also to the proxies included in each of the DA experiments, and their associated error (Sect. 4.2.5).

Finally, we observe an increase of the reconstructed variability in the precipitation of the South-Western Andes (Fig. 4.9), particularly for TIC-MDN, from around 1800–1850 CE, i.e., when most of the ice core records start to become available (Fig. D.12). Before 1830 CE, the standard deviation of the reconstruction is 30.7 and 21.0 mm year^{-1} and, after 1830 CE, 56.3 and 44.2 mm year^{-1} for TIC-reg and TIC-MDN, respectively. Additionally, in this region, two out of three sites assimilated with MAIDEN start before the 18th century. Similarly, for TIC-reg, only two sites out of five in the South-Western Andes start before the 18th century. More-

over, those two assimilated sites are regressed against temperature in TIC-reg. The South-Western Andes, due to their proximity to the Antarctic Peninsula, are likely more influenced by the presence of numerous ice core records, compared with New Zealand (TIC-reg and TIC-MDN) or Tasmania (TIC-reg) for example, where this increase of interannual variability is not observed in the reconstructed near-surface air temperature (Fig. 4.8). Moreover, in Tasmania (TIC-reg), there are four proxy records on a small area (Figs. D.4 and D.10) that all start before 1600 CE.

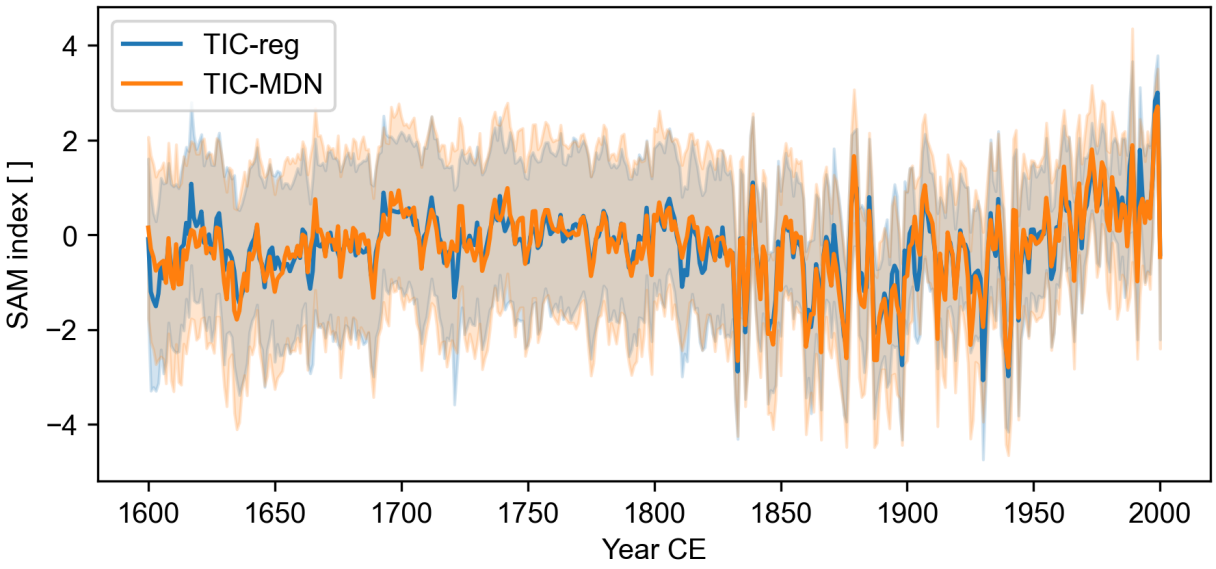


Figure 4.10: *Z-scored (relative to 1901–2000 CE) TIC-reg (in blue) and TIC-MDN (in orange) reconstructed SAM index over 1600–2000 CE (Table 4.1). The uncertainty associated with each reconstruction is represented by the shaded areas.*

This increase of interannual variability is even more striking in the reconstructed SAM index for both reconstructions (Fig. 4.10). Before around 1830 CE particularly, too few TRW proxy sites have been assimilated in the mid-latitudes to be able to reconstruct the large-scale variability adequately with less ice core records (Fig. D.12). The standard deviation of the z-scored reconstructed SAM index is 0.52 and 0.51 before 1830 CE and 1.05 and 1.11 after 1830 CE for TIC-reg et TIC-MDN, respectively. However, the SAM reconstructions are still highly and significantly correlated with each other (r = 0.91), and look essentially the same over the whole 1600-2000 CE period (Fig. 4.10). Before 1830 CE, when the number of ice core records is more limited (Fig. D.12), the reconstructions are less correlated (r = 0.77; and r = 0.95 after 1830 CE).

Lastly, over the last 400 years, the MAIDEN model generally reproduces the observed tree growth well in terms of correlation coefficients at the six assimilated sites (with a mean correlation of 0.53; Fig. D.13). However, as previously

highlighted in Sect. 4.4.1, the simulated variance is largely underestimated compared to the observations, which is not surprising regarding the reconstructions of near-surface air temperature and precipitation of the past 400 years.

4.5 Conclusion

In this study, we have included for the first time a dendroclimatic process-based model into a data-assimilation procedure to reconstruct the past climate variability of the Southern Hemisphere. We have then compared all the results from our DA experiments with the commonly used regression-based PSM.

First, we have shown that including the ecophysiological model MAIDEN into a data-assimilation procedure is technically possible. The assimilation of actual TRW records with a tree-growth mechanistic model has never been done before. Knowing that it is at least achievable is promising. The general pattern of near-surface air temperature, precipitation and the atmospheric circulation of the mid- to high-latitudes of the SH is well reproduced by the DA experiment with MAIDEN over the recent period. Over the last century, the DA experiment with MAIDEN is also able to produce reconstructions that are well correlated with different climate fields, such as near-surface air temperature, precipitation and atmospheric circulation in some regions of the Southern Hemisphere, with only a few TRW proxy records. The DA-based reconstructions with the regression have been similarly validated against state-of-the-art climate datasets as MAIDEN. The skill of MAIDEN as a PSM in the DA framework is not better but at least as good as the regression-based PSM. Given the advantages that a process-based PSM can bring in terms of non-linearity of the relationship between climate and tree growth, but also in terms of climate variables included as inputs of the model (e.g. atmospheric CO_2 concentration), having a comparable skill to a regression-based PSM is encouraging. There are still opportunities for improvement with the MAIDEN model while for the regression, the perspectives are more limited. For instance, we could improve the model-data comparison by using an observed tree growth index that is closer to what MAIDEN simulates, i.e., forest carbon accumulation. Different shortcomings related to the calibration of the MAIDEN model have also been addressed in Rezsöhazy et al. [2020] and Rezsöhazy et al. [2021]. If solved, this may likely help to increase the number of proxy sites where MAIDEN could be validated, but also improve the performance of MAIDEN in simulating the relationship between climate and tree growth, and so enhance the skill of the DA-based reconstruction using MAIDEN as a PSM. Moreover, in this study, the criteria for including a TRW proxy record with the regression had to be less strict than for MAIDEN. MAIDEN was indeed validated at all the assimilated sites while the regression was not. This may provide a better stability of the MAIDEN model.

However, it appears clearly that our DA framework does not include enough TRW proxy records in the mid-latitudes to properly reproduce the observed variance of near-surface air temperature and precipitation with both TRW PSMs, particularly at larger spatial scale (e.g., South America). The Southern Hemisphere counts indeed few TRW proxy records compared with the Northern Hemisphere [PAGES 2k Consortium, 2017] but offers an interesting framework as few reconstructions of the Southern Hemisphere climate exist to date [Neukom et al., 2011, 2014]. This pattern of variance becomes even more striking before 1830 CE, where we observe a smaller interannual variability of the reconstructed near-surface air temperature and precipitation in some regions of the mid-latitudes, and of the reconstructed SAM index, compared to the last 150 years. However, the timing of the climate changes is well reconstructed in some localized areas of the mid-latitudes, e.g., the South-Western Andes, New Zealand and Tasmania, as shown by the significant and relatively high correlations with the observations. As a consequence, the MAIDEN model simulates tree-ring growth series that are generally well correlated with the observations over the last 400 years, but which display a small variance compared to the observations.

At the local scale, we have highlighted a difference between the two DA experiments in the reconstructed amplitude of the climate change in the preindustrial era relative to the 20th century. Using MAIDEN as a PSM for TRW records tends to reconstruct an average warmer and wetter climate than the regression-based PSM. However, this would need an in-depth investigation with more TRW proxy records in order to be confirmed.

For now, our framework only offers a limited skill of the reconstructions, but our results are encouraging for MAIDEN, and more generally for the use of dendroclimatic process-based models in DA. We are far from providing a complete hemispheric reconstruction of atmospheric fields in the Southern Hemisphere. We are still in the testing phase of our approach, so that comparing our DA-based reconstructions with state-of-the-art reconstructions [e.g. Tardif et al., 2019] would not make sense in this study.

In the future, mechanistic models like MAIDEN will likely become an important tool of the DA framework that would help overcome the potential bias associated with regression models. However, this would require to improve the calibration procedure of MAIDEN, so that the model could be applied more efficiently and more skillfully at large spatial scale. In particular, the calibration procedure could be more informative in the future, for instance in the definition of the prior ranges of the calibrated parameters, that could be set by species or biome. Different data sources, such as satellite data and the associated vegetation indexes, could also be used to better inform the different biological processes in the model (e.g. related to photosynthesis or phenology). More investigation of the performance of

the MAIDEN model as a PSM in the DA procedure compared with the commonly used regression model would also be needed using more TRW proxy records.

5

Conclusions and perspectives

Insight into the past variations of climate beyond the instrumental era is given by proxies of climate, particularly abundant during the last millennium. Among them, tree-ring proxies, and more specifically tree-ring width, are the most widely available, which make them of particular interest for large-scale climate reconstructions. To date, most methods used for inferring past climate variability from tree rings at large spatial scale have been based on the estimation of a statistical relationship between tree-ring proxy and the climate target variable, generally with a linear regression. Statistical approaches have well-known limitations related to the assumptions that tree-growth variations are linearly and stationarily driven by local climate factors only. Process-based dendroclimatic models may be able to overcome some of the limitations of the statistical models by incorporating an explicit representation of the main biological processes driving the potential non-linear response of tree-ring proxies to climate. This provides the opportunity to improve reconstructions of climate variations and thereby, our general understanding of the past climate variability. This thesis was committed to increase our ability to withdraw meaningful climate information from tree-ring proxy networks using mechanistic modelling. To this end, we incorporated for the first time a process-based dendroclimatic model, MAIDEN, into a data assimilation procedure, to answer the following overarching question: "*Can we improve large-scale climate reconstructions based on tree-ring width proxies by taking into account explicitly the links between climate and tree growth with a process-based dendroclimatic model?*". To answer this research question, the thesis has been divided into three chapters, each of them addressing a specific question and corresponding to the steps required for the incorporation of MAIDEN into a data assimilation framework. We

summarize the main achievements related to the Chapters 2 to 4 and answer the associated questions here below.

5.1 What is the adequate method to robustly calibrate MAIDEN in an automatised way when only limited information on the local conditions are available?

Many challenges can arise when applying dendroclimatic process-based models at large spatial scale as required in climate field reconstruction. In particular, the need for meteorological data at high spatial and temporal resolution to run the model and the setting of different constants related to the site characteristics (e.g., soil conditions) can be an obstacle. In Chapter 2, we have developed a protocol to calibrate and apply the MAIDEN model at potentially any tree-ring width site in the extratropical latitudes. The protocol is tested over the 20th century in the Eastern Canadian taiga, with a network of *Picea mariana* tree-ring width chronologies, and in Europe, at three individual tree-ring width sites with different tree species. The Bayesian calibration of the MAIDEN model focuses on the most sensitive parameters of the model related to the photosynthesis and carbon allocation modules, as identified by Gennaretti et al. [2017]. The constants linked to the climate station and site conditions are fixed on the basis of available observations. All other parameters are set to the values given in Gennaretti et al. [2017].

More generally, this chapter has highlighted the possibility of MAIDEN to be applied at large spatial scale for paleoclimate exercises using the calibration protocol developed. Our main results have shown that, for now, a site-specific calibration of MAIDEN is the most adapted for a good performance of the model. It is, however, important to stay aware of the potential overfitting problems that can arise from the systematic application of MAIDEN to a large number of sites. To avoid those problems as far as possible, the model must be calibrated over a long enough period of time using high-resolution or bias-corrected climate inputs, and subsequently validated.

In particular, we have highlighted the sensitivity of the model to the quality of the climate data used as inputs of the model. Even if this does not translate significantly in varying correlation coefficients over the calibration period, the calibrated parameters can highly change between the experiments using climate datasets at different resolutions as inputs of the model. This indicates a potential compensation of the bias related to the climate inputs in the calibration procedure, which may lead to overfitting issues. Simple bias-correction techniques could be used in order to increase the quality of the climate inputs and, as a consequence, the resulting calibration. Additionally, the split-sample validation of the MAIDEN model points out the risk of overfitting related to the limitations of the calibration procedure, with

sometimes high and significant correlation coefficients over the calibration period and low correlation coefficients over the validation period. This is particularly true when calibrating the model over a short period of time (25 years).

At last, we compare our results with MAIDEN by applying the same split-sample validation procedure to the simple VS-Lite model [Tolwinski-Ward et al., 2011]. It has already been applied at the global scale because of the simplicity of its calibration [Breitenmoser et al., 2014] and has been used here as a benchmark. The VS-Lite model displays lower calibration correlation coefficients at our study sites but show more stable calibration and validation correlation coefficients compared to MAIDEN, so that it is less exposed to overfitting problems, likely due to the small number of parameters to be calibrated.

5.2 To which extent is a complex dendroclimatic model such as MAIDEN adapted for application to a large number of sites?

In Chapter 3, the protocol developed in Chapter 2 is tested at global scale and refined, by making use of the tree-ring width records of the PAGES2k database [PAGES 2k Consortium, 2017] over the 20th century.

More generally, this chapter has shown that, even though the calibration of such process-based model is challenging, MAIDEN can be applied at large spatial scale, with a skill similar to a simpler dendroclimatic model such as VS-Lite but with clear benefits associated with the complexity of the model. Consequently, the MAIDEN model has the potential to be incorporated in a data assimilation procedure for improving the large-scale reconstruction of past climate variations, compared to the commonly used regression.

In particular, compared to VS-Lite, MAIDEN has been successfully calibrated and verified at an equivalent number of sites (63 and 64 out of 302 sites for VS-Lite and MAIDEN, respectively; 18 in common), but with less stable correlation coefficients over the calibration and verification periods. We have highlighted important differences in the factors influencing the performance of both models. Contrary to MAIDEN, the performance of VS-Lite is highly sensitive to the strength of the climate signal imprinted in the tree-ring series, in particular temperature. As a result, while the application of VS-Lite can be limited to tree-ring sites displaying a strong temperature signal, which characterizes the extreme growth environments, MAIDEN may be skillful in vast regions where the climate signal in tree rings is complex, incorporating the influence of multiple climatic factors. The performance of MAIDEN is still hindered by the lack of information given to the model during the initialization and calibration procedure (large parameter priors, absence of observed gross primary production (GPP) data to calibrate the parameters in the

photosynthesis module, for instance). However, at the sites where the models are skillfully calibrated, the tree growth dependency on climate is on average better simulated by MAIDEN compared to VS-Lite, which can largely overestimate it. This is an important point to consider when using such simple model for paleoclimate reconstructions. Finally, in this chapter, important challenges related to the calibration of MAIDEN at global scale have been pointed out, in particular to simulate a consistent phenology. The calibration protocol has been slightly updated to avoid potential phenological discrepancies.

5.3 What is the added value of using a dendroclimatic process-based model as a proxy system model in reconstruction of past climates with data assimilation?

On the basis of the developments made in Chapters 2 and 3, we are now able to incorporate, in Chapter 4, the MAIDEN model into a data assimilation procedure. The first and important achievement of this last chapter is that it is technically possible to use MAIDEN as a forward proxy system model (PSM) for tree-ring width observations in the data assimilation framework and, secondly, that the resulting data assimilation-based reconstructions with MAIDEN are at least as good as with a regression-based PSM over the validation period. We have thus been able to prove that the methodology is promising and provides interesting perspective for the future. However, additional work is still needed to fully document the added value of using a dendroclimatic process-based model in the data assimilation framework.

In particular, the procedure has been tested by focusing on the Southern Hemisphere. To do so, we have also made use of ice core records in Antarctica, in order to reconstruct a consistent hemispheric circulation pattern. Over the last century, both data assimilation reconstructions have been similarly validated against observations of near-surface air temperature, precipitation and winds. For now, the MAIDEN model does not surpass the standard regression model used as a PSM for the assimilation of tree-ring data. However, there are clear advantages related to mechanistic modelling, for instance the non-linearity of the tree-growth-to-climate relationship and the inclusion of CO_2 effect on tree growth, which may still result in more robust reconstructions beyond the instrumental era. Moreover, there is still room for large improvements when using MAIDEN, while there are few perspectives with the regression. The results of this chapter are encouraging for MAIDEN, but more tests are required in order to draw stronger conclusions.

5.4 General conclusions

In this thesis, we have shown that calibrating and applying a dendroclimatic process-based model at large spatial scale is possible (Chapters 2 and 3). However, this represents an important challenge and, as a consequence, overfitting problems and biological discrepancies can arise from the calibration procedure, that we must account for. Calibrating the model over a long period of time with high-resolution climate inputs and, most importantly, validating the calibrated parameters is required to avoid overfitting of the calibration as far as possible (Chapters 2 and 3). A screening of the resulting simulated phenology can partly resolve the biological discrepancies arising from the automatised calibration of MAIDEN (Chapter 3). However, this only offers downstream solutions to the identified calibration problems. Therefore, the main limitation to the application of MAIDEN to a large number of sites still lies in the initialization and calibration procedure of the model, in particular because information is missing for an efficient and robust calibration and initialization of the model, as highlighted in Chapter 3.

Despite these challenges, the MAIDEN model offers a skill as good as the simple and easily calibrated VS-Lite model to reproduce the observed tree growth at global scale, but with important benefits for paleoclimate applications. For instance, MAIDEN can be successfully applied to a wider range of environments, in particular where the tree-growth-to-climate relationship is complex, giving the opportunity to reconstruct climate from tree-ring proxies in areas less often used. The complexity of the response of tree growth to climate as shaped by the many biological processes modelled in MAIDEN likely explains why it can, on average, better simulate the climate signal imprinted in tree-ring width series. By effectively incorporating the influence of CO_2 concentration on forest carbon fluxes, the model may be able to better account for the potential non-stationarity of the relationship between climate and tree growth. In this regard, this thesis has highlighted the potential of the mechanistic MAIDEN model to improve our ability to retrieve a robust and relevant climate signal from tree-ring width networks over vast regions of the mid-latitudes, making its complexity worthy (Chapter 3). Subsequently, we have shown that the inclusion of the mechanistic model MAIDEN into a data assimilation framework for assimilating tree-ring width observations is achievable on a technical point of view. Our test case in the Southern Hemisphere highlights the capacity of MAIDEN to be used as a PSM to make the link between climate model outputs at low resolution and tree-ring width proxies. The resulting data assimilation-based reconstructions are overall consistent in terms of correlation coefficients with the large-scale pattern of past near-surface air temperature, precipitation or atmospheric circulation. However, we could not show that it actually improves the reconstruction of past climate variations compared to a regression-based PSM (Chapter 4).

5.5 Perspectives

In this thesis, we have made important steps to demonstrate that the MAIDEN model could improve the large-scale climate reconstructions with data assimilation. In the future, MAIDEN could become a valuable tool to overcome the limitations of the statistical models, provided that some elements are addressed.

When willing to apply MAIDEN, and more generally a process-based model, at large spatial scale, there is a balance to find in order to robustly initialize and calibrate the model at the greatest number of proxy sites, i.e., being informative enough given the available data while not resulting in a calibration procedure that is too costly in terms of processing and computing time.

In the calibration procedure of MAIDEN, we decide to collect only information available globally (or nearly globally) for the initialization and calibration of the model (e.g. high-resolution climate data at a daily time step, site constants such as soil characteristics), and neglect data that are actually not available or easily retrievable for each site (e.g. slope, aspect, root profile, GPP at a daily resolution). This also implies to focus on a minimum but sufficient number of parameters to calibrate, and thus omit the calibration of less sensitive parameters of the model. Those non-calibrated parameters are fixed to their previously calibrated value, in Gea-Izquierdo et al. [2015] and Gennaretti et al. [2017]. We also set large prior ranges for the Bayesian calibration of the most sensitive parameters, which incorporate as much site conditions as possible for an application at large spatial scale, but can result in a less efficient Bayesian calibration at the local scale. Finally, as underlined throughout the manuscript, the tree-ring width observations against which we calibrate and evaluate MAIDEN can not be directly compared with the output of the model (i.e., carbon accumulation in the forest stand). As a result, the normalization of the observations and simulations hinders a complete calibration and evaluation of the variance of the simulated tree growth index against the tree-ring width observations. It is in theory possible to compute a wood biomass production index as in Gennaretti et al. [2018] to directly compare observations with the output of MAIDEN, but this would require to have access to density data as extensively as tree-ring width data, both for the earlywood and latewood fractions, which does not seem feasible given their availability at large spatial scale.

Unavoidably, all this can translate into overfitting problems and biological discrepancies at the calibrated sites, as pointed out in this thesis. Even though our calibration procedure has produced encouraging results with MAIDEN, these shortcomings of the calibration procedure still limit the application of MAIDEN at a large number of sites. If solved, the calibration and application of MAIDEN at large spatial scale would become far more effective. In order to mitigate those shortcomings, different solutions may exist that tackle the problem at the source,

i.e the lack of information needed to robustly initialize and calibrate MAIDEN, and not the consequences of it, as we have done up to now.

For instance, the calibration of the sensitive parameters related to the photosynthesis module in MAIDEN could be improved. In this thesis, these parameters are calibrated at the study site by comparing the normalized tree-ring width observations with the normalized annual quantity of carbon allocated to the stem simulated by MAIDEN. In Gennaretti et al. [2017], the photosynthesis parameters are calibrated against GPP data. In particular, Gennaretti et al. [2017] extracted the gross ecosystem production, assumed to be comparable to the simulated GPP of MAIDEN in the study, from an eddy covariance (i.e., a method to measure exchange rates of trace gases between the atmosphere and the ecosystems; Baldocchi et al., 2001) station of the Fluxnet network (Baldocchi et al., 2001; `https://fluxnet.org/`) closest to the study site. Using machine learning techniques to combine the carbon flux measurements from the network of Fluxnet eddy covariance stations with remote sensing and meteorological data, the FLUXCOM initiative (`http://www.fluxcom.org/`) has recently provided different global and spatially gridded products, among which, gridded daily GPP data at 0.5° resolution over 1980-2013 CE [Tramontana et al., 2016; Jung et al., 2017], synthesized, evaluated and made publicly available [Jung et al., 2020]. In the future, such data could be retrieved at the cell grid closest to the study site to calibrate the photosynthesis parameters of the MAIDEN model at large spatial scale by directly comparing daily simulated and observed GPP.

We have also highlighted in Chapter 3 the difficulty to properly set the phenology at many sites, because we do not provide the necessary information during the calibration of the model. For instance, in the future, the phenology of MAIDEN could be informed more efficiently during the calibration procedure or set more explicitly by making use of remote sensing data that can provide different vegetation indexes such as the Normalized Difference Vegetation Index (NDVI) [e.g. Zhang et al., 2003; Ganguly et al., 2010; Hmimina et al., 2013; Testa et al., 2018]. For instance, the U.S. Geological Survey (USGS) Earth Resources Observation and Science (EROS) provides phenological metrics derived from NDVI time series built on the basis of satellite sensor data and informing on the timing of the vegetative growing season (`https://www.usgs.gov/core-science-systems/eros/phenology`; Meier and Brown, 2014) in the United States. In MAIDEN, the phenology of a specific site results from different parameters that are calibrated or not. This is the case, for example, for the calibrated parameters *vegphase23*, *day23_flex* and *GDD1* (Tables B.2 and B.3) that influence the start of the growing season, or *photoper*, a photoperiod threshold, that influences the end of the growing season. As a consequence, setting the phenology in MAIDEN against existing data would also reduce the number of parameters considered in the Bayesian calibration procedure as some of them would become meaningless in the model.

This could be done, for example, by a priori setting the phenology at the study site on the basis of the available data over the satellite era. Alternatively, the phenological module of MAIDEN could be simplified on the basis of the observed relationship between phenology (as provided by satellite data) and climate to explicitly set the timing of the phenological phases without relying on calibrated or non-calibrated parameters of the MAIDEN model. Therefore, this would prevent unrealistic lengths of the growth period to arise from the calibration of MAIDEN, as highlighted in Chapter 3.

In this thesis, we defined large prior ranges for the calibrated parameters because we do not have easily access to the information required to refine them depending on the environmental conditions or the species to which the model is applied. In the future, however, a more in-depth investigation of the sensitivity of the model calibration to the definition of the prior for each biome or species could be useful. As MAIDEN is regularly used and calibrated for new sites by different groups, the number of species and environmental conditions for which it is calibrated is increasing and we could also take advantage of this to set species-specific or biome-specific prior ranges for the calibrated parameters. More informative prior ranges will obviously help guide the Bayesian calibration towards a more biologically plausible set of parameters. More generally, the site-by-site calibration of the most sensitive parameters has been preferred here over a multi-site optimization. Yet, on the long term, the latter would facilitate the application of MAIDEN at large spatial scale and likely improve the performance of the model and the robustness of the calibration. As a consequence, in the future, the most sensitive species-dependent parameters of the model could be calibrated using a network of site chronologies with the same species. The less sensitive species-dependent parameters that are currently not calibrated could be a priori set on the basis of previous studies in order to improve the performance of the model (in particular the version from Gennaretti et al. [2017] that has not been applied to deciduous species so far, as elaborated in Chapter 3).

Improving the calibration procedure of MAIDEN will undoubtedly lead to a more efficient and more skillful application of the model at large spatial scale. As a result, the data assimilation procedure in which we can already incorporate MAIDEN, may benefit from these improvements, whether by an increased number of proxy sites to which MAIDEN can be applied, or by an improved performance of the model to extract meaningful climate information at the assimilated site. However, as mentioned above, this implies to solve the issue of setting meaningful units for the tree growth observations that are compared with the output of the MAIDEN model during the calibration of the carbon allocation parameters.

Aside from the low number of tree-ring proxies incorporated in the data assimilation experiments, we have highlighted in Chapter 4 the difficulty to attribute the skill of the data assimilation-based reconstructions to the statistical or process-

based PSM or to the specificities of the data assimilation experiments (e.g. number of proxy sites included, calibration period, among others). Pseudoproxy experiments [e.g. Acevedo et al., 2017; Steiger and Smerdon, 2017] could help evaluate the actual performance of MAIDEN as a PSM in the data assimilation framework compared to a regression-based PSM in a controlled environment.

Using a mechanistic model such as MAIDEN has also the great advantage of benefiting from the updates that are regularly made in the model to improve the way it simulates the response of tree growth to climate variability. For instance, a snow module has been recently added to the model by Hermoso de Mendoza et al. [2021]. It has shown to improve the skill of MAIDENiso in simulating hydrological cycle components and is expected to enhance the reconstructions of the hydrological cycle or isotope-related processes. It has also been pointed out in the thesis that MAIDEN, and more generally ecophysiological models, tends to overestimate the actual effect of CO_2 on tree growth [Peñuelas et al., 2011; Gea-Izquierdo et al., 2017]. Yet, the precise quantification of a potential CO_2 fertilization effect on tree growth, for instance through an improved water use efficiency, is still lacking [e.g. Peñuelas et al., 2011; Giguère-Croteau et al., 2019; Marchand et al., 2020]. Improvements can be made in this regard, in order to better take into account the effect of the increasing CO_2 concentration on tree growth and, as a consequence, enhance the performance of the model. For instance, MAIDEN does not incorporate nutrient dynamics, and thus the potential limiting effect of nitrogen, phosphore availability or hydraulic constraints on a potential positive CO_2 fertilization effect on tree growth [Gea-Izquierdo et al., 2017]. Other physiological processes could also be affected more directly by CO_2 concentration in the model, for example autotrophic respiration (which depends on temperature and GPP in MAIDEN) or the allocation rules (which depend on climate and soil water content), as suggested by Gea-Izquierdo et al. [2017].

The MAIDEN model also offers the opportunity to investigate the so-called divergence problem [D'Arrigo et al., 2008], because it explicitly includes, as other mechanistic models, multiple and non-linear drivers of tree-growth response to climate whose individual effects can be assessed. However, this would likely require to incorporate a better representation of the factors that have been identified as potential causes for the divergent pattern of tree growth compared to the rapidly increasing instrumental temperature over the last decades in northern latitudes. This is for instance the case for decreasing levels of stratospheric ozone that have been suspected of causing the decrease of tree productivity, or for dimming in some regions (i.e., decreasing solar radiation reaching the ground) [D'Arrigo et al., 2008]. As discussed above, the influence of CO_2 concentration on tree growth, through its potential offsetting effect on forest productivity, must also be accurately accounted for in ecophysiological models like MAIDEN, in order to robustly address the divergence problem.

Finally, an isotopic module is available with MAIDEN through the isotope-enabled version MAIDENiso [Danis et al., 2012]. Few dendroclimatic models simultaneously provide tree-ring growth indexes and cellulose isotopes. The protocol developed in this thesis may be adapted to also incorporate stable isotopes of carbon and oxygen, i.e., δ^{13}C and δ^{18}O in tree-ring cellulose.

A

Supplement to Chapter 1

A.1 Dendroclimatic models

Throughout the thesis, we make use of two dendroclimatic models, MAIDEN (Sect. A.1.1) and VS-Lite (Sect. A.1.2), that we present in detail hereafter.

A.1.1 MAIDEN

The MAIDEN model is a comprehensive ecophysiological model that has been initially developed by Laurent Misson [Misson, 2004] in order to analyze the relationship between tree growth and climate variability using dendroecological data at the stand level. In particular, the MAIDEN model uses daily maximum and minimum temperature, precipitation and CO_2 atmospheric concentration to simulate the daily course of photosynthesis and allocate the daily available carbon to different compartments (stem, canopy, roots, storage) on the basis of phenology-dependent rules. Two versions of the model have been derived from the initial version of Misson [2004]: a version that has been developed by Gea-Izquierdo et al. [2015] for the Mediterranean forest, and a version developed by Gennaretti et al. [2017] for boreal tree species. In this thesis, we use a combined version developed by Fabio Gennaretti (unpublished), which offers the possibility to switch between the two versions. We detail here below the main equations for modelling the Net Primary Production (NPP) and the carbon allocation in the two current versions of the model. The description of the model is based on Misson [2004], Gea-Izquierdo et al. [2015] and Gennaretti et al. [2017]. We first detail the version of Gea-Izquierdo et al. [2015] and then elaborate the modifications that have been made to this version by Gennaretti et al. [2017] (Sect. A.1.1.3)

A.1.1.1 Modelling the net primary production

The coupled photosynthesis-stomatal conductance system is estimated on a daily basis for the sunlit and shaded fractions of the canopy, depending on the photosyn-

thetic photon flux density that each fraction receives. The photosynthetic photon flux density is computed from the photosynthetically active radiation transmitted to and then absorbed by the canopy following the Beer's law of radiation attenuation as a function of the Leaf Area Index (LAI) of the stand. The radiation, from which the photosynthetically active radiation is derived, and the humidity variables (i.e., the atmospheric vapor pressure deficit) are computed in the MT-CLIM model [Running et al., 1987] that is coupled to MAIDEN. The computation of radiation is directly related to the elevation, slope and aspect of the study site. The LAI is computed as follows (in square meter of leaves per square meter of stand; hereafter m^2 of leaves . m^{-2} of stand):

$$LAI(i) = C_{canopy}(i) \times \left(\frac{1}{SLA} \times PercCLeaf \right)^{-1} \quad \text{(A.1)}$$

where $C_{canopy}(i)$ corresponds to the leaf carbon reservoir at day *i* (in grams of carbon per square metre of stand per day; hereafter $gC.m^{-2}$ of stand . day^{-1}); *SLA*, to the specific leaf area (a parameter, in $m^2.g^{-1}$) and *PercCLeaf* to the percentage of carbon in leaves (a parameter between 0 and 1). The sunlit and shaded fractions of the LAI are computed as follows: $LAI_{sun}(i)$ = 1 - exp(-*LAI(i)*) and $LAI_{shade}(i)$ = *LAI(i)* - $LAI_{sun}(i)$.

The leaf photosynthesis or Gross Primary Production (GPP; in $gC.m^{-2}$ of stand . day^{-1}) is estimated on a daily time step following the biochemical model of Farquhar et al. [1980]. *Asun* and *Ashade* correspond to the gross primary production for the sun and shade leaves, respectively (in μmol of carbon per square meter of leaves per second; hereafter, μmol C . m^{-2} of leaves . s^{-1}), and are computed similarly. A_n (i.e., *Asun* or *Ashade*) depends on the carboxylation (V_c), oxygenation (V_o) and dark respiration (R_d) rates, as follows: $A_n = V_c - 0.5V_o - R_d$, where $A_c = V_c - 0.5V_o$. R_d is calculated as a fixed rate of A_c ($R_d = 0.006 \times A_c$). Leaf photosynthesis at day *i* can be limited by the carboxylation rate either when the activity of the enzyme Rubisco is limiting (W_c) or when the electron transport is limiting (W_j): $A_c = \min\{W_c, W_j\}$.

V_{cmax} (in μmol C. m^{-2} of leaves . s^{-1}; equation (A.2)) controls the dependence of W_c on the daytime temperature (T_{day}, in °C) on a daily basis. The equivalent J_{max} for W_j is computed as a fixed rate of V_{cmax}. V_{cmax} at day *i* is expressed as a logistic function of T_{day}:

$$V_{cmax}(i) = \frac{V_{max}}{1 + exp(V_b((T_{day}(i) + 273) - V_{ip}))} \cdot \theta_p \quad \text{(A.2)}$$

where the parameters V_{max} (in μmol C. m^{-2} of leaves . s^{-1}), V_b (in $°C^{-1}$) and V_{ip} (in °C) are respectively the asymptote, the slope and the inflection point of

V_{cmax} as a function of *Tday*. θ_p is a function of the soil water stress that depends on the soil moisture conditions of the previous year.

The leaf photosynthesis is then integrated over the whole canopy by making use of the shaded (LAI_{shade}) and sunlit (LAI_{sun}) fractions of the LAI at day *i* (in m^2 of leaves . m^{-2} of stand):

$$Asuncanopy(i) = Asun(i) \times LAI_{sun}(i) \times sday(i) \times 12.011e-6 \quad \text{(A.3)}$$

$$Ashadecanopy(i) = Ashade(i) \times LAI_{shade}(i) \times sday(i) \times 12.011e-6 \quad \text{(A.4)}$$

where *sday(i)* is the day length of day *i* in seconds; *Asuncanopy(i)* and *Ashadecanopy(i)* correspond to the GPP for the sunlit and shaded fractions of the canopy, respectively (in $gC.m^{-2}$ of stand . day^{-1}). *Acanopy(i)* corresponds to the GPP at day *i* integrated over the whole canopy (= *Asuncanopy(i)* + *Ashadecanopy(i)*).

The stomatal conductance g_s is computed on a daily basis following a modified version of the Leuning equation [Leuning, 1995; Gea-Izquierdo et al., 2015]. The stomatal conductance directly depends on the leaf photosynthesis and on θ_g, a non-linear function of the soil water stress (equation (A.5)). In turn, the stomatal conductance directly influences the intensity of the gas exchange and so the photosynthesis. The equation for θ_g is similar to V_{cmax} (equation (A.2)) with an asymptote equal to 1, a slope represented by the parameter $soil_b$ (in mm^{-1}), and an inflection point corresponding to the parameter $soil_{ip}$ (in mm) (equation (A.5)). The soil water stress at day *i*, $\theta_g(i)$, depends on the daily soil water content *SWC(i)* (in mm) as follows:

$$\theta_g(i) = \frac{1}{1 + exp(soil_b \cdot (SWC(i) - soil_{ip})} \quad \text{(A.5)}$$

The soil water content at day *i* is estimated from the precipitation used as input of the model. The soil is divided into a certain number of layers that is determined for the study site. Each layer has characteristics that are defined by the user on the basis of observations (percentage of clay and sand, percentage of fine roots and layer thickness). The characteristics of each soil layer determine the path followed by the precipitated water (infiltration, evaporation, runoff or infiltration and drainage) and, subsequently, the water content of each layer. The sum of the water content of each layer defines the soil water content. In the absence of soil water stress (θ_g = 1), the stomatal conductance is maximum. Conversely, when the soil water stress is maximum (θ_g = 0), the stomatal conductance is nul, and so the photosynthesis.

Finally, the Net Primary Production (NPP) at day *i* (in $gC.m^{-2}$ of stand . day^{-1}) corresponds to the GPP minus the quantity of carbon used for autotrophic respiration R_a: $A_N(i)$ = *Acanopy*(*i*) - $R_a(i)$. R_a is computed as a percentage of the gross primary production *Acanopy*, defined as a function of maximum daily temperature.

A.1.1.2 Modelling the carbon allocation

The daily quantity of carbon from photosynthesis $A_N(i)$ is then allocated to different tree compartments: canopy, stem, roots and storage. The carbon allocation depends on the phenological phase. There are five phenological phases in MAIDEN (Fig. A.1). The first phenological period or P1 corresponds to winter. For evergreens, all the available carbon from photosynthesis is allocated to the storage of non-structural carbohydrates (NSC; Fig. A.1). At the beginning of each year *j*, the variable *AlloCcanopy(j)* (in gC.m^{-2} of stand) is calculated by the model, i.e., the maximum quantity of carbon that the canopy can potentially contain during year *j*. In Gea-Izquierdo et al. [2015], *AlloCcanopy(j)* depends on the moisture conditions of the previous year, through θ_{LAI}*(j)*:

$$AlloCcanopy(j) = \theta_{LAI}(j) \times MaxCcanopy \tag{A.6}$$

where,

$$\theta_{LAI}(j) = \left(1 - 2 \cdot \frac{perc_{LAI} - SWC_{250}}{perc_{LAI}}\right) \tag{A.7}$$

where the parameter $perc_{LAI}$ (in mm) corresponds to the threshold value beyond which θ_{LAI} = 1; and SWC_{250} corresponds to the mean soil water content of May-December of the previous year. θ_{LAI} (*j*) can vary between 0.7 and 1. When equal to 1, the canopy can reach its maximum in year *j*, as defined by *MaxCcanopy* (in gC.m^{-2} of stand). *MaxCcanopy* is calculated on the basis of the parameters *SLA* (see Sect. A.1.1.1) and *LAImax*, the maximum LAI (in m^2.m^{-2}). The transition from the first (P1) to the second (P2) phenological phase is fixed on day d_{12}.

During P2, there is accumulation of growing degree days (GDD). Once the threshold of GDD sum has been reached (the parameter GDD_1, in ℃), the third phenological phase (P3) starts with budburst. However, P3 can not start later than a selected day of the year, as defined by the parameter *vegphase23*. During P3, the total quantity of carbon available C_T (*i*) (= A_N + C_{bud}) comes from photosynthesis A_N and storage carbon as NSC (C_{bud}). The carbon is allocated either to the stem (C_{stem}), the canopy (C_{canopy}), or the roots (C_{roots}) (Fig. A.1). The parameter C_{bud} corresponds to the stored carbon that is used each day by the tree (in gC.m-2 of stand . day^{-1}). The carbon allocated to the canopy at day *i* is computed as follows:

$$C_{canopy}(i) = C_T(i) \times (1 - 0.2 \times h_{3_1}(i)) \times ratio^{-1}_{root/leaf} \tag{A.8}$$

where $ratio_{root/leaf}$ corresponds to the ratio between the quantity of carbon allocated to the roots and to the canopy. $h_{3_1}(i)$ determines the proportion of carbon

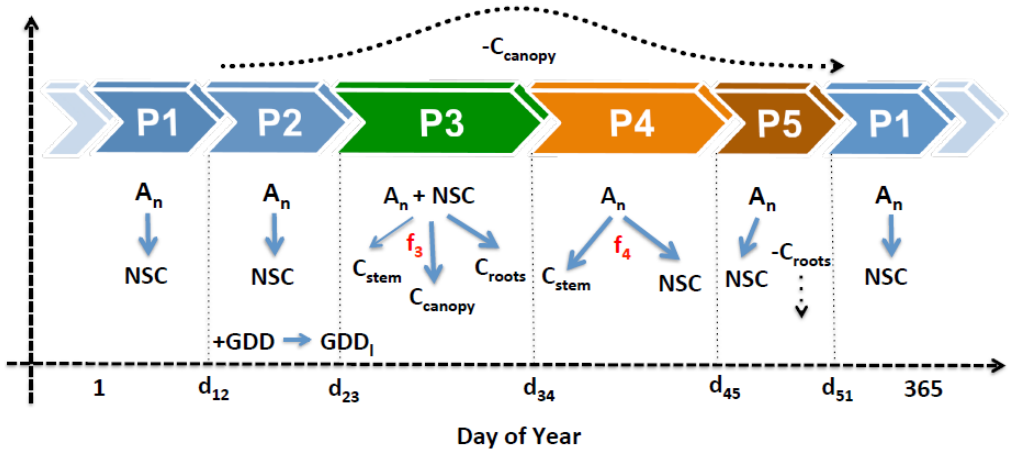


Figure A.1: *Phenological phases (P1 to P5) of the MAIDEN model and associated carbon allocation rules to different tree compartments during one year. A_n stands for the net daily carbon assimilation from photosynthesis A_N (in the text); NSC for non-structural carbohydrates or storage; GDD for growing degree days; GDD_1 is a parameter determining the start of the P3 phenological phase (see the text); C is the carbon allocated to the different pools (stem, roots, canopy); d is the day of the year for the transition from one phenological phase to another. Allocation within the plant is represented by solid arrows while litterfall (canopy or roots) is represented by dashed arrows. f_3 and f_4 are phenology-dependent rules determining the allocation to the different pools as a function of soil moisture and temperature (see the text for more details). Figure from Gea-Izquierdo et al. [2015].*

($C_T(i)$) allocated to the roots and to the canopy (between 0 and 1), and depends on the climatic conditions via three parameters: p_{3moist} (in mm^{-1}), which represents the dependence of $h_{3_1}(i)$ on the soil water content at day *i*, *SWC(i)*; p_{3temp} (in ℃) and p_{3sd} (in ℃), which represent the optimum and dispersion, respectively, of the dependence of $h_{3_1}(i)$ to daily maximum temperature T_{max}. The carbon allocated to the stem at day *i* is computed as follows:

$$C_{stem}(i) = C_T(i) \times 0.5 \times h_{3_1}(i) \times h_{3_2}(i) \tag{A.9}$$

where $h_{3_2}(i)$ corresponds to the proportion of carbon allocated to the stem in P3 (between 0 and 1) and also depends on the climatic conditions via three parameters: st_{3moist} (in mm^{-1}), st_{3temp} (in ℃) and st_{3sd_temp} (in ℃), similarly to $h_{3_1}(i)$. The rest of the available carbon is allocated to the roots. The third phenological phase ends when the quantity of carbon in the canopy has reached *AlloCcanopy*(*j*), or when the quantity of carbon stored in the form of NSC is below a threshold value (in $gC.m^{-2}$ of stand).

The phenological phase 4 (P4) corresponds to the summer. During summer, all the carbon from photosynthesis is allocated to the stem or to the storage (Fig.

A.1). The allocation between the storage and the stem depends on the climatic conditions via $h_4(i)$:

$$C_{stem}(i) = A_N(i) \times (1 - h_4(i)) \tag{A.10}$$

$$C_{stor}(i) = A_N(i) \times h_4(i) \tag{A.11}$$

where $h_4(i)$ corresponds to the proportion of carbon from photosynthesis that is allocated to the storage pool in the form of NSC:

$$h_4(i) = (1 - exp(st_{4temp} \cdot T_{max}(i))) \cdot \left(exp\left(-0.5 \cdot \left(\frac{SWC(i)}{st_{4sd_moist}} \right)^2 \right) \right) \tag{A.12}$$

where the parameters st_{4temp} (in $°C^{-1}$) and std_{4sd_moist} (in mm) represent the intensity and direction of the dependence of the proportion of carbon allocated to the stem or storage on the daily maximum temperature $T_{max}(i)$ and on the soil water content *SWC(i)*, respectively.

The last phenophase (P5), which corresponds to autumn, starts when the photoperiod is lower than a threshold of duration of daylight (*photoper*, in hours). During this period, all the photosynthates are allocated to the storage pool (Fig. A.1). The fine roots die throughout the phenophase following a constant turnover rate. This phenological phase lasts for a fixed number of days, than can be parametrized.

Throughout the year, the carbon losses from the canopy are calculated differently for evergreens and deciduous (-C_{canopy} *(i)*, Fig. A.1). They directly affect the photosynthetic capacity of the tree via the LAI (equation A.1). For deciduous, the carbon losses only occur in P5 (autumn) and are uniformly distributed throughout the period. For evergreens, the losses are calculated each day of the year following a function that depends on *AlloCcanopy*(*j*) (equation (A.6)) and on three parameters: the yearly canopy turnover rate *PercentFall* (between 0 and 1); the day of the year with maximum losses *OutMax*; and the length of the period with losses *OutLength* (an index proportional to the length of the period with losses, with no units):

$$\begin{aligned} outCcanopy(i) = (PercentFall \cdot AlloCcanopy_j) \cdot \\ exp\left(-0.5 \left(\frac{DOY_i - 1}{OutMax} \right)^{OutLength} \right) - (PercentFall \cdot AlloCcanopy_j) \cdot \\ exp\left(-0.5 \left(\frac{DOY_i}{OutMax} \right)^{OutLength} \right) \end{aligned} \tag{A.13}$$

where DOY_i corresponds to the day of the year.

A.1.1.3 Modifications of MAIDEN for the North American boreal forest

The version of MAIDEN as in Gea-Izquierdo et al. [2015] has been specifically developed for Mediterranean tree species at sites where precipitation is the main limiting factor of tree growth. Different modifications have been made by Gennaretti et al. [2017] to the version of Gea-Izquierdo et al. [2015] in order to better account for specific processes occurring in the boreal forests, where temperature plays a dominant role. In particular, the daytime temperature *Tday* (Sect. A.1.1.1) has been replaced by a function *S*, in order to allow for a smooth response of photosynthesis to the increasing temperature in equation (A.2) and prevent the overestimation of the GPP in spring. The function *S* is computed each day *i* with the following differential equation [Mäkelä et al., 2004], solved with the Euler's method:

$$\frac{dS_i}{di} = \frac{Tday_i - S_i}{\tau} \tag{A.14}$$

where the parameter τ is a constant that takes into account the acclimation of the photosynthesis to changing temperature. Its value is higher when the number of days needed for the acclimation of photosynthesis is important. When equal to 1, this is equivalent to using the daytime temperature directly.

The equation for computing the maximum quantity of carbon in the canopy *AlloCcanopy*(*j*) (equation (A.6)) has also been modified, as it now depends on both temperature and precipitation:

$$AlloCcanopy(j) = 0.7 \times MaxCcanopy + 0.3 \times MaxCcanopy \times \theta_{LAI}(j) \tag{A.15}$$

where,

$$\theta_{LAI}(j) = \frac{1}{1 + exp(CanopyT \cdot T_{j-1})} \cdot \frac{1}{1 + exp(CanopyP \cdot P_{j-1})} \tag{A.16}$$

where T_{j-1} corresponds to the mean July-August temperature of the previous year (detrended and transformed to z-scores); P_{j-1}, to April precipitation of the previous year (detrended and transformed to z-scores); *CanopyT* and *CanopyP* correspond to the slope of the relationship between θ_{LAI} and temperature (T_{j-1}) or precipitation (P_{j-1}), respectively.

In order to decrease the interannual variability of the budburst date (i.e., the transition from P2 to P3) related to the overreaction of the start of the growing season to GDD yearly variations, a parameter has been added (*day23_flex*, in years) that smooths the yearly time series of budburst dates (as defined by GDD_1 and *vegphase23*) using a *n*-year cubic smoothing spline at the beginning of the simulation with MAIDEN. *n* corresponds to *day23_flex*. A maximum duration of

the P3 phase has also been defined in the model. During P3, the equation for the allocation of carbon to the stem (equation (A.9)) has been simplified:

$$C_{stem}(i) = C_T(i) \times (1 - h_3) \tag{A.17}$$

where h_3 is a parameter between 0 and 1 corresponding to the proportion of carbon allocated to the canopy and to the roots in P3. The carbon is allocated to the roots or to the canopy following the ratio $ratio_{root/leaf}$. In P4, the equation (A.11) has also been modified, so that $h_4(i)$ (equation (A.12)) only depends on daily maximum temperature:

$$C_{stem}(i) = A_N(i) \cdot \left(1 - 0.8 \cdot exp\left(-0.5\left(\frac{T_{max}(i)}{st_{4temp}}\right)^2\right)\right) \tag{A.18}$$

where the parameter st_{4temp} corresponds to the inflection point of the function. An additional criterion has also been added for the transition from P4 to P5, i.e., the occurrence of negative minimum daily temperature after the 1^{st} of September.

A.1.2 VS-Lite

The Vaganov-Shashkin-Lite or VS-Lite model is a simple numerical model that has been developed as a light version of the full Vaganov-Shashkin (VS) model to capture the primary response of tree-ring growth to climate variability in the extratropical region [Tolwinski-Ward et al., 2011]. In particular, VS-Lite models the non-linear response of tree growth to monthly mean temperature and cumulative precipitation, used as inputs of the model, and to insolation (derived from the latitude of the site, also used as input of the model). The model does not include any biological processes but relies instead on the principle of limiting factors and on threshold growth response functions (equations (A.19), (A.20) and (A.22)) to simulate an annual tree-ring growth index. In practice, the model computes, for each month *s* of the year *t*, the response $g_T(s,t)$ of tree growth to monthly mean temperature $T(s,t)$ (in °C) (equation (A.19)) and the response $g_M(s,t)$ of tree growth to monthly soil moisture $M_S(s,t)$ (in volume of water per volume of soil, v/v) (equation (A.20)), between 0 and 1 (with no units).

$$g_T(s,t) = \begin{cases} 0 & \text{if } T(s,t) \leq T_1; \\ \dfrac{(T(s,t) - T_1)}{(T_2 - T_1)} & \text{if } T_1 \leq T(s,t) \leq T_2; \\ 1 & \text{if } T_2 \leq T(s,t) \end{cases} \tag{A.19}$$

$$g_M(s,t) = \begin{cases} 0 & \text{if } M_S(s,t) \leq M_1; \\ \dfrac{(M_S(s,t) - M_1)}{(M_2 - M_1)} & \text{if } M_1 \leq M_S(s,t) \leq M_2; \\ 1 & \text{if } M_2 \leq M_S(s,t) \end{cases} \tag{A.20}$$

where T_1 and M_1 are parameters corresponding to the threshold temperature and soil moisture, respectively, below which tree growth at the study site is considered as equal to zero; T_2 and M_2 are parameters corresponding to the threshold temperature and soil moisture, respectively, beyond which tree growth at the study site is considered as optimal.

The monthly soil moisture $M_S(s,t)$ is computed based on the National Oceanic and Atmospheric Administration's Climate Prediction Center (CPC) "Leaky Bucket Model" [Huang et al., 1996]. It estimates the evapotranspiration, surface runoff and groundwater flow with empirical functions using the input data of the VS-Lite model (monthly mean temperature and cumulative precipitation). These three components are subtracted from the incoming precipitation. The result of the subtraction is then added to the previous month soil moisture to compute $M_S(s,t)$.

Finally, the VS-Lite model computes for each month *s* of year *t* a response of tree growth to the monthly insolation, as a function of the latitude Φ of the study site, $g_E(s,t)$ (equation (A.21)). This corresponds to the ratio between the monthly mean day length ($L(s,t)$) and the mean day length of the summer solstice month:

$$g_E(s,t) = \frac{L(s,t)}{max\{L(s,t)\}} \tag{A.21}$$

Based on these three growth responses, $g_T(s,t)$, $g_M(s,t)$ and $g_E(s,t)$, the principle of limiting factors is used to compute the overall growth response of month *s* and year *t*, $g(s,t)$, by taking the minimum of $g_T(s,t)$ and $g_M(s,t)$, modulated by $g_E(s,t)$:

$$g(s,t) = g_E(s,t) \times min\{g_T(s,t), g_M(s,t)\} \tag{A.22}$$

For each year *t*, the growth response function $g(s,t)$ is integrated over a variable window of months as delimited by the parameters I_0 (start month) and I_f (end month; Table A.1), in order to build an annual growth response time series. The resulting series is then normalized by removing the mean and dividing by the standard deviation.

Among the 12 tunable parameters of the model (Table A.1), the first four are devoted to the non-linear response of tree-ring growth to the monthly climatic conditions as in equations (A.19) and (A.20). The optimal values for those parameters can be obtained using the Bayesian calibration procedure described in Tolwinski-Ward et al. [2013]. The next six parameters used for computing the soil humidity

in the CPC's "Leaky Bucket Model" are usually set to their default values, which have been shown to be suitable for an application at global scale [Tolwinski-Ward et al., 2011]. The values for the parameters l_0 and l_f controlling the length of the integration window for *g(s,t)* can be adapted in order to incorporate previous year's months.

Table A.1: *VS-Lite parameters as in Tolwinski-Ward et al. [2011].*

Temperature response parameters	
Threshold temperature for $g_T > 0$	T_1 [℃]
Threshold temperature for $g_T = 1$	T_2 [℃]
Soil moisture response parameters	
Threshold soil moisture for $g_M > 0$	M_1 [v/v]
Threshold soil moisture for $g_M = 1$	M_2 [v/v]
Soil moisture parameters	
Runoff parameter 1	α [mois^{-1}]
Runoff parameter 2	μ [ ]
Runoff parameter 3	m [ ]
Maximum moisture held by soil	W_{max} [v/v]
Minimum moisture held by soil	W_{min} [v/v]
Root (bucket) depth	d_r [mm]
Integration window parameters	
Integration start month	l_0
Integration end month	l_f

B

Supplement to Chapter 2

B.1 Supplementary tables

Table B.1: *Main constants linked to site conditions and control parameters in the MAIDEN model.*

Parameter	Meaning	Units
exp_site	Indicates if the species at the site is a deciduous (1) or evergreen (2) tree	no unit (1 or 2)
base_elev_cst	Station elevation	meters
base_isoh_cst	Station isohyet	centimeters
site_lat_cst	Site latitude	degrees
site_elev_cst	Site elevation	meters
site_slp_cst	Site slope	degrees
site_asp_cst	Site aspect	degrees
site_isoh_cst	Site isohyet	centimeters
site_ehoriz_cst	Site East slope	degrees
site_whoriz_cst	Site West slope	degrees
thick1-2-3 or 4	Soil layer thickness	meters
finefrac1-2-3 or 4	% of fine roots in the soil layer	Coeff. between 0-1
clay1-2-3 or 4	% of clay in the soil layer	%
sand1-2-3 or 4	% of sand in the soil layer	%

Table B.2: *GHCN (Table 2.2) stations used for daily climate data at the European sites (Fig. 2.2).*

Site	Time period	Station name	Station lat/lon	Station elevation
FINL	1900-1944/1950-2000	Sodankyla	67.37N26.65E	179m
EALP	1950-2000	Zugspitze	47.42N10.99E	2964m
	1910-1949	Innsbruck	47.27N11.4E	577m
SWIT179	1910-2000	Saentis	47.25N9.35E	2502m

Table B.3: *Calibrated parameters of the MAIDEN model [Gennaretti et al., 2017].*

	Process		Parameter	Units
Photosynthesis	Temperature dependence of photosynthesis	Asymptote	V_{max}	μmol C.m^{-2} of leaves . s^{-1}
		Slope	V_b	°C^{-1}
		Inflection point	V_{ip}	°C
	Water stress dependence of stomatal conductance	Slope	$soil_b$	mm^{-1}
		Inflection point	$soil_{ip}$	mm
	Acclimation to temperature of photosynthesis	Needed days	τ	days
Carbon allocation	Definition of canopy maximum amount of carbon	Slope of temperature dependence	*CanopyT*	°C^{-1}
		Slope of precipitation dependence	*CanopyP*	mm^{-1}
	Start of the growing season (budburst)	GDD sum threshold	GDD_1	°C
		Day before the later start	*vegphase23*	day of the year
		Acclimation to changing GDD sums	*day23_flex*	years
	Daily available carbon from buds reservoir	Storage C used by the tree	C_{bud}	gC.m^{-2} of stand . day^{-1}
	Partition of carbon to different tree compartments during growing season	Portion allocated to canopy and roots	*h3*	fraction (0-1)
	Partition of carbon to different tree compartments during summer period	Inflection point of the temperature dependence	st_{4temp}	°C
	Photoperiod for transition from summer to fall season	Photoperiod threshold	*photoper*	hours
	Carbon losses from the canopy	Yearly canopy turnover rate	*PercentFall*	fraction (0-1)
		Approximate day of the year with maximum losses	*OutMax*	day of the year
		Index proportional to the length of the period with losses	*OutLength*	NA

B.2 Supplementary figures

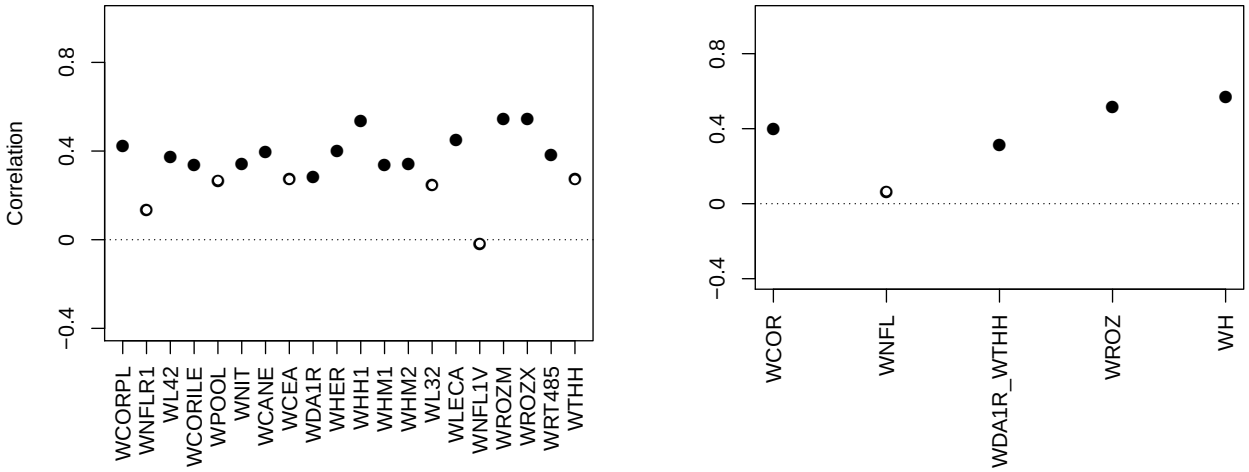


Figure B.1: *Pearson correlation coefficients between tree-growth observations and simulations at the Eastern Canadian taiga sites (Fig. 2.1) with MAIDEN using NRCAN (5 arcmin) as climatic inputs (Table 2.2) for the 1950-2000 period with QC_taiga calibrated parameters from Gennaretti et al. [2017]. Individual (left) and aggregated sites (right). The long-term decadal trends have been removed in observations and simulations. White inner circles stand for non-significant correlations (p-value > 0.05). Plain circles stand for significant correlations (p-value < 0.05).*

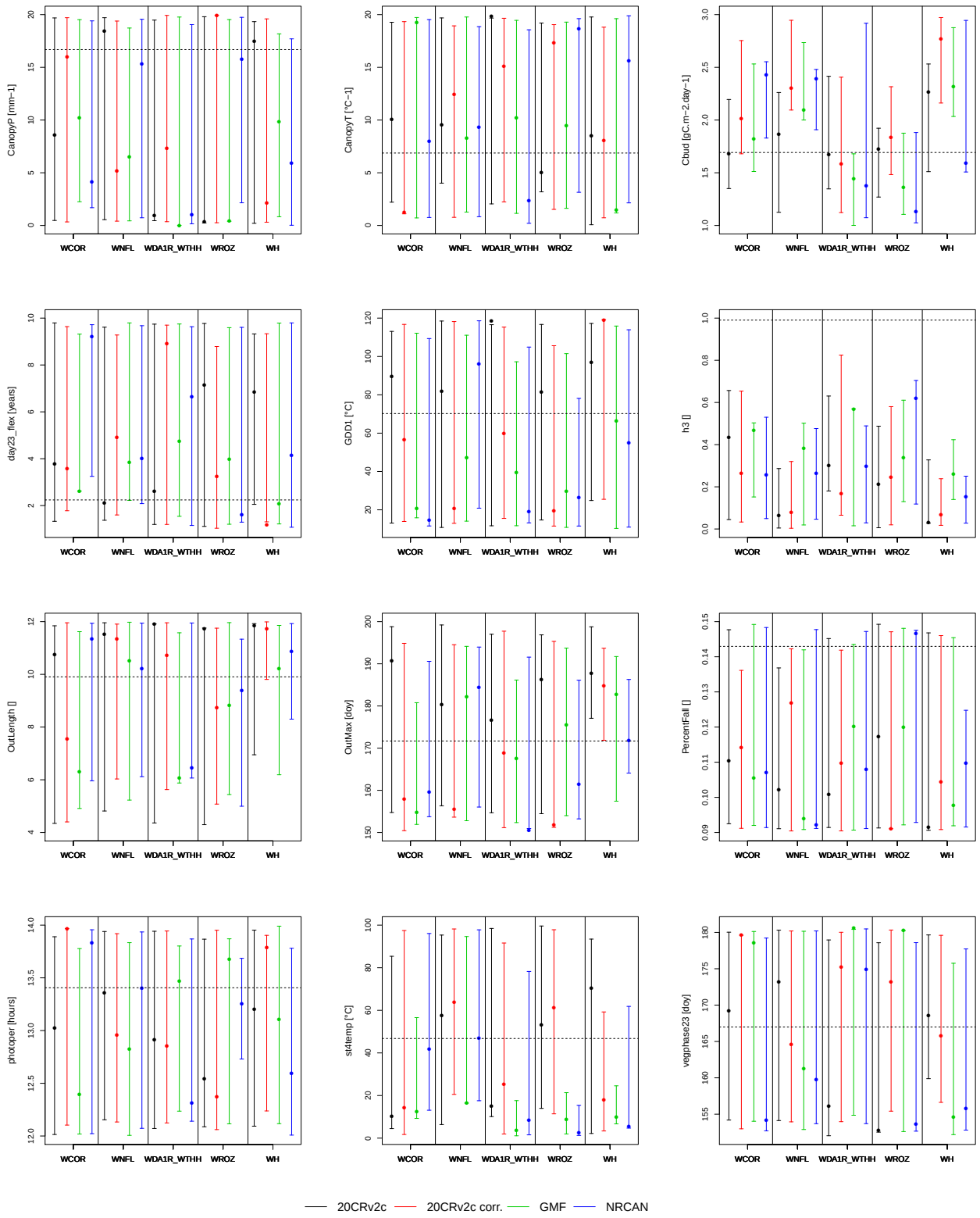


Figure B.2: *Selected carbon allocation parameters value (Table B.3) based on the calibration procedure detailed in Sect. 2.2.3.1 and 95% confidence interval of each parameter (computed based on all iterations of the third step of the calibration process, with a five iterations thinning and a burn-in period of 3000 iterations, see Sect. 2.2.3.1) for the five aggregated Eastern Canadian sites (Fig. 2.1b) and for all climatic datasets (Table 2.2) over the 1950-2000 time period. Dashed line corresponds to the parameter value at QC_taiga site from Gennaretti et al. [2017].*

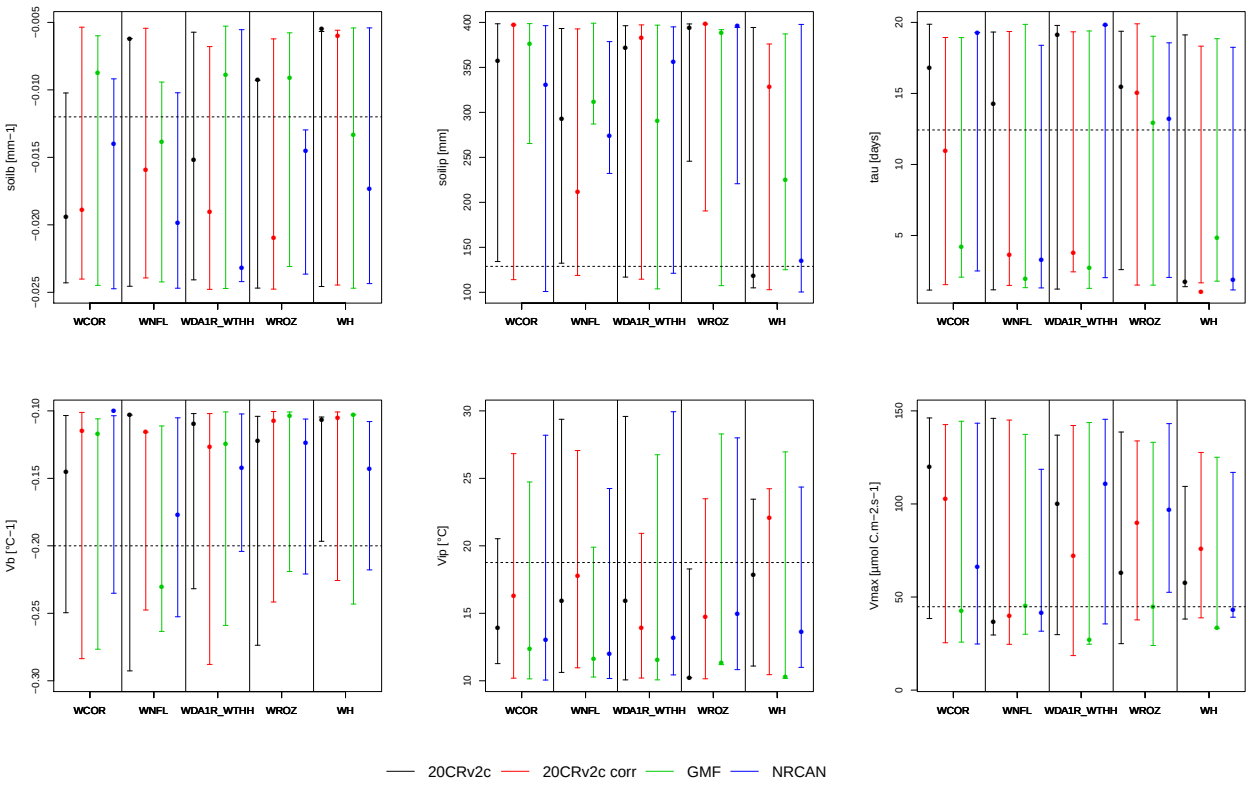


Figure B.3: *Selected photosynthesis parameters value (Table B.3) based on the calibration procedure detailed in Sect. 2.2.3.1 and 95% confidence interval of each parameter (computed based on all iterations of the second step of the calibration process, with a five iterations thinning and a burn-in period of 1000 iterations, see Sect. 2.2.3.1) for the five aggregated Eastern Canadian sites (Fig. 2.1b) and for all climatic datasets (Table 2.2) over the 1950-2000 time period. Dashed line corresponds to the parameter value at QC_taiga site from Gennaretti et al. [2017].*

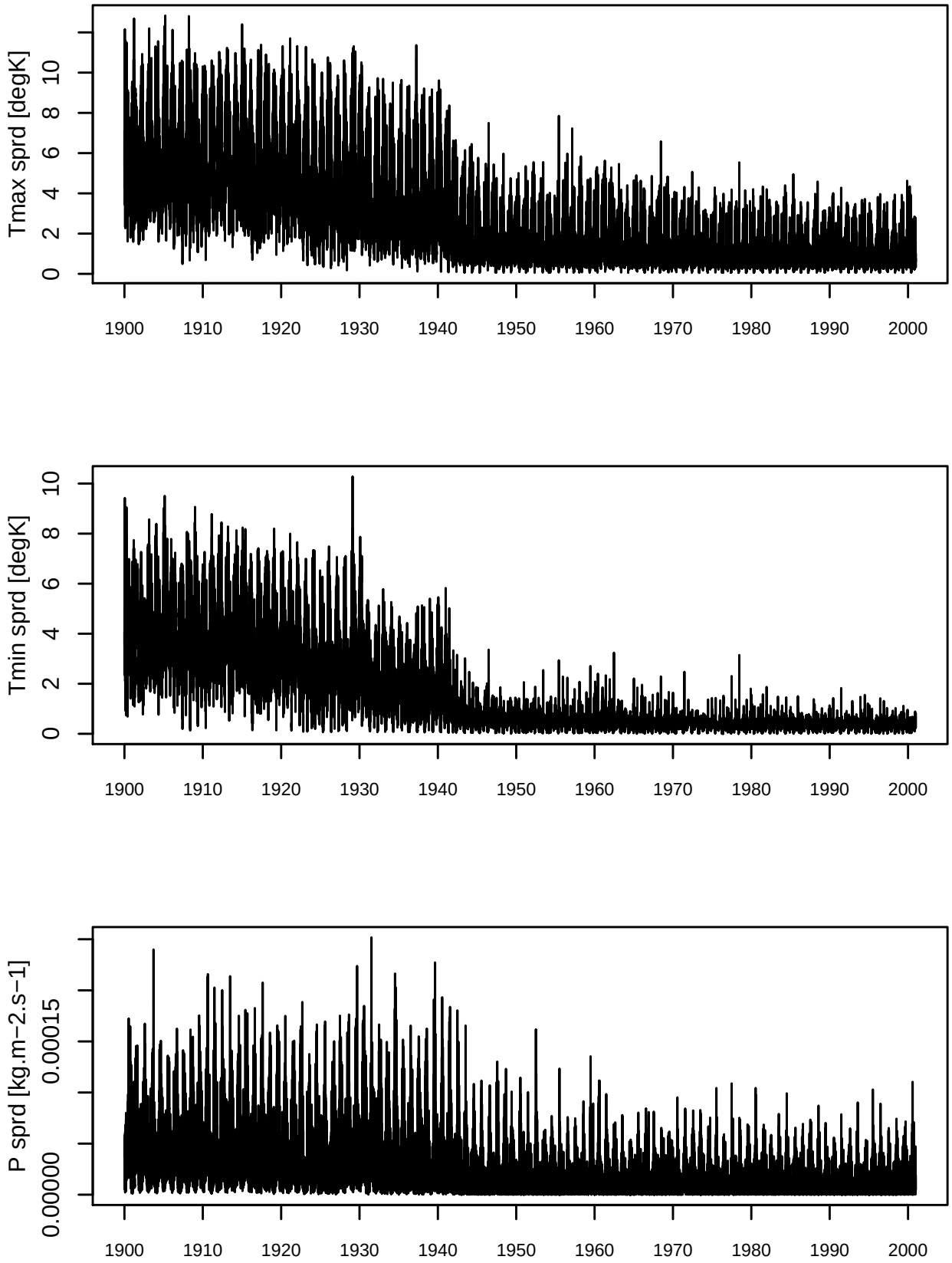
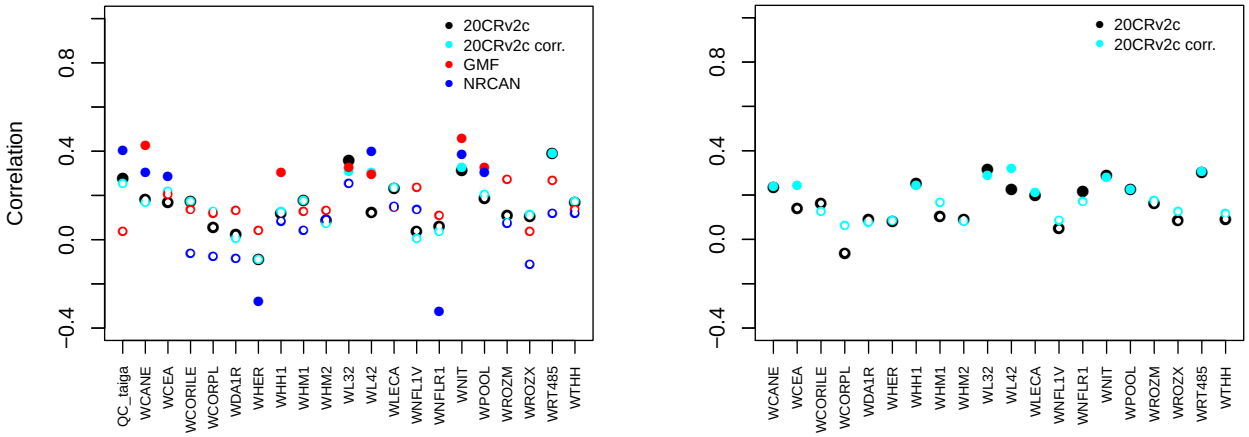


Figure B.4: *WL42 (Fig. 2.1a). Ensemble spread of maximum temperature (Tmax sprd), minimum temperature (Tmin sprd) and precipitations (P sprd) for the NOAA-CIRES 20th Century Reanalysis V2c (Table 2.2) for the 1900-2000 time period.*



(a) 1950-2000 **(b)** 1900-2000

Figure B.5: *Pearson correlation coefficients between tree-growth observations and simulations at the Eastern Canadian taiga sites (Fig. 2.1a) with VS-Lite using the different climatic datasets described in Table 2.2 for the 1950-2000 (a) and 1900-2000 (b) calibration periods. White inner circles stand for non-significant correlations (p-value > 0.05).*

C

Supplement to Chapter 3

C.1 Supplementary tables

Table C.1: *Main constants linked to site conditions and control parameters in the MAIDEN model.*

Parameter	Meaning	Units
exp_site	Indicates if the species at the site is a deciduous (1) or evergreen (2) tree	no unit (1 or 2)
base_elev_cst	Station elevation	meters
base_isoh_cst	Station isohyet	centimeters
site_lat_cst	Site latitude	degrees
site_elev_cst	Site elevation	meters
site_slp_cst	Site slope	degrees
site_asp_cst	Site aspect	degrees
site_isoh_cst	Site isohyet	centimeters
site_ehoriz_cst	Site East slope	degrees
site_whoriz_cst	Site West slope	degrees
thick1-2-3 or 4	Soil layer thickness	meters
finefrac1-2-3 or 4	% of fine roots in the soil layer	Coeff. between 0-1
clay1-2-3 or 4	% of clay in the soil layer	%
sand1-2-3 or 4	% of sand in the soil layer	%

Table C.2: *Calibrated parameters of the MAIDEN model [Gennaretti et al., 2017].*

	Process		Parameter	Units
Photosynthesis	Temperature dependence of photosynthesis	Asymptote	V_{max}	μmol C.m^{-2} of leaves . s^{-1}
		Slope	V_b	°C^{-1}
		Inflection point	V_{ip}	°C
	Water stress dependence of stomatal conductance	Slope	$soil_b$	mm^{-1}
		Inflection point	$soil_{ip}$	mm
	Acclimation to temperature of photosynthesis	Needed days	τ	days
Carbon allocation	Definition of canopy maximum amount of carbon	Slope of temperature dependence	*CanopyT*	°C^{-1}
		Slope of precipitation dependence	*CanopyP*	mm^{-1}
	Start of the growing season (budburst)	GDD sum threshold	GDD_1	°C
		Day before the later start	*vegphase23*	day of the year
		Acclimation to changing GDD sums	*day23_flex*	years
	Daily available carbon from buds reservoir	Storage C used by the tree	C_{bud}	gC.m^{-2} of stand . day^{-1}
	Partition of carbon to different tree compartments during growing season	Portion allocated to canopy and roots	*h3*	fraction (0-1)
	Partition of carbon to different tree compartments during summer period	Inflection point of the temperature dependence	st_{4temp}	°C
	Photoperiod for transition from summer to fall season	Photoperiod threshold	*photoper*	hours
	Carbon losses from the canopy (evergreen only)	Yearly canopy turnover rate	*PercentFall*	fraction (0-1)
		Approximate day of the year with maximum losses	*OutMax*	day of the year
		Index proportional to the length of the period with losses	*OutLength*	NA

Table C.3: *Calibrated parameters of the MAIDEN model [Gea-Izquierdo et al., 2015].*

	Process		Parameter	Units
Photosynthesis	Temperature dependence of photosynthesis	Asymptote	V_{max}	μmol C.m^{-2} of leaves . s^{-1}
		Slope	V_b	℃$^{-1}$
		Inflection point	V_{ip}	℃
	Water stress dependence of stomatal conductance	Slope	$soil_b$	mm^{-1}
		Inflection point	$soil_{ip}$	mm
Carbon allocation	Definition of canopy maximum amount of carbon	Slope of temperature dependence	$perc_{LAI}$	℃$^{-1}$
	Start of the growing season (budburst)	GDD sum threshold	GDD_1	℃
		Day before the later start	*vegphase23*	day of the year
	Daily available carbon from buds reservoir	Storage C used by the tree	C_{bud}	gC.m^{-2} of stand . day^{-1}
	Partition of carbon to different tree compartments during growing season	Definition of carbon allocated to the stem as a function of soil water	p_{3moist}	mm^{-1}
		Definition of carbon allocated to the stem as a function of maximum temperature	p_{3temp}	℃
			p_{3sd}	℃
		Definition of carbon allocated to the stem as a function of soil water	st_{3moist}	mm^{-1}
		Definition of carbon allocated to the stem as a function of maximum temperature	st_{3temp}	℃
			st_{3sd_temp}	℃
	Partition of carbon to different tree compartments during summer period	Definition of carbon allocated to stem or storage as a function of maximum temperature	st_{4temp}	℃$^{-1}$
		Definition of carbon allocated to stem or storage as a function of soil water	st_{4sd_moist}	mm
	Photoperiod for transition from summer to fall season	Photoperiod threshold	*photoper*	hours

Table C.4: *Ranges of calibrated parameters prior uniform distributions, for the MAIDEN model [Gennaretti et al., 2017]. See Table C.2 for details on calibrated parameters.*

	Parameter	Lower bound	Upper bound
Photosynthesis	V_{max}	5	150
	V_b	-0.3	-0.05
	V_{ip}	5	30
	$soil_b$	-0.06	-0.005
	$soil_{ip}$	3	400
	τ	1	20
Carbon allocation	*CanopyT*	0	20
	CanopyP	0	20
	GDD_1	10	250
	vegphase23	90	190
	day23_flex	1	10
	C_{bud}	1	16
	h3	0	1
	st_{4temp}	1	100
	photoper	9	14
	PercentFall	0.09	0.5
	OutMax	120	250
	OutLength	2	15

Table C.5: *Ranges of calibrated parameters prior uniform distributions, for the MAIDEN model [Gea-Izquierdo et al., 2015]. See Table C.3 for details on calibrated parameters.*

	Parameter	Lower bound	Upper bound
Photosynthesis	V_{max}	5	150
	V_b	-0.3	-0.05
	V_{ip}	5	30
	$soil_b$	-0.06	-0.005
	$soil_{ip}$	3	400
Carbon allocation	$perc_{LAI}$	40	250
	GDD_1	10	250
	vegphase23	90	190
	C_{bud}	1	16
	p_{3moist}	-0.7	-0.001
	p_{3temp}	-160	185
	p_{3sd}	5	200
	st_{3moist}	-0.8	-0.005
	st_{3temp}	-170	230
	st_{3sd_temp}	5	300
	st_{4temp}	0.008	0.95
	st_{4sd_moist}	45	1090
	photoper	9	14

Table C.6: *Pearson correlations between different climate indicators and MAIDEN or VS-Lite verification correlations (1901-1949). O-S stands for the year starting from October (previous year) to September (current year); P for precipitation; JAS for July-August-September; T for temperature. Asterisks stand for significant correlations (p-value < 0.05). The difference in the number of sites on which correlations are computed is due to the phenological criterion that has been applied to MAIDEN calibrated sites (see Sect. 3.2.4.1 for more details).*

Model (version)	**Correlation**
Correlations between O-S mean cumulative P correlation and verification correlation	
MAIDEN (Ge2017; 189 sites)	0.073
MAIDEN (GI2015; 160 sites)	0.076
VS-Lite (302 sites)	-0.067
Correlations between annual mean T correlation and verification correlation	
MAIDEN (Ge2017; 189 sites)	0.036
MAIDEN (GI2015; 160 sites)	0.036
VS-Lite (302 sites)	-0.052
Correlations between JAS mean T correlation and verification correlation	
MAIDEN (Ge2017; 189 sites)	0.027
MAIDEN (GI2015; 160 sites)	0.049
VS-Lite (302 sites)	-0.053

Table C.7: *Pearson correlations between correlations of observed TRW with different climate indicators and MAIDEN or VS-Lite verification correlations (1901-1949). O-S stands for the year starting from October (previous year) to September (current year); P for precipitation; JAS for July-August-September; T for temperature. Asterisks stand for significant correlations (p-value < 0.05). The difference in the number of sites on which correlations are computed is due to the phenological criterion that has been applied to MAIDEN calibrated sites (see Sect. 3.2.4.1 for more details).*

Model (version)	**Correlation**
Correlations between observed TRW and O-S P correlation and verification correlation	
MAIDEN (Ge2017; 189 sites)	0.114
MAIDEN (GI2015; 160 sites)	0.155
VS-Lite (302 sites)	0.149*
VS-Lite (189 Ge2017 selected sites)	0.190*
VS-Lite (160 GI2015 selected sites)	0.091
Correlations between observed TRW and annual T correlation and verification correlation	
MAIDEN (Ge2017; 189 sites)	0.074
MAIDEN (GI2015; 160 sites)	0.059
VS-Lite (302 sites)	0.467*
VS-Lite (189 Ge2017 selected sites)	0.471*
VS-Lite (160 GI2015 selected sites)	0.503*
Correlations between observed TRW and JAS T correlation and verification correlation	
MAIDEN (Ge2017; 189 sites)	-0.039
MAIDEN (GI2015; 160 sites)	-0.097
VS-Lite (302 sites)	0.506*
VS-Lite (189 Ge2017 selected sites)	0.496*
VS-Lite (160 GI2015 selected sites)	0.494*

Table C.8: *Pearson correlations of correlations between different climate indicators and tree-ring width observations with correlations between the same climate indicators and MAIDEN or VS-Lite tree-growth simulations (1901-1949 verification period). O-S stands for the year starting from October (previous year) to September (current year); P for precipitation; JAS for July-August-September; T for temperature; TRindex for tree-ring index. Asterisks stand for significant correlations (p-value < 0.05). The difference in the number of sites on which correlations are computed is due to the phenological criterion that has been applied to MAIDEN calibrated sites (see Sect. 3.2.4.1 for more details).*

Model (version)	**Correlation**
Correlations between observed TRW and O-S P correlation and simulated TRindex and O-S P correlation	
MAIDEN (Ge2017; 189 sites)	0.388*
MAIDEN (GI2015; 160 sites)	0.322*
VS-Lite (302 sites)	0.515*
VS-Lite (189 Ge2017 selected sites)	0.552*
VS-Lite (160 GI2015 selected sites)	0.552*
MAIDEN (well-fitted sites only)	0.694*
VS-Lite (well-fitted sites only)	0.837*
MAIDEN (common well-fitted sites only)	0.747*
VS-Lite (common well-fitted sites only)	0.886*
Correlations between observed TRW and annual T correlation and simulated TRindex and annual T correlation	
MAIDEN (Ge2017; 189 sites)	0.053
MAIDEN (GI2015; 160 sites)	0.171*
VS-Lite (302 sites)	0.241*
VS-Lite (189 Ge2017 selected sites)	0.203*
VS-Lite (160 GI2015 selected sites)	0.291*
MAIDEN (well-fitted sites only)	0.648*
VS-Lite (well-fitted sites only)	0.678*
MAIDEN (common well-fitted sites only)	0.608*
VS-Lite (common well-fitted sites only)	0.772*
Correlations between observed TRW and JAS T correlation and simulated TRindex and JAS T correlation	
MAIDEN (Ge2017; 189 sites)	0.130
MAIDEN (GI2015; 160 sites)	0.216*
VS-Lite (302 sites)	0.338*
VS-Lite (189 Ge2017 selected sites)	0.329*
VS-Lite (160 GI2015 selected sites)	0.328*
MAIDEN (well-fitted sites only)	0.759*
VS-Lite (well-fitted sites only)	0.704*
MAIDEN (common well-fitted sites only)	0.739*
VS-Lite (common well-fitted sites only)	0.787*

C.2 Supplementary figures

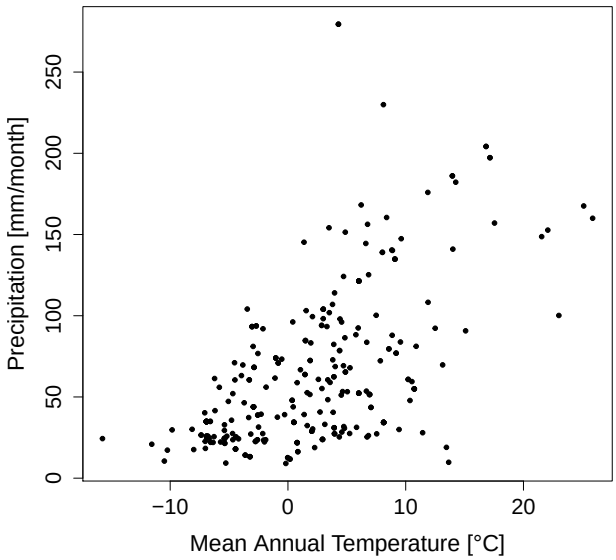


Figure C.1: *Mean monthly cumulative precipitation (in millimeters per month) as a function of mean annual temperature (in ℃) at the 302 PAGES2k TRW sites used in this study. The climate data are from the Global Meteorological Forcing Dataset for land surface modelling (v2) at 0.5° resolution (Section 3.2.3) over the 1901-2000 time period.*

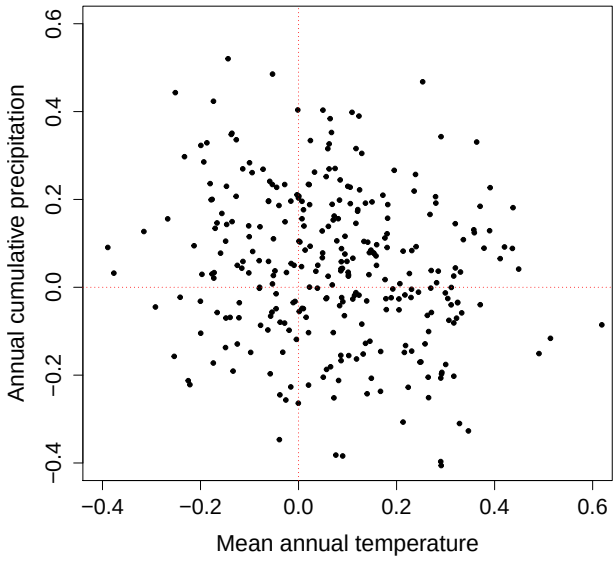


Figure C.2: *Correlations between annual cumulative precipitation and TRW observations as a function of correlations between mean annual temperature and TRW observations at the 302 PAGES2k TRW sites used in this study, over the 1901-2000 period. The climate data are from the Global Meteorological Forcing Dataset for land surface modelling (v2) at 0.5° resolution (Section 3.2.3).*

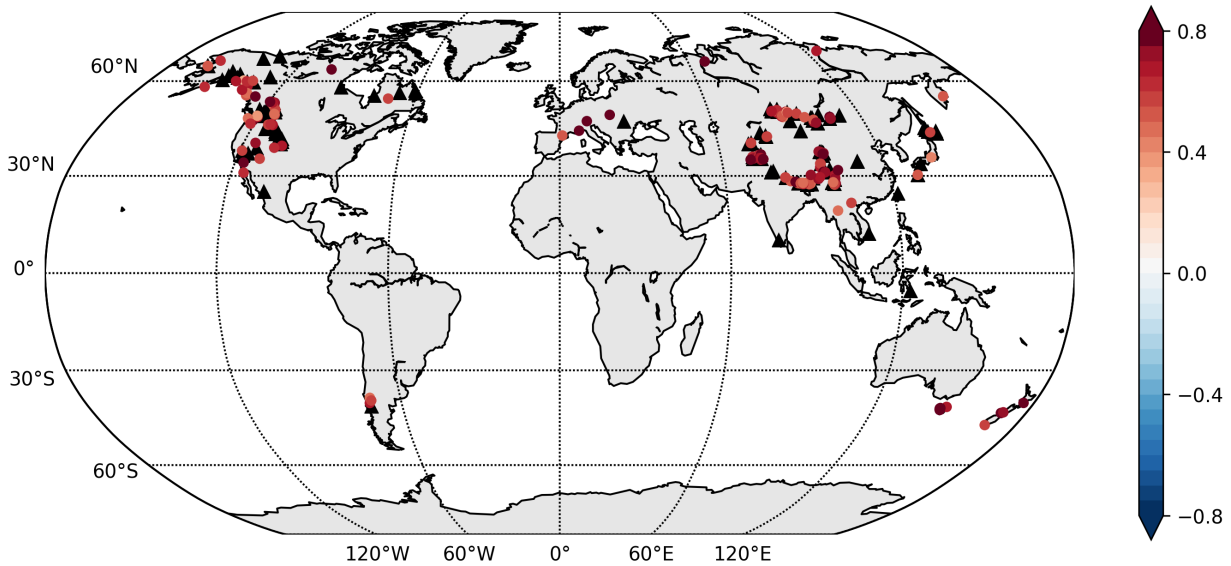


Figure C.3: *MAIDEN [Gea-Izquierdo et al., 2015] calibration correlations for selected sites (Sect. 3.2.4.1; 160 sites out of 302). Background map from Hunter [2007].*

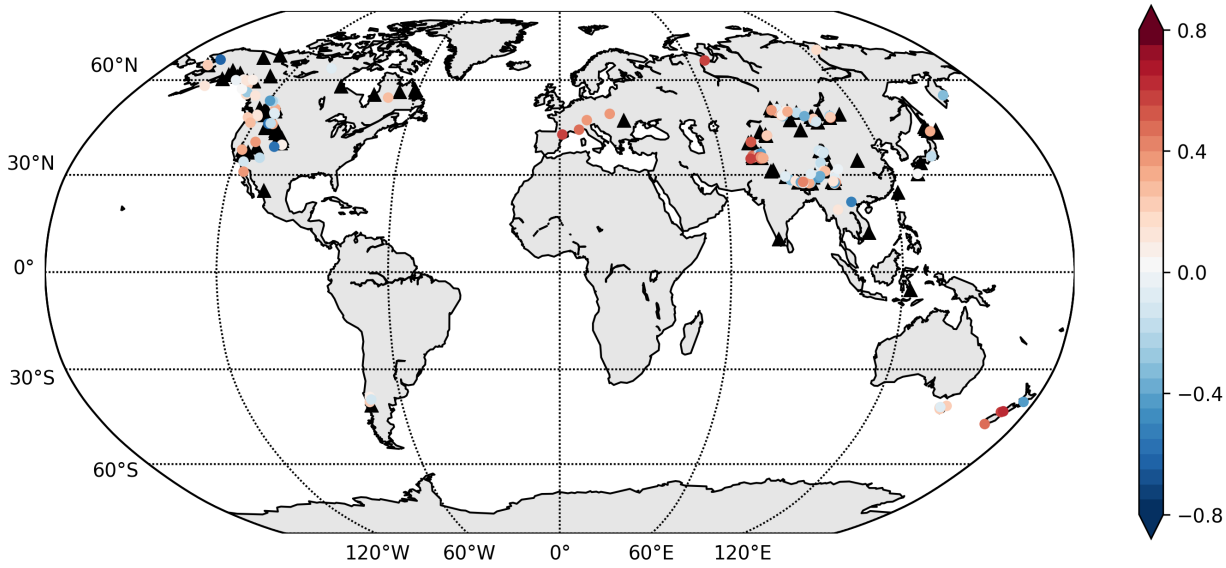


Figure C.4: *MAIDEN [Gea-Izquierdo et al., 2015] verification correlations for selected sites (Sect. 3.2.4.1; 160 sites out of 302). Background map from Hunter [2007].*

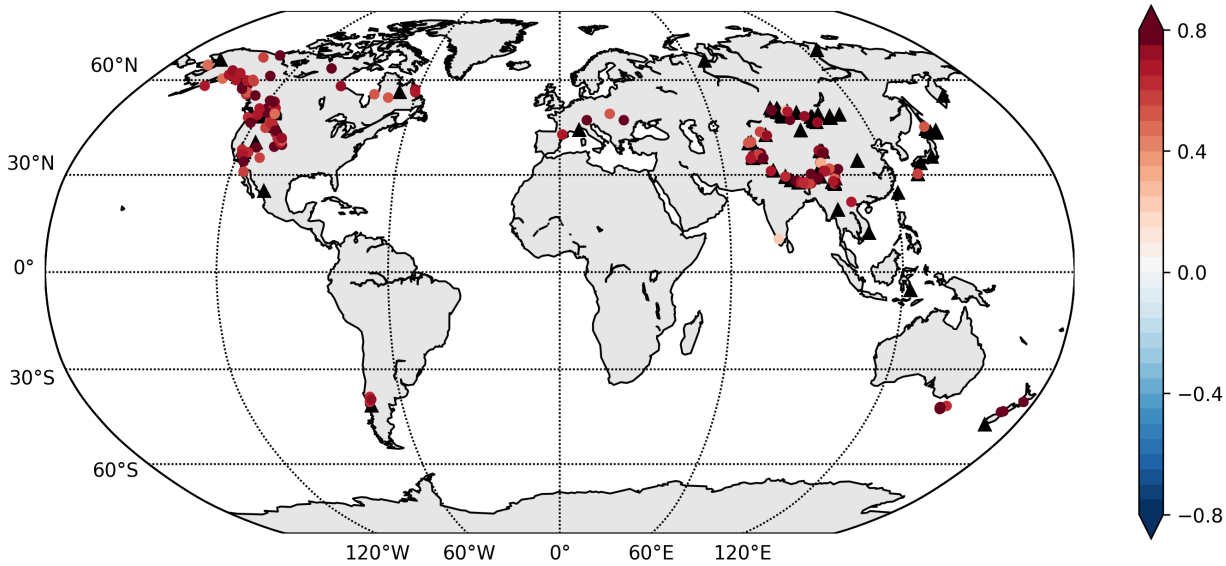


Figure C.5: *MAIDEN [Gennaretti et al., 2017] calibration correlations for selected sites (Sect. 3.2.4.1; 189 sites out of 302). Background map from Hunter [2007].*

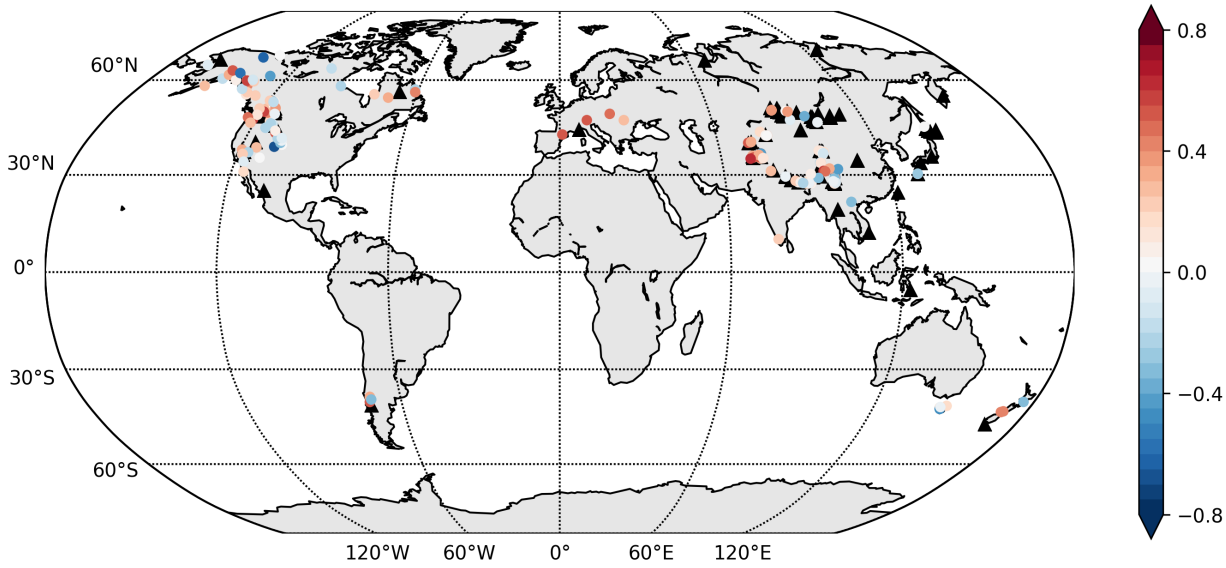


Figure C.6: *MAIDEN [Gennaretti et al., 2017] verification correlations for selected sites (Sect. 3.2.4.1; 189 sites out of 302). Background map from Hunter [2007].*

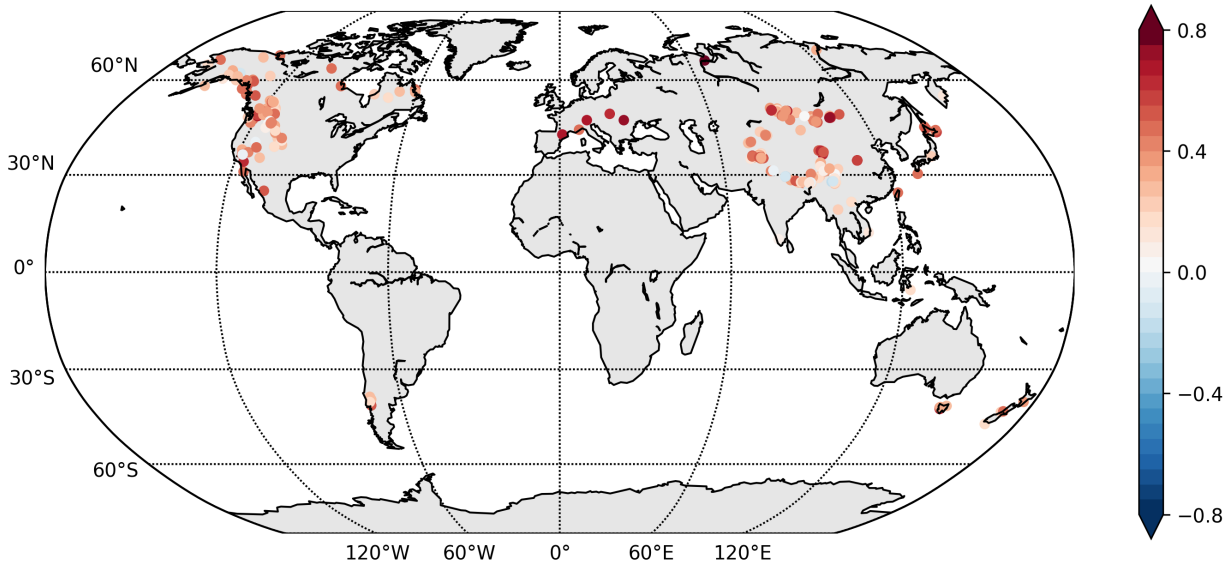


Figure C.7: *VS-Lite calibration correlations for 302 sites. Background map from Hunter [2007].*

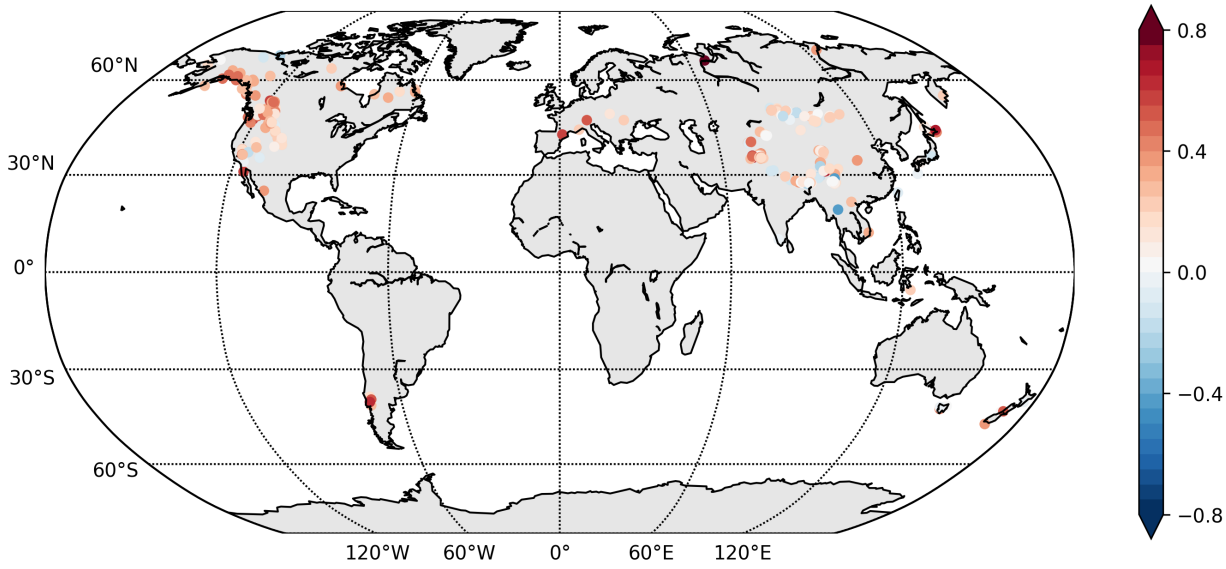
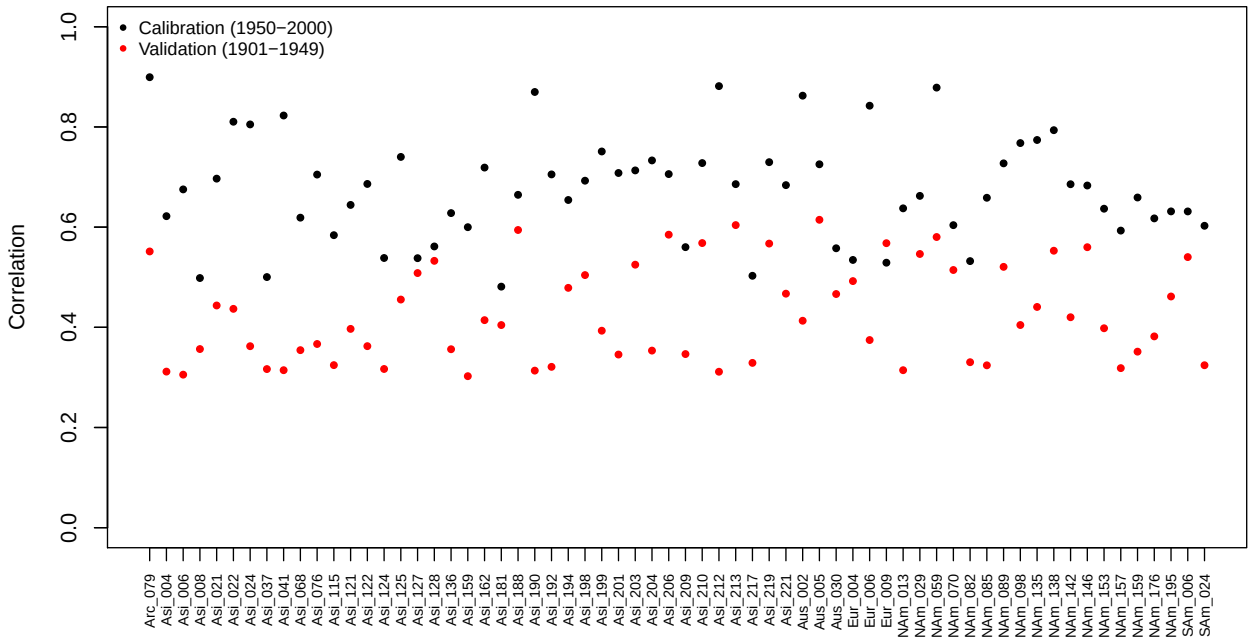
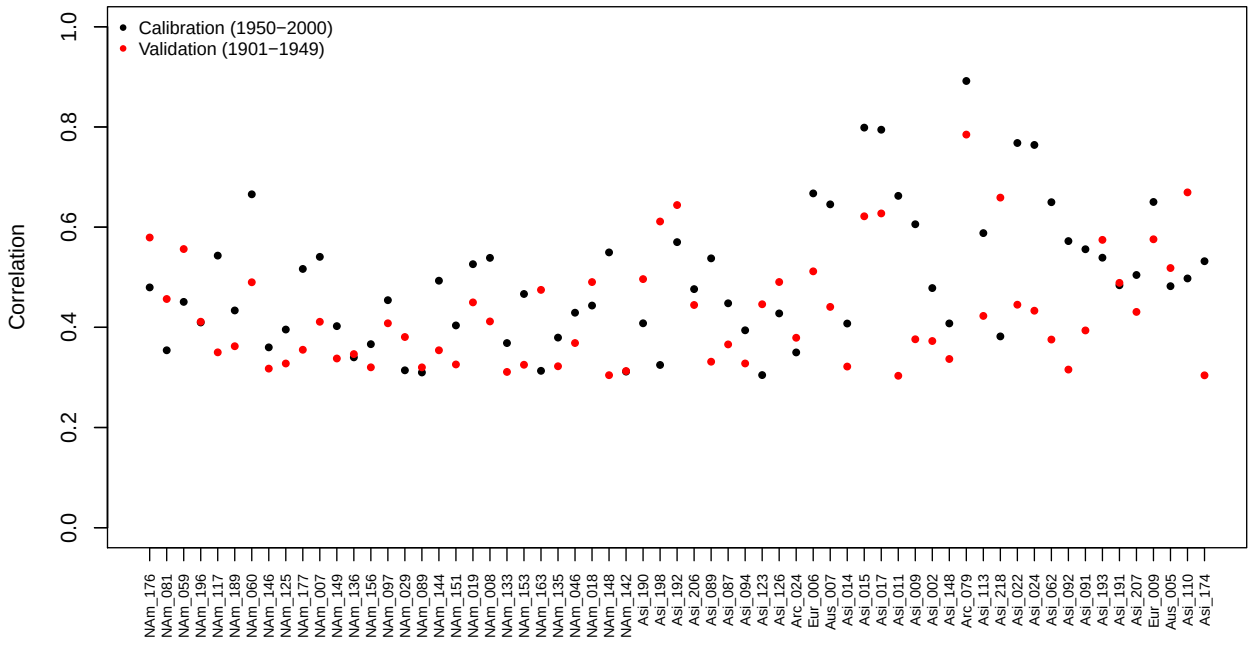


Figure C.8: *VS-Lite verification correlations for 302 sites. Background map from Hunter [2007].*



(a) MAIDEN



(b) VS-Lite

Figure C.9: *(a) MAIDEN (64 sites) and (b) VS-Lite (63 sites) calibration (1950-2000) and verification (1901-1949) correlations (all significant at the 95% confidence level) for well-fitted sites (Sect. 3.3.1) (with names from the PAGES2k database: NAm for North American sites; Asi for Asian sites; Eur for European sites; Arc for Arctic sites; Aus for Australian, Tasmanian or New Zealand sites; SAm for South American sites).*

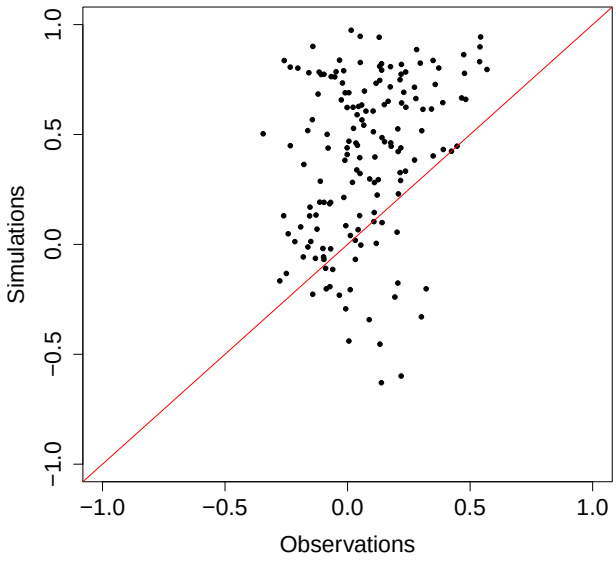


Figure C.10: *Correlations between mean annual temperature and VS-Lite tree-ring index simulations as a function of correlations between mean annual temperature and TRW observations for MAIDEN [Gea-Izquierdo et al., 2015] selected sites (Sect. 3.2.4.1; 160 sites out of 302), over the 1901-1949 verification period.*

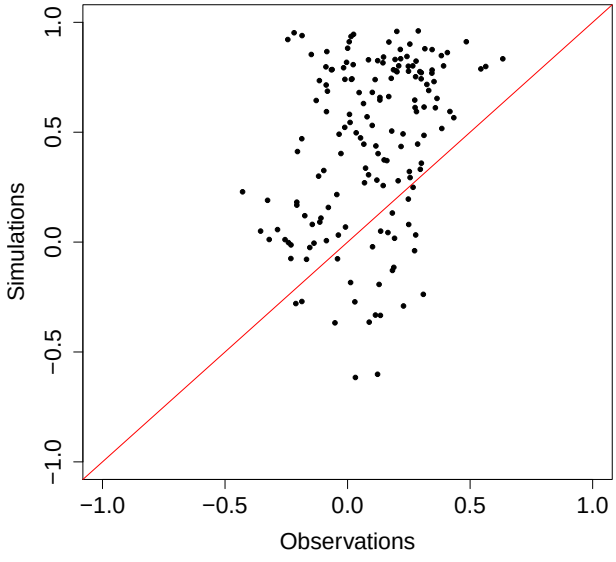


Figure C.11: *Correlations between mean July-August-September temperature and VS-Lite tree-ring index simulations as a function of correlations between mean July-August-September temperature and TRW observations for MAIDEN [Gea-Izquierdo et al., 2015] selected sites (Sect. 3.2.4.1; 160 sites out of 302), over the 1901-1949 verification period.*

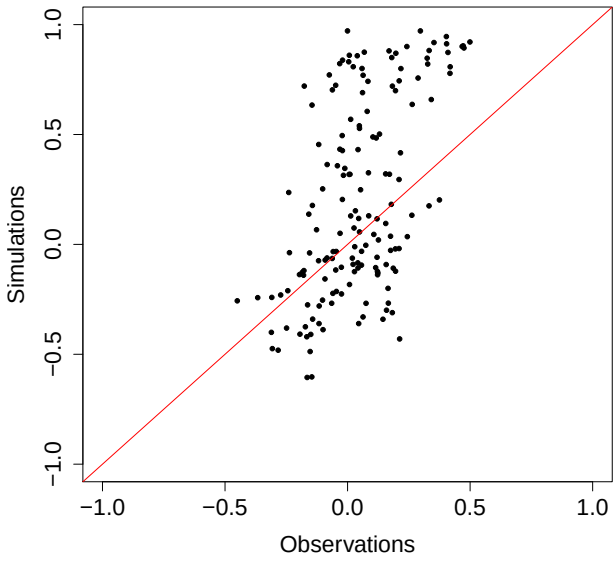


Figure C.12: *Correlations between October-September cumulative precipitation and VS-Lite tree-ring index simulations as a function of correlations between October-September cumulative precipitation and TRW observations for MAIDEN [Gea-Izquierdo et al., 2015] selected sites (Sect. 3.2.4.1; 160 out of 302), over the 1901-1949 verification period.*

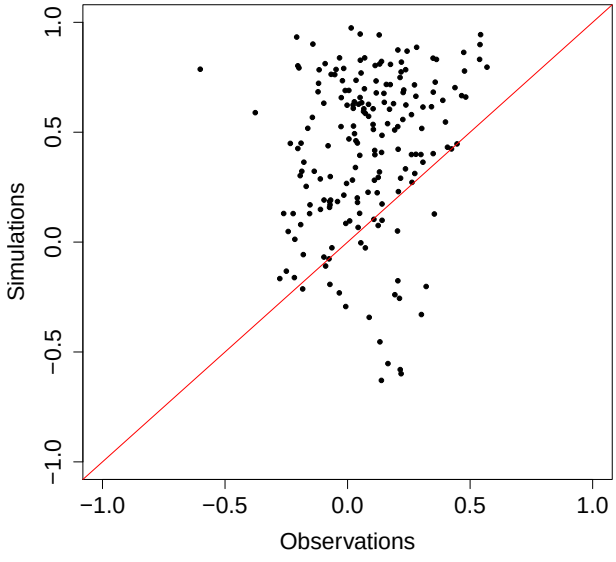


Figure C.13: *Correlations between mean annual temperature and VS-Lite tree-ring index simulations as a function of correlations between mean annual temperature and TRW observations for MAIDEN [Gennaretti et al., 2017] selected sites (Sect. 3.2.4.1; 189 sites out of 302), over the 1901-1949 verification period.*

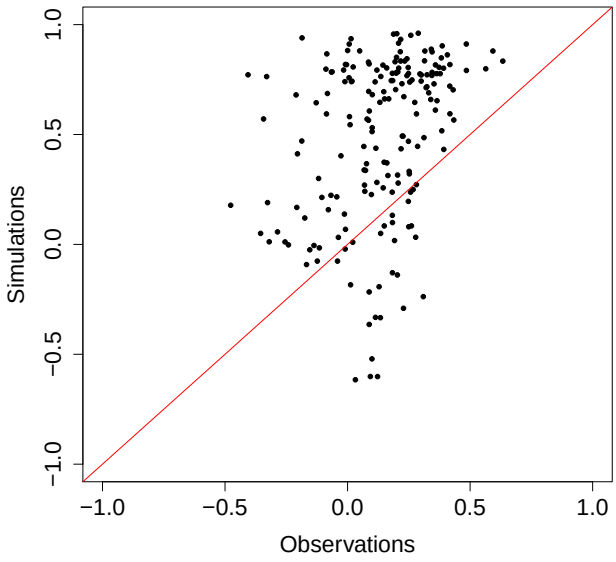


Figure C.14: *Correlations between mean July-August-September temperature and VS-Lite tree-ring index simulations as a function of correlations between mean July-August-September temperature and TRW observations for MAIDEN [Gennaretti et al., 2017] selected sites (Sect. 3.2.4.1; 189 sites out of 302), over the 1901-1949 verification period.*

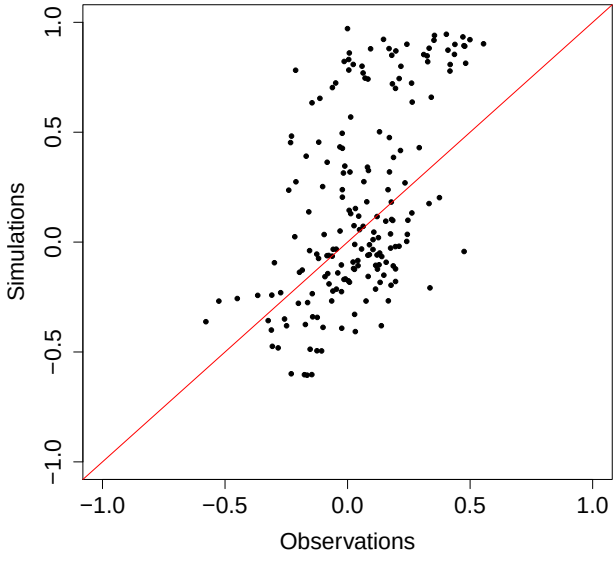


Figure C.15: *Correlations between October-September cumulative precipitation and VS-Lite tree-ring index simulations as a function of correlations between October-September cumulative precipitation and TRW observations for MAIDEN [Gennaretti et al., 2017] selected sites (Sect. 3.2.4.1; 189 out of 302), over the 1901-1949 verification period.*

D

Supplement to Chapter 4

D.1 Data assimilation and particle filtering in paleoclimatology

In paleoclimatology, the objective of data assimilation is to provide an estimate of the state of the climate system that is as accurate as possible given the available observations by optimally combining climate model outputs and observations. In this regard, data assimilation can be commonly represented within a Bayesian framework. Starting from the prior estimate of the climate variables of interest as given by a climate model, the data assimilation framework provides a posterior estimate (i.e., the reanalysis) of these climate variables according to the observations.

A probability density function (hereafter pdf) describes each climate variable of interest in the model. Let define $\mathbf{x}^p$, the model state, and $\mathbf{y}$, the available observations that potentially bring information on $\mathbf{x}^p$. Following the Bayes' theorem:

$$p(\mathbf{x}^p|\mathbf{y}) = \frac{p(\mathbf{y}|\mathbf{x}^p)p(\mathbf{x}^p)}{p(\mathbf{y})} \tag{D.1}$$

where $p(\mathbf{x}^p)$ is the joint prior pdf of all variables of interest; $p(\mathbf{y}|\mathbf{x}^p)$, the pdf of the available observations given the model state, also called the likelihood; $p(\mathbf{x}^p|\mathbf{y})$, the posterior pdf, i.e., the probability of observing $\mathbf{x}^p$ given the available observations $\mathbf{y}$ and model constraint, or the reanalysis. The temporal resolution of the available observations $\mathbf{y}$ defines the time step of the assimilation and the period over which the prior is averaged (one year in this thesis). In the data assimilation framework, we often assume the likelihood to be Gaussian:

$$p(\mathbf{y}|\mathbf{x}^p) = K^{-1} \exp\left[-\frac{1}{2}(\mathbf{y} - H(\mathbf{x}^p))^T C^{-1}(\mathbf{y} - H(\mathbf{x}^p))\right] \tag{D.2}$$

where K is a normalization constant; H is the observation operator, a function that makes the link between the prior defined by the climate variables of interest, here

given by the model results, and the observations (also called the mapping of the prior to the observational phase space). For proxy records, H can range from a simple linear regression, that links the proxy records with climate variables, to a more complex proxy system model, for instance here MAIDEN [Evans et al., 2013; Dee et al., 2016]. C is the error covariance of the observations, generally assumed to be diagonal (i.e., the errors are assumed to be independent); T is the symbol for matrix transpose.

In this thesis, we make use of a probabilistic approach as described in van Leeuwen [2009] to define the state of the climate system, leading to what is referred to as particle filtering. In this approach, the model prior pdf is represented discretely with a set of independent model states, i.e., the particles. The prior pdf is defined as follows:

$$p(\mathbf{x}^p) = \frac{1}{N}\sum_{i=1}^{N}\delta(\mathbf{x}^p - \mathbf{x}_i^p) \tag{D.3}$$

where N is the number of random particles, ranging from i = 1 to $i = N$, and δ is a kernel density. Each particle in the prior is assumed to have the same probability. In the thesis, the N particles are sampled from a pre-existing ensemble of climate model simulations at an annual resolution to build the prior (i.e., the offline approach). The prior is thus the same for any reconstructed years, that are assumed to be independent of each other. This assumption is valid when reconstructing atmospheric variables, as is the case in this thesis, since their predictability is smaller than one year (the time step of the assimilation). On the contrary, the online approach sequentially builds the prior, year by year, propagating forward the updates made on the previous steps [e.g. Goosse, 2017]. Matsikaris et al. [2015] have shown that the online approach does not surpass the offline approach when focusing on the atmosphere.

Combining equation (D.1) with equation (D.3) gives us:

$$p(\mathbf{x}^p|\mathbf{y}) = \frac{1}{N}\sum_{i=1}^{N} w_i\delta(\mathbf{x}^p - \mathbf{x}_i^p) \tag{D.4}$$

where,

$$w_i = \frac{p(\mathbf{y}|\mathbf{x}_i^p)}{\sum_{j=1}^{N} p(\mathbf{y}|\mathbf{x}_j^p)} \tag{D.5}$$

where w_i is commonly called the weight of the particle i. The weight of a particle is derived from the likelihood associated with the particle regarding the available observations, $p(\mathbf{y}|\mathbf{x}^p)$. The weight for a particle closer to the observations will be higher, and lower for particles characterized by a state less consistent with the observations. In this thesis, for each time step of the assimilation, the posterior mean, i.e., the weighted mean of the sampled particles, is considered as the reconstruction for that time step (one year):

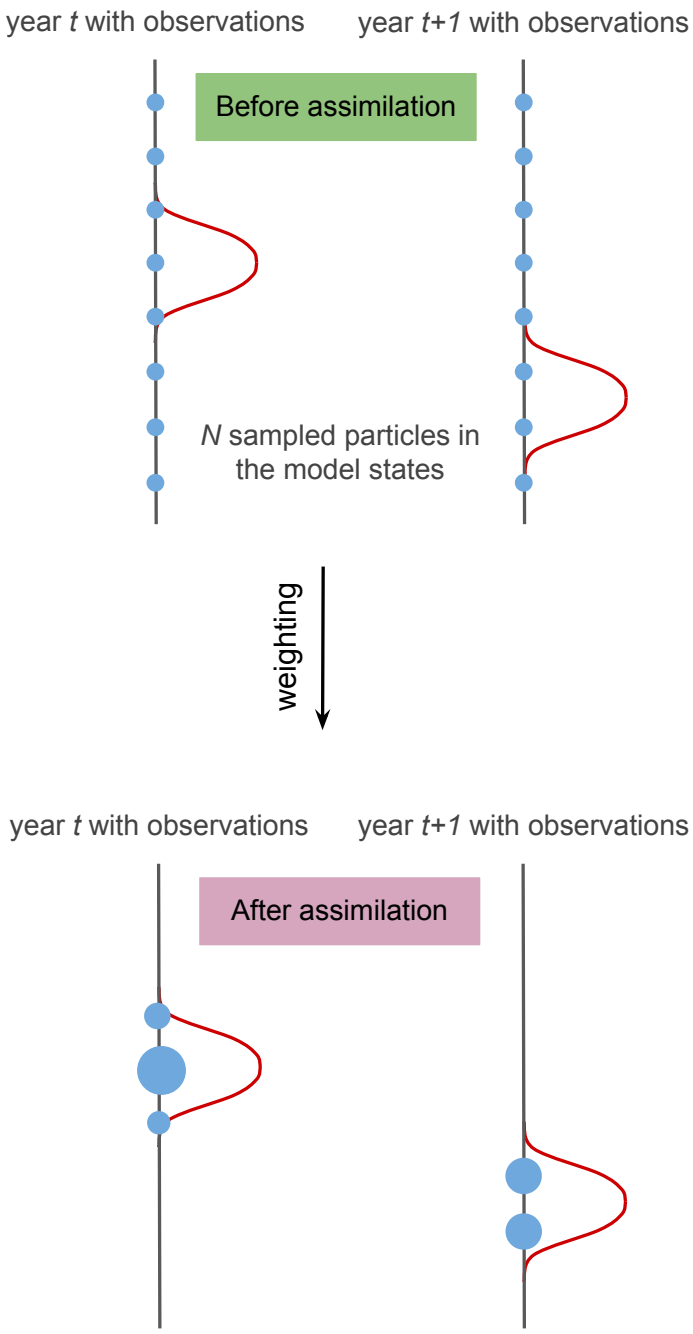


Figure D.1: *Schematic representation of the procedure of offline data assimilation with a particle filter. Before the assimilation, all the* N *(= 8 in our example) particles (blue circles) sampled in the model states (vertical axis) have the same weight, which is proportional to the size of the circle, whatever the year considered (t and t+1 in the example). The distribution of the available observations with uncertainties (*C *in equation* (D.2)*) for each year is represented by the red curve. After the assimilation, the particles have been weighted relatively to their associated likelihood, given the available observations for each year, and the size of the circle is thus modified. When the weight of a particle is zero, it does not appear anymore on the figure.*

$$\overline{p(\mathbf{x}^p)|\mathbf{y}} = \sum_{i=1}^{N} w_i \mathbf{x}_i^p \tag{D.6}$$

The weighted standard deviation of the sampled particles gives an estimate of the range of the reconstruction (i.e., the ensemble spread).

The same methodology is applied for each year of the reconstruction, i.e., the period covered by observations (Fig. D.1). First, the prior estimate of the state of the climate system for that year is estimated by sampling N particles from an ensemble of model simulations, for all the variables of interest (i.e., the assimilated and the analyzed variables). Then, all the sampled particles are compared to the available observations for that year, directly or by means of a proxy system model. A weight is given to each particle on the basis of its associated likelihood regarding the available observations. The weighted mean of the particles provides the reconstruction for that year.

This method has the advantage of respecting the dynamics of the climate system as included in the climate model since only the weight of the sampled particles are updated throughout the procedure according to the available observations. The particle filter does not require an inversion or linearization of the observation operator H, which is an important advantage as well. Additionally, there are no assumptions made on the prior and posterior distributions. Finally, particle filtering can be easily implemented without any a priori information on the model.

D.2 Supplementary tables

Table D.1: *Pearson correlation coefficient between the observed tree-ring width (TRW) time series and the tree-ring index time series simulated by the regression model (Sect. 4.2.4.2) over 1950-2000 (calibration period) and 1901-1949 (verification period) at the 21 TRW sites of the PAGES2k databases [PAGES 2k Consortium, 2013, 2017]. The site names are from the PAGES2k database: Aus for Tasmanian or New Zealand sites; SAm for South American sites. Asterisks stand for significant correlation coefficients at the 95% confidence level.*

Site	Calibration	Verification
Aus_001	0.42*	-0.09
Aus_002	0.31*	-0.08
Aus_004	0.24	0.15
Aus_005	0.52*	-0.03
Aus_007	0.65*	0.35*
Aus_009	0.43*	-0.06
Aus_030	0.16	0.31*
Aus_031	0.25	-0.05
SAm_006	0.65	0.01
SAm_024	0.09	0.03
SAm_025	030*	0.50*
SAm_029	0.25	0.12
SAm_9	0.29*	-0.06
SAm_10	0.17	0.07
SAm_11	0.57*	0.22
SAm_12	0.31*	0.09
SAm_15	0.18	-0.04
SAm_16	0.18	0.21
SAm_17	0.20	0.22
SAm_18	0.09	-0.07
SAm_19	0.13	-0.15

D.3 Supplementary figures

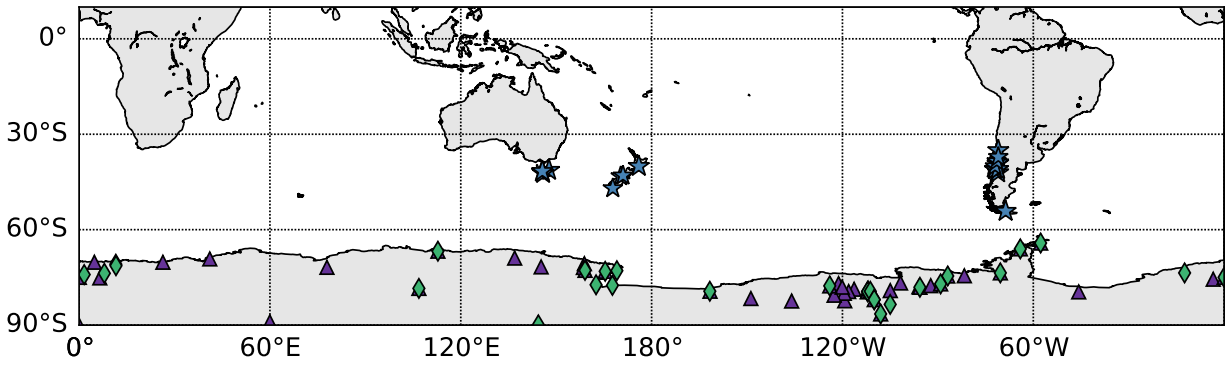


Figure D.2: *Location of the 21 tree-ring width (TRW) records (blue stars) from the PAGES2k databases [PAGES 2k Consortium, 2013, 2017]; the 49 ice core snow accumulation records (purple triangles) from Thomas et al. [2017] and Medley et al. [2018]; and the 29 $\delta^{18}O$ records (green diamonds) from Stenni et al. [2017] (Sect. 4.2.3). Background map from Hunter [2007].*

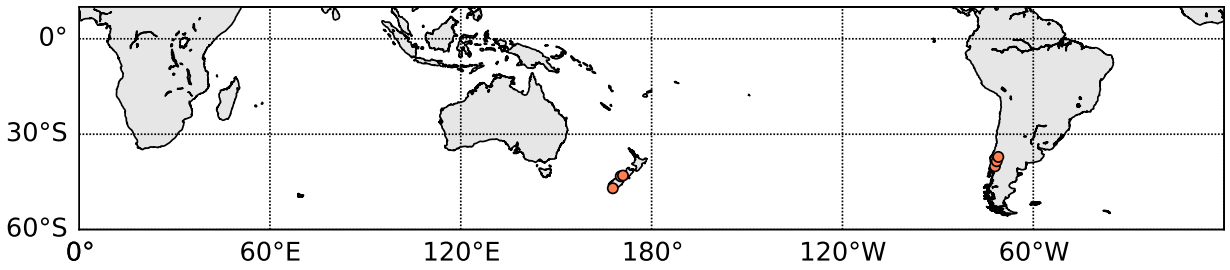


Figure D.3: *Location of the six tree-ring width (TRW) records (orange circles) from the PAGES2k databases [PAGES 2k Consortium, 2013, 2017] assimilated with the MAIDEN model calibrated over the 1950-2000 CE time period (see Sect. 4.2.4.1 for more details). Background map from Hunter [2007].*

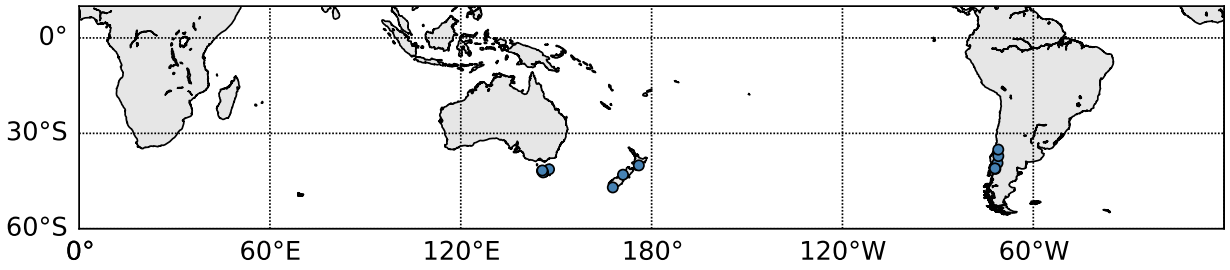


Figure D.4: *Location of the 12 tree-ring width (TRW) records (blue circles) from the PAGES2k databases [PAGES 2k Consortium, 2013, 2017] assimilated with the regression-based model calibrated over the 1901-2000 CE time period (see Sect. 4.2.4.2 for more details). Background map from Hunter [2007].*

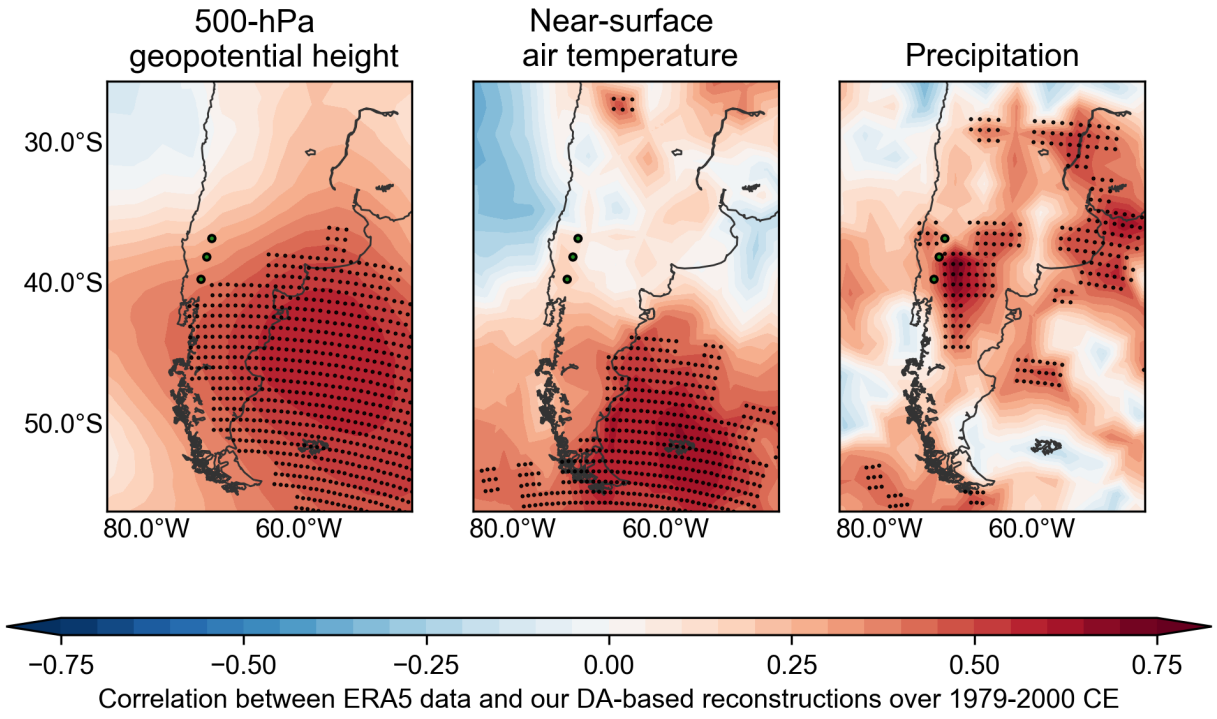


Figure D.5: *Pearson correlation coefficient between the reconstructed and ERA5 geopotential height at 500 hPa, near-surface air temperature or cumulative precipitation in South America over 1979-2000 CE for the TIC-MDN experiment (see Sect. 4.3 and Table 4.1 for details on the experiment). The green dots indicate the localization of the assimilated tree-ring width records. The black dots indicate a significant correlation coefficient at the 95% confidence level.*

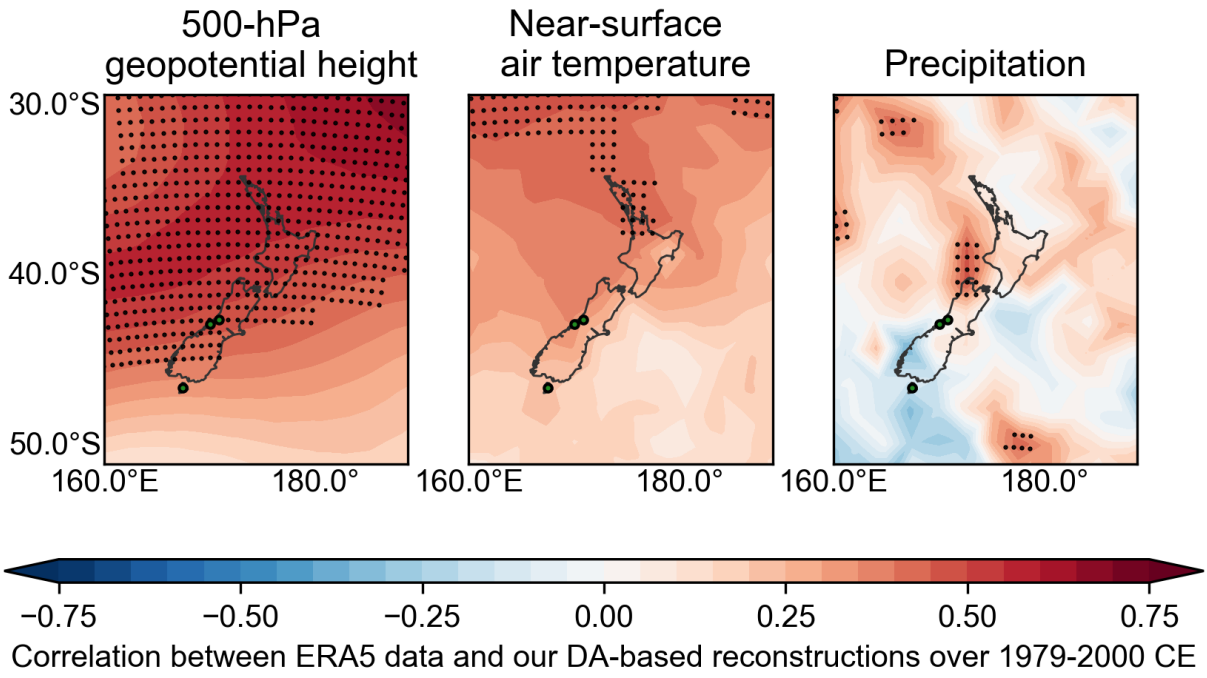


Figure D.6: *Pearson correlation coefficient between the reconstructed and ERA5 geopotential height at 500 hPa, near-surface air temperature or cumulative precipitation in New Zealand over 1979-2000 CE for the TIC-MDN experiment (see Sect. 4.3 and Table 4.1 for details on the experiment). The green dots indicate the localization of the assimilated tree-ring width records. The black dots indicate a significant correlation coefficient at the 95% confidence level.*

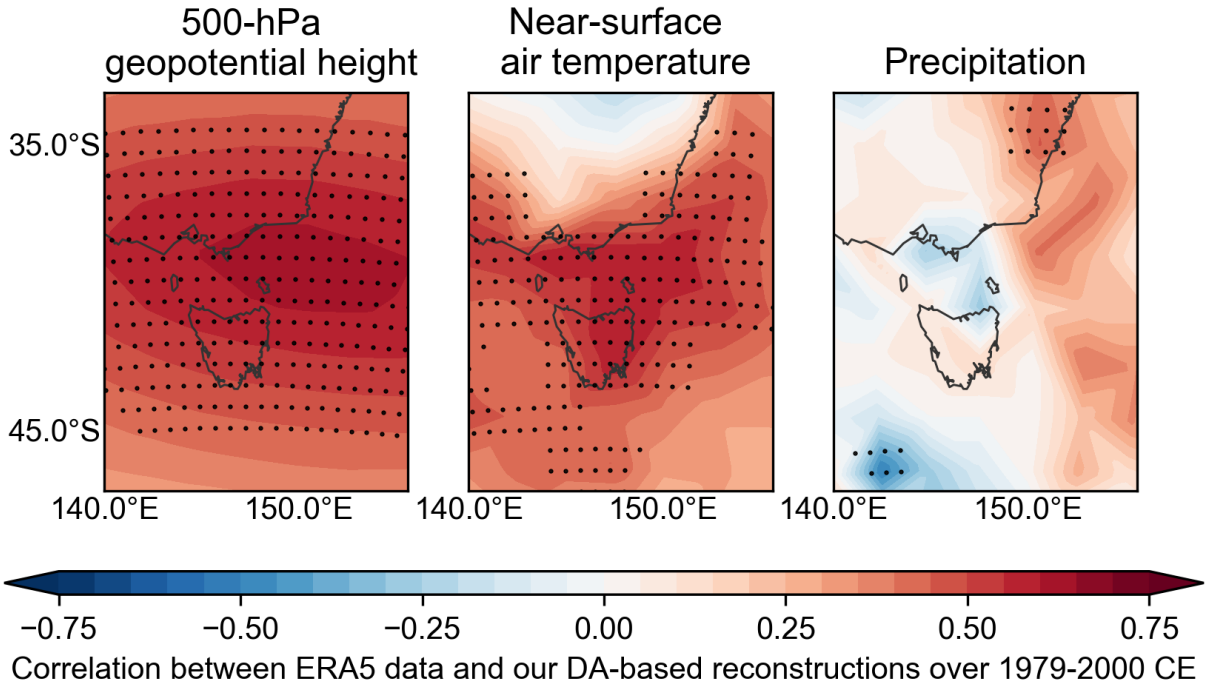


Figure D.7: *Pearson correlation coefficient between the reconstructed and ERA5 geopotential height at 500 hPa, near-surface air temperature or cumulative precipitation in Tasmania over 1979-2000 CE for the TIC-MDN experiment (see Sect. 4.3 and Table 4.1 for details on the experiment). The green dots indicate the localization of the assimilated tree-ring width records. The black dots indicate a significant correlation coefficient at the 95% confidence level.*

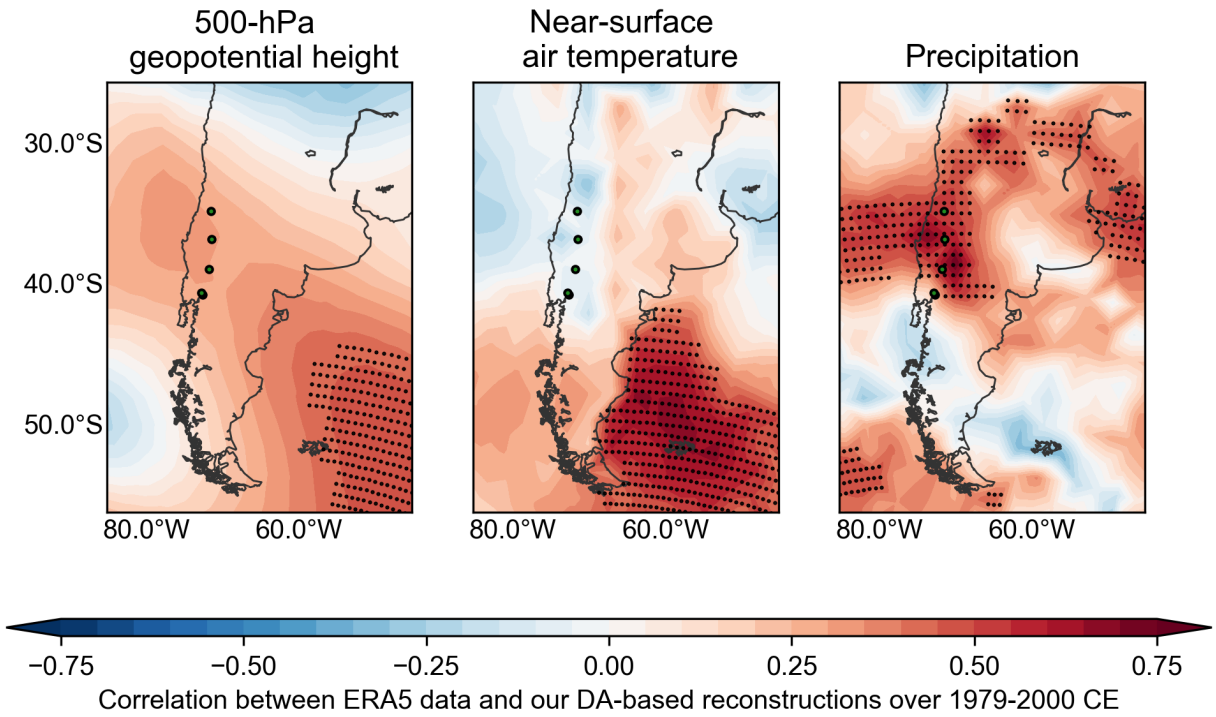


Figure D.8: *Pearson correlation coefficient between the reconstructed and ERA5 geopotential height at 500 hPa, near-surface air temperature or cumulative precipitation in South America over 1979-2000 CE for the TIC-reg experiment (see Sect. 4.3 and Table 4.1 for details on the experiment). The green dots indicate the localization of the assimilated tree-ring width records. The black dots indicate a significant correlation coefficient at the 95% confidence level.*

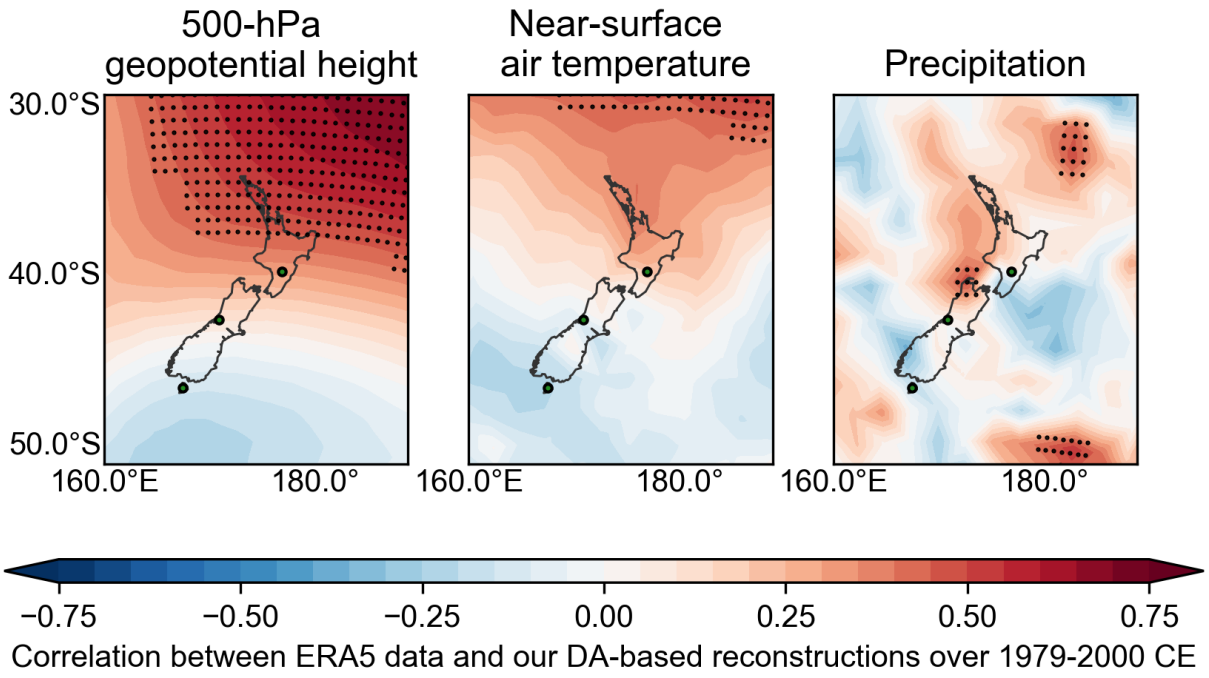


Figure D.9: *Pearson correlation coefficient between the reconstructed and ERA5 geopotential height at 500 hPa, near-surface air temperature or cumulative precipitation in New Zealand over 1979-2000 CE for the TIC-reg experiment (see Sect. 4.3 and Table 4.1 for details on the experiment). The green dots indicate the localization of the assimilated tree-ring width records. The black dots indicate a significant correlation coefficient at the 95% confidence level.*

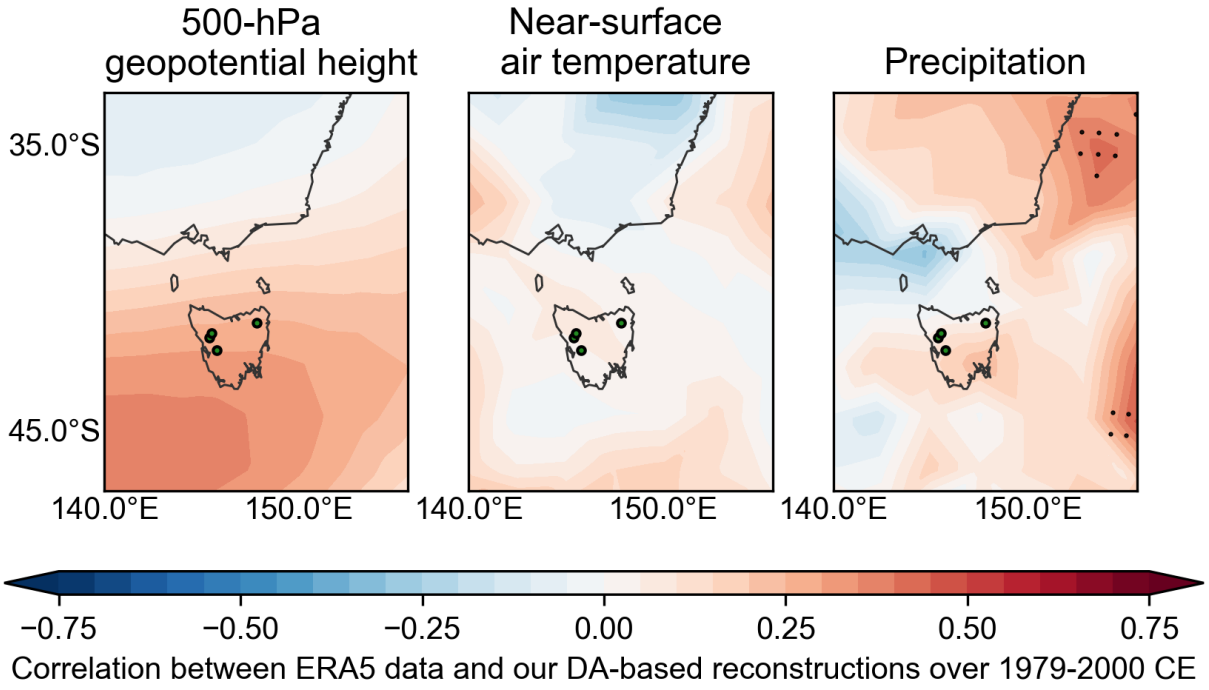


Figure D.10: *Pearson correlation coefficient between the reconstructed and ERA5 geopotential height at 500 hPa, near-surface air temperature or cumulative precipitation in Tasmania over 1979-2000 CE for the TIC-reg experiment (see Sect. 4.3 and Table 4.1 for details on the experiment). The green dots indicate the localization of the assimilated tree-ring width records. The black dots indicate a significant correlation coefficient at the 95% confidence level.*

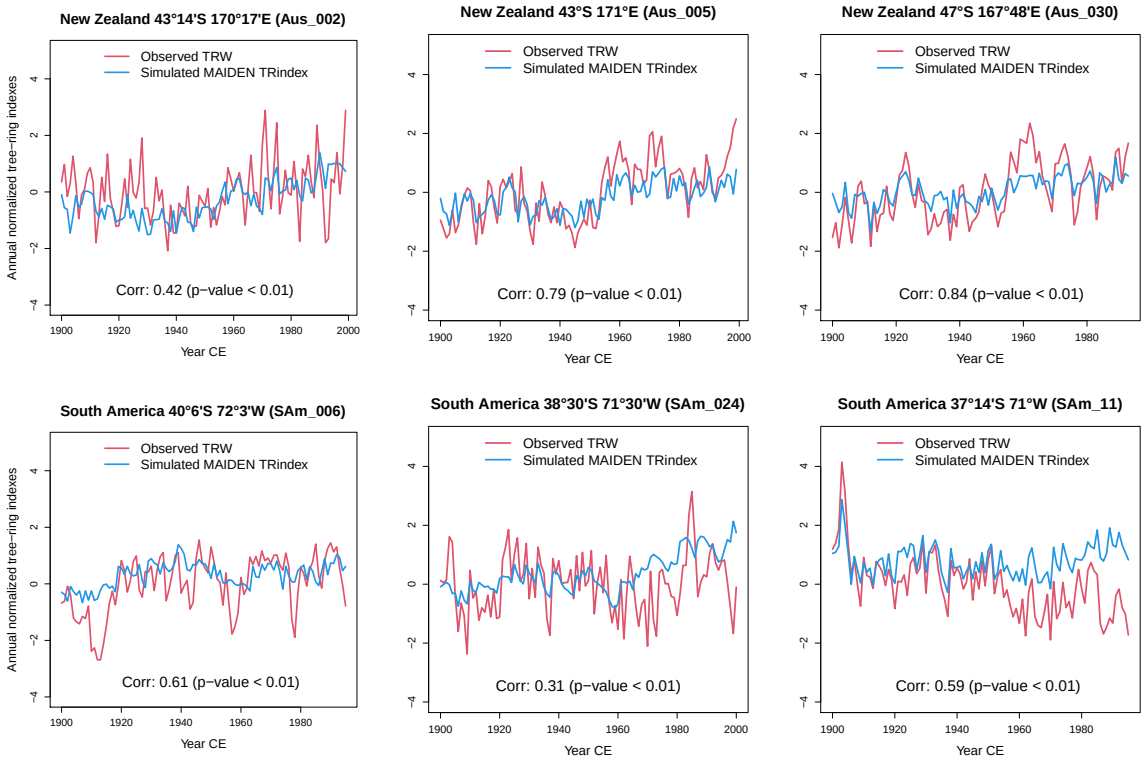


Figure D.11: *Observed tree-ring width and simulated tree-ring index by MAIDEN over 1900-2000 CE at the six assimilated tree-ring width sites (Sect. 4.2.4.1). Pearson correlation coefficient (Corr) between observed and simulated tree-ring index and associated p-value. The observations are normalized relative to 1900-2000 CE. The simulations are normalized relative to 1900-2000 CE using the mean and the standard deviation of the reference run of MAIDEN with the iCESM1 data used in the data assimilation procedure (Sect. 4.2.4.1). The TIC-MDN reanalysis is used to run MAIDEN (see Sect. 4.3 for details on the data assimilation experiment).*

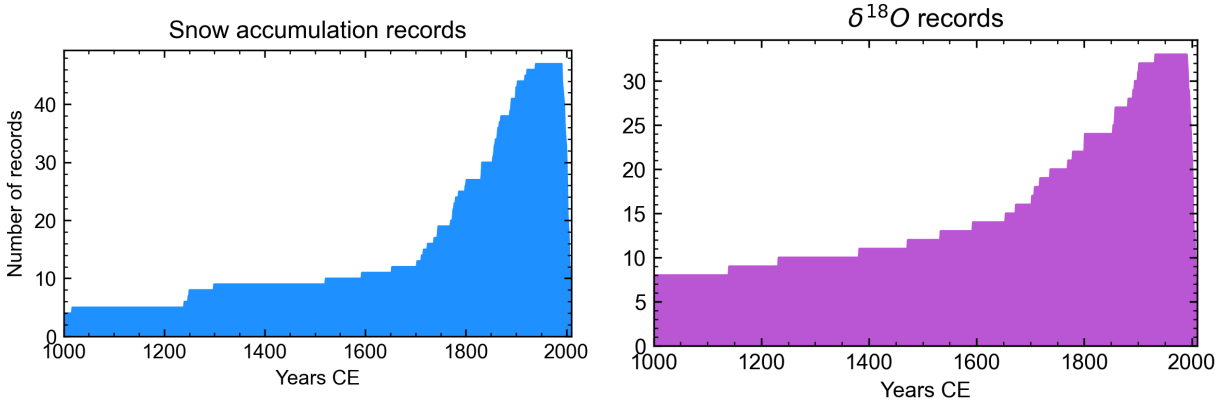


Figure D.12: *Number of snow accumulation and $\delta^{18}O$ records used in this study (Sect. 4.2.3.2) over 1000-2000 CE. Figures from Dalaiden et al. [2021].*

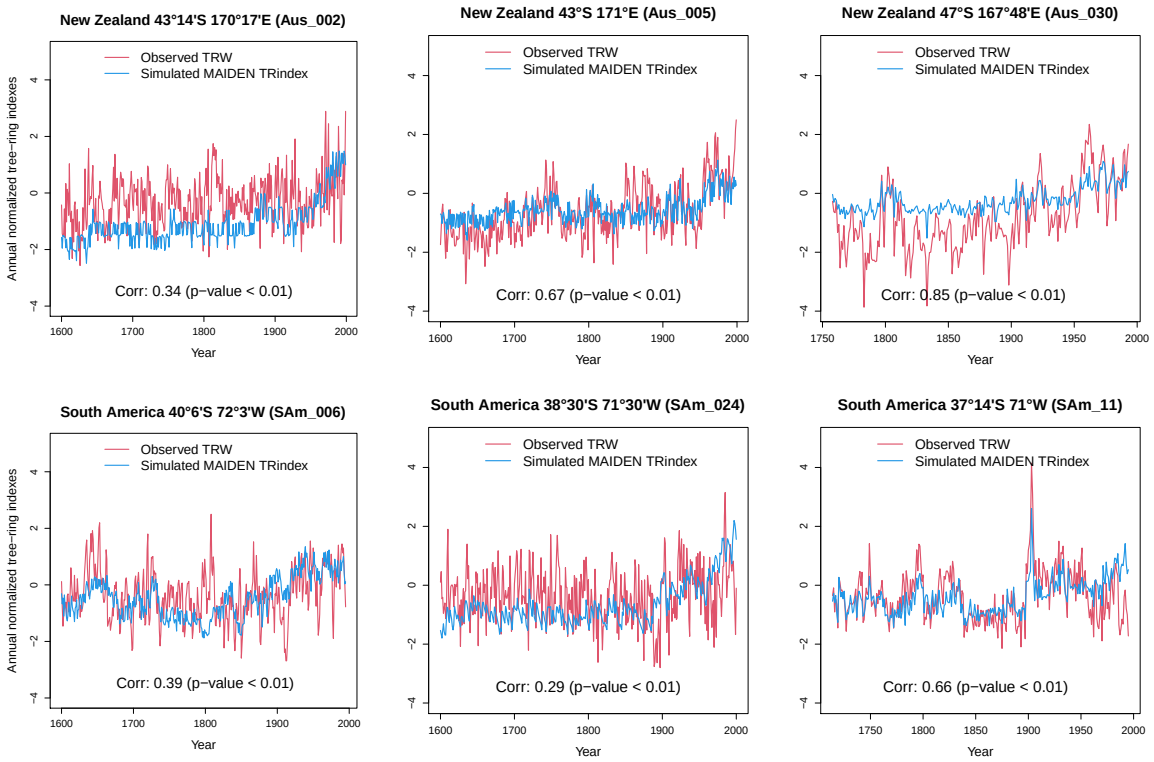


Figure D.13: *Observed tree-ring width and simulated tree-ring index by MAIDEN over 1600-2000 CE at the six assimilated tree-ring width sites (Sect. 4.2.4.1). Pearson correlation coefficient (Corr) between observed and simulated tree-ring index and associated p-value. The observations are normalized relative to 1900-2000 CE. The simulations are normalized relative to 1900-2000 CE using the mean and the standard deviation of the reference run of MAIDEN with the iCESM1 data used in the data assimilation procedure (Sect. 4.2.4.1). The TIC-MDN reanalysis is used to run MAIDEN (see Sect. 4.3 for details on the data assimilation experiment).*

E

List of publications related to the thesis

First author

- Rezsöhazy, J., Goosse , H., Guiot, J., Gennaretti, F., Boucher, E., André, F., and Jonard, M. (2020). Application and evaluation of the dendroclimatic process-based model MAIDEN during the last century in Canada and Europe, *Climate of the Past*, **16**, 1043–1059, https://doi.org/10.5194/cp-16-1043-2020. (Chapter 2)

- Rezsöhazy, J., Gennaretti, F., Goosse, H., Guiot, J. (2021). Testing the performance of dendroclimatic process-based models at global scale with the PAGES2k tree-ring width database, *Climate Dynamics*, **57**, 2005-2020, https://doi.org/10.1007/s00382-021-05789-7. (Chapter 3)

- Rezsöhazy, J., Dalaiden, Q., Klein, F., Goosse, H, and Guiot, J. (2021). Using a process-based dendroclimatic proxy system model in a data assimilation framework: a test case in the Southern Hemisphere over the past centuries, In preparation. (Chapter 4)

Co-author

- Dalaiden, Q., Goosse, H., Rezsöhazy, J. and Thomas, E.R. (2021). Reconstructing atmospheric circulation and sea-ice extent in the West Antarctic over the past 200 years using data assimilation, *Climate Dynamics*, https://doi.org/10.1007/s00382-021-05879-6.

References

Acevedo, W., Fallah, B., Reich, S., and Cubasch, U. (2017). Assimilation of pseudo-Tree-ring-width observations into an atmospheric general circulation model. *Climate of the Past*, 13(5):545–557.

Agosta, C., Amory, C., Kittel, C., Orsi, A., Favier, V., Gallée, H., Van Den Broeke, M. R., Lenaerts, J. T., Van Wessem, J. M., Van De Berg, W. J., and Fettweis, X. (2019). Estimation of the Antarctic surface mass balance using the regional climate model MAR (1979-2015) and identification of dominant processes. *Cryosphere*, 13:281–296.

Anchukaitis, K. J., Evans, M. N., Kaplan, A., Vaganov, E. A., Hughes, M. K., Grissino-Mayer, H. D., and Cane, M. A. (2006). Forward modeling of regional scale tree-ring patterns in the southeastern United States and the recent influence of summer drought. *Geophysical Research Letters*, 33(4):2–5.

Anchukaitis, K. J., Wilson, R., Briffa, K. R., Büntgen, U., Cook, E. R., D'Arrigo, R., Davi, N., Esper, J., Frank, D., Gunnarson, B. E., Hegerl, G., Helama, S., Klesse, S., Krusic, P. J., Linderholm, H. W., Myglan, V., Osborn, T. J., Zhang, P., Rydval, M., Schneider, L., Schurer, A., Wiles, G., and Zorita, E. (2017). Last millennium Northern Hemisphere summer temperatures from tree rings: Part II, spatially resolved reconstructions. *Quaternary Science Reviews*, 163:1–22.

Anderson, D. M., Tardif, R., Horlick, K., Erb, M. P., Hakim, G. J., Noone, D., Perkins, W. A., and Steig, E. (2019). Additions to the Last Millennium Reanalysis Multi-Proxy Database. *Data Science Journal*, 18(1):2.

Atsawawaranunt, K., Comas-bru, L., Mozhdehi, S. A., and Deininger, M. (2018). The SISAL database : a global resource to document oxygen and carbon isotope records from speleothems. 10:1687–1713.

Ault, T. R., Cole, J. E., Evans, M. N., Barnett, H., Abram, N. J., Tudhope, A. W., and Linsley, B. K. (2009). Intensified decadal variability in tropical climate during the late 19th century. *Geophysical Research Letters*, 36:1–5.

Babst, F., Bodesheim, P., Charney, N., Friend, A. D., Girardin, M. P., Klesse, S., Moore, D. J., Seftigen, K., Björklund, J., Bouriaud, O., Dawson, A., DeRose, R. J., Dietze, M. C., Eckes, A. H., Enquist, B., Frank, D. C., Mahecha, M. D., Poulter, B., Record, S., Trouet, V., Turton, R. H., Zhang, Z., and Evans, M. E. (2018). When tree rings go global: Challenges and opportunities for retro- and prospective insight. *Quaternary Science Reviews*, 197:1–20.

Babst, F., Bouriaud, O., Poulter, B., Trouet, V., Girardin, M. P., and Frank, D. C. (2019). Twentieth century redistribution in climatic drivers of global tree growth. *Science Advances*, 5:1–9.

Babst, F., Poulter, B., Trouet, V., Tan, K., Neuwirth, B., Wilson, R., Carrer, M., Grabner, M., Tegel, W., Levanic, T., Panayotov, M., Urbinati, C., Bouriaud, O., Ciais, P., and Frank, D. (2013). Site- and species-specific responses of forest growth to climate across the European continent. *Global Ecology and Biogeography*, 22(6):706–717.

Badgeley, J. A., Steig, E. J., Hakim, G. J., and Fudge, T. J. (2020). Greenland temperature and precipitation over the last 20 000 years using data assimilation. *Climate of the Past*, 16(4):1325–1346.

Baker, A., C. Hellstrom, J., Kelly, B. F., Mariethoz, G., and Trouet, V. (2015). A composite annual-resolution stalagmite record of North Atlantic climate over the last three millennia. *Scientific Reports*, 5:1–8.

Baldocchi, D., Falge, E., Gu, L., Olson, R., Hollinger, D., Running, S., Anthoni, P., Bernhofer, C., Davis, K., Evans, R., Fuentes, J., Goldstein, A., Katul, G., Law, B., Lee, X., Malhi, Y., Meyers, T., Munger, W., Oechel, W., Paw, U. K., Pilegaard, K., Schmid, H. P., Valentini, R., Verma, S., Vesala, T., Wilson, K., and Wofsy, S. (2001). FLUXNET: A New Tool to Study the Temporal and Spatial Variability of Ecosystem-Scale Carbon Dioxide, Water Vapor, and Energy Flux Densities. *Bulletin of the American Meteorological Society*, 82(11):2415–2434.

Barron, J. A., Bukry, D., and Hendy, I. L. (2015). High-resolution paleoclimatology of the Santa Barbara Basin during the Medieval Climate Anomaly and early Little Ice Age based on diatom and silicoflagellate assemblages in Kasten core SPR0901-02KC. *Quaternary International*, 387:13–22.

Becker, M. (1989). The role of climate on present and past vitality of silver fir forests in the Vosges mountains of northeastern France. *Canadian Journal of Forest Research*, 19(9):1110–1117.

Berger, A. (1978). Long-term variations of daily insolation and Quaternary climatic changes. *Journal of the Atmospheric Sciences*, 35:2362–2367.

Bird, B. W., Abbott, M. B., Finney, B. P., and Kutchko, B. (2009). A 2000 year varve-based climate record from the central Brooks Range, Alaska. *Journal of Paleolimnology*, 41:25–41.

Björklund, J. A., Gunnarson, B. E., Seftigen, K., Esper, J., and Linderholm, H. W. (2014). Blue intensity and density from northern fennoscandian tree rings, exploring the potential to improve summer temperature reconstructions with earlywood information. *Climate of the Past*, 10:877–885.

Black, D. E., Peterson, L. C., Overpeck, J. T., Kaplan, A., Evans, M. N., and Kashgarian, M. (1999). Eight centuries of North Atlantic ocean atmosphere variabitity. *Science*, 286:1709–1713.

Boucher, E., Guiot, J., Hatté, C., Daux, V., Danis, P. A., and Dussouillez, P. (2014). An inverse modeling approach for tree-ring-based climate reconstructions under changing atmospheric CO2 concentrations. *Biogeosciences*, 11(12):3245–3258.

Boucher, E., Nicault, A., Arseneault, D., Bégin, Y., and Karami, M. P. (2017). Decadal variations in Eastern Canada's taiga wood biomass production forced by ocean-atmosphere interactions. *Scientific Reports*, 7(1):1–13.

Bradley, R. S. and Jonest, P. D. (1993). 'Little ice age' summer temperature variations: Their nature and relevance to recent global warming trends. *The Holocene*, 3(4):367–376.

Brady, E., Stevenson, S., Bailey, D., Liu, Z., Noone, D., Nusbaumer, J., Otto-Bliesner, B. L., Tabor, C., Tomas, R., Wong, T., Zhang, J., and Zhu, J. (2019). The Connected Isotopic Water Cycle in the Community Earth System Model Version 1. *Journal of Advances in Modeling Earth Systems*, 11:2547–2566.

Breitenmoser, P., Brönnimann, S., and Frank, D. (2014). Forward modelling of tree-ring width and comparison with a global network of tree-ring chronologies. *Climate of the Past*, 10(2):437–449.

Breitsprecher, A. and Bethel, J. S. (1990). Stem-Growth Periodicity of Trees in a Tropical Wet Forest of Costa Rica. *Ecology*, 71(3):1156–1164.

Briffa, K. and Jones, P. (1992). Tree-ring density reconstructions of summer temperature patterns across Western North America since 1600. *Journal of Climate*, 5:735–754.

Briffa, K., Schweingruber, F. H., Jones, P., Osborn, T. J., Shiyatov, S. G., and Vaganov, E. A. (1998a). Reduced sensitivity of recent tree-growth to temperature at high northern latitudes. *Nature*, 391:678–685.

Briffa, K. R. (1999). Interpreting high-resolution proxy climate data — the example of dendroclimatology. In von Storch, H. and Navarra, A., editors, *Analysis of Climate Variability*, pages 77–94, Berlin, Heidelberg. Springer Berlin Heidelberg.

Briffa, K. R., Jones, P. D., Bartholin, T. S., Eckstein, D., Schweingruber, F. H., Karlén, W., Zetterberg, P., and Eronen, M. (1992). Fennoscandian summers from ad 500: temperature changes on short and long timescales. *Climate Dynamics*, 7:111–119.

Briffa, K. R., Jones, P. D., Wigley, T. M. L., Pilcher, J. R., and Baillie, M. G. L. (1986). Climate reconstruction from tree rings: Part 2, spatial reconstruction of summer mean sea-level pressure patterns over great britain. *Journal of Climatology*, 6(1):1–15.

Briffa, K. R., Osborn, T. J., Schweingruber, F. H., Harris, I. C., Jones, P. D., Shiyatov, S. G., and Vaganov, E. A. (2001). Low-frequency temperature variations from a northern tree ring density network. *Journal of Geophysical Research Atmospheres*, 106(D3):2929–2941.

Briffa, K. R., Schweingruber, F. H., Jones, P. D., Osborn, T. J., Harris, I. C., Shiyatov, S. G., Vaganov, E. A., and Grudd, H. (1998b). Trees tell of past climates: but are they speaking less clearly today? *Philosophical Transactions of the Royal Society of London. Series B: Biological Sciences*, 353(1365):65–73.

Büntgen, U., Arseneault, D., Boucher, É., Churakova (Sidorova), O. V., Gennaretti, F., Crivellaro, A., Hughes, M. K., Kirdyanov, A. V., Klippel, L., Krusic, P. J., Linderholm, H. W., Ljungqvist, F. C., Ludescher, J., McCormick, M., Myglan, V. S., Nicolussi, K., Piermattei, A., Oppenheimer, C., Reinig, F., Sigl, M., Vaganov, E. A., and Esper, J. (2020). Prominent role of volcanism in Common Era climate variability and human history. *Dendrochronologia*, 64.

Büntgen, U., Frank, D., Trouet, V., and Esper, J. (2010). Diverse climate sensitivity of Mediterranean tree-ring width and density. *Trees - Structure and Function*, 24:261–273.

Büntgen, U., Frank, D. C., Schmidhalter, M., Neuwirth, B., Seifert, M., and Esper, J. (2006). Growth/climate response shift in a long subalpine spruce chronology. *Trees - Structure and Function*, 20:99–110.

Büntgen, U., Kyncl, T., Ginzler, C., Jacks, D. S., Esper, J., Tegel, W., Heussner, K.-U., and Kyncl, J. (2013). Filling the Eastern European gap in millennium-long temperature reconstructions. *Proceedings of the National Academy of Sciences*, 110:1773–1778.

Büntgen, U., Tegel, W., Nicolussi, K., McCormick, M., Frank, D., Trouet, V., Kaplan, J., Herzig, F., Heussner, K.-U., Wanner, H., Luterbacher, J., and Esper, J. (2011). 2500 Years of European Climate Variability and Human Susceptibility. *Science*, 331:578–582.

Buras, A. (2017). A comment on the expressed population signal. *Dendrochronologia*, 44:130–132.

Camenisch, C., Keller, K. M., Salvisberg, M., Amann, B., Bauch, M., Blumer, S., Brázdil, R., Brönnimann, S., Büntgen, U., Campbell, B. M., Fernández-Donado, L., Fleitmann, D., Glaser, R., González-Rouco, F., Grosjean, M., Hoffmann, R. C., Huhtamaa, H., Joos, F., Kiss, A., Kotyza, O., Lehner, F., Luterbacher, J., Maughan, N., Neukom, R., Novy, T., Pribyl, K., Raible, C. C., Riemann, D., Schuh, M., Slavin, P., Werner, J. P., and Wetter, O. (2016). The 1430s: A cold period of extraordinary internal climate variability during the early Spörer Minimum with social and economic impacts in north-western and central Europe. *Climate of the Past*, 12:2107–2126.

Cernusak, L. A. and English, N. B. (2015). Beyond tree-ring widths: Stable isotopes sharpen the focus on climate responses of temperate forest trees. *Tree Physiology*, 35:1–3.

Comas-Bru, L., Rehfeld, K., Roesch, C., Amirnezhad-Mozhdehi, S., Harrison, S., Atsawawaranunt, K., Ahmad, S. M., Ait Brahim, Y., Baker, A., Bosomworth, M., Breitenbach, S., Burstyn, Y., Columbu, A., Deininger, M., Demény, A., Dixon, B., Fohlmeister, J., Hatvani, I. G., Hu, J., Kaushal, N., Kern, Z., Labuhn, I., Lechleitner, F., Lorrey, A., Martrat, B., Novello, V. F., Oster, J., Pérez-Mejías, C., Scholz, D., Scroxton, N., Sinha, N., Ward, B. M., Warken, S., and Zhang, H. (2020). SISALv2: A comprehensive speleothem isotope database with multiple age-depth models. *Earth System Science Data Discussions*, 12:1–47.

Cook, A. E. R., Seager, R., Kushnir, Y., Briffa, K. R., Frank, D., Krusic, P. J., Tegel, W., Schrier, G. V. D., Baillie, M., Baittinger, C., Bleicher, N., Bonde, N., Carrer, M., Cooper, R., Katarina, Č., and Dittmar, C. (2015). Old World Megadroughts and Pluvials During the Common Era. 1(10):1–22.

Cook, E. and Peters, K. (1981). The smoothing spline, a new approach to standardising forest interior tree-ring. *Trre-ring Bulletin*, 41:45–53.

Cook, E. R., Anchukaitis, K. J., Buckley, B. M., D'Arrigo, R. D., Jacoby, G. C., and Wright, W. E. (2010). Asian monsoon failure and megadrought during the last millennium. *Science*, 328:486–489.

Cook, E. R., Briffa, K. R., Meko, D. M., Graybill, D. A., and Funkhouser, G. (1995). The 'segment length curse' in long tree-ring chronology development for palaeoclimatic studies. *The Holocene*, 5(2):229–237.

Cook, E. R. and Kairiukstis, L. (1990). *Methods of dendrochronology: Applications in the Environmental Sciences*. Kluwer Academic, Boston.

Cook, E. R., Krusic, P. J., Anchukaitis, K. J., Buckley, B. M., Nakatsuka, T., and Sano, M. (2013). Tree-ring reconstructed summer temperature anomalies for temperate East Asia since 800 C.E. *Climate Dynamics*, 41:2957–2972.

Cook, E. R., Meko, D. M., Stahle, D. W., and Cleaveland, M. K. (1999). Drought reconstructions for the continental United States. *Journal of Climate*, 12:1145–1163.

Cook, E. R., Palmer, J. G., and D'Arrigo, R. D. (2002). Evidence for a 'Medieval Warm Period' in a 1,100 year tree-ring reconstruction of past austral summer temperatures in New Zealand. *Geophysical Research Letters*, 29(14):14–17.

Cook, E. R., Seager, R., Cane, M. A., and Stahle, D. W. (2007). North American drought: Reconstructions, causes, and consequences. *Earth-Science Reviews*, 81:93–134.

Cook, E. R., Solomina, O., Matskovsky, V., Cook, B. I., Agafonov, L., Berdnikova, A., Dolgova, E., Karpukhin, A., Knysh, N., Kulakova, M., Kuznetsova, V., Kyncl, T., Kyncl, J., Maximova, O., Panyushkina, I., Seim, A., Tishin, D., Ważny, T., and Yermokhin, M. (2020). The European Russia Drought Atlas (1400–2016 CE). *Climate Dynamics*, 54:2317–2335.

Cook, E. R., Woodhouse, C. A., Eakin, C. M., Meko, D. H., and Stahle, D. W. (2004). Long-term aridity changes in the western United States. *Science*, 306:1015–1018.

Cook, T. L., Bradley, R. S., Stoner, J. S., and Francus, P. (2009). Five thousand years of sediment transfer in a high arctic watershed recorded in annually laminated sediments from Lower Murray Lake, Ellesmere Island, Nunavut, Canada. *Journal of Paleolimnology*, 41:77–94.

Cooper, R. J., Melvin, T. M., Tyers, I., Wilson, R. J. S., and Briffa, K. R. (2013). A tree-ring reconstruction of East Anglian (UK) hydroclimate variability over the last millennium. *Climate Dynamics*, 40:1019–1039.

Craig, H. (1961). Isotopic variations in meteoric waters. *Science*, 133:1702–1703.

Crespin, E., Goosse, H., Fichefet, T., and Mann, M. E. (2009). The 15th century Arctic warming in coupled model simulations with data assimilation. *Climate of the Past*, 5:389–401.

Crowley, T. J., Zielinski, G., Vinther, B., Udisti, R., Kreutz, K., Cole-Dai, J., and Castellano, E. (2008). Volcanism and the Little Ice Age. *PAGES News*, 16(2):22–23.

Dalaiden, Q., Goosse, H., Rezsöhazy, J., and Thomas, E. (2021). Reconstructing atmospheric circulation and sea-ice extent in the West Antarctic over the past 200 years using data assimilation. *Climate Dynamics*.

Danis, P.-A., Hatté, C., Misson, L., and Guiot, J. (2012). MAIDENiso: a multiproxy biophysical model of tree-ring width and oxygen and carbon isotopes. *Canadian Journal of Forest Research*, 42(9):1697–1713.

Dansgaard, W. (1964). Stable isotopes in precipitation. *Tellus*, 16:436–468.

Dansgaard, W., Clausen, H. B., Gundestrup, N., Hammer, C. U., Johnsen, S. F., Kristinsdottir, P. M., and Reeh, N. (1982). A new Greenland deep ice core. *Science*, 218:1273–1277.

D'Arrigo, R., Davi, N., Jacoby, G., Wilson, R., and Wiles, G. (2014). *Dendroclimatic Studies: Tree Growth and Climate Change in Northern Forests*. John Wiley & Sons and American Geophysical Union.

D'Arrigo, R., Palmer, J., Ummenhofer, C. C., Kyaw, N. N., and Krusic, P. (2011). Three centuries of Myanmar monsoon climate variability inferred from teak tree rings. *Geophysical Research Letters*, 38:1–5.

D'Arrigo, R., Wilson, R., and Jacoby, G. (2006a). On the long-term context for late twentieth century warming. *Journal of Geophysical Research Atmospheres*, 111:1–12.

D'Arrigo, R., Wilson, R., Liepert, B., and Cherubini, P. (2008). On the 'Divergence Problem' in Northern Forests: A review of the tree-ring evidence and possible causes. *Global and Planetary Change*, 60(3-4):289–305.

D'Arrigo, R., Wilson, R., Palmer, J., Krusic, P., Curtis, A., Sakulich, J., Bijaksana, S., Zulaikah, S., and Ngkoimani, L. O. (2006b). Monsoon drought over Java, Indonesia, during the past two centuries. *Geophysical Research Letters*, 33:4–7.

D'Arrigo, R. D., Kaufmann, R. K., Davi, N., Jacoby, G. C., Laskowski, C., Myneni, R. B., and Cherubini, P. (2004). Thresholds for warming-induced growth decline at elevational tree line in the Yukon Territory, Canada. *Global Biogeochemical Cycles*, 18:1–7.

Davi, N., Jacoby, R., D'Arrigo, R., Naartarbileg, N., Jinbao, L., and Curtis, A. (2009). A tree-ring-based drought index reconstruction for far-western Mongolia: 1565–2004. *International Journal of Climatology*, 29:1508–1514.

Dee, S. G., Steiger, N. J., Emile-Geay, J., and Hakim, G. J. (2016). On the utility of proxy system models for estimating climate states over common era. *Journal of Advances in Modeling Earth Systems*, 8:1164–1179.

Delpierre, N., Vitasse, Y., Chuine, I., Guillemot, J., Bazot, S., Rutishauser, T., and Rathgeber, C. B. (2016). Temperate and boreal forest tree phenology: from organ-scale processes to terrestrial ecosystem models. *Annals of Forest Science*, 73:5–25.

Denne, M. and Dodd, R. (1981). The Environmental Control of Xylem Differentiation. In Barnett, J., editor, *Xylem Cell Development*, pages 236–255. Kent, UK: Castle House.

Deslauriers, A., Rossi, S., Anfodillo, T., and Saracino, A. (2008). Cambial phenology, wood formation and temperature thresholds in two contrasting years at high altitude in southern Italy. *Tree Physiology*, 28(6):863–871.

Dolgova, E. (2016). June-September temperature reconstruction in the Northern Caucasus based on blue intensity data. *Dendrochronologia*, 39:17–23.

Douglass, A. E. (1941). Crossdating in Dendrochronology. *Journal of Forestry*, 39(10):825–831.

Drew, D. M., Downes, G. M., and Battaglia, M. (2010). CAMBIUM, a process-based model of daily xylem development in Eucalyptus. *Journal of Theoretical Biology*, 264(2):395–406.

Dubinkina, S., Goosse, H., Sallaz-Damaz, Y., Crespin, E., and Crucifix, M. (2011). Testing a Particle Filter To Reconstruct Climate Changes Over the Past Centuries. *International Journal of Bifurcation and Chaos*, 21(12):3611–3618.

Duchesne, L., Houle, D., Ouimet, R., Caldwell, L., Gloor, M., and Brienen, R. (2019). Large apparent growth increases in boreal forests inferred from tree-rings are an artefact of sampling biases. *Scientific Reports*, 9(1):1–9.

Dufrêne, E., Davi, H., François, C., Le Maire, G., Le Dantec, V., and Granier, A. (2005). Modelling carbon and water cycles in a beech forest. Part I: Model description and uncertainty analysis on modelled NEE. *Ecological Modelling*, 185(2-4):407–436.

Dunbar, R. B. and Cole, J. E. (1999). Annual Records of Tropical Systems (ARTS): Recommendations for Research. *PAGES Workshop Report 99-1*.

Erb, M. P., Emile-Geay, J., Hakim, G. J., Steiger, N., and Steig, E. J. (2020). Atmospheric dynamics drive most interannual U.S. droughts over the last millennium. *Science Advances*, 6:1–13.

Erni, S., Arseneault, D., Parisien, M. A., and Bégin, Y. (2017). Spatial and temporal dimensions of fire activity in the fire-prone eastern Canadian taiga. *Global Change Biology*, 23(3):1152–1166.

Esper, J., Cook, E., Krusic, P., Peters, K., and Schweingruber, F. (2003). Tests of the RCS method for preserving low-frequency variability in long tree-ring chronologies. *Tree-ring research*, 59(2):81–98.

Esper, J., Cook, E. R., and Schweingruber, F. H. (2002). Low-frequency signals in long tree-ring chronologies for reconstructing past temperature variability. *Science*, 295:2250–2253.

Esper, J., Frank, D., Büntgen, U., Verstege, A., Luterbacher, J., and Xoplaki, E. (2007). Long-term drought severity variations in Morocco. *Geophysical Research Letters*, 34(17):1–5.

Esper, J., George, S. S., Anchukaitis, K., D'Arrigo, R., Ljungqvist, F., Luterbacher, J., Schneider, L., Stoffel, M., Wilson, R., and Büntgen, U. (2018). Large-scale, millennial-length temperature reconstructions from tree-rings. *Dendrochronologia*, 50:81–90.

Esper, J., Schneider, L., Smerdon, J. E., Schöne, B. R., and Büntgen, U. (2015). Signals and memory in tree-ring width and density data. *Dendrochronologia*, 35:62–72.

Evans, M., Kaplan, A., Cane, M., and Villalba, R. (2001). Chapter 4 - globality and optimality in climate field reconstructions from proxy data. In Markgraf, V., editor, *Interhemispheric Climate Linkages*, pages 53–XV. Academic Press, San Diego.

Evans, M. N., Kaplan, A., and Cane, M. A. (2002). Pacific sea surface temperature field reconstruction from coral δ18O data using reduced space objective analysis. *Paleoceanography*, 17(1).

Evans, M. N., Reichert, B. K., Kaplan, A., Anchukaitis, K. J., Vaganov, E. A., Hughes, M. K., and Cane, M. A. (2006). A forward modeling approach to paleoclimatic interpretation of tree-ring data. *Journal of Geophysical Research: Biogeosciences*, 111(3):1–13.

Evans, M. N., Tolwinski-Ward, S. E., Thompson, D. M., and Anchukaitis, K. J. (2013). Applications of proxy system modeling in high resolution paleoclimatology. *Quaternary Science Reviews*, 76:16–28.

Fang, M. and Li, X. (2019). An Artificial Neural Networks-Based Tree Ring Width Proxy System Model for Paleoclimate Data Assimilation. *Journal of Advances in Modeling Earth Systems*, 11(4):892–904.

FAO/IIASA/ISRIC/ISSCAS/JRC (2012). Harmonized World Soil Database (version 1.2). FAO, Rome, Italy and IIASA, Laxenburg, Austria.

Farquhar, G. D., Caemmerer, S., and Berry, J. A. (1980). A biochemical model of photosynthetic CO2 assimilation in leaves of C3 species. *Planta*, 149(1):78–90–90.

Fatichi, S., Leuzinger, S., and Körner, C. (2014). Moving beyond photosynthesis: From carbon source to sink-driven vegetation modeling. *New Phytologist*, 201(4):1086–1095.

Fatichi, S., Pappas, C., Zscheischler, J., and Leuzinger, S. (2019). Modelling carbon sources and sinks in terrestrial vegetation. *New Phytologist*, 221(2):652–668.

Fisher, D. A., Koerner, R. M., Kuivinen, K., Clausen, H. B., Johnsen, S. J., Steffensen, J.-P., Gundestrup, N., and Hammer, C. U. (1996). Inter-comparison of Ice Core δ18O and Precipitation Records from Sites in Canada and Greenland over the last 3500 years and over the last few Centuries in detail using EOF Techniques. In Jones, P., Bradley, R., and Jouzel, J., editors, *Climatic Variations and Forcing Mechanisms of the Last 2000 Years*, volume 41. Springer, Berlin, Heidelberg.

Flato, G., Marotzke, J., Abiodun, B., Braconnot, P., Chou, S., Collins, W., Cox, P., Driouech, F., Emori, S., Eyring, V., Forest, C., Gleckler, P., Guilyardi, E., Jakob, C., Kattsov, V., Reason, C., and Rummukainen, M. (2013). Evaluation of Climate Models. In *Climate Change 2013: The Physical Science Basis. Contribution of Working Group I to the Fifth Assessment Report of the Intergovernmental Panel on Climate Change*. Cambridge University Press, Cambridge, United Kingdom and New York, USA.

Fleitmann, D., Dunbar, R. B., McCulloch, M., Mudelsee, M., Vuille, M., McClanahan, T. R., Cole, J. E., and Eggins, S. (2007). East African soil erosion recorded in a 300 year old coral colony from Kenya. *Geophysical Research Letters*, 34:1–5.

Franke, J., Brönnimann, S., Bhend, J., and Brugnara, Y. (2017). A monthly global paleo-reanalysis of the atmosphere from 1600 to 2005 for studying past climatic variations. *Scientific Data*, 4:1–19.

Fritts, H., Blasing, T., Hayden, B. P., and Kutzbach, J. (1971). Multivariate Techniques for Specifying Tree-Growth and Climate Relationships and for Reconstructing Anomalies in Paleoclimate. *Journal of Applied Meteorology*, 10(5):845–864.

Fritts, H. C. (1976). *Tree rings and climate*. Academic Press, London.

Fritts, H. C. (1991). *Reconstructing large-scale climatic patterns from tree-ring data: A diagnostic analysis.* University of Arizona Press, Tucson, Arizona, USA.

Fritts, H. C., Mosimann, J. E., and Bottorff, C. P. (1969). A revised computer program for standardizing tree-ring series. University of Arizona, Laboratory of Tree-Ring Research. *Tree-Ring Bulletin*, pages 3–18.

Ganguly, S., Friedl, M. A., Tan, B., Zhang, X., and Verma, M. (2010). Land surface phenology from MODIS: Characterization of the Collection 5 global land cover dynamics product. *Remote Sensing of Environment*, 114(8):1805–1816.

Gea-Izquierdo, G., Guibal, F., Joffre, R., Ourcival, J. M., Simioni, G., and Guiot, J. (2015). Modelling the climatic drivers determining photosynthesis and carbon allocation in evergreen Mediterranean forests using multiproxy long time series. *Biogeosciences*, 12(12):3695–3712.

Gea-Izquierdo, G., Nicault, A., Battipaglia, G., Dorado-Liñán, I., Gutiérrez, E., Ribas, M., and Guiot, J. (2017). Risky future for Mediterranean forests unless they undergo extreme carbon fertilization. *Global Change Biology*, 23(7):2915–2927.

Gennaretti, F. (2017). MAIDEN ecophysiological forest model, figshare, Software.

Gennaretti, F., Arseneault, D., and Bégin, Y. (2014a). Millennial disturbance-driven forest stand dynamics in the Eastern Canadian taiga reconstructed from subfossil logs. *Journal of Ecology*, 102:1612–1622.

Gennaretti, F., Arseneault, D., Nicault, A., Perreault, L., and Begin, Y. (2014b). Volcano-induced regime shifts in millennial tree-ring chronologies from northeastern North America. *Proceedings of the National Academy of Sciences*, 111(28):10077–10082.

Gennaretti, F., Boucher, E., Nicault, A., Gea-Izquierdo, G., Arseneault, D., Berninger, F., Savard, M. M., Bégin, C., and Guiot, J. (2018). Underestimation of the Tambora effects in North American taiga ecosystems. *Environmental Research Letters*, 13(3).

Gennaretti, F., Gea-Izquierdo, G., Boucher, E., Berninger, F., Arseneault, D., and Guiot, J. (2017). Ecophysiological modeling of the climate imprint on photosynthesis and carbon allocation to the tree stem in the North American boreal forest. *Biogeosciences*, 14:4851–4866.

Giguère-Croteau, C., Boucher, É., Bergeron, Y., Girardin, M. P., Drobyshev, I., Silva, L. C., Hélie, J. F., and Garneau, M. (2019). North America's oldest boreal trees are more efficient water users due to increased [CO2], but do not grow faster. *Proceedings of the National Academy of Sciences of the United States of America*, 116(7):2749–2754.

Girardin, M. P., Bouriaud, O., Hogg, E. H., Kurz, W., Zimmermann, N. E., Metsaranta, J. M., De Jong, R., Frank, D. C., Esper, J., Büntgen, U., Guo, X. J., and Bhatti, J. (2016a). No growth stimulation of Canada's boreal forest under half-century of combined warming and CO2 fertilization. *Proceedings of the National Academy of Sciences of the United States of America*, 113(52):E8406–E8414.

Girardin, M. P., Hogg, E. H., Bernier, P. Y., Kurz, W. A., Guo, X. J., and Cyr, G. (2016b). Negative impacts of high temperatures on growth of black spruce forests intensify with the anticipated climate warming. *Global Change Biology*, 22(2):627–643.

Gong, D. and Wang, S. (1999). Definition of Antarctic oscillation index. *Geophysical Research Letters*, 26:459–462.

Goosse, H. (2015). *Climate System Dynamics and Modelling*. Cambridge University Press.

Goosse, H. (2016). An additional step toward comprehensive paleoclimate reanalyses. *Journal of Advances in Modeling Earth Systems*, 6:1501–1503.

Goosse, H. (2017). Reconstructed and simulated temperature asymmetry between continents in both hemispheres over the last centuries. *Climate Dynamics*, 48(5-6):1483–1501.

Goosse, H., Arzel, O., Luterbacher, J., Mann, M. E., Renssen, H., Riedwyl, N., Timmermann, A., Xoplaki, E., and Wanner, H. (2006). The origin of the European "Medieval Warm Period". *Climate of the Past*, 2:99–113.

Goosse, H., Crespin, E., de Montety, A., Mann, M. E., Renssen, H., and Timmermann, A. (2010). Reconstructing surface temperature changes over the past 600 years using climate model simulations with data assimilation. *Journal of Geophysical Research*, 115:1–17.

Goosse, H., Crespin, E., Dubinkina, S., Loutre, M. F., Mann, M. E., Renssen, H., Sallaz-Damaz, Y., and Shindell, D. (2012). The role of forcing and internal dynamics in explaining the "Medieval Climate Anomaly". *Climate Dynamics*, 39:2847–2866.

Goosse, H., Renssen, H., Timmermann, A., and Bradley, R. S. (2005). Internal and forced climate variability during the last millennium: A model-data comparison using ensemble simulations. *Quaternary Science Reviews*, 24:1345–1360.

Griffin, D., Woodhouse, C. A., Meko, D. M., Stahle, D. W., Faulstich, H. L., Carrillo, C., Touchan, R., Castro, C. L., and Leavitt, S. W. (2013). North American monsoon precipitation reconstructed from tree-ring latewood. *Geophysical Research Letters*, 40:954–958.

Grissino-Mayer, H. (2001). Evaluating Crossdating Accuracy: A Manual and Tutorial for the Computer Program COFECHA. *Tree-ring research*.

Gruber, A., Strobl, S., Veit, B., and Oberhuber, W. (2010). Impact of drought on the temporal dynamics of wood formation in Pinus sylvestris. *Tree Physiology*, 30:490–501.

Guiot, J., Boucher, E., and Gea-Izquierdo, G. (2014). Process models and model-data fusion in dendroecology. *Frontiers in Ecology and Evolution*, 2:1–12.

Guiot, J. and Corona, C. (2010). Growing season temperatures in Europe and climate forcings over the past 1400 years. *PLoS ONE*, 5(4).

Guiot, J., Keller, T., and Tessier, L. (1995). Relational databases in dendroclimatology and new nonlinear methods to analyse the tree response to climate and pollution. In *Tree rings: from the past to the future, Proceedings of the International Workshop on Asian and Pacific Dendrochronology. Forestry and Forest Products Research Institute Scientific Meeting Report*, volume 1, pages 17–23.

Guiot, J., Torre, F., Jolly, D., Peyron, O., Boreux, J. J., and Cheddadi, R. (2000). Inverse vegetation modeling by Monte Carlo sampling to reconstruct palaeoclimates under changed precipitation seasonality and CO2 conditions: Application to glacial climate in Mediterranean region. *Ecological Modelling*, 127:119–140.

Hakim, G. J., Emile-Geay, J., Steig, E. J., Noone, D., Anderson, D. M., Tardif, R., Steiger, N., and Perkins, W. A. (2016). The last millennium climate reanalysis project: Framework and first results. *Journal of Geophysical Research*, 121(12):6745–6764.

Hararuk, O., Campbell, E. M., Antos, J. A., and Parish, R. (2019). Tree rings provide no evidence of a CO 2 fertilization effect in old-growth subalpine forests of western Canada. *Global Change Biology*, 25(4):1222–1234.

Harris, I., Jones, P. D., Osborn, T. J., and Lister, D. H. (2014). Updated high-resolution grids of monthly climatic observations - the CRU TS3.10 Dataset. *International Journal of Climatology*, 34(3):623–642.

Harris, I., Osborn, T. J., Jones, P., and Lister, D. (2020). Version 4 of the CRU TS monthly high-resolution gridded multivariate climate dataset. *Scientific Data*, 7:1–18.

Hartig, F., Minunno, F., and Paul, S. (2019). BayesianTools: General-Purpose MCMC and SMC Samplers and Tools for Bayesian Statistics. R package version 0.1.6.

Heeter, K. J., Harley, G. L., Van De Gevel, S. L., and White, P. B. (2019). Blue intensity as a temperature proxy in the eastern United States: A pilot study from a southern disjunct population of Picea rubens (Sarg.). *Dendrochronologia*, 55:105–109.

Hegerl, G. C., Crowley, T. J., Baum, S. K., Kim, K. Y., and Hyde, W. T. (2003). Detection of volcanic, solar and greenhouse gas signals in paleo-reconstructions of Northern Hemispheric temperature. *Geophysical Research Letters*, 30(5):94–97.

Helama, S., Lindholm, M., Timonen, M., and Eronen, M. (2004). Detection of climate signal in dendrochronological data analysis: A comparison of tree-ring standardization methods. *Theoretical and Applied Climatology*, 79:239–254.

Helama, S., Melvin, T. M., and Briffa, K. R. (2017). Regional curve standardization: State of the art. *Holocene*, 27:172–177.

Hemming, D. L., Switsur, V. R., Waterhouse, J. S., Heaton, T. H., and Carter, A. H. (1998). Climate variation and the stable carbon isotope composition of tree ring cellulose: An intercomparison of Quercus robur, Fagus sylvatica and Pinus silvestris. *Tellus*, 50B:25–33.

Hereid, K. A., Quinn, T. M., and Okumura, Y. M. (2013). Assessing spatial variability in El Niño-Southern Oscillation event detection skill using coral geochemistry. *Paleoceanography*, 28:14–23.

Hermoso de Mendoza, I., Boucher, E., Gennaretti, F., Lavergne, A., Andreu-Hayles, L., and Field, R. (2021). A new snow module improves predictions of isotope-enabled MAIDENiso forest growth model. *Geoscientific Model Development Discussions*.

Hersbach, H., Bell, B., Berrisford, P., Hirahara, S., Horányi, A., Muñoz-Sabater, J., Nicolas, J., Peubey, C., Radu, R., Schepers, D., Simmons, A., Soci, C., Abdalla, S., Abellan, X., Balsamo, G., Bechtold, P., Biavati, G., Bidlot, J., Bonavita, M., De Chiara, G., Dahlgren, P., Dee, D., Diamantakis, M., Dragani, R., Flemming, J., Forbes, R., Fuentes, M., Geer, A., Haimberger, L., Healy, S., Hogan, R. J., Hólm, E., Janisková, M., Keeley, S., Laloyaux, P., Lopez, P., Lupu, C., Radnoti, G., de Rosnay, P., Rozum, I., Vamborg, F., Villaume, S., and Thépaut, J. N. (2020). The ERA5 global reanalysis. *Quarterly Journal of the Royal Meteorological Society*, 146:1999–2049.

Hessl, A. E., Anchukaitis, K. J., Jelsema, C., Cook, B., Byambasuren, O., Leland, C., Nachin, B., Pederson, N., Tian, H., and Hayles, L. A. (2018). Past and future drought in Mongolia. *Science Advances*, 4:1–8.

Hmimina, G., Dufrêne, E., Pontailler, J. Y., Delpierre, N., Aubinet, M., Caquet, B., de Grandcourt, A., Burban, B., Flechard, C., Granier, A., Gross, P., Heinesch, B., Longdoz, B., Moureaux, C., Ourcival, J. M., Rambal, S., Saint André, L., and Soudani, K. (2013). Evaluation of the potential of MODIS satellite data to predict vegetation phenology in different biomes: An investigation using ground-based NDVI measurements. *Remote Sensing of Environment*, 132:145–158.

Hofgaard, A., Ols, C., Drobyshev, I., Kirchhefer, A. J., Sandberg, S., and Söderström, L. (2019). Non-stationary Response of Tree Growth to Climate Trends Along the Arctic Margin. *Ecosystems*, 22:434–451.

Holmes, R. (1983). Computer-Assisted Quality Control in Tree-Ring Dating and Measurement. *Tree-ring bulletin*.

Huang, J., van den Dool, H., and Georgarakos, K. (1996). Analysis of Model-Calculated Soil Moisture over the United States (1931–1993) and Applications to Long-Range Temperature Forecasts. *Journal of Climate*, 9:1350–1362.

Huang, J.-G., Ma, Q., Rossi, S., Biondi, F., Deslauriers, A., Fonti, P., Liang, E., Mäkinen, H., Oberhuber, W., Rathgeber, C. B. K., Tognetti, R., Treml, V., Yang, B., Zhang, J.-L., Antonucci, S., Bergeron, Y., Camarero, J. J., Campelo, F., Čufar, K., Cuny, H. E., De Luis, M., Giovannelli, A., Gričar, J., Gruber, A., Gryc, V., Güney, A., Guo, X., Huang, W., Jyske, T., Kašpar, J., King, G., Krause, C., Lemay, A., Liu, F., Lombardi, F., Martinez del Castillo, E., Morin, H., Nabais, C., Nöjd, P., Peters, R. L., Prislan, P., Saracino, A., Swidrak, I., Vavrčík, H., Vieira, J., Yu, B., Zhang, S., Zeng, Q., Zhang, Y., and Ziaco, E. (2020). Photoperiod and temperature as dominant environmental drivers triggering secondary growth resumption in Northern Hemisphere conifers. *Proceedings of the National Academy of Sciences*, 117(34):202007058.

Hughes, M. K. and Diaz, H. F. (1994). Was there a 'medieval warm period', and if so, where and when? *Climatic Change*, 26:109–142.

Hughes, M. K., Guiot, J., and Ammann, C. (2010). An emerging paradigm: Process-based climate reconstructions. *PAGES news*, 18(2):87–89.

Hughes, M. K., Swetnam, T. W., and Diaz, H. F. (2011). *Dendroclimatology: Progress and Prospects*, volume 11. New York, springer edition.

Hunter, J. D. (2007). Matplotlib: A 2D graphics environment. *Computing in Science and Engineering*, 9(3):90–95.

Hutchinson, M. F., McKenney, D. W., Lawrence, K., Pedlar, J. H., Hopkinson, R. F., Milewska, E., and Papadopol, P. (2009). Development and testing of Canada-wide interpolated spatial models of daily

minimum-maximum temperature and precipitation for 1961-2003. *Journal of Applied Meteorology and Climatology*, 48(4):725–741.

Huybers, P. and Curry, W. (2006). Links between annual, Milankovitch and continuum temperature variability. *Nature*, 441(7091):329–332.

Imbrie, J., Hays, J. D., Martinson, D. G., Mclntyre, A., Mix, A. C., Morley, J. J., Pisias, N. G., Prell and, W. L., and Shackleton, N. J. (1984). The orbital theory of pleistocene climate: support from a revised chronology of the marine 18O record. In Berger, A., Imbrie, J., Hays, J., Kukla, G., and Saltzman, B., editors, *Milankovitch and Climate*, pages 269–305. Plenum Reidel, Dordrecht.

IPCC (2019). IPCC Special Report on the Ocean and Cryosphere in a Changing Climate [H.-O. Pörtner, D.C. Roberts, V. Masson-Delmotte, P. Zhai, M. Tignor, E. Poloczanska, K. Mintenbeck, A. Alegría, M. Nicolai, A. Okem, J. Petzold, B. Rama, N.M. Weyer (eds.)]. *In press*.

Jimenez, G., Cole, J. E., Thompson, D. M., and Tudhope, A. W. (2018). Northern Galápagos Corals Reveal Twentieth Century Warming in the Eastern Tropical Pacific. *Geophysical Research Letters*, 45:1981–1988.

Johnson, S. E. and Abrams, M. D. (2009). Age class, longevity and growth rate relationships: Protracted growth increases in old trees in the eastern United States. *Tree Physiology*, 29(11):1317–1328.

Jones, P. D., Briffa, K. R., Barnett, T. P., and Tett, S. F. B. (1998). High-resolution palaeoclimatic records for the last millennium. *The Holocene*, 4:455–471.

Jones, P. D., Briffa, K. R., Osborn, T. J., Lough, J. M., Van Ommen, T. D., Vinther, B. M., Luterbacher, J., Wahl, E. R., Zwiers, F. W., Mann, M. E., Schmidt, G. A., Ammann, C. M., Buckley, B. M., Cobb, K. M., Esper, J., Goosse, H., Graham, N., Jansen, E., Kiefer, T., Kull, C., Küttel, M., Mosley-Thompson, E., Overpeck, J. T., Riedwyl, N., Schulz, M., Tudhope, A. W., Villalba, R., Wanner, H., Wolff, E., and Xoplaki, E. (2009). High-resolution palaeoclimatology of the last millennium: A review of current status and future prospects. *Holocene*, 19(1):3–49.

Jones, P. D. and Mann, M. E. (2004). Climate over past millennia. *Reviews of Geophysics*, 42:1–42.

Jones, P. D., Osborn, T. J., and Briffa, K. R. (2001). The evolution of climate over the last millennium. *Science*, 292(5517):662–667.

Jonsson, B. and Matern, B. (1974). On the computation of annual ring indices. *International Workshop on Dendroclimatology, Univeristy of Arizona, Tucson*.

Jouzel, J., Lorius, C., Petit, J. R., Genthon, C., Barkov, N. I., Kotlyakov, V. M., and Petrov, V. M. (1987). Vostok ice core: A continuous isotope temperature record over the last climatic cycle (160,000 years). *Nature*, 329:403–408.

Jung, M., Reichstein, M., Schwalm, C. R., Huntingford, C., Sitch, S., Ahlström, A., Arneth, A., Camps-Valls, G., Ciais, P., Friedlingstein, P., Gans, F., Ichii, K., Jain, A. K., Kato, E., Papale, D., Poulter, B., Raduly, B., Rödenbeck, C., Tramontana, G., Viovy, N., Wang, Y. P., Weber, U., Zaehle, S., and Zeng, N. (2017). Compensatory water effects link yearly global land CO 2 sink changes to temperature. *Nature*, 541(7638):516–520.

Jung, M., Schwalm, C., Migliavacca, M., Walther, S., Camps-Valls, G., Koirala, S., Anthoni, P., Besnard, S., Bodesheim, P., Carvalhais, N., Chevallier, F., Gans, F., S Goll, D., Haverd, V., Köhler, P., Ichii, K., K Jain, A., Liu, J., Lombardozzi, D., E M S Nabel, J., A Nelson, J., O'Sullivan, M., Pallandt, M., Papale, D., Peters, W., Pongratz, J., Rödenbeck, C., Sitch, S., Tramontana, G., Walker, A., Weber, U., and Reichstein, M. (2020). Scaling carbon fluxes from eddy covariance sites to globe: Synthesis and evaluation of the FLUXCOM approach. *Biogeosciences*, 17(5):1343–1365.

Kaczka, R. J., Spyt, B., Janecka, K., Beil, I., Büntgen, U., Scharnweber, T., Nievergelt, D., and Wilmking, M. (2018). Different maximum latewood density and blue intensity measurements techniques reveal similar results. *Dendrochronologia*, 49:94–101.

Kalnay, E. (2003). *Atmospheric Modeling, Data Assimilation and Predictability*. Cambridge University Press.

Kaufman, D. (2014). A community-driven framework for climate reconstructions. *Eos*, 95(40):361–362.

Keeling, C. D., Bacastow, R. B., and Bainbridge, A. E. (1976). Atmospheric carbon dioxide variations at Mauna Loa Observatory, Hawaii. *Tellus*, 28(6):538–551.

King, J. M., Tierney, J. E., Hakim, G. J., Emile-Geay, J., Zhu, F., and Wilson, R. (2021). A data assimilation approach to last millennium temperature field reconstruction using a limited high-sensitivity proxy network 2. *Journal of Climate*, published.

Konecky, B., McKay, N., Churakova (Sidorova), O., Comas-Bru, L., Dassié, E., DeLong, K., Falster, G., Fischer, M., Jones, M., Jonkers, L., Kaufman, D., Leduc, G., Managave, S., Martrat, B., Opel, T., Orsi, A., Partin, J., Sayani, H., Thomas, E., Thompson, D., Tyler, J., Abram, N., Atwood, A., Conroy, J., Kern, Z., Porter, T., Stevenson, S., and von Gunten, L. (2020). The Iso2k Database: A global compilation of paleo-δ18O and δ2H records to aid understanding of Common Era climate. *Earth System Science Data*, 12:2261–2288.

Körner, C. (2015). Paradigm shift in plant growth control. *Current Opinion in Plant Biology*, 25:107–114.

Körner, C., Asshoff, R., Bignucolo, O., Hättenschwiler, S., Keel, S. G., Peláez-Riedl, S., Pepin, S., Siegwolf, R. T., and Zotz, G. (2005). Ecology: Carbon flux and growth in mature deciduous forest trees exposed to elevated CO2. *Science*, 309(5739):1360–1362.

Kress, A., Saurer, M., Siegwolf, R. T., Frank, D. C., Esper, J., and Bugmann, H. (2010). A 350 year drought reconstruction from Alpine tree ring stable isotopes. *Global Biogeochemical Cycles*, 24:1–16.

Labuhn, I., Daux, V., Girardclos, O., Stievenard, M., Pierre, M., and Masson-Delmotte, V. (2016). French summer droughts since 1326 CE: A reconstruction based on tree ring cellulose δ18O. *Climate of the Past*, 12:1101–1117.

Lauritzen, S. E. and Lundberg, J. (1999). Speleothems and climate: A special issue of The Holocene. *Holocene*, 9(6):643–647.

Lavergne, A., Daux, V., Villalba, R., and Barichivich, J. (2015). Temporal changes in climatic limitation of tree-growth at upper treeline forests: Contrasted responses along the west-to-east humidity gradient in Northern Patagonia. *Dendrochronologia*, 36:49–59.

Lavergne, A., Gennaretti, F., Risi, C., Daux, V., Savard, M., Naulier, M., Villalba, R., Begin, C., Lavergne, A., Gennaretti, F., Risi, C., Daux, V., Boucher, E., Lavergne, A., Gennaretti, F., Risi, C., Daux, V., Boucher, E., and Savard, M. M. (2017). Modelling tree ring cellulose δ 18 O variations in two temperature-sensitive tree species from North and South America. *Climate of the Past*, 13:1515–1526.

Leuning, R. (1995). A critical appraisal of a combined stomatal-photosynthesis model for C3 plants. *Plant, Cell & Environment*, 18(4):339–355.

Lévesque, M., Siegwolf, R., Saurer, M., Eilmann, B., and Rigling, A. (2014). Increased water-use efficiency does not lead to enhanced tree growth under xeric and mesic conditions. *New Phytologist*, 203(1):94–109.

Linderholm, H. W., Björklund, J., Seftigen, K., Gunnarson, B. E., and Fuentes, M. (2015). Fennoscandia revisited : a spatially improved tree - ring reconstruction of summer temperatures for the last 900 years. *Climate Dynamics*, 45:933–947.

Liu, Y., Wang, Y., Li, Q., Song, H., Linderhlom, H. W., Leavitt, S. W., Wang, R., and An, Z. (2014). Tree-ring stable carbon isotope-based May-July temperature reconstruction over Nanwutai, China, for the past century and its record of 20th century warming. *Quaternary Science Reviews*, 93:67–76.

Lough, J. M. (2010). Climate records from corals. *Wiley Interdisciplinary Reviews: Climate Change*, 1:318–331.

Luterbacher, J., Dietrich, D., Xoplaki, E., Grosjean, M., and Wanner, H. (2004). European Seasonal and Annual Temperature Variability, Trends, and Extremes since 1500. *Science*, 303:1499–1503.

Luterbacher, J., Werner, J. P., Smerdon, J. E., Fernández-Donado, L., González-Rouco, F. J., Barriopedro, D., Ljungqvist, F. C., Büntgen, U., Zorita, E., Wagner, S., Esper, J., McCarroll, D., Toreti, A., Frank, D., Jungclaus, J. H., Barriendos, M., Bertolin, C., Bothe, O., Brázdil, R., Camuffo, D., Dobrovolný, P., Gagen, M., García-Bustamante, E., Ge, Q., Gómez-Navarro, J. J., Guiot, J., Hao, Z., Hegerl, G. C., Holmgren, K., Klimenko, V. V., Martín-Chivelet, J., Pfister, C., Roberts, N., Schindler,

A., Schurer, A., Solomina, O., Von Gunten, L., Wahl, E., Wanner, H., Wetter, O., Xoplaki, E., Yuan, N., Zanchettin, D., Zhang, H., and Zerefos, C. (2016). European summer temperatures since Roman times. *Environmental Research Letters*, 11(2).

Mäkelä, A., Hari, P., Berninger, F., Hänninen, H., and Nikinmaa, E. (2004). Acclimation of photosynthetic capacity in Scots pine to the annual cycle of temperature. *Tree Physiology*, 24(4):369–376.

Malevich, S. B., Woodhouse, C. A., and Meko, D. M. (2013). Tree-ring reconstructed hydroclimate of the Upper Klamath basin. *Journal of Hydrology*, 495:13–22.

Mangini, A., Spötl, C., and Verdes, P. (2005). Reconstruction of temperature in the Central Alps during the past 2000 yr from a δ18O stalagmite record. *Earth and Planetary Science Letters*, 235(3-4):741–751.

Mann, M. E., Bradley, R. S., and Hughes, M. K. (1998). Global-scale temperature patterns and climate forcing over the past six centuries. *Nature*, 392:779–787.

Mann, M. E., Bradley, R. S., and Hughes, M. K. (1999). Northern Hemisphere temperatures during the past millennium. *Geophysical Research Letters*, 26(6):759–762.

Mann, M. E. and Rutherford, S. (2002). Climate reconstruction using "Pseudoproxies". *Geophysical Research Letters*, 29(10):1–4.

Mann, M. E., Rutherford, S., Wahl, E., and Ammann, C. (2007). Robustness of proxy-based climate field reconstruction methods. *Journal of Geophysical Research Atmospheres*, 112(12):1–18.

Mann, M. E., Zhang, Z., Hughes, M. K., Bradley, R. S., Miller, S. K., Rutherford, S., and Ni, F. (2008). Proxy-based reconstructions of hemispheric and global surface temperature variations over the past two millennia. *Proceedings of the National Academy of Sciences*, 105(36):13252–13257.

Mann, M. E., Zhang, Z., Rutherford, S., Bradley, R. S., Hughes, M. K., Shindell, D., Ammann, C., Faluvegi, G., and Ni, F. (2009). Global Signatures and Dynamical Origins of the Little Ice Age and Medieval Climate Anomaly. *Science*, 326:1256–1260.

Marchand, W., Girardin, M. P., Hartmann, H., Depardieu, C., Isabel, N., Gauthier, S., Boucher, É., and Bergeron, Y. (2020). Strong overestimation of water-use efficiency responses to rising CO2 in tree-ring studies. *Global Change Biology*, 26(8):4538–4558.

Marshall, G. J. (2003). Trends in the Southern Annular Mode from observations and reanalyses. *Journal of Climate*, 16:4134–4143.

Masson-Delmotte, V., Raffalli-Delerce, G., Danis, P. A., Yiou, P., Stievenard, M., Guibal, F., Mestre, O., Bernard, V., Goosse, H., Hoffmann, G., and Jouzel, J. (2005). Changes in European precipitation seasonality and in drought frequencies revealed by a four-century-long tree-ring isotopic record from Brittany, western France. *Climate Dynamics*, 24:57–69.

Matsikaris, A., Widmann, M., and Jungclaus, J. (2015). On-line and off-line data assimilation in palaeoclimatology: A case study. *Climate of the Past*, 11:81–93.

McCarroll, D. and Loader, N. J. (2004). Stable isotopes in tree rings. *Quaternary Science Reviews*, 23:771–801.

McCarroll, D., Pettigrew, E., Luckman, A., Guibal, F., and Edouard, J.-L. (2002). Blue Reflectance Provides a Surrogate for Latewood Density of High-latitude Pine Tree Rings. *Arctic, Antarctic, and Alpine Research*, 34(4):450–453.

Medley, B., McConnell, J. R., Neumann, T. A., Reijmer, C. H., Chellman, N., Sigl, M., and Kipfstuhl, S. (2018). Temperature and Snowfall in Western Queen Maud Land Increasing Faster Than Climate Model Projections. *Geophysical Research Letters*, 45(3):1472–1480.

Medley, B. and Thomas, E. R. (2019). Increased snowfall over the Antarctic Ice Sheet mitigated twentieth-century sea-level rise. *Nature Climate Change*, 9:34–39.

Meier, G. A. and Brown, J. F. (2014). Remote sensing of land surface phenology. Technical report, Reston, VA.

Melvin, T. M., Brifffa, K. R., Nicolussi, K., and Grabner, M. (2007). Time-varying-response smoothing. *Dendrochronologia*, 25:65–69.

Menne, M., Durre, I., Korzeniewski, B., McNeal, S., Thomas, K., Yin, X., Anthony, S., Ray, R., Vose, R., Gleason, B., and Houston, T. (2012a). Global Historical Climatology Network - Daily (GHCN-Daily), Version 3.24. NOAA National Climatic Data Center.

Menne, M. J., Durre, I., Vose, R. S., Gleason, B. E., and Houston, T. G. (2012b). An overview of the global historical climatology network-daily database. *Journal of Atmospheric and Oceanic Technology*, 29(7):897–910.

Misson, L. (2004). MAIDEN: a model for analyzing ecosystem processes in dendroecology. *Canadian Journal of Forest Research*, 34(4):874–887.

Myhre, G., Shindell, D., Bréon, F.-M., Collins, W., Fuglestvedt, J., Huang, J., Koch, D., Lamarque, J.-F., Lee, D., Mendoza, B., Nakajima, T., Robock, A., Stephens, G., Takemura, T., and Zhang, H. (2013). Anthropogenic and Natural Radiative Forcing. In *Climate Change 2013: The Physical Science Basis. Contribution of Working Group I to the Fifth Assessment Report of the Intergovernmental Panel on Climate Change*. Cambridge University Press, Cambridge, United Kingdom and New York, USA.

Nash, J. E. and Sutcliffe, J. V. (1970). River flow forecasting through conceptual models part I - A discussion of principles. *Journal of Hydrology*, 10(3):282–290.

Naulier, M., Savard, M. M., Bégin, C., Gennaretti, F., Arseneault, D., Marion, J., Nicault, A., and Bégin, Y. (2015). A millennial summer temperature reconstruction for northeastern Canada using oxygen isotopes in subfossil trees. *Climate of the Past*, 11:1153–1164.

Neukom, R., Gergis, J., Karoly, D. J., Wanner, H., Curran, M., Elbert, J., González-Rouco, F., Linsley, B. K., Moy, A. D., Mundo, I., Raible, C. C., Steig, E. J., Van Ommen, T., Vance, T., Villalba, R., Zinke, J., and Frank, D. (2014). Inter-hemispheric temperature variability over the past millennium. *Nature Climate Change*, 4:362–367.

Neukom, R., Luterbacher, J., Villalba, R., Kttel, M., Frank, D., Jones, P. D., Grosjean, M., Esper, J., Lopez, L., and Wanner, H. (2010). Multi-centennial summer and winter precipitation variability in southern South America. *Geophysical Research Letters*, 37:1–6.

Neukom, R., Luterbacher, J., Villalba, R., Küttel, M., Frank, D., Jones, P. D., Grosjean, M., Wanner, H., Aravena, J. C., Black, D. E., Christie, D. A., D'Arrigo, R., Lara, A., Morales, M., Soliz-Gamboa, C., Srur, A., Urrutia, R., and von Gunten, L. (2011). Multiproxy summer and winter surface air temperature field reconstructions for southern South America covering the past centuries. *Climate Dynamics*, 37:35–51.

Neukom, R., Steiger, N., Gómez-Navarro, J. J., Wang, J., and Werner, J. P. (2019). No evidence for globally coherent warm and cold periods over the preindustrial Common Era. *Nature*, 571(7766):550–554.

Nicault, A., Alleaume, S., Brewer, S., Carrer, M., Nola, P., and Guiot, J. (2008). Mediterranean drought fluctuation during the last 500 years based on tree-ring data. *Climate Dynamics*, 31:227–245.

Nicault, A., Bégin, Y., and Guiot, J. (2010a). Standardisation des séries dendrochronologiques. In Payette, S. and Fillion, L., editors, *La dendroécologie, principes, méthodes et applications*, pages 199–227. Les Presses de l'Université Laval, Québec.

Nicault, A., Boucher, E., Tapsoba, D., Arseneault, D., Berninger, F., Bégin, C., DesGranges, J., Guiot, J., Marion, J., Wicha, S., and Bégin, Y. (2014). Spatial analysis of black spruce (Picea mariana (Mill.) B.S.P.) radial growth response to climate in northern Québec – Labrador Peninsula, Canada . *Canadian Journal of Forest Research*, 45(3):343–352.

Nicault, A., Guiot, J., Edouard, J. L., and Brewer, S. (2010b). Preserving long-term fluctuations in standardisation of tree-ring series by the adaptative regional growth curve (ARGC). *Dendrochronologia*, 28:1–12.

Oke, P. R. and Sakov, P. (2008). Representation error of oceanic observations for data assimilation. *Journal of Atmospheric and Oceanic Technology*, 25:1004–1017.

Osborn, T. J., Jones, P. D., Lister, D. H., Morice, C. P., Simpson, I. R., Winn, J. P., Hogan, E., and Harris, I. C. (2021). Land Surface Air Temperature Variations Across the Globe Updated to 2019: The CRUTEM5 Data Set. *Journal of Geophysical Research: Atmospheres*, 126:1–22.

PAGES 2k Consortium (2013). Continental-scale temperature variability during the past two millennia. *Nature Geoscience*, 6(5):339–346.

PAGES 2k Consortium (2017). A global multiproxy database for temperature reconstructions of the Common Era. *Scientific Data*, 4(1):170088.

Palmer, J. G., Cook, E. R., Turney, C. S., Allen, K., Fenwick, P., Cook, B. I., O'Donnell, A., Lough, J., Grierson, P., and Baker, P. (2015). Drought variability in the eastern Australia and New Zealand summer drought atlas (ANZDA, CE 1500-2012) modulated by the Interdecadal Pacific Oscillation. *Environmental Research Letters*, 10:1–12.

Partin, J. W., Cobb, K. M., Adkins, J. F., Clark, B., and Fernandez, D. P. (2007). Millennial-scale trends in west Pacific warm pool hydrology since the Last Glacial Maximum. *Nature*, 449(7161):452–455.

Pauling, A., Luterbacher, J., Casty, C., and Wanner, H. (2006). Five hundred years of gridded high-resolution precipitation reconstructions over Europe and the connection to large-scale circulation. *Climate Dynamics*, 26(4):387–405.

Payette, S., Filion, L., and Delwaide, A. (2008). Spatially explicit fire-climate history of the boreal forest-tundra (Eastern Canada) over the last 2000 years. *Philosophical Transactions of the Royal Society B: Biological Sciences*, 363(1501):2301–2316.

Pearl, J. K., Keck, J. R., Tintor, W., Siekacz, L., Herrick, H. M., Meko, M. D., and Pearson, C. L. (2020). New frontiers in tree-ring research. *The Holocene*, page 095968362090223.

Peng, C., Guiot, J., Wu, H., Jiang, H., and Luo, Y. (2011). Integrating models with data in ecology and palaeoecology: Advances towards a model-data fusion approach. *Ecology Letters*, 14:522–536.

Peñuelas, J., Canadell, J. G., and Ogaya, R. (2011). Increased water-use efficiency during the 20th century did not translate into enhanced tree growth. *Global Ecology and Biogeography*, 20(4):597–608.

Perkins, W. A. and Hakim, G. J. (2017). Reconstructing paleoclimate fields using online data assimilation with a linear inverse model. *Climate of the Past*, 13:421–436.

Petit, J. R., Jouzel, J., Raynaud, D., Barkov, N. I., Barnola, J. M., Basile, I., Bender, M., Chappellaz, J., Davis, M., Delaygue, G., Delmotte, M., Kotiyakov, V. M., Legrand, M., Lipenkov, V. Y., Lorius, C., Pépin, L., Ritz, C., Saltzman, E., and Stievenard, M. (1999). Climate and atmospheric history of the past 420,000 years from the Vostok ice core, Antarctica. *Nature*, 399:429–436.

Prislan, P., Čufar, K., Koch, G., Schmitt, U., and Gričar, J. (2013). Review of cellular and subcellular changes in the cambium. *IAWA Journal*, 34(4):391–407.

Pumijumnong, N., Eckstein, D., and Sass, U. (1995). Tree-Ring Research on Tectona Grandis in Northern Thailand. *IAWA Journal*, 16(4):385–392.

Rathgeber, C. B., Cuny, H. E., and Fonti, P. (2016). Biological basis of tree-ring formation: A crash course. *Frontiers in Plant Science*, 7(MAY2016):1–7.

Rezsöhazy, J., Gennaretti, F., Goosse, H., and Guiot, J. (2021). Testing the performance of dendroclimatic process-based models at global scale with the PAGES2k tree-ring width database. *Climate Dynamics*, 57:2005–2020.

Rezsöhazy, J., Goosse, H., Guiot, J., Gennaretti, F., Boucher, E., André, F., and Jonard, M. (2020). Application and evaluation of the dendroclimatic process-based model MAIDEN during the last century in Canada and Europe. *Climate of The Past*, 16:1043–1059.

Riedwyl, N., Küttel, M., Luterbacher, J., and Wanner, H. (2009). Comparison of climate field reconstruction techniques: Application to Europe. *Climate Dynamics*, 32:381–395.

Rinne, K. T., Loader, N. J., Switsur, V. R., and Waterhouse, J. S. (2013). 400-year May-August precipitation reconstruction for Southern England using oxygen isotopes in tree rings. *Quaternary Science Reviews*, 60:13–25.

Rossi, S., Deslauriers, A., Anfodillo, T., and Carraro, V. (2007). Evidence of threshold temperatures for xylogenesis in conifers at high altitudes. *Oecologia*, 152(1):1–12.

Rossi, S., Deslauriers, A., Anfodillo, T., Morin, H., Saracino, A., Motta, R., and Borghetti, M. (2006). Conifers in cold environments synchronize maximum growth rate of tree-ring formation with day length. *New Phytologist*, 170(2):301–310.

Rossi, S., Deslauriers, A., Griçar, J., Seo, J. W., Rathgeber, C. B., Anfodillo, T., Morin, H., Levanic, T., Oven, P., and Jalkanen, R. (2008). Critical temperatures for xylogenesis in conifers of cold climates. *Global Ecology and Biogeography*, 17:696–707.

Rubino, M., Etheridge, D. M., Thornton, D. P., Howden, R., Allison, C. E., Francey, R. J., Langenfelds, R. L., Steele, P. L., Trudinger, C. M., Spencer, D. A., Curran, M. A. J., Van Ommen, T. D., and Smith, A. M. (2019). Revised records of atmospheric trace gases CO2, CH4, N2O and d13C-O2 over the last 2000 years from Law Dome, Antarctica. *Earth System Science Data*, pages 473–492.

Running, S. W., Nemani, R. R., and Hungerford, R. D. (1987). Extrapolation of synoptic meteorological data in mountainous terrain and its use for simulating forest evapotranspiration and photosynthesis. *Canadian Journal of Forest Research*, 17(6):472–483.

Rutherford, S., Mann, M. E., Osborn, T. J., Bradley, R. S., Briffa, K. R., Hughes, M. K., and Jones, P. D. (2005). Proxy-based Northern Hemisphere surface temperature reconstructions: Sensitivity to method, predictor network, target season, and target domain. *Journal of Climate*, 18(13):2308–2329.

Rydval, M., Larsson, L. Å., McGlynn, L., Gunnarson, B. E., Loader, N. J., Young, G. H., and Wilson, R. (2014). Blue intensity for dendroclimatology: Should we have the blues? Experiments from Scotland. *Dendrochronologia*, 32:191–204.

Rydval, M., Loader, N. J., Gunnarson, B. E., Druckenbrod, D. L., Linderholm, H. W., Moreton, S. G., Wood, C. V., and Wilson, R. (2017). Reconstructing 800 years of summer temperatures in Scotland from tree rings. *Climate Dynamics*, 49:2951–2974.

Saurer, M., Siegenthaler, U., and Schweingruber, F. (1995). The climate-carbon isotope relationship in tree rings and the significance of site conditions. *Tellus*, 47B:320–330.

Schneider, S. H. and Dickinson, R. E. (1974). Climate modeling. *Reviews of Geophysics*, 12(3):447–493.

Schöngart, J., Orthmann, B., Hennenberg, K. J., Porembski, S., and Worbes, M. (2006). Climate-growth relationships of tropical tree species in West Africa and their potential for climate reconstruction. *Global Change Biology*, 12:1139–1150.

Schwarz, G. (1978). Estimating the Dimension of a Model. *The Annals of Statistics*, 6(2):461–464.

Schweingruber, F., Fritts, H., Braker, O., Drew, L., and Schar, E. (1978). The Xray technique as applied to dendroclimatology. *Tree-Ring Bulletin*, 38:61–91.

Schweingruber, F. H. (1996). *Tree rings and environment: dendroecology.* Haupt, Berne, Switzerland.

Seftigen, K., Frank, D. C., Björklund, J., Babst, F., and Poulter, B. (2018). The climatic drivers of normalized difference vegetation index and tree-ring-based estimates of forest productivity are spatially coherent but temporally decoupled in Northern Hemispheric forests. *Global Ecology and Biogeography*, 27(11):1352–1365.

Sheffield, J., Goteti, G., and Wood, E. F. (2006). Development of a 50-year high-resolution global dataset of meteorological forcings for land surface modeling. *Journal of Climate*, 19(13):3088–3111.

Sheppard, P. R. (2010). Dendroclimatology: Extracting climate from trees. *Wiley Interdisciplinary Reviews: Climate Change*, 1(3):343–352.

Shi, J. F., Liu, Y., Vaganov, E. A., Li, J., and Cai, Q. (2008). Statistical and process-based modeling analyses of tree growth response to climate in semi-arid area of north central China: A case study of Pinus tabulaeformis. *Journal of Geophysical Research: Biogeosciences*, 113(1):1–10.

Silva, L. C., Anand, M., and Leithead, M. D. (2010). Recent widespread tree growth decline despite increasing atmospheric CO2. *PLoS ONE*, 5(7):e11543.

Smerdon, J. E., Kaplan, A., Chang, D., and Evans, M. N. (2010). A pseudoproxy evaluation of the CCA and RegEM methods for reconstructing climate fields of the last millennium. *Journal of Climate*, 23(18):4856–4880.

Souverijns, N., Gossart, A., Gorodetskaya, I. V., Lhermitte, S., Mangold, A., Laffineur, Q., Delcloo, A., and Van Lipzig, N. P. (2018). How does the ice sheet surface mass balance relate to snowfall? Insights from a ground-based precipitation radar in East Antarctica. *Cryosphere*, 12:1987–2003.

St. George, S. and Esper, J. (2019). Concord and discord among Northern Hemisphere paleotemperature reconstructions from tree rings. *Quaternary Science Reviews*, 203:278–281.

Stahle, D. W. (1999). Useful strategies for the development of tropical tree-ring chronologies. *IAWA Journal*, 20(3):249–253.

Stahle, D. W., Cook, E. R., Burnette, D. J., Villanueva, J., Cerano, J., Burns, J. N., Griffin, D., Cook, B. I., Acuña, R., Torbenson, M. C., Szejner, P., and Howard, I. M. (2016). The Mexican Drought Atlas: Tree-ring reconstructions of the soil moisture balance during the late pre-Hispanic, colonial, and modern eras. *Quaternary Science Reviews*, 149:34–60.

Steiger, N. J., Hakim, G. J., Steig, E. J., Battisti, D. S., and Roe, G. H. (2014). Assimilation of time-averaged pseudoproxies for climate reconstruction. *Journal of Climate*, 27:426–441.

Steiger, N. J. and Smerdon, J. E. (2017). A pseudoproxy assessment of data assimilation for reconstructing the atmosphere-ocean dynamics of hydroclimate extremes. *Climate of the Past*, 13(10):1435–1449.

Steiger, N. J., Smerdon, J. E., Cook, E. R., and Cook, B. I. (2018). A reconstruction of global hydroclimate and dynamical variables over the Common Era. *Scientific Data*, 5:1–15.

Stenni, B., Curran, M. A., Abram, N. J., Orsi, A., Goursaud, S., Masson-Delmotte, V., Neukom, R., Goosse, H., Divine, D., Van Ommen, T., Steig, E. J., Dixon, D. A., Thomas, E. R., Bertler, N. A., Isaksson, E., Ekaykin, A., Werner, M., and Frezzotti, M. (2017). Antarctic climate variability on regional and continental scales over the last 2000 years. *Climate of the Past*, 13:1609–1634.

Stevenson, S., Otto-Bliesner, B. L., Brady, E. C., Nusbaumer, J., Tabor, C., Tomas, R., Noone, D. C., and Liu, Z. (2019). Volcanic Eruption Signatures in the Isotope-Enabled Last Millennium Ensemble. *Paleoceanography and Paleoclimatology*, 34:1534–1552.

Stoffel, M., Khodri, M., Corona, C., Guillet, S., Poulain, V., Bekki, S., Guiot, J., Luckman, B. H., Oppenheimer, C., Lebas, N., Beniston, M., and Masson-Delmotte, V. (2015). Estimates of volcanic-induced cooling in the Northern Hemisphere over the past 1,500 years. *Nature Geoscience*, 8:784–788.

Tardif, R., Hakim, G. J., Perkins, W. A., Horlick, K. A., Erb, M. P., Emile-Geay, J., Anderson, D. M., Steig, E. J., and Noone, D. (2019). Last Millennium Reanalysis with an expanded proxy database and seasonal proxy modeling. *Climate of the Past*, 15(4):1251–1273.

Testa, S., Soudani, K., Boschetti, L., and Borgogno Mondino, E. (2018). MODIS-derived EVI, NDVI and WDRVI time series to estimate phenological metrics in French deciduous forests. *International Journal of Applied Earth Observation and Geoinformation*, 64:132–144.

Thomas, E. R., Melchior Van Wessem, J., Roberts, J., Isaksson, E., Schlosser, E., Fudge, T. J., Vallelonga, P., Medley, B., Lenaerts, J., Bertler, N., Van Den Broeke, M. R., Dixon, D. A., Frezzotti, M., Stenni, B., Curran, M., and Ekaykin, A. A. (2017). Regional Antarctic snow accumulation over the past 1000 years. *Climate of the Past*, 13:1491–1513.

Tierney, J. E., Abram, N. J., Anchukaitis, K. J., Evans, M. N., Giry, C., Kilbourne, K. H., Saenger, C. P., Wu, H. C., and Zinke, J. (2015). Tropical sea surface temperatures for the past four centuries reconstructed from coral archives. *Paleoceanography*, 30:226–252.

Tingley, M. P. and Huybers, P. (2010a). A Bayesian algorithm for reconstructing climate anomalies in space and time. Part I: Development and applications to paleoclimate reconstruction problems. *Journal of Climate*, 23(10):2759–2781.

Tingley, M. P. and Huybers, P. (2010b). A bayesian algorithm for reconstructing climate anomalies in space and time. Part II: Comparison with the regularized expectation-maximization algorithm. *Journal of Climate*, 23(10):2782–2800.

Tingley, M. P. and Huybers, P. (2013). Recent temperature extremes at high northern latitudes unprecedented in the past 600 years. *Nature*, 496:201–205.

Tolwinski-Ward, S. E., Anchukaitis, K. J., and Evans, M. N. (2013). Bayesian parameter estimation and interpretation for an intermediate model of tree-ring width. *Climate of the Past*, 9(4):1481–1493.

Tolwinski-Ward, S. E., Evans, M. N., Hughes, M. K., and Anchukaitis, K. J. (2011). An efficient forward model of the climate controls on interannual variation in tree-ring width. *Climate Dynamics*, 36(11-12):2419–2439.

Tolwinski-Ward, S. E., Tingley, M. P., Evans, M. N., Hughes, M. K., and Nychka, D. W. (2015). Probabilistic reconstructions of local temperature and soil moisture from tree-ring data with potentially time-varying climatic response. *Climate Dynamics*, 44(3-4):791–806.

Touchan, R., Anchukaitis, K. J., Meko, D. M., Kerchouche, D., Slimani, S., Ilmen, R., Hasnaoui, F., Guibal, F., Julio Camarero, J., Sánchez-Salguero, R., Piermattei, A., Sesbou, A., Cook, B. I., Sabir, M., and Touchane, H. (2017). Climate controls on tree growth in the Western Mediterranean. *Holocene*, 27(10):1429–1442.

Touchan, R., Anchukaitis, K. J., Meko, D. M., Sabir, M., Attalah, S., and Aloui, A. (2011a). Spatiotemporal drought variability in northwestern Africa over the last nine centuries. *Climate Dynamics*, 37:237–252.

Touchan, R., Funkhouser, G., Hughes, M. K., and Erkan, N. (2005a). Standardized precipitation index reconstructed from Turkish tree-ring widths. *Climatic Change*, 72(3):339–353.

Touchan, R., Woodhouse, C. A., Meko, D. M., and Allen, C. (2011b). Millennial precipitation reconstruction for the Jemez Mountains, New Mexico, reveals changingb drought signal. *International Journal of Climatology*, 31:896–906.

Touchan, R., Xoplaki, E., Funkhouser, G., Luterbacher, J., Hughes, M. K., Erkan, N., Akkemik, Ü., and Stephan, J. (2005b). Reconstructions of spring/summer precipitation for the Eastern Mediterranean from tree-ring widths and its connection to large-scale atmospheric circulation. *Climate Dynamics*, 25:75–98.

Tramontana, G., Jung, M., Schwalm, C. R., Ichii, K., Camps-Valls, G., Ráduly, B., Reichstein, M., Arain, M. A., Cescatti, A., Kiely, G., Merbold, L., Serrano-Ortiz, P., Sickert, S., Wolf, S., and Papale, D. (2016). Predicting carbon dioxide and energy fluxes across global FLUXNET sites with regression algorithms. *Biogeosciences*, 13(14):4291–4313.

Tsvetanov, N., Dolgova, E., and Panayotov, M. (2020). First measurements of Blue intensity from Pinus peuce and Pinus heldreichii tree rings and potential for climate reconstructions. *Dendrochronologia*, 60(February):125681.

University of East Anglia Climatic Research Unit (CRU) (2017). CRU TS4.01: Climatic Research Unit (CRU) Time-Series (TS) version 4.01 of high-resolution gridded data of month-by-month variation in climate (Jan. 1901 - Dec. 2016). *Centre for Environmental Data Analysis (CEDA)*.

Vaganov, E. A., Anchukaitis, K. J., and Evans, M. N. (2011). *How Well Understood Are the Processes that Create Dendroclimatic Records? A Mechanistic Model of the Climatic Control on Conifer Tree-Ring Growth Dynamics*, pages 37–75. Springer Netherlands, Dordrecht.

Vaganov, E. A., Hughes, M. K., Kirdyanov, A., Schweingruber, F. H., and Silkin, P. (1999). Influence of snowfall and melt timing on tree growth in subarctic Eurasia. *Nature*, 400:149–151.

Vaganov, E. A., Hughes, M. K., and Shashkin, A. (2006). *Growth dynamics of conifer tree rings*. New York, springer edition.

Valler, V., Brugnara, Y., and Bronnimann, S. (2020). Assimilating monthly precipitation data in a paleoclimate data assimilation framework. *Climate of the Past*, 16:1309–1323.

Van Der Sleen, P., Groenendijk, P., Vlam, M., Anten, N. P., Boom, A., Bongers, F., Pons, T. L., Terburg, G., and Zuidema, P. A. (2015). No growth stimulation of tropical trees by 150 years of CO2 fertilization but water-use efficiency increased. *Nature Geoscience*, 8(1):24–28.

van Leeuwen, P. J. (2009). Particle Filtering in Geophysical Systems. *Monthly Weather Review*, 137(12):4089–4114.

van Wessem, J. M., van de Berg, W. J., Noël, B. P. Y., van Meijgaard, E., Birnbaum, G., Jakobs, C. L., Krüger, K., Lenaerts, J. T. M., Lhermitte, S., Ligtenberg, S. R. M., Medley, B., Reijmer, C. H., van Tricht, K., Trusel, L. D., van Ulft, L. H., Wouters, B., Wuite, J., and van den Broeke, M. R. (2018). Modelling the climate and surface mass balance of polar ice sheets using RACMO2, part 2: Antarctica (1979-2016). *The Cryosphere*, 12:1479–1498.

Vinther, B. M., Johnsen, S. J., Andersen, K. K., Clausen, H. B., and Hansen, A. W. (2003). NAO signal recorded in the stable isotopes of Greenland ice cores. *Geophysical Research Letters*, 30(7):1–4.

Visser, H., Büntgen, U., D'Arrigo, R., and Petersen, A. C. (2010). Detecting instabilities in tree-ring proxy calibration. *Climate of the Past*, 6:367–377.

Von Storch, H., Zorita, E., Jones, J. M., Dimitriev, Y., González-Rouco, F., and Tett, S. F. (2004). Recontructing past climate from noisy data. *Science*, 306:679–682.

Wang, J., Emile-Geay, J., Guillot, D., Smerdon, J. E., and Rajaratnam, B. (2014). Evaluating climate field reconstruction techniques using improved emulations of real-world conditions. *Climate of the Past*, 10:1–19.

Wang, J., Yang, B., and Ljungqvist, F. C. (2015). A millennial summer temperature reconstruction for the eastern tibetan plateau from tree-ring width. *Journal of Climate*, 28(13):5289–5304.

Weinheimer, A. and Biondi, F. (2003). PALEOCLIMATOLOGY | Varves. In Holton, J., editor, *Encyclopedia of Atmospheric Sciences*, pages 1680–1685. Academic Press, Oxford.

Werner, J. P., Divine, D. V., Ljungqvist, F. C., Nilsen, T., and Francus, P. (2018). Spatio-Temporal variability of Arctic summer temperatures over the past 2 millennia. *Climate of the Past*, 14:527–557.

Werner, J. P. and Tingley, M. P. (2015). Technical Note: Probabilistically constraining proxy age-depth models within a Bayesian hierarchical reconstruction model. *Climate of the Past*, 11(3):533–545.

White, W. B. (2019). Speleothems. In White, W., Culver, D., and Pipan, T., editors, *Encyclopedia of Caves (Third Edition)*, pages 1006–1017. Academic Press.

Widmann, M., Goosse, H., Van Der Schrier, G., Schnur, R., and Barkmeijer, J. (2010). Using data assimilation to study extratropical Northern Hemisphere climate over the last millennium. *Climate of the Past*, 6:627–644.

Wilmking, M., van der Maaten-Theunissen, M., van der Maaten, E., Scharnweber, T., Buras, A., Biermann, C., Gurskaya, M., Hallinger, M., Lange, J., Shetti, R., Smiljanic, M., and Trouillier, M. (2020). Global assessment of relationships between climate and tree growth. *Global Change Biology*, 26(6):3212–3220.

Wilson, R., Anchukaitis, K., Briffa, K. R., Büntgen, U., Cook, E., D'Arrigo, R., Davi, N., Esper, J., Frank, D., Gunnarson, B., Hegerl, G., Helama, S., Klesse, S., Krusic, P. J., Linderholm, H. W., Myglan, V., Osborn, T. J., Rydval, M., Schneider, L., Schurer, A., Wiles, G., Zhang, P., and Zorita, E. (2016). Last millennium northern hemisphere summer temperatures from tree rings: Part I: The long term context. *Quaternary Science Reviews*, 134:1–18.

Wilson, R., Cook, E., D'Arrigo, R., Riedwyl, N., Evans, M., Tudhope, A., and Allan, R. (2010). Reconstructing ENSO: the influence of method, proxy data, climate forcing and teleconnections. *Journal of Quaternary Science*, 25(18):62–78.

Wilson, R., D'Arrigo, R., Buckley, B., Büntgen, U., Esper, J., Frank, D., Luckman, B., Payette, S., Vose, R., and Youngblut, D. (2007). A matter of divergence: Tracking recent warming at hemispheric scales using tree ring data. *Journal of Geophysical Research Atmospheres*, 112:1–17.

Wilson, R. and Elling, W. (2004). Temporal instability in tree-growth/climate response in the Lower Bavarian Forest region: Implications for dendroclimatic reconstruction. *Trees - Structure and Function*, 18(1):19–28.

Wilson, R., Tudhope, A., Brohan, P., Briffa, K., Osborn, T., and Tett, S. (2006). Two-hundred-fifty years of reconstructed and modeled tropical temperatures. *Journal of Geophysical Research: Oceans*, 111:1–13.

Wong, C. I. and Breecker, D. O. (2015). Advancements in the use of speleothems as climate archives. *Quaternary Science Reviews*, 127:1–18.

Yang, B., Qin, C., Wang, J., He, M., Melvin, T. M., Osborn, T. J., and Briffa, K. R. (2014). A 3,500-year tree-ring record of annual precipitation on the northeastern Tibetan Plateau. *Proceedings of the National Academy of Sciences of the United States of America*, 111:2903–2908.

Yuan, Y. J., Zhang, T. W., Wei, W. S., Nievergelt, D., Verstege, A., Yu, S. L., Zhang, R. B., and Esper, J. (2013). Development of tree-ring maximum latewood density chronologies for the Western Tien Shan Mountains, China: Influence of detrending method and climate response. *Dendrochronologia*, 31:192–197.

Zaw, Z., Fan, Z. X., Bräuning, A., Xu, C. X., Liu, W. J., Gaire, N. P., Panthi, S., and Than, K. Z. (2020). Drought Reconstruction Over the Past Two Centuries in Southern Myanmar Using Teak Tree-Rings: Linkages to the Pacific and Indian Oceans. *Geophysical Research Letters*, 47:1–10.

Zhang, H., Werner, J. P., García-Bustamante, E., González-Rouco, F., Wagner, S., Zorita, E., Fraedrich, K., Jungclaus, J. H., Ljungqvist, F. C., Zhu, X., Xoplaki, E., Chen, F., Duan, J., Ge, Q., Hao, Z., Ivanov, M., Schneider, L., Talento, S., Wang, J., Yang, B., and Luterbacher, J. (2018). East Asian warm season temperature variations over the past two millennia. *Scientific Reports*, 8:1–11.

Zhang, X., Friedl, M. A., Schaaf, C. B., Strahler, A. H., Hodges, J. C., Gao, F., Reed, B. C., and Huete, A. (2003). Monitoring vegetation phenology using MODIS. *Remote Sensing of Environment*, 84(3):471–475.

Zhang, Y. X., Shao, X. M., Xu, Y., and Wilmking, M. (2011). Process-based modeling analyses of Sabina przewalskii growth response to climate factors around the northeastern Qaidam Basin. *Chinese Science Bulletin*, 56(14):1518–1525.

Zhao, S., Pederson, N., D'Orangeville, L., HilleRisLambers, J., Boose, E., Penone, C., Bauer, B., Jiang, Y., and Manzanedo, R. D. (2019). The International Tree-Ring Data Bank (ITRDB) revisited: Data availability and global ecological representativity. *Journal of Biogeography*, 46:355–368.

Zhu, F., Emile-Geay, J., Hakim, G. J., King, J., and Anchukaitis, K. J. (2020). Resolving the Differences in the Simulated and Reconstructed Temperature Response to Volcanism. *Geophysical Research Letters*, 47(8):1–17.

Zinke, J., Reuning, L., Pfeiffer, M., Wassenburg, J. A., Hardman, E., Jhangeer-Khan, R., Davies, G. R., Ng, C. K., and Kroon, D. (2016). A sea surface temperature reconstruction for the southern Indian Ocean trade wind belt from corals in Rodrigues Island (19°S, 63°E). *Biogeosciences*, 13:5827–5847.

Zolitschka, B., Francus, P., Ojala, A. E., and Schimmelmann, A. (2015). Varves in lake sediments - a review. *Quaternary Science Reviews*, 117:1–41.